

## MIT Open Access Articles

*The First Hundred Brown Dwarfs Discovered by  
the Wide-field Infrared Survey Explorer (WISE)*

The MIT Faculty has made this article openly available. **Please share**  
how this access benefits you. Your story matters.

**Citation:** Davy Kirkpatrick, J. et al. "The First Hundred Brown Dwarfs Discovered by the Wide-field Infrared Survey Explorer (WISE)." The Astrophysical Journal Supplement Series 197.2 (2011): 19.

**As Published:** <http://dx.doi.org/10.1088/0067-0049/197/2/19>

**Publisher:** IOP Publishing

**Persistent URL:** <http://hdl.handle.net/1721.1/76592>

**Version:** Author's final manuscript: final author's manuscript post peer review, without publisher's formatting or copy editing

**Terms of use:** Creative Commons Attribution-Noncommercial-Share Alike 3.0



To be submitted to *The Astrophysical Journal*

## The First Hundred Brown Dwarfs Discovered by the Wide-field Infrared Survey Explorer (WISE)

J. Davy Kirkpatrick<sup>a</sup>, Michael C. Cushing<sup>b</sup>, Christopher R. Gelino<sup>a</sup>, Roger L. Griffith<sup>a</sup>,  
Michael F. Skrutskie<sup>d</sup>, Kenneth A. Marsh<sup>a</sup>, Edward L. Wright<sup>c</sup>, Amanda K. Mainzer<sup>b</sup>,  
Peter R. Eisenhardt<sup>b</sup>, Ian S. McLean<sup>c</sup>, Maggie A. Thompson<sup>j</sup>, James M. Bauer<sup>b</sup>, Dominic J.  
Benford<sup>l</sup>, Carrie R. Bridge<sup>k</sup>, Sean E. Lake<sup>c</sup>, Sara M. Petty<sup>c</sup>, S. Adam Stanford<sup>m</sup>, Chao-Wei  
Tsai<sup>a</sup>, Vanessa Bailey<sup>t</sup>, Charles A. Beichman<sup>a</sup>, John J. Bochanski<sup>g,u</sup>, Adam J. Burgasser<sup>h</sup>,  
Peter L. Capak<sup>n</sup>, Kelle L. Cruz<sup>i</sup>, Philip M. Hinz<sup>t</sup>, Jeyhan S. Kartaltepe<sup>o</sup>, Russell P. Knox<sup>t</sup>,  
Swarnima Manohar<sup>p</sup>, Daniel Masters<sup>q</sup>, Maria Morales-Calderón<sup>n</sup>, Lisa A. Prato<sup>e</sup>, Timothy  
J. Rodigas<sup>t</sup>, Mara Salvato<sup>r</sup>, Steven D. Schurr<sup>s</sup>, Nicholas Z. Scoville<sup>p</sup>, Robert A. Simcoe<sup>g</sup>,  
Karl R. Stapelfeldt<sup>b</sup>, Daniel Stern<sup>b</sup>, Nathan D. Stock<sup>t</sup>, William D. Vacca<sup>f</sup>

## ABSTRACT

We present ground-based spectroscopic verification of six Y dwarfs (see also Cushing et al.), eighty-nine T dwarfs, eight L dwarfs, and one M dwarf identified by the Wide-field Infrared Survey Explorer (WISE). Eighty of these are cold brown dwarfs with spectral types  $\geq T6$ , six of which have been announced earlier in Mainzer et al. and Burgasser et al. We present color-color and color-type diagrams showing the locus of M, L, T, and Y dwarfs in WISE color space.

---

<sup>a</sup>Infrared Processing and Analysis Center, MS 100-22, California Institute of Technology, Pasadena, CA 91125; davy@ipac.caltech.edu

<sup>b</sup>NASA Jet Propulsion Laboratory, 4800 Oak Grove Drive, Pasadena, CA 91109

<sup>c</sup>Department of Physics and Astronomy, UCLA, Los Angeles, CA 90095-1547

<sup>d</sup>Department of Astronomy, University of Virginia, Charlottesville, VA, 22904

<sup>e</sup>Lowell Observatory, 1400 West Mars Hill Road, Flagstaff, AZ, 86001

<sup>f</sup>SOFIA-USRA, NASA Ames Research Center, Moffett Field, CA 94035

<sup>g</sup>Massachusetts Institute of Technology, 77 Massachusetts Avenue, Building 37, Cambridge, MA 02139

<sup>h</sup>Department of Physics, University of California, San Diego, CA 92093

<sup>i</sup>Department of Physics and Astronomy, Hunter College, New York, NY 10065

<sup>j</sup>The Potomac School, 1301 Potomac School Road, McLean, VA 22101

<sup>k</sup>Division of Physics, Mathematics, and Astronomy, MS 220-6, California Institute of Technology, Pasadena, CA 91125

<sup>l</sup>Infrared Astrophysics Branch, NASA-Goddard Space Flight Center, 8800 Greenbelt Road, Greenbelt, MD 20771

<sup>m</sup>University of California, Davis, CA 95616

<sup>n</sup>Spitzer Science Center, California Institute of Technology, Pasadena, CA 91125

<sup>o</sup>National Optical Astronomy Observatory, 950 North Cherry Avenue, Tucson, AZ 85719

<sup>p</sup>California Institute of Technology, MC 104-24, Pasadena, CA 91125

<sup>q</sup>University of California, Riverside

<sup>r</sup>Max-Planck-Institut für Plasmaphysik, Boltzmanstrasse 2, D-85741 Garching, Germany

<sup>s</sup>Planck Science Center, MS 220-6, California Institute of Technology, Pasadena, CA 91125

<sup>t</sup>Steward Observatory, The University of Arizona, 933 N. Cherry Ave., Tucson, AZ 85721

<sup>u</sup>Astronomy and Astrophysics Department, Pennsylvania State University, 525 Davey Laboratory, University Park, PA 16802

Near-infrared and, in a few cases, optical spectra are presented for these discoveries. Near-infrared classifications as late as early Y are presented and objects with peculiar spectra are discussed. Using these new discoveries, we are also able to extend the optical T dwarf classification scheme from T8 to T9. After deriving an absolute WISE 4.6  $\mu\text{m}$  (W2) magnitude vs. spectral type relation, we estimate spectrophotometric distances to our discoveries. We also use available astrometric measurements to provide preliminary trigonometric parallaxes to four of our discoveries, which have types of L9 pec (red), T8, T9, and Y0; all of these lie within 10 pc of the Sun. The Y0 dwarf, WISE 1541–2250, is the closest at  $2.8^{+1.3}_{-0.6}$  pc; if this 2.8 pc value persists after continued monitoring, WISE 1541–2250 will become the seventh closest stellar system to the Sun. Another ten objects, with types between T6 and >Y0, have spectrophotometric distance estimates also placing them within 10 pc. The closest of these, the T6 dwarf WISE 1506+7027, is believed to fall at a distance of  $\sim 4.9$  pc. WISE multi-epoch positions supplemented with positional info primarily from *Spitzer*/IRAC allow us to calculate proper motions and tangential velocities for roughly one half of the new discoveries. This work represents the first step by WISE to complete a full-sky, volume-limited census of late-T and Y dwarfs. Using early results from this census, we present preliminary, lower limits to the space density of these objects and discuss constraints on both the functional form of the mass function and the low-mass limit of star formation.

## 1. Introduction

Brown dwarfs, objects whose central temperatures never reach the critical threshold for stable thermonuclear burning (Kumar 1963; Hayashi & Nakano 1963), are the lowest mass products of star formation. Hundreds of examples are now known<sup>1</sup>, enabling the study of brown dwarfs as a population in their own right (Kirkpatrick 2005). The study of brown dwarfs helps to constrain mechanisms for small-object formation, which include turbulent fragmentation (Padoan et al. 2005; Boyd & Whitworth 2005), magnetic field confinement (Boss 2004), stellar embryo ejection through dynamical interactions (Reipurth & Clarke 2001; Bate & Bonnell 2005), and photo-evaporation of embryos by nearby hot stars (Whitworth & Zinnecker 2004).

Brown dwarfs also represent a “fossilized” record of star formation throughout the

---

<sup>1</sup>See DwarfArchives.org.

Galaxy’s history because their mass is never ejected back into the interstellar medium. They therefore preserve information on metallicity enrichment over the lifetime of the Milky Way (Burgasser 2008). Solitary brown dwarfs have also proven to be excellent calibrators of the atmospheric models on which our inference of the properties of giant exoplanets depends (Fortney et al. 2005; Barman et al. 2005; Marois et al. 2008). Their effective temperatures are similar to those of the exoplanets discovered thus far but their spectra lack the complication of irradiation from a host star.

Despite uncovering hundreds of brown dwarfs, previous surveys have allowed us to identify only the warmest examples. The latest object currently having a measured spectrum is UGPS J072227.51–054031.2, whose effective temperature is estimated to be  $520 \pm 40$  K (Lucas et al. 2010; Bochanski et al., submitted, find  $T_{eff} = 500\text{--}600\text{K}$ ) and whose spectrum is used as the near-infrared T9 spectral standard (Cushing et al., accepted)<sup>2</sup>. Two other objects – WD 0806–661B (also known as GJ 3483B; Luhman et al. 2011) and CFBDSIR J145829+101343B (Liu et al. 2011) – are probably even colder and later in type than UGPS J072227.51–054031.2, although both currently lack spectroscopic confirmation. Both of these objects underscore the fact that the coldest brown dwarfs are extremely faint even at near-infrared wavelengths where ground-based spectroscopy has its best chance of characterizing the spectra. WD 0806–661B, a common proper motion companion to a white dwarf with a measured distance of  $19.2 \pm 0.6$  pc, has yet to be detected in ground-based imaging observations down to  $J=23.9$  mag (Luhman et al., submitted; see also Rodriguez et al. 2011). CFBDSIR J145829+101343B is the secondary in a system with a composite spectral type of T9 and a measured distance of  $23.1 \pm 2.4$  pc (Liu et al. 2011). A combination of its close proximity (0.11 arcsec) to the primary along with a faint magnitude ( $J=21.66 \pm 0.34$ ) make the acquisition of a spectrum challenging. Of the two, WD 0806–661B is less luminous at J band and presumably intrinsically fainter bolometrically (see also Wright et al. 2011). Finding even closer and brighter examples of cold brown dwarfs will be necessary to maximize our chances of best characterizing them.

Canvassing the immediate Solar Neighborhood for such cold objects is one of the goals of the all-sky mission performed by the Wide-field Infrared Survey Explorer (Wright et al. 2010). Discoveries will directly measure the low-mass cutoff of star formation (Figure 12 of Burgasser 2004) and provide even colder fiducial atmospheres for modeling cold exoplanets and understanding the gas giants of our own Solar System. The discovery of cold objects raises the question of whether a new spectral class, dubbed “Y” (Kirkpatrick 2000; Kirkpatrick 2008; see also Kirkpatrick et al. 1999), will be needed beyond the T class. In this

---

<sup>2</sup>Previously published objects with spectral types  $\geq T8.5$  have been reclassified now that the end of the T dwarf sequence and beginning of the Y dwarf sequence has been defined (Cushing et al., accepted).

paper we present an overview of the our first  $\sim 100$  WISE brown dwarf discoveries and show that objects colder than those previously known, including Y-class brown dwarfs, are being uncovered.

## 2. Brown Dwarf Selection

WISE is an Earth-orbiting NASA mission that surveyed the entire sky simultaneously at wavelengths of 3.4, 4.6, 12, and 22  $\mu\text{m}$ , hereafter referred to as bands W1, W2, W3, and W4, respectively. As shown in Figures 6, 7, and 13 of Wright et al. (2010) as well as Figure 2 of Mainzer et al. (2011), the W1 and W2 bands were specifically designed to probe the deep, 3.3  $\mu\text{m}$   $\text{CH}_4$  absorption band in brown dwarfs and the region relatively free of opacity at  $\sim 4.6 \mu\text{m}$ . Since the peak of the Planck function at low temperatures is in the mid-infrared, a large amount of flux emerges in the 4.6  $\mu\text{m}$  window, and this makes the W1-W2 colors of cool brown dwarfs extremely red (see §2.1). Such red colors, which are almost unique among astronomical sources, make the identification of cool brown dwarfs much easier.

WISE launched on 2009 Dec 14 and, after an in-orbit checkout, began surveying the sky on 2010 Jan 14. Its Sun-synchronous polar orbit around the Earth meant that each location along the ecliptic was observed a minimum of eight times, with larger numbers of re-visits occurring at locations nearer the ecliptic poles. WISE completed its first full pass of the sky on 2010 Jul 17 and its second pass on 2011 Jan 09. During this second pass, the outer, secondary tank depleted its cryogen on 2010 Aug 05, rendering the W4 band unusable, and the inner, primary tank depleted its cryogen on 2010 Sep 30, rendering the W3 band unusable. Thus, this second full sky pass is partly missing bands W3 and W4. Fortunately, the bands most crucial for brown dwarf selection – W1 and W2 – were little affected by this cryogen exhaustion. WISE continued to collect data on a third, incomplete sky pass in bands W1 and W2 until data acquisition was halted on 2011 Jan 31.

Preliminary processing of the data, including single-frame and coadded images and photometrically and astrometrically characterized detections, has been used to search for cold brown dwarf candidates, as described in detail below. This is the same version of the pipeline software that produced the WISE Preliminary Data Release, details of which can be found in the Explanatory Supplement<sup>3</sup>. For a more detailed description of the WISE mission and data products, see Wright et al. (2010) and the NASA/IPAC Infrared Science Archive (IRSA; <http://irsa.ipac.caltech.edu>). Because processing of the data continues as of this writing, our candidate selection is on-going, and only a fraction of our candidates

---

<sup>3</sup>See <http://wise2.ipac.caltech.edu/docs/release/prelim/expsup/>.

has been followed up, it is not possible to estimate the sky coverage or volume surveyed for discoveries presented herein. However, objects discussed here can be added to the growing census of brown dwarfs in the Solar Neighborhood and can be used to place lower limits, as we do in §5.3 below, to the brown dwarf space density as a function of type or temperature. As such, this paper should be regarded as a progress report on the continuing WISE search for previously missed brown dwarfs in the Sun’s immediate vicinity.

## 2.1. Comparison to Known M, L, and T Dwarfs

Before beginning the hunt for brown dwarfs, it is necessary to establish empirically the locus of known brown dwarfs in WISE color space and to understand what other kinds of astrophysical objects might fall in the same area. This will not only inform the search of WISE color space itself but also dictate the kinds of photometric follow-up that need to take place before time-intensive spectroscopic characterization begins.

We have performed a positional cross-correlation of nearby stars from Dwarf Archives<sup>4</sup> against source lists derived from the WISE coadded data. Many of these stars are known to have substantial proper motion, so it was necessary to verify each cross-match by visually inspecting the WISE and Two Micron All-Sky Survey (2MASS; Skrutskie et al. 2006) images. The final cross-identifications are given in Table 1, which lists photometry<sup>5</sup> from 2MASS (when detected) and WISE for 118 previously cataloged T dwarfs, 142 L dwarfs, and 92 M dwarfs. Figure 1 shows the resulting trend of WISE W1-W2 color as a function of spectral type for these objects, ranging from early-M through late-T. Note that there is a slow increase in the W1-W2 color between early-M and early-L, with the color stagnating near 0.3 mag between early- and mid-L. The W1-W2 color then rapidly increases at types later than mid-L, corresponding to the appearance of the methane fundamental band at  $3.3\ \mu\text{m}$  (Noll et al. 2000). The average W1-W2 color is  $\sim 0.6$  mag at T0 and  $\sim 1.5$  mag at T5, with the color increasing to above 3.0 mag at late T.

The red W1-W2 colors ( $>1.7$  mag) of dwarfs of type mid-T and later are almost, but not entirely, unique among astrophysical sources. Dust-obscured galaxies (DOGs) and asymptotic giant branch stars (AGBs) are the major sources of contamination at these red W1-W2 colors, as analysis of the Spitzer Deep Wide-Field Survey (SDWFS) results of Eisenhardt et al. (2010) has shown. The three short-wavelength bands of WISE – which are close in

---

<sup>4</sup>See <http://DwarfArchives.org>.

<sup>5</sup>In this and all subsequent tables, the errors listed are one-sigma values.

wavelength to the 3.6, 4.5, and 8.0  $\mu\text{m}$  bands (hereafter denoted as ch1, ch2, and ch4, respectively) of the Infrared Array Camera (IRAC) onboard the *Spitzer* Space Telescope – can help to distinguish between these populations. As Figure 1 of Eisenhardt et al. (2010) shows, most AGBs with very red W1-W2 (or ch1-ch2) colors can be distinguished by their very red W2-W3 (or ch2-ch4) colors. Brown dwarfs with similar W1-W2 colors are much *bluer* in W2-W3 color than these contaminants. Similarly, DOGs should be easily separable from brown dwarfs because, like AGBs, their W2-W3 (or ch2-ch4) colors tend to the red for objects with very red W1-W2 colors. This is further demonstrated in Figure 12 of Wright et al. (2010), where the bulk of the extragalactic menagerie, including red Active Galactic Nuclei, can be distinguished from cold brown dwarfs using a color of  $W2-W3 \approx 2.5$  as the dividing line.

As with any set of generic color cuts, however, one should be ever vigilant for exceptions. As Figure 1 and Figure 2 show, very late-T dwarfs have colors approaching  $W2-W3 \sim 2.0$  mag, near the locus of extragalactic sources, but their W1-W2 colors are extreme ( $> 3.0$  mag). Few extragalactic sources have W1-W2 colors this red, so the W2-W3 color criterion can be relaxed for the coldest objects (see Figure 3). Indeed, brown dwarfs with  $T_{\text{eff}} < 300\text{K}$  are expected to turn to the red in W2-W3 color (Figure 14 of Wright et al. 2010). It should also be noted that the location of low-gravity or low-metallicity brown dwarfs may not follow the general rule set by normal-gravity, solar-metallicity cases, so it is important to use other data (proper motion, parallax) when possible to identify brown dwarfs independent of photometric selections. Nonetheless, a number of possibly low-metallicity T dwarfs have been uncovered using these same photometric selections, as further discussed in the Appendix.

## 2.2. Search for New Candidates

We have used two different sets of criteria to search the WISE source lists for nearby brown dwarfs:

(1) To find the coldest brown dwarfs, we selected high signal-to-noise ( $\text{SNR} > 3$  at W2) detections having W1-W2 colors (or limits) greater than 1.5 mag, corresponding roughly to types  $\geq \text{T5}$ . (Because of the relative depths of the W1 and W2 bands, the W1-W2 requirement imposes a more severe W2 SNR limit of its own, generally  $W2 \text{ SNR} > 7$ .) In order to assure that an object is real, we required it to have been detected at least eight times in the individual W2 exposures; this eliminated spurious sources like cosmic rays and satellite trails that would otherwise not be eliminated during the outlier rejection step in coadd image creation (see section IV.5.a.v of the Explanatory Supplement to the WISE



Preliminary Data Release<sup>6</sup>). For our initial candidate selection, we also required  $W2-W3 < 3.0$  mag if the object has a detection in W3.

(2) To find bright, nearby (i.e., high proper motion) L and T dwarfs that other surveys have missed, we searched for objects with  $W1-W2$  colors greater than 0.4 mag (roughly types  $\geq L5$ ),  $W2$  SNR values greater than 30, and no association with a 2MASS source (implying that the  $J-W2$  color is either very red or the object has moved). It should be noted that the WISE source lists report 2MASS associations falling within 3 arcseconds of each WISE source<sup>7</sup>. As with the first search, we required the object to have been detected at least eight times in W2 to assure its reliability. To eliminate extragalactic contaminants, we imposed one additional criterion that  $W1-W2 > 0.96(W2-W3) - 0.96$  (see dashed line in Figure 3)<sup>8</sup>.

For both searches, no constraint on galactic latitude was imposed, although additional constraints were placed on object detections in order to assure that they were real, particularly for our earliest searches of the WISE source lists. First, the reduced  $\chi^2$  value from the PSF photometric fitting (“rchi2” in the WISE Preliminary Release Source Catalog) was required to fall between 0.5 and 3.0 to assure that the source was pointlike. Second, the early version of the WISE data processing pipeline automatically flagged artifacts – bright star halos, diffraction spikes, latent images, ghost reflections from bright stars, etc. – only on individual frames and not on the coadded images. For search #2 above, because those objects all have high-SNR  $W2$  detections, we are able to use these individual frame flags to remove objects marked as spurious. For fainter objects found in search #1, we created three-color images from the  $W1$  (blue),  $W2$  (green), and  $W3$  (red) coadded images, which were then inspected by eye to eliminate artifacts. Third, for all objects passing the above tests, we created finder charts showing the Digitized Sky Survey (DSS;  $B$ ,  $R$ ,  $I$ ), the Sloan Digital Sky Survey (SDSS; York et al. 2000 –  $u$ ,  $g$ ,  $r$ ,  $i$ , and  $z$ , if available), 2MASS ( $J$ ,  $H$ ,  $K_s$ ), and WISE ( $W1$ ,  $W2$ ,  $W3$ ,  $W4$ , + 3-color image made from  $W1+W2+W3$ ) images. A visual inspection of these finder charts allowed us to remove other spurious sources and

---

<sup>6</sup>Available at <http://wise2.ipac.caltech.edu/docs/release/prelim/expsup/>.

<sup>7</sup>See section IV.7.a.i of <http://wise2.ipac.caltech.edu/docs/release/prelim/expsup/>.

<sup>8</sup>It should be noted that five objects from Table 1 fall more than one sigma to the right of this line. These objects are the M dwarfs CTI 064951.4+280442 and CTI 065950.5+280228 and the L dwarfs SDSS J082030.12+103737.0, SDSS J102947.68+483412.2, and SDSS J204317.69–155103.4. Visual inspection of the WISE images for each of these shows that the  $W3$  detections for all five sources are almost certainly spurious, the photometry code having found a low-level  $W3$  “detection” at the sky location of the object. The signal-to-noise values for each of these  $W3$  detections are 3.1, 2.2, 3.1, 2.0, and 4.4, respectively. Because the  $W3$  band is sensitive to extended structure within the Milky Way as well as background variations by bright stars and the Moon, low-level  $W3$  detections should be regarded with caution.

objects clearly visible in the short wavelength optical bands, while also allowing us to check for proper motion between surveys for objects bright enough to have been detected at shorter wavelengths, such as  $J$  and  $H$  for brighter T dwarf candidates.

Example images are shown in Figure 4.1 through Figure 4.19 for our spectroscopically confirmed candidates. WISE photometry for these same sources is given in Table 2.

### 3. Follow-up Imaging Observations

#### 3.1. Ground-based Near-infrared Follow-up

Follow-up imaging observations of WISE candidates are important not only for verifying that the source has the characteristics of a brown dwarf at shorter wavelengths but also for determining how bright the object is at wavelengths observable from the ground. This latter knowledge is necessary for determining which facility to use for spectroscopic confirmation.

Ground-based near-infrared observations at  $J$  and  $H$  bands are technically the easiest to acquire. Before discussing specifics, it should be noted that the two main near-infrared filter systems being used today – the 2MASS system and the Mauna Kea Observatories Near-infrared (MKO-NIR, or just MKO) system – will yield somewhat different results for the same objects. The 2MASS bandpasses are illustrated in Figure 2 of Skrutskie et al. (2006), and the MKO filter profiles are shown in Figure 1 of Tokunaga et al. (2002). A comparison of the two filter sets is illustrated in Figure 4 of Bessell (2005). For  $J$  and  $H$  bands, the main difference between the two systems lies in the width of the  $J$ -band filter; the  $H$ -band filters are very similar. The 2MASS  $J$ -band profile extends to bluer wavelengths than does the MKO  $J$ -band profile, and the overall shapes of the two  $J$  filters are quite different, the 2MASS  $J$  filter lacking the top-hat shape that is characteristic of most filter profiles. As a result, the measured  $J$ -band magnitude of a brown dwarf, whose spectral signature is also quite complex at these same wavelengths, can be considerably different between the two systems. This is dramatically illustrated in Figure 3 of Stephens & Leggett (2004), which shows that although the  $H$ -band magnitudes are (as expected) very similar between the two systems for a wide range of brown dwarf types, the  $J$ -band magnitudes (and hence,  $J - H$  colors) can differ by as much as 0.5 mag for late-type T dwarfs. In the discussion that follows, we note the systems on which our photometry was obtained and we mark photometry from the two systems with different colors and symbols on the plots.

As Figure 5 and Figure 6 show, mid- to late-T dwarfs ( $W1 - W2 > 1.5$  mag) have relatively blue colors,  $J - H \lesssim 0.4$  mag, on the 2MASS filter system. The upper righthand panel of Figure 5 of Leggett et al. 2010 shows the trend of  $J - H$  color versus spectral type using the

MKO filter system, and there we find that  $J - H \lesssim -0.1$  mag for dwarfs  $\geq T5$ . These blue colors in both systems are a consequence of stronger methane bands and collision-induced  $H_2$  absorption at  $H$ -band compared to  $J$ -band. This color stands in contrast to the majority of other astrophysical sources, whose  $J - H$  colors are much redder than this. For example, Figure 19 of Skrutskie et al. (2006) shows the 2MASS  $J - H$  color distribution of detected sources at high Galactic latitude and confirms that most 2MASS objects have colors redder than those of mid- to late-T dwarfs. Nevertheless, there are true astrophysical sources – e.g., main sequence stars earlier than type K0 (Table 2 of Bessell & Brett 1988); certain AGNs, particularly those with  $0.7 < z < 1.1$  (Figure 2 of Kozuma & Yamaoka 2010) – that aren’t brown dwarfs and have  $J - H$  colors below 0.4 mag.

Fortunately, other colors like  $J$ -W2 and  $H$ -W2 can also be used to distinguish populations. Figure 7 and Figure 8 show these colors as a function of spectral type and demonstrate that the  $J$ -W2 color of mid- to late-T dwarfs runs from  $\sim 2.0$  mag at T5 to  $> 4.0$  mag at late-T;  $H$ -W2 color runs from  $\sim 1.5$  mag to  $\sim 5.0$  mag for the same range of types. Figure 9 and Figure 10 show the trend of  $J$ -W2 and  $H$ -W2 with W1-W2 color. The correlation is very tight for M and L dwarfs ( $W1-W2 < 0.6$  mag), but at redder W1-W2 colors, corresponding to the L/T transition and beyond, there is a much larger spread of  $J$ -W2 and  $H$ -W2 colors at a given W1-W2 color. Nonetheless, both  $J$ -W2 and  $H$ -W2 color increase dramatically beyond  $W1-W2 > 1.5$  mag ( $> T5$ ).

With our list of brown dwarf candidates in hand, we have obtained  $J$  and  $H$  observations – and in some cases,  $Y$  and  $K_s$  as well – using a variety of different facilities in both hemispheres. Details of those observations are given below, and a listing of the resultant photometry can be found in Table 3.

### 3.1.1. *Fan Mountain/FanCam*

The Fan Mountain Near-infrared Camera (FanCam) at the University of Virginia’s 31-inch telescope has a  $1024 \times 1024$ -pixel HAWAII-1 array (pixel scale of 0.51 arcsec/pix) that images an 8.7-arcminute square field of view (Kanneganti et al. 2009). Observations of eight of our candidates were obtained in 2MASS  $J$  and  $H$  bands, and for some objects  $Y$ -band observations were also acquired. Details on observing strategy and data reduction are described further in Mainzer et al. (2011).

### 3.1.2. *Magellan/PANIC*

Persson’s Auxiliary Nasmyth Infrared Camera (PANIC) at the 6.5m Magellan Baade Telescope has a  $1024 \times 1024$  HAWAII array with a plate scale of  $0''.125 \text{ pixel}^{-1}$ , resulting in a  $2 \times 2$ -arcminute field of view (Martini et al. 2004). Observations of three of our candidates were obtained in Carnegie (essentially MKO)  $J$  and  $H$  bands. A series of dithered images of short integration times was obtained in each band, as is the standard in near-infrared imaging observations.

The data were reduced using custom Interactive Data Language (IDL) routines written by one of us (M.C.C.). Each image was first corrected for non-linearity using the relation given in the PANIC Observer’s Manual<sup>9</sup>. Sky flat fields were constructed by first subtracting a median-averaged dark frame from each twilight flat frame. The dark-subtracted twilight flats were then scaled to a common flux level and then medianed. After each frame was sky subtracted and flat fielded, we corrected for optical distortions as described in the PANIC Observer’s Manual. Frames were then aligned and combined using a median average to produce the final mosaic. 2MASS stars in the field of view were used to both astrometrically calibrate the mosaic as well as determine the zero points for the images.

### 3.1.3. *Mt. Bigelow/2MASS*

The 2MASS camera on the 1.5m Kuiper Telescope on Mt. Bigelow, Arizona, has three  $256 \times 256$  NICMOS3 arrays capable of observing simultaneously in 2MASS  $J$ ,  $H$ , and  $K_s$  filters (Milligan et al. 1996). The plate scale for all three arrays is  $1''.65 \text{ pixel}^{-1}$ , resulting in a  $7 \times 7$  arcmin field of view. Images for twenty-three of our candidates were obtained using a  $3 \times 3$  box dither pattern, and to reduce the overheads associated with nodding the telescope four images were taken at each of nine dither positions. At the conclusion of each dither sequence, the telescope was offset slightly before the start of the next sequence.

The data were reduced using custom IDL routines. Flat fields in each band were constructed using on-source frames. These images were scaled to a common flux level and combined using an average, the latter process rejecting the lowest 10 and highest 20 values at each pixel location to eliminate imprinting of real objects. Each raw frame was then flat fielded with these derived flats. Sky subtraction was then accomplished in a two-step process. First, all of the coadded frames were median averaged to produce a first-order sky

---

<sup>9</sup>See <http://www.lco.cl/telescopes-information/magellan/instruments/panic/panic-online-documentation/panic-manual/panic-observers-s-manual/panic-manual>

frame. This frame was then subtracted from each of the coadded frames so that stars could be easily identified. A sky frame was then constructed for each coadded image using the five previous frames in the sequence and the next five frames in the sequence. Stars identified in the previous step were masked out before the ten frames were median averaged. The sky frame was then scaled to the same flux level as the image and subtracted. After all of the coadded frames had been sky subtracted, the frames were co-registered on the sky and averaged. 2MASS stars in the field of view were used to both astrometrically calibrate the mosaic as well as determine the zero points for the images.

#### 3.1.4. *PAIRITEL*

The Peters Automated Infrared Imaging Telescope (PAIRITEL; Bloom et al. 2006) on Mt. Hopkins, Arizona, is a 1.3m telescope equipped with three  $256 \times 256$  NICMOS3 arrays with  $2''$  pixels that cover an  $8.5 \times 8.5$  arcminute field of view simultaneously in 2MASS  $J$ ,  $H$ , and  $K_s$  filters (Milligan et al. 1996). This camera is, in fact, one of the original 2MASS cameras (Skrutskie et al. 2006) and the telescope is the original 2MASS northern facility, now roboticized for transient follow-up and other projects. Thirty-three of our candidates were observed here.

Upon acquiring a target field, the system acquires a series of 7.8 s exposures until the desired integration time (1200 s) is met. After every third exposure the telescope shifts to a position offset by about one tenth of the field of view in order to account for bad pixels on the arrays. Within hours of a night’s observations an automated data pipeline delivers Flexible Image Transport System (FITS; Hanisch et al. 2001) mosaic images of the combined stack of observations for each object in each of the three wavebands. The pipeline subtracts a background from each raw image based on the median of several images adjacent in time. The resulting individual frames are calibrated with a flat field constructed from sky observations spanning many nights. Astrometric and photometric calibrations were accomplished using observations of 2MASS-detected stars in the field of view.

#### 3.1.5. *Palomar/WIRC*

The Wide-field Infrared Camera (WIRC) at the 5m Hale Telescope at Palomar Observatory has a pixel scale of  $0''.2487 \text{ pixel}^{-1}$  and uses a  $2048 \times 2048$ -pixel HAWAII-2 array to image an 8.7-arcminute square field of view (Wilson et al. 2003). Observations of eighteen of our candidates were obtained in MKO  $J$  and  $H$  bands.

Images were reduced using a suite of IRAF<sup>10</sup> scripts and FORTRAN programs kindly provided by T. Jarrett. The images were first linearized and dark subtracted. Sky background and flat field images were created from the list of input images, and then these were subtracted from and divided into, respectively, each input image. At this stage, WIRC images still contained a significant bias not removed by the flat field. Comparison of 2MASS and WIRC photometric differences across the array showed that this flux bias had a level of  $\approx 10\%$  and the pattern was roughly the same for all filters. Using these 2MASS-WIRC differences for many fields, we created a flux bias correction image that was then applied to each of the “reduced” images. Finally, we astrometrically calibrated the images using 2MASS stars in the field. The images were then mosaicked together. This final mosaic was photometrically calibrated using 2MASS stars and a custom IDL script. Magnitudes were calculated using the zero points computed using 2MASS stars.

### 3.1.6. *Shane/Gemini*

The Gemini Infrared Imaging Camera at the 3m Shane Telescope at Lick Observatory uses two  $256 \times 256$ -pixel arrays (pixel scale of 0.70 arcsec/pix) for simultaneous observations of a  $3 \times 3$ -arcminute field of view (McLean et al. 1994) over each array. The short-wavelength channel uses a NICMOS3 HgCdTe array, and the long-wavelength channel uses an InSb array. Observations were obtained for three of our candidates and used 2MASS  $J$ ,  $H$ , and  $K_s$  filters. Observations were acquired in pairs ( $J + K_s$  or  $H + K_s$ ) so that twice as much integration time could be obtained on the InSb array at  $K_s$  as in either the  $J$  or  $H$  filter on the HgCdTe array. Observations were obtained in dithered sequences. Data reduction was handled similarly to that described for the Mt. Bigelow/2MASS data.

### 3.1.7. *SOAR/SpartanIRC*

The Spartan Infrared Camera (SpartanIRC) at the 4.1m Southern Astrophysics Research (SOAR) Telescope on Cerro Pachón, Chile, uses a mosaic of two  $2048 \times 2048$ -pixel HAWAII-2 arrays to cover either a 3-arcminute square (0.04 arcsec/pix) or 5-arcminute square (0.07 arcsec/pix) field of view (Loh et al. 2004). For seven of our candidates, we used the  $5 \times 5$ -arcminute mode and acquired observations in the MKO  $J$  and  $H$  (and for one object

---

<sup>10</sup>The Image Reduction and Analysis Facility (Tody 1986) is distributed by the National Optical Astronomy Observatory, which is operated by the Association of Universities for Research in Astronomy, Inc., under cooperative agreement with the National Science Foundation.

object,  $K$ ) filters. Observing strategy and data reductions followed the same prescription discussed in Burgasser et al. (2011).

### 3.1.8. *Keck/NIRC2*

The second-generation Near-infrared Camera (NIRC2) at the 10m W. M. Keck Observatory atop Mauna Kea, Hawai‘i, employs a  $1024 \times 1024$  Aladdin-3 array. Used with the Keck II laser guide star adaptive optics system (Wizinowich et al. 2006; van Dam et al. 2006), it can provide deep, high-resolution, imaging for our faintest targets. In the wide-field mode, the camera has a plate scale of 0.039686 arcsec/pix resulting in a field of view of  $40 \times 40$  arcsec. WISEPA J182831.08+265037.8 and WISEPC J205628.90+145953.3 are the only targets in this paper whose photometry comes solely from the NIRC2 data because they were undetected in  $J$ - and/or  $H$ -band at other facilities. The camera employs MKO  $J$  and  $H$  filters.

For WISEPA J182831.08+265037.8 we used the  $R=16$  star USNO-B 1168-0346313 (Monet et al. 2003), located  $41''$  from the target, for the tip-tilt reference star. The tip-tilt reference star for WISEPC J205628.90+145953.3 was USNO-B 1050-0583683 ( $R=13$ , separation= $13''$ ). A three-position dither pattern was used to avoid the noisy lower-left quadrant. Each position of the dither pattern consisted of a 120 s exposure; the pattern was repeated two or three times with a different offset for each repeat in order to build up deeper exposures.

The images were reduced using a custom set of IDL scripts written by one of us (C.R.G.). The raw images were first sky-subtracted using a sky frame constructed from all of the images. Next, a dome flat was used to correct for pixel-to-pixel sensitivity variations. In order to shift the reduced images to a common astrometric grid for the creation of the mosaic, we used the header keywords AOTSX and AOTSY, which record the position of the AO tip-tilt sensor stage. As the telescope is dithered, this sensor must move so that the tip-tilt star stays properly centered. Although this method of computing image offsets is more precise than using the right ascension and declination offsets in the header, it can be prone to small positional errors. To account for this, we computed the minimum of the residuals of the shifted image relative to the reference image (the first image of the stack) over a  $5 \times 5$  pixel grid centered on the AOTSX/AOTSY-computed offset. This correction was generally  $< 2$  pixels. The aligned images were then medianed to form the final mosaic.

There are typically very few, if any, 2MASS stars in the NIRC2 field of view that can be used to determine the photometric zero point. We therefore bootstrapped a photometric

zero point using faint stars in the NIRC2 images that are also present in the much wider field-of-view Palomar/WIRC images that have been calibrated using 2MASS stars. For this ensemble we computed the average difference between the calibrated WIRC magnitudes and the NIRC2 instrumental magnitudes. We used the standard deviation of the differences as the error in the photometric calibration and note that it is the dominant source of uncertainty.

### 3.1.9. CTIO-4m/NEWFIRM

The NOAO Extremely Wide Field Infrared Imager (NEWFIRM) at the 4m Victor M. Blanco Telescope on Cerro Tololo, Chile, consists of four 2048×2048 InSb arrays arranged in a 2×2 grid. With a pixel scale of 0.40 arcsec/pixel, this grid covers a total field of view of 27.6×27.6 arcmin. (Swaters et al. 2009). The only source in this paper with NEWFIRM photometry is WISEPA J1541521.66–225025.2, so the discussion that follows is specific to this set of observations.

At *J*-band, ten sets of images were obtained with integration times of 30 s and two coadds; at *H*-band ten sets with exposure times of 5 s and twelve coadds were obtained. Thus, the total integration time was 600 s in each filter, and these are on the MKO system. Because of the large field of view and the 35'' gap between the arrays, we positioned the target near the center of the North-East array, designated SN013 in the Proposal Preparation Guide<sup>11</sup>.

Photometry was performed on the mosaics produced by the NEWFIRM pipeline (Swaters et al. 2009). Although the pipeline computed a magnitude zero-point based on the photometry of 2MASS stars in the mosaic, the default aperture used was so large ( $\approx 6$  pixel radius) that WISEPA J1541521.66–225025.2 overlapped with a close neighbor. Furthermore, WISEPA J1541521.66–225025.2 was barely visible on the mosaics, meaning that a smaller aperture was warranted to increase the S/N of our measurement. We therefore re-calibrated the mosaics using an aperture of 2-pixel radius.

### 3.1.10. 2MASS and UKIDSS

Some of the WISE brown dwarf candidates were detected by 2MASS or by the United Kingdom Infrared Deep Sky Survey (UKIDSS; Lawrence et al. 2007). For 2MASS, we have

---

<sup>11</sup>[http://www.noao.edu/ets/newfirm/documents/Quick\\_Guide\\_for\\_Proposal\\_Preparation.pdf](http://www.noao.edu/ets/newfirm/documents/Quick_Guide_for_Proposal_Preparation.pdf)



searched the All-Sky Point Source Catalog and the Reject Table<sup>12</sup> and found photometry for forty-five of our sources, the other fifty-one being too faint for 2MASS detection. For UKIDSS, we searched Data Release 6 (or 5 for those mini-surveys not released in 6) and found five of our objects – three in the Large Area Survey and two in the Galactic Clusters Survey.

### 3.2. Follow-up Using Spitzer/IRAC

Some of the coldest brown dwarf candidates detected by WISE have W1-W2 color *limits* because these sources are too faint to be detected in the W1 band. Acquiring deeper images at similar bandpasses would therefore be extremely beneficial in further deciding which of the candidates are the most interesting for spectroscopic follow-up. Fortunately, the two shortest wavelength bandpasses of the Infrared Array Camera (IRAC; Fazio et al. 2004) onboard the *Spitzer* Space Telescope (Werner et al. 2004) are operating during the Warm *Spitzer* mission and can be used to provide this missing info. Although these bandpasses – at 3.6 and 4.5  $\mu\text{m}$  (aka ch1 and ch2, respectively) – are similar to the two shortest wavelength bands of WISE (see Figure 2 of Mainzer et al. 2011), they were not designed specifically for brown dwarf detection and therefore yield less extreme colors (ch1-ch2 vs. W1-W2) for objects of the same spectral type. Nonetheless, IRAC photometry in the Warm Spitzer era provides a powerful verification tool for WISE brown dwarf candidates.

Figure 11 shows the trend of ch1-ch2 color versus spectral type for early-M through late-T dwarfs taken from Patten et al. (2006), Leggett et al. (2009), and Leggett et al. (2010). As noted by these authors, there is a clear trend of increasing ch1-ch2 color with later spectral type, as expected. Figure 12 maps the ch1-ch2 color onto W1-W2 color for these same sources. Two additional plots, Figure 13 and Figure 14, show composite colors made from ground-based near-infrared and *Spitzer* follow-up and demonstrate that both *J*-ch2 and *H*-ch2 colors can serve as proxies for spectral type for objects of type mid-T and later. Plots of *H*-ch2 color versus type have been presented in earlier papers (the upper lefthand panel of Figure 6 of Leggett et al. 2010; Figure 5 of Eisenhardt et al. 2010). Even earlier, Warren et al. (2007) noted the tight correlation between *H*-ch2 color and effective temperature for later T dwarfs and suggested that the color is relatively insensitive to gravity and metallicity, which makes it a reliable indicator of  $T_{\text{eff}}$  or type (see also Burningham et al. 2008).

We have therefore obtained IRAC ch1 and ch2 photometry of many of our WISE brown dwarf candidates (Program ID=70062; J.D. Kirkpatrick, PI). Data were collected in both

---

<sup>12</sup>See <http://www.ipac.caltech.edu/2mass/releases/allsky/doc/explsup.html> for details.

channels using a 5-position, medium-scale “cycling” dither script. Single images were 30s per position, for a total on-source exposure time of 150s per channel.

Although the *Spitzer* Science Center (SSC) suggests performing photometry on custom-built mosaics from the basic calibrated data (BCD) rather than the post-BCD mosaics, we have found that the photometric differences between the two mosaics are negligible for our data sets. Therefore, photometry of our sources was measured on the post-BCD mosaics as produced by the SSC IRAC Pipeline, software version S18.18. The post-BCD mosaics have a pixel scale of  $0.6''/\text{pixel}$ , which is half of the native pixel scale. We used a 4-pixel aperture, a sky annulus of 24-40 pixels, and applied the aperture corrections listed in Table 4.7 of the IRAC Instrument Handbook<sup>13</sup> to account for our non-standard aperture size. Resulting IRAC photometry for those confirmed candidates observed so far is listed in Table 3.

#### 4. Follow-up Spectroscopic Observations

For candidates whose follow-up imaging strengthened their credibility as a bona fide brown dwarf, we obtained spectroscopic confirmation at near-infrared wavelengths. The facilities and instruments we have used, along with the data reductions employed, are discussed below.

##### 4.1. Keck/LRIS

The Low Resolution Imaging Spectrometer (LRIS, Oke et al. 1995) at the 10m W. M. Keck Observatory atop Mauna Kea, Hawai’i, uses two channels to simultaneously observe blue and red optical wavelengths. Our observational setup employed only the two  $2k \times 4k$  CCDs in the red channel. When used with the 400 lines/mm grating blazed at  $8500 \text{ \AA}$  and a  $1''$  slit, the red channel produces  $10\text{-}\text{\AA}$ -resolution spectra covering the range from 6300 to  $10100 \text{ \AA}$ . The OG570 order-blocking filter was used to eliminate second-order light. Flat-field exposures of the interior of the telescope dome were used to normalize the response of the detector, and HgNeAr arc lamps were taken after each program object to obtain the wavelength calibration. Because our targets were late-T dwarfs, for which the  $9300\text{-}\text{\AA}$  band of  $\text{H}_2\text{O}$  is the most important spectral diagnostic, observations of G0 dwarf stars near in airmass and near in time were needed to correct for telluric  $\text{H}_2\text{O}$  at these same wavelengths. Observations were typically acquired with the slit oriented to the parallactic angle to minimize

---

<sup>13</sup><http://ssc.spitzer.caltech.edu/irac/iracinstrumenthandbook>

wavelength-dependent slit losses. Once per night, a standard star from the list of Hamuy et al. (1994) was observed to provide flux calibration. The data were reduced and calibrated using standard IRAF routines as described in Kirkpatrick et al. (1999) and Kirkpatrick et al. (2006).

#### 4.2. IRTF/SpeX

SpeX, a medium-resolution spectrograph and imager at NASA’s 3m Infrared Telescope Facility (IRTF) on Mauna Kea, Hawai’i, uses a  $1024 \times 1024$  InSb array for its spectroscopic observations (Rayner et al. 2003). We used the prism mode with a  $0''.5$  wide slit to achieve a resolving power of  $R \equiv \lambda/\Delta\lambda \approx 150$  over the range  $0.8\text{--}2.5 \mu\text{m}$ . A series of 120s or 180s exposures were typically obtained at two different nod positions along the  $15''$  long slit. A0 dwarf stars at similar airmass to the target were observed near in time for telluric correction and flux calibration. Observations were typically obtained with the slit oriented to the parallactic angle to minimize slit losses and spectral slope variations due to differential atmospheric refraction. Finally, a set of exposures of internal flat field and argon arc lamps were obtained for flat fielding and wavelength calibration.

The data were reduced using Spextool (Cushing et al. 2004) the IDL-based data reduction package for SpeX. The raw images were first corrected for non-linearity, pair subtracted, and then flat fielded. For some of the fainter sources, multiple pair-subtracted images were averaged in order to facilitate tracing. The spectra were then optimally extracted (e.g., Horne 1986) and wavelength calibrated using the argon lamp exposures. Multiple spectra were then averaged and the resulting spectrum was corrected for telluric absorption and flux calibrated using observations of an A0 V star using the technique described in Vacca et al. (2003).

#### 4.3. Keck/NIRSPEC

The Near-Infrared Spectrometer (NIRSPEC, McLean et al. 1998, 2000) at the 10m W. M. Keck Observatory on Mauna Kea, Hawai’i, uses a  $1024 \times 1024$  InSb array for spectroscopy. In low-resolution mode, use of the  $42 \times 0''.38$  slit results in a resolving power of  $R \equiv \lambda/\Delta\lambda \approx 2500$ . Our brown dwarf candidates were observed in either or both of the N3 and N5 configurations (see McLean et al. 2003) that cover the portion of the *J*-band window from  $1.15$  to  $1.35 \mu\text{m}$  and the portion of the *H*-band window from  $1.5$  to  $1.8 \mu\text{m}$ .

Data were typically obtained in four or more sets of dithered pairs, with a 300-second

exposure obtained at each dither position. To measure telluric absorption and to calibrate the flux levels, A0 dwarf stars were observed near in time and airmass to the target. Other calibrations consisted of neon and argon arc lamp spectra, dark frames, and spectra of a flat-field lamp. We employed standard reductions using the REDSPEC package, as described in McLean et al. (2003).

#### 4.4. Magellan/FIRE

The Folded-port Infrared Echellette (FIRE; Simcoe et al. 2008, Simcoe et al. 2010) at the 6.5m Magellan Baade Telescope uses a  $2048 \times 2048$  HAWAII-2RG array. In its high-throughput prism mode, it covers the wavelength range from 0.8 to  $2.5 \mu\text{m}$  at a resolution ranging from  $R=500$  at  $J$ -band to  $R=300$  at  $K$ -band for a slit width of  $0''.6$ . Typically, each observation used the  $50''$ -long slit aligned to the parallactic angle, and consisted of a series of nod pairs taken with exposure times not exceeding 120s per position. The spectrograph detector was read out using the 4-amplifier mode at “high gain” (1.2 counts per  $e^-$ ) with the Fowler-8 sampling mode. We also obtained exposures of a variable voltage quartz lamp (set at 1.2 V and 2.2 V) for flat fielding purposes and neon/argon arc lamps were used for wavelength calibration. A0 dwarf stars were used for telluric and flux calibration.

Data were reduced using a modified version of Spextool. In contrast to SpeX, the spatial axis of the FIRE slit is not aligned with the columns of the detector so that the wavelength solution is not only a function of the column number but also of the row number. We therefore derived a two-dimensional wavelength solution in two steps. First, a one-dimensional wavelength solution applicable to the center of the slit was determined using the night-sky OH emission lines (Cushing et al. 2004). Second, the OH emission lines were used to map the optical distortions in the spatial and dispersion axes within each order. The 1D wavelength solution and distortion maps were then combined to assign a wavelength and spatial position to each pixel in each order.

With the wavelength calibration completed, the remainder of the reduction steps could proceed. Pairs of images taken at different positions along the slit were subtracted in order to remove the bias and dark current as well as to perform a first-order sky subtraction. The resulting pair-subtracted image was then flat fielded using a normalized flat constructed from dome flats taken at the start of each night. The spectral extraction followed the technique described in Smith et al. (2007). A set of “pseudorectangles” was defined spanning each order to map out positions of constant wavelength on the detector. These rectangles are themselves composed of pseudopixels with a width and height of  $\sim 1$  detector pixel. The pseudorectangles were then extracted using a polygon clipping algorithm (Sutherland &

Hodgman 1974), producing 1D profiles of the slit at each wavelength. Spectral extraction including residual background subtraction could then proceed in the standard way. The raw spectra were then combined and corrected for telluric absorption and flux calibrated using the observations of an A0 V star and the technique described in Vacca et al. (2003).

#### 4.5. Palomar/TSpec

The Triple Spectrograph (TSpec) at the 5m Hale Telescope at Palomar Observatory uses a  $1024 \times 2048$  HAWAII-2 array to cover simultaneously the range from 1.0 to  $2.45 \mu\text{m}$  (Herter et al. 2008). With a  $1 \times 30$ -arcsecond slit, it achieves a resolution of  $\sim 2700$ . Observations were acquired in an ABBA nod sequence with an exposure time per nod position not exceeding 300s to mitigate problems with changing OH background levels. Observations of A0 dwarf stars were taken near in time and near in airmass to the target objects and were used for telluric correction and flux calibration. Dome flats were taken to calibrate the pixel-to-pixel response. Data reduction is identical to that discussed above for FIRE because Spextool required the same changes for TSpec reductions as it did for FIRE reductions.

#### 4.6. SOAR/OSIRIS

The Ohio State Infrared Imager/Spectrometer (OSIRIS) mounted at the 4.1m Southern Astrophysical Research Telescope (SOAR) located at Cerro Pachón, Chile, uses a  $1024 \times 1024$  HgCdTe array. The  $1''0$ -wide slit yields a resolving power of  $R \approx 1400$  across the 1.18-2.35  $\mu\text{m}$  wavelength range in three spectral orders. Short exposures (180s) were taken at six or seven positions noddled along the  $24''$ -long slit. A0 dwarf stars were observed for telluric correction and flux calibration. Wavelength calibration was based on the OH airglow lines. The data were reduced using a modified version of the Spextool data reduction package. (See § 4.2 for a description of Spextool.) The three spectral orders were then merged into a single spectrum covering the entire wavelength range.

#### 4.7. HST/WFC3

The Wide Field Camera 3 (WFC3) onboard the *Hubble* Space Telescope employs a  $1024 \times 1024$  HgCdTe detector with a plate scale of  $0''.13 \text{ pixel}^{-1}$  to image a field of view of  $123 \times 126$  arcseconds. We used the G141 grism to acquire slitless spectroscopy over the 1.1-1.7  $\mu\text{m}$  range for faint targets not observable from ground-based facilities (Program 12330,

PI Kirkpatrick). The resulting resolving power,  $R \approx 130$ , is ideal for the broad characterization of faint sources. Three spectra – those of WISEPC J145018.40+553421.4, WISEPA J173835.53+273258.9, and WISEPA J182831.08+265037.8 – were obtained with this setup. For each target, we first obtained four direct images through the F140W filter in MULTI-ACCUM mode using the SPARS25 sampling sequence. The telescope was offset slightly between each exposure. We then obtained four dispersed images with the G141 grism using MUTLIACCUM mode and a SPARS50 sequence. These dispersed images were acquired at the same positions/dithers as used in the direct images.

Bias levels and dark current were first subtracted from the data images using version 2.3 of the CALWFC3 pipeline. CALWFC3 also flat fields the direct images, but the grism images are flat fielded during the extraction process described below. Spectra were then extracted using the aXe software (Kümmel et al. 2009). Because aXe requires knowledge of the position and brightness of the targets in the field of view, we combined the four direct images using MULTIDRIZZLE (Koekemoer et al. 2002) and the latest Instrument Distortion Coefficient Table (IDCTAB). SExtractor (Bertin & Arnouts 1996) was then used to produce a catalog of objects in the field. For each cataloged object, two-dimensional subimages centered on the first-order spectra of each object were combined using AXEDRIZZLE to produce a final spectral image. These subimages were used to extract flux-calibrated spectra. Additional details on the data reduction process are discussed in Cushing et al. (accepted).

## 5. Analysis

### 5.1. Deriving Spectral Types

The list of spectroscopically confirmed WISE brown dwarfs is given in Table 4. Abbreviated source names<sup>14</sup> are shown in column 1; optical spectral types are shown in column 2; near-infrared types are shown in column 3; and the source of the spectrum, integration time, telluric corrector star (for ground-based observations), and observation date are shown in columns 4 through 7. The optical and near-infrared classifications of these sources are discussed further below.

---

<sup>14</sup>Throughout the rest of the paper, we will abbreviate WISE source names to the form “WISE hhmm±ddmm”. Full designations can be found in Table 2.

### 5.1.1. Optical Spectral Types

Keck/LRIS spectra were obtained for seven of our candidates. Reduced spectra from 8000 to 10000 Å are shown in Figure 15, all of which have been corrected for telluric absorption over the regions 6867–7000 Å (the Fraunhofer B band, caused by O<sub>2</sub> absorption), 7594–7685 Å (the Fraunhofer A band, again caused by O<sub>2</sub>), and 7186–7273, 8162–8282, and ~8950–9650 Å (all caused by H<sub>2</sub>O absorption). These spectra show the hallmarks of T dwarf optical spectra: strong H<sub>2</sub>O absorption with a bandhead at 9250 Å, along with Cs I absorption at 8521 and 8943 Å in the earlier objects and CH<sub>4</sub> absorption between 8800 and 9200 Å in the later objects.

By-eye comparisons to the T dwarf optical spectral standards of Burgasser et al. (2003) show that these spectra range in type from T<sub>o</sub>5 for WISE 1841+7000 to later than T<sub>o</sub>8 for WISE 1741+2553. (The “o” subscript is used to denote spectral types assigned based on optical spectra.) This latter spectrum is unusual in that it has stronger 8800–9200 Å CH<sub>4</sub>, stronger 9250–9400 Å H<sub>2</sub>O bands of the 3( $\nu_1, \nu_3$ ) transition, and stronger 9450–9800 Å H<sub>2</sub>O bands of the 2( $\nu_1, \nu_3$ ) + 2( $\nu_2$ ) transition than the latest T dwarf optical standard, the T<sub>o</sub>8 dwarf 2MASS J04151954–0935066 (Burgasser et al. 2003). We therefore propose that WISE 1741+2553 be the spectral standard for a newly adopted T<sub>o</sub>9 spectral class. Figure 16 illustrates the entire sequence of T dwarf optical standards from Burgasser et al. (2003) appended with the proposed T<sub>o</sub>0 standard SDSSp J083717.22–000018.3 from Kirkpatrick (2008) and this newly proposed T<sub>o</sub>9 standard.

Further evidence in support of a new optical standard is shown in Figure 17. Shown here is a comparison of the spectrum of WISE 1741+2553 with our LRIS spectrum of the bright, late-T dwarf UGPS J072227.51–054031.2, which Cushing et al. (accepted) have proposed as the infrared spectral standard for type T9. As our comparison shows, the CH<sub>4</sub> and H<sub>2</sub>O depths are very similar between these two objects and both are distinctly different from the T<sub>o</sub>8 standard. Thus, identifying WISE 1741+2553 as the new, T<sub>o</sub>9 anchor point would help link the optical and near-infrared sequences, especially since WISE 1741+2553 is also classified as a T9 on the near-infrared scheme. See further discussion in the Appendix.

### 5.1.2. Near-infrared Spectral Types

All of the confirmed brown dwarfs listed in Table 4 have near-infrared follow-up spectra. These spectra were classified using the the near-infrared M and L sequences of Kirkpatrick et al. (2010) and the near-infrared T0-to-T8 dwarf sequence of Burgasser et al. (2006). Cushing et al. (accepted) have extended classifications to T9 and Y0 and have reclassified previously

discovered  $>T8$  dwarfs from the literature on this system. This extension of the classification system uses UGPS 0722–0540 as the near-infrared T9 standard and WISE 1738+2732 as the Y0 standard.

Assignment of spectral types was done by overplotting spectra of these standards onto the candidate spectra and determining by-eye which standard provided the best match. In some cases two adjacent standards, such as T7 and T8, provided an equally good match, so the candidate spectrum was assigned an intermediate type, in this case, of T7.5. For L dwarfs, the comparison was done at  $J$ -band and, following the prescription discussed in Kirkpatrick et al. (2010), any anomalies at  $H$ - and  $K$ -bands were noted. Spectra that did not match any of the standards well are marked with a “pec” suffix to indicate that they are peculiar. As a further example, an object that best fit the L9 spectral standard at  $J$ -band but failed to provide a good match to the L9 standard at longer wavelengths because it was considerably redder than the standard was assigned a type of “L9 pec (red).” See Kirkpatrick et al. (2010) for examples of similar classifications.

In Figure 18 through Figure 25, we show the near-infrared spectra for each of our sources. Because of the narrow wavelength ranges covered by the Keck/NIRSPEC and SOAR/OSIRIS spectra, those data are plotted separately in Figure 26 and Figure 27.

### 5.1.3. Discussion

Near-infrared spectral types (and optical spectral types, for those with Keck/LRIS spectra) are listed in Table 4 for all WISE brown dwarf discoveries. For objects with near-infrared spectral types of T0 or later, Figure 28 shows the number of newly discovered objects per spectral type bin compared to the number of objects previously published. Whereas there were 16 objects known previously with types of T8 or later (Burgasser et al. 2002, Tinney et al. 2005, Looper et al. 2007, Warren et al. 2007, Delorme et al. 2008, Burningham et al. 2008, Burningham et al. 2009, Burningham et al. 2010b, Goldman et al. 2010, Lucas et al. 2010, Delorme et al. 2010, Burningham et al. 2011b), the tally now stands at 58 once our objects are added. WISE has already identified seventeen new objects with types equal to or later than the T9 UGPS J072227.51–054031.2, the previous record holder for latest measured spectral type, and six of these belong to the Y dwarf class (Cushing et al., accepted).

Figure 1 through Figure 3 and Figure 5 through Figure 14, discussed previously, show the locations of these newly discovered WISE brown dwarfs (black symbols) in color space. The T9, T9.5, and early-Y dwarfs continue the trend toward redder W1-W2, ch1-ch2,  $J$ -W2,  $H$ -W2,  $J$ -ch2, and  $H$ -ch2 colors, with the reddest object being the  $>Y0$  dwarf WISE



1828+2650 ( $J-W2 = 9.39 \pm 0.35$  mag;  $J$  on the MKO filter system). The blueward trend in  $J-H$  color seen for later T dwarfs, however, begins to reverse near a spectral type of Y0. In particular, the  $J-H$  color of WISE 1828+1650 is dramatically redder ( $J-H = 0.72 \pm 0.42$  mag; MKO filter system) than any of the late-T or Y0 dwarfs, the latter of which show a large scatter in  $J-H$  colors themselves. Cushing et al. (accepted) explore the trend of  $J-H$  colors in more detail and show that the synthetic photometry derived from our observed spectra generally agree with photometry measured from direct imaging. Given the large spread in  $J-H$  color observed for the six Y dwarfs already identified,  $JHK_s$  colors alone cannot be used to confirm or deny objects as cold as Y dwarfs.

## 5.2. Distances and Proper Motions

Distances to the new WISE brown dwarf discoveries can be estimated based on their W2 magnitudes and measured spectral types. First, however, the relation between absolute W2 magnitude and spectral type needs to be established using objects with measured trigonometric parallaxes and WISE W2 detections. Figure 29 shows the trend of absolute W2 magnitude as a function of near-infrared spectral type for previously published objects whose measured parallaxes are at least three times the measurement error (Table 5). A third-order least squares relation, weighted by the errors on the  $M_{W2}$  values, is shown by the black curve in Figure 29. For this fit, objects known to be binary (red points) have been omitted. The resulting relation is

$$M_{W2} = 9.692 + 0.3602( Type ) - 0.02660( Type )^2 + 0.001020( Type )^3$$

where  $Type$  is the near-infrared spectral type on the system where L0=0, L5=5, T0=10, T5=15, and Y0=20.

Using this relation, we have estimated distances to our WISE discoveries. These are given in column 2 of Table 6. (The distance to the lone M dwarf, WISE 0106+1518, was estimated using 2MASS magnitudes and the near-infrared absolute magnitudes listed in Table 3 of Kirkpatrick & McCarthy 1994.) These distance estimates for the late-T dwarfs and Y dwarfs are shown graphically in Figure 30. Also shown in the figure are previously published late-T dwarfs from other surveys. WISE has sufficient sensitivity to detect the latest T dwarfs out to 15 to 20 pc and because of its all-sky coverage can complete the census of the Solar Neighborhood for these objects. As the figure shows, twelve of our objects have estimated distances placing them within 10 pc of the Sun, and two of these have estimates placing them within 5 pc. It should also be noted that the fitted relation

shown in Figure 29 may lead to overestimated distances for objects at the latest types because the relation falls above all four of the previously published T8.5 and T9 dwarfs on that plot. Furthermore, the extrapolation of this relation to even later Y dwarf types may lead to even more discrepant distance overestimates, as discussed further in the caption to Figure 29. Measuring trigonometric parallaxes for more of these latest T dwarfs and early Y dwarfs will be an important, early step in characterizing the physical nature of these objects.

Because these objects should all lie very close to the Sun, their observed parallaxes will be large. Thanks to its survey strategy, WISE performed its two passes of the sky with observations always near  $90^\circ$  solar elongation, thus capitalizing on the maximum parallactic angle at both epochs. (For objects observed during the final  $\sim 2$  weeks of WISE operations, three epochs of WISE data are available.) Objects will, of course, also show displacements due to proper motion, so observations at other epochs and/or from other surveys are necessary to disentangle the two effects. Hence, ancillary astrometry from 2MASS and SDSS and our own follow-up observations from the ground and from space (*Spitzer* and *HST*) are invaluable. Currently available astrometric data points<sup>15</sup> are shown in columns 3 through 8 of Table 6.

It should be noted here that positions of objects in the WISE preliminary data release may be offset from their true positions by many times the quoted positional uncertainty. Approximately 20% of the sources fainter than  $W1 \approx 14.5$  mag in the Preliminary Release Source Catalog suffer from a pipeline coding error that biases the reported position by  $\sim 0.2$ – $1.0$  arcsec in the declination direction while an increasingly smaller fraction of the sources suffer this effect to magnitudes as bright as  $W1 \approx 13.0$  mag. The Cautionary Notes section of the WISE Preliminary Release Explanatory Supplement describes the origin and nature of this effect in detail. For this paper, we have rerun the WISE images for our sources through a version of the WISE pipeline that eliminates this source of systematic error, and we list those remeasured positions in Table 6. This version of the pipeline is essentially the same one used to process data for the WISE Final Data Release.

Astrometric fits were made to the multiple observations of each source. These fits solved for five parameters: initial (time =  $t_i$ ) positional offsets of  $\Delta\alpha$  and  $\Delta\delta$  in Right Ascension ( $\alpha$ ) and in Declination ( $\delta$ ), the Right Ascension component of proper motion ( $\mu_\alpha = (\cos \delta) d\alpha/dt$ ), the Declination component of proper motion ( $\mu_\delta = d\delta/dt$ ), and the parallax ( $\pi_{trig}$ ). For all but four sources, the data were not sufficient to find an accurate distance, so the distance was forced to equal the spectrophotometric estimate, and the fit only solved for the first four

---

<sup>15</sup>Future papers will include astrometry taken from our various ground-based imaging campaigns, once data over a longer time baseline have been acquired.

parameters; the four sources with a preliminary parallax measurement are listed in Table 7 and are discussed individually in the Appendix. The equations used are

$$\cos \delta_1(\alpha_i - \alpha_1) = \Delta\alpha + \mu_\alpha(t_i - t_1) + \pi_{trig} \vec{R}_i \cdot \hat{W}, \text{ and}$$

$$\delta_i - \delta_1 = \Delta\delta + \mu_\delta(t_i - t_1) - \pi_{trig} \vec{R}_i \cdot \hat{N}.$$

Subscript  $i$  refers to the individual astrometric measurements, where  $t_i$  is the observation time in years, and  $R_i$  is the vector position of the observer relative to the Sun in celestial coordinates and astronomical units.  $\hat{N}$  and  $\hat{W}$  are unit vectors pointing North and West from the position of the source.  $R_i$  is the position of the Earth for 2MASS, SDSS, WISE, and *HST* observations; for *Spitzer* observations,  $R_i$  is the position of the spacecraft. The observed positional difference on the left hand side is in arcseconds, the parameters  $\Delta\alpha$  and  $\Delta\delta$  are in arcseconds, the proper motion  $\mu_\alpha$  and  $\mu_\delta$  are in arcseconds/year, and the parallax  $\pi_{trig}$  is in arcseconds.

These equations are solved using standard weighted least-squares techniques, which also provide the uncertainties in the parameters. These uncertainties come from propagating the uncertainties in the input. The  $\chi^2$  and number of degrees of freedom are also given and can be used to assess the quality of the fit. The resulting proper motions in RA and Dec are listed in columns 9 and 10 of Table 6. For motions with a significance of  $> 3\sigma$ , the total proper motion is listed in column 11 along with the tangential velocity in column 12.

### 5.3. Space Density of late-T dwarfs

The brown dwarf discoveries presented here represent only a fraction of the brown dwarf candidates identified so far from WISE data. WISE coadded data are not available across the entire sky, and many of those coadds do not reach the full survey depth. Nonetheless, we can use these preliminary results to assess our progress toward completing the tally of cold brown dwarfs in the Solar Neighborhood and gauging the functional form of the mass function for these objects by using lower limits to their space densities.

Our goal is to complete an all-sky census of objects out to a specified maximum distance for each spectral subtype of T6 or later. Table 8 divides our discoveries into six spectral type bins (column 1) from T6 through  $>Y0$ . The approximate range in effective temperature is given for each bin in column 2. These temperature bins are assigned as follows. We took the values of  $T_{eff}$  for T dwarfs of type T6 and later as computed by Warren et al.

(2007), Delorme et al. (2008), Burningham et al. (2008), Burgasser et al. (2010b), Lucas et al. (2010), Burgasser et al. (2011), Burningham et al. (2011), Burningham et al. (2011b), Bochanski et al. (submitted), and Cushing et al. (accepted) or compiled by Kirkpatrick (2005). Then, when necessary, we re-assigned spectral types to these objects so that they matched the near-infrared spectral classification scheme of Burgasser et al. (2006) or its extension beyond T8 by Cushing et al. (accepted). We then examined the distribution of temperature within each integral spectral type bin and found that a 150K width for each bin was enough to encompass the  $T_{eff}$  values for most of the objects. The final assignments are given in column 2 of Table 8.

As shown in Figure 30, the depth of our current search translates to different distances for each bin. In the spirit of determining the space density using a well defined census of the Solar Neighborhood, we limit our sample to those objects falling within 20 pc of the Sun even if WISE can sample that spectral type to larger distances. Only in the last three bins – the T9-T9.5 bin and the Y dwarf bins – is WISE incomplete at this distance, so those bins are limited to volumes with smaller radii. These values, called  $d_{max}$ , are listed in column 3.

Next, the number of objects per spectral type bin lying closer than the value of  $d_{max}$  is tabulated for previously published objects (column 4), for our new WISE discoveries (column 5), and in total (column 6). Distances are determined using trigonometric parallaxes, if available, or spectrophotometric estimates if no parallax has been measured. The resulting space density in each bin is given in column 7.

This simple calculation of the space densities can be overestimated for the following reasons:

(1) Spectrophotometric distance estimates have an inherent bias. The absolute magnitude versus spectral type relation is based on parallaxes, and those parallax measurements lead to a bias in estimated distances because a parallax value of  $\pi_{trig} \pm \sigma$  is more likely to represent an object further away ( $\pi_{trig} - \sigma$ ) than an object closer ( $\pi_{trig} + \sigma$ ) because the volume of space between parallax values of  $\pi_{trig}$  and  $\pi_{trig} - \sigma$  is larger than that sampled between parallax values of  $\pi_{trig}$  and  $\pi_{trig} + \sigma$ . Thus, the observed values of  $\pi_{trig}$  are larger than the true values and the measured absolute values will be systematically too large. A correction can be applied that depends only on the value of  $\sigma/\pi_{trig}$  (see Table 1 of Lutz & Kelker 1973). Most of the parallaxes in Table 5 have  $\sigma/\pi_{trig}$  values of less than 5% where the correction to the absolute magnitude is  $\leq 0.02$  mag, and those with larger errors have already been downweighted in our fit. We therefore conclude that the Lutz-Kelker effect is negligible here.

(2) Both the Malmquist bias and the Eddington bias can be largely accounted for by limiting

the sample over which we derive our space densities. Malmquist bias (Malmquist 1920), in which more luminous objects can preferentially bias statistics in a magnitude limited sample, can be eliminated by calculating space densities in narrow spectral type bins in which all objects have the same (or nearly the same) intrinsic luminosity. The Eddington bias (Eddington 1913; Eddington 1940), in which random errors will bias magnitude measures to brighter values due to the fact that there are more objects in the more distant (fainter) population than in the closer (brighter) one, can be reduced by operating at magnitudes where the random errors are still small. By using the brighter and better measured  $W2$  values to estimate distances, we can reduce the effects of Eddington bias on our derived densities. (For further discussion, see also Teerikorpi 2004.)

(3) Unresolved binarity will cause distances to be underestimated. This may cause a more distant object to appear closer than it really is and falsely inflate the space density. Empirical data presented earlier can be used to estimate this degree of binary contamination. Figure 29 shows a well-defined binary sequence (red) overlying the sequence of single objects on the  $M_{W2}$  versus spectral type diagram. If we compute the ratio of known binaries to total objects between L0 and T4, we find that 12/35, or 34%, are binary. (See also section 7.4 of Burgasser et al. 2006 for an in-depth discussion of intrinsic binarity, which varies from  $\sim 20\%$  at early-L to  $\sim 42\%$  at the L/T transition.) While this is a sizable percentage, it does not mean that all of the unresolved binaries fall outside of the sample considered. Some small fraction will still be contained within the distance limit and will have been undercounted by a factor of two. Nonetheless, binarity is likely the largest contributor to inflating density estimates.

On the other hand, other biases discussed below lead to an underestimate in the space densities. These effects are believed to overwhelm the effects detailed above, and hence our simple space density calculations, although preliminary, can be considered as lower limits to the true densities:

(1) Although WISE has taken data covering the entire sky at multiple epochs, the available coadded data cover less than 75% of the entire sky. Also none of the sky has been coadded to its full depth using all available frames and the detection threshold for first-pass processing was set higher, in units of signal-to-noise ratio, than it will be for final processing. The latter points are particularly important as they will, in the future, enable more robust colors or color limits for potential Y dwarf candidates. Moreover, we have followed up less than 50% of the brown dwarf candidates already culled from sections of the sky for which we have access. Thus, we believe that our current space density estimates are gross underestimates.

(2) Except for 2MASS, other surveys providing data in column 4 of Table 8 do not have all-sky coverage and can only provide limited help in completing this nearby sample. Moreover, none of the current or planned ground-based surveys canvassing the sky for brown dwarfs

can reach sizable populations of the coldest objects because Y dwarfs are intrinsically dim at ground-observable wavelengths. This is highlighted in Figure 31, which shows the absolute  $H$ -band magnitude as a function of spectral type. Note that the Y0 dwarf WISE 1541–2250 has  $M_H = 23.7 \pm 0.9$  mag; its absolute magnitude is  $M_J = 23.9 \pm 0.8$  mag and it is presumably even fainter than this shortward of  $J$  band. WISE operates at wavelengths where these objects are their brightest – five thousand times brighter at W2 than at  $J$  and  $H$  bands, in the case of WISE 1828+2650 – so it is the only survey capable of detecting the coldest brown dwarfs in significant numbers.

(3) As mentioned earlier, the  $M_{W2}$  vs. spectral type relation of Figure 29 likely overpredicts distances to dwarfs of type  $\geq T9$ . This means that our surveyed volume may be overestimated, leading to an underestimate of the space density.

(4) Despite the all-sky coverage of WISE, the galactic plane will restrict our ability to probe to the same depths as other parts of the sky due to higher backgrounds and confusion. This loss of coverage is not currently accounted for in our density estimates.

We have checked the distance distribution of objects in each spectral type bin by performing the  $V/V_{max}$  test (column 8 of Table 8). This test was first proposed by Schmidt (1968) to check the uniformity of a distribution of objects in space. The quantity  $V$  is the volume of space interior to object  $i$  at distance  $d_i$ , and  $V_{max}$  is the full volume of space contained within the distance limit,  $d_{max}$ , of the sample. For a uniform sample, the average value,  $\langle V/V_{max} \rangle$ , should be 0.5 because half of the sample should lie in the nearer half of the volume and the rest should lie in the farther half. If this number is not near 0.5, then the sample is either non-isotropic or incomplete. For our sample we find that the T dwarf bins have  $\langle V/V_{max} \rangle$  values considerably less than 0.5. This points to incompleteness in the sample – our low  $\langle V/V_{max} \rangle$  values are almost certainly a consequence of the fact that the brighter (closer) candidates tend to be followed up first. This gives further credence to the assertion that our number densities are lower limits only. For the Y dwarf bins, however, the values of  $\langle V/V_{max} \rangle$  are above 0.5, which is further suggestive that our assumed distances to these objects are overestimates.

Figure 32 shows these preliminary results (column 9 of Table 8) relative to measurements made by other surveys and relative to predictions based on different forms of the underlying mass function. Previous results by Metchev et al. (2008), Burningham et al. (2010b), and Reyl   et al. (2010) are shown by the open symbols and, with the possible exception of the Burningham et al. (2010b) point, support values of  $\alpha$  of zero or greater, where the functional form is given as  $dN/dM \propto M^{-\alpha}$ . Our incomplete, volume-limited sample so far fails to put tighter constraints on the mass function at warmer temperatures than previously published work, but the preliminary lower limit to the Y0 space density already rules out the  $\alpha = -1.0$

model and may soon, with additional Y0 discoveries, be able to distinguish between the  $\alpha = 0.0$  and  $\alpha = +1.0$  models. Results for the early-Y dwarfs already suggest that the low-mass cutoff of star formation must be below  $10 M_{Jup}$  if  $\alpha \leq 0$ . This result is in accordance with findings in young star formation regions (e.g., Luhman et al. 2000, Muench et al. 2002, Lucas et al. 2006, Luhman 2007), but the derived masses for those objects should be considered cautiously, as discussed in Baraffe et al. (2003), because models with ages of  $\sim 1$  Myr or younger are highly sensitive to untested assumptions about initial conditions. Using models of older ages is far less sensitive to these assumptions, so field brown dwarfs provide a better check of star formation’s low-mass cutoff. Model fits by Cushing et al. (accepted) suggest that our Y dwarf discoveries have masses as high as  $30 M_{Jup}$  or as low as  $3 M_{Jup}$  or less, which agrees roughly with the mass values inferred from Figure 32.

## 6. Conclusions

This paper represents the culmination of a year’s worth of effort following up the first batch of brown dwarf candidates identified by WISE. There are many hundreds more candidates still being scrutinized, and there are still areas of sky not yet searched. It is therefore clear that these first hundred brown dwarf discoveries are harbingers of a much larger trove of brown dwarfs yet to be uncovered by WISE. Not only is the WISE data archive uniquely suited to finding even colder objects than the current batch of early-Y dwarfs, the all-sky and multi-epoch nature of the mission will enable many other brown dwarf studies – the search for the lowest mass objects in nearby moving groups, hunting for low-metallicity objects via their high proper motions, etc. – that are well beyond the scope of the photometric search presented here.

## 7. Acknowledgments

This publication makes use of data products from the Wide-field Infrared Survey Explorer, which is a joint project of the University of California, Los Angeles, and the Jet Propulsion Laboratory/California Institute of Technology, funded by the National Aeronautics and Space Administration. We acknowledge fruitful discussions with Tim Conrow, Roc Cutri, and Frank Masci, and acknowledge assistance with Magellan/FIRE observations by Emily Bowsher. This publication also makes use of data products from 2MASS, SDSS, and UKIDSS. 2MASS is a joint project of the University of Massachusetts and the Infrared Processing and Analysis Center/California Institute of Technology, funded by the National Aeronautics and Space Administration and the National Science Foundation. SDSS is funded

by the Alfred P. Sloan Foundation, the Participating Institutions, the National Science Foundation, the U.S. Department of Energy, the National Aeronautics and Space Administration, the Japanese Monbukagakusho, the Max Planck Society, and the Higher Education Funding Council for England. UKIDSS uses the Wide Field Camera at the United Kingdom Infrared Telescope atop Mauna Kea, Hawai'i. We are grateful for the efforts of the instrument, calibration, and pipeline teams that have made the UKIDSS data possible. We acknowledge use of the DSS, which were produced at the Space Telescope Science Institute under U.S. Government grant NAG W-2166. The images of these surveys are based on photographic data obtained using the Oschin Schmidt Telescope on Palomar Mountain and the UK Schmidt Telescope. This research has made use of the NASA/IPAC Infrared Science Archive (IRSA), which is operated by the Jet Propulsion Laboratory, California Institute of Technology, under contract with the National Aeronautics and Space Administration. Our research has benefited from the M, L, and T dwarf compendium housed at DwarfArchives.org, whose server was funded by a NASA Small Research Grant, administered by the American Astronomical Society. We are also indebted to the SIMBAD database, operated at CDS, Strasbourg, France. This work is based in part on observations made with the *Spitzer* Space Telescope, which is operated by the Jet Propulsion Laboratory, California Institute of Technology, under a contract with NASA. Support for this work was provided by NASA through an award issued to program 70062 by JPL/Caltech. This work is also based in part on observations made with the NASA/ESA *Hubble* Space Telescope, obtained at the Space Telescope Science Institute, which is operated by the Association of Universities for Research in Astronomy, Inc., under NASA contract NAS 5-26555. These observations are associated with program #12330. Support for program #12330 was provided by NASA through a grant from the Space Telescope Science Institute. Some of the spectroscopic data presented herein were obtained at the W.M. Keck Observatory, which is operated as a scientific partnership among the California Institute of Technology, the University of California and the National Aeronautics and Space Administration. The Observatory was made possible by the generous financial support of the W.M. Keck Foundation. In acknowledgement of our observing time at Keck and the IRTF, we further wish to recognize the very significant cultural role and reverence that the summit of Mauna Kea has always had within the indigenous Hawai'ian community. We are most fortunate to have the opportunity to conduct observations from this mountain. We acknowledge use of PAIRITEL, which is operated by the Smithsonian Astrophysical Observatory (SAO) and was made possible by a grant from the Harvard University Milton Fund, the camera loaned from the University of Virginia, and the continued support of the SAO and UC Berkeley. The PAIRITEL project is supported by NASA Grant NNG06GH50G. This paper also includes data gathered with the 6.5 m Magellan Telescopes located at Las Campanas Observatory, Chile.



## Appendix: Notes on Special Objects

Notes are given below for objects with unusual spectra, spectrophotometric distance estimates placing them within 10 parsecs of the Sun, spectral types later than T9, or possible companionship with a nearby object previously cataloged. In the sections below, the spectra of objects are assumed to be normal unless peculiarities are specifically mentioned.

### A. WISEPC J003119.76–384036.4 ( $J=14.1$ mag, $W2=12.0$ mag)

The  $J$ -band spectrum of this object, which was earlier cataloged as SIPS J0031–3840 and identified to be nearby star via its high proper motion by Deacon et al. (2005), is a good match to the spectrum of the L2 standard (Figure A1), but the spectrum is much bluer than the standard at  $H$  and  $K$  bands. Because this source does not exhibit other telltale signs of low metallicity, such as strong hydride bands, we classify it as an “L2 pec (blue)”. Martín et al. (2010) give an optical spectral type of L2.5 and do not note any peculiarities that might be attributable to low metallicity, either. Its near-infrared spectral morphology and discrepancy relative to its nearest standard is most similar to the “L1 pec (sl. blue)” object 2MASS J14403186–1303263 shown in Figure 32 of Kirkpatrick et al. (2010). Furthermore, this object has a larger  $W1$ - $W2$  color than a typical L2 (see Figure 1) and a bluer  $J-H$  color (see Figure 5). As discussed in Kirkpatrick et al. (2010), the physical interpretation of these “blue L dwarfs” is not fully known and may differ from object to object. Some blue L dwarfs are blue, for example, because they are composite L + T dwarf binaries (e.g., Burgasser 2007). Model fitting suggests that others have thin cloud decks and/or large grains in their atmosphere, though neither seems to be directly attributable to gravity or metallicity effects (Burgasser et al. 2008). Kinematic analysis by Faherty et al. (2009) has shown that the blue L dwarfs have kinematics older than the field L dwarf population, but not nearly as old as that of low-metallicity M dwarfs. It is possible that some of the blue L dwarfs may be slightly metal poor, and that even a subtle lowering of the metal abundance in these objects may result in the directly measurable effects on the spectral energy distribution seen here.

### B. WISEPC J010637.07+151852.8 ( $J=14.4$ mag, $W2=12.7$ mag)

Despite the fact that the spectrum of this object matches very well to the  $J$ -band spectrum of the M8 standard, the  $H$ -band spectrum is more peaked than that seen in a normal M8, with the  $H_2O$  bands on either side of the  $H$  peak being stronger than in the standard (Figure A2). This object, which we classify as “M8 pec”, is similar to the peculiar

late-M dwarf 2MASS J18284076+1229207 shown in Figure 38 of Kirkpatrick et al. (2010). The cause of the peculiarity is not known, but appears not to be due to low gravity, as there are no peculiarities in the strength of the FeH bands between 0.9 and 1.3  $\mu\text{m}$  when compared to the M8 standard. (See, for example, near-IR spectra of low-gravity late-M dwarfs in Figure 14 of Kirkpatrick et al. 2010.) This object also has a larger W1-W2 color than a typical M8 (see Figure 1) and a bluer  $J - H$  color (see Figure 5). Curiously, this object has a sizable motion –  $\mu = 0.412 \pm 0.006$  arcsec/yr – and a tangential velocity of  $85.5 \pm 1.3$  km/s, suggesting that it may belong to an old population. The peculiar spectroscopic features may be caused in part by a slightly subsolar metallicity. Deacon et al. (2009) also identified this object as the high motion source ULAS2MASS J0106+1518, and their proper motion determination ( $\mu = 0.407$  arcsec/yr) agrees with the one we derive here.

### C. WISEPC J014807.25–720258.7 ( $J=19.0$ mag, $W2=14.6$ mag)

The near-infrared spectrum of this object, discussed in Cushing et al. (accepted), is distinctly later in type than the T9 near-infrared standard, UGPS J072227.51–054031.2, and is therefore classified as T9.5. Our spectrophotometric distance places it at 12.1 pc (Table 6). This is the only one of our  $\geq T9.5$  discoveries not detected in W3 and along with WISE 1738+2732 is one of only two  $\geq T9.5$  dwarfs detected in W1 (Table 2).

### D. WISEPA J020625.26+264023.6 ( $J=16.5$ mag, $W2=12.8$ mag)

The  $J$ -band spectrum of this object closely matches that of the L9 spectral standard, but the  $H$ - and  $K$ -band portions are much redder than those of the standard L9 (Figure A3). This extremely red color is supported by independent photometry, namely  $J - K_s = 2.007 \pm 0.137$  mag, from the 2MASS All-Sky Point Source Catalog. This color is somewhat redder than the mean  $J - K_s$  color,  $\sim 1.78$  mag, of very late L’s (Figure 14 of Kirkpatrick 2008). Because of its spectral peculiarity, we classify this object as “L9 pec (red)”, and add it to the growing list of L dwarfs that appear red for reasons not obviously attributable to low gravity (see Table 6 of Kirkpatrick et al. 2010). The underlying physical cause for these “red L dwarfs” is not known, although two have been studied in detail by Looper et al. (2008). Using the small sample of red L dwarfs then known, Kirkpatrick et al. (2010) found that these objects, unlike young, low-gravity L dwarfs that are also redder than spectral standards of the same type, appear to have older kinematics than that of the field L dwarf population.

**E. WISEPA J025409.45+022359.1 ( $J=15.9$  mag,  $W2=12.7$  mag)**

This object is a nearby T8 dwarf at a spectrophotometric distance of  $d=6.9$  pc. Our astrometry (Table 6) over a 10.4yr baseline indicates a high motion of  $\mu = 2.546 \pm 0.046$  arcsec/yr and a large tangential velocity of  $83.3 \pm 1.5$  km/s. Our preliminary trigonometric parallax measurement (Table 7) places this object at  $6.1^{+2.3}_{-1.4}$  pc, in excellent agreement with the spectrophotometric estimate.

**F. WISEPA J031325.96+780744.2 ( $J=17.7$  mag,  $W2=13.2$  mag)**

This T8.5 dwarf has a spectrophotometric distance estimate of only 8.1 pc.

**G. WISEPA J041022.71+150248.5 ( $J=19.3$  mag,  $W2=14.2$  mag)**

The near-infrared spectrum of this object, discussed in Cushing et al. (accepted), is classified as Y0. Our distance estimate places it 9.0 pc from the Sun, and our measurement of the proper motion indicates that it may also be a high mover –  $\mu = 2.429 \pm 0.334$  arcsec/yr – although the error bar is large (Table 6). As with most of the other Y dwarf discoveries, this object is detected by WISE only in bands W2 and W3 and not in W1 or W4 (Table 2).

**H. WISEPA J044853.29–193548.5 ( $J=17.0$  mag,  $W2=14.2$  mag)**

The depths of the  $H_2O$  and  $CH_4$  absorption bands in the  $J$ - and  $H$ -band spectra of this object best fit the T5 standard; however, the spectrum shows excess flux in the  $Y$  band around 0.95 to 1.10  $\mu m$  and a flattening of the entire  $K$ -band spectrum (Figure A4). We therefore classify this object as a “T5 pec”. Excess flux at  $Y$  band and a flattening at  $K$  have also been noted in Burgasser et al. (2006) for the T6 pec dwarf 2MASS J09373487+2931409, which may be slightly metal-poor ( $[M/H] \approx -0.5$  to  $-0.1$ ) based on fits to model spectra. Burgasser et al. (2011) and Burgasser et al. (2010) have noted the same peculiarities in the spectrum of the T7.5 dwarf ULAS J141623.94+134836.3 (Scholz 2010; Burningham et al. 2010), which is a common proper motion companion to the nearby, late-L dwarf SDSS J141624.08+134826.7 (Schmidt et al. 2010; Bowler et al. 2010). The latter is classified by Kirkpatrick et al. (2010) as sdL7 and by Burningham et al. (2010) as d/sdL7. Given that the two objects are presumably coeval, it can be assumed that they have the same metallicity and that the peculiar features in the spectrum of ULAS J141623.94+134836.3 –

and by extension, WISE 0448–1935 – are caused by a metal content below solar. The high motion of WISE 0448–1935 –  $\mu = 1.168 \pm 0.029$  arcsec/yr, which translates into a tangential velocity of  $118.5 \pm 2.9$  km/s for an estimated distance of 21.4 pc – also indicates that this object belongs to an old kinematic population.

### **I. WISEPA J045853.89+643452.9 ( $J=18.3$ mag, $W2=13.0$ mag)**

This object was discussed in detail by Mainzer et al. (2011). Our distance estimate of 7.3 pc assumes a single source, but analysis of laser guide star adaptive optics data from Gelino et al. (2011) indicates that the source is a double in which the components have  $\Delta J \approx \Delta H \approx 1$  mag. Individual magnitudes are measured as  $J_A = 17.50 \pm 0.09$ ,  $J_B = 18.48 \pm 0.12$  and  $H_A = 17.81 \pm 0.13$ ,  $H_B = 18.81 \pm 0.17$  on the MKO filter system. Gelino et al. (2011) suggest an actual distance to the system of  $12.3 \pm 2.3$  pc and individual spectral types of T8.5 and T9.

### **J. WISEPA J052536.33+673952.3 ( $J=17.5$ mag, $W2=14.9$ mag)**

The  $J$ -band spectrum of this object best fits the T6 standard, but there are discrepancies at  $Y$  and  $K$  bands. At  $Y$  band the spectrum of WISE 0525+6739 shows excess flux relative to the standard, and at  $K$  band the spectrum shows less flux relative to the standard (Figure A5). We therefore classify this object as a “T6 pec”. The physical cause, as discussed above for WISE 0448–1935, may be low metal content.

### **K. WISEPA J052844.51–330823.9 ( $J=16.7$ mag, $W2=14.5$ mag)**

The  $J$ -band spectrum of this object best fits the T7 standard, but there are discrepancies at  $Y$  and  $K$  bands. At  $Y$  band the spectrum of WISE 0528–3308 shows excess flux relative to the standard, and at  $K$  band the spectrum shows less flux relative to the standard (Figure A6). We therefore classify this object as a “T7 pec”. The physical cause, as discussed above for both WISE 0448–1935 and WISE 0525+6739, may be low metal content.

### L. WISEPC J083641.12–185947.2 ( $J$ =unknown, $W2$ =15.0 mag)

The  $J$ -band spectrum of this object best fits the T8 standard, but there are major discrepancies at  $Y$  and  $K$  bands. At  $Y$  band the spectrum of WISE 0836–1859 shows excess flux relative to the standard, and at  $K$  band the spectrum shows less flux relative to the standard (Figure A7). We therefore classify this object as a “T8 pec”. Several other objects discussed in this section – WISE 0448–1935, WISE 0525+6739, WISE 0528–3308, WISE 1436–1814, WISE 2134–7137, and WISE 2325–4105 – have similar  $Y$ - and  $K$ -band discrepancies, which may result from low metal content, but none are as severe as the discrepancies in this object. Unlike in those objects, the  $H$ -band flux in WISE 0836–1859 is markedly lower than the closest matching standard at  $J$ , making this object the most peculiar one of the group, and perhaps also the most metal poor.

Ideally, we would like to study the frequency of these metal-poor T dwarfs to see if the numbers found are what star formation theory would predict for an old, field population. Unfortunately, we do not have cold models across a large grid of metallicities with which to determine the  $[M/H]$  values of our spectra. We suspect that in cool objects such as these, slight changes in the metal content can have profound effects on the emergent spectra. As a result, we may be able to detect via spectroscopy smaller changes in  $[M/H]$  for T dwarfs than are possible in hotter stars due to the richness of molecular species and the important role of condensation in determining the absorbing species of colder objects. In other words, the metal content of these T dwarfs may not be too different from solar. As discussed above for WISE 0448–1935, the T7.5 dwarf ULAS J141623.94+134836.3 shows peculiarities in its spectrum that are similar to the ones seen in these unusual WISE T dwarfs, yet models with a subsolar abundance of only  $[M/H] = -0.3$  provide good fits to the emergent spectrum of that object (Burgasser et al. 2010).

### M. WISEPC J112254.73+255021.5 ( $J$ =16.7 mag, $W2$ =14.0 mag)

This object, a normal T6 dwarf, lies 265 arcseconds away from the nearby M5 V star LHS 302 (GJ 3657). Our spectrophotometric distance estimate for WISE 1122+2550 (16.9 pc; Table 6) is very similar to the distance of 17.2 pc obtained via trigonometric parallax ( $0.0581 \pm 0.0039$  arcsec) for LHS 302 (Dahn et al. 1988). Moreover, the Right Ascension and Declination components of the proper motion of WISE 1122+2550 are measured by us to be  $-0.954 \pm 0.016$  and  $-0.276 \pm 0.018$  arcsec/yr, respectively, which are only  $\sim 3\sigma$  different from those measured for LHS 302 ( $-1.002 \pm 0.001$  arcsec/yr and  $-0.330 \pm 0.001$  arcsec/yr; Dahn et al. 1988). If these two objects are a common proper motion binary, the projected separation between them is  $\sim 4500$  AU.

Other stellar + substellar binaries of large separation are known. Examples are the Gliese 570 system comprised of K4 V, M1.5 V + M3 V, and T7.5 components with the latter having a projected separation of 1500 AU from the K star; the Gliese 584 system comprised of G1 V + G3 V and L8 components with a projected separation of 3600 AU (Kirkpatrick et al. 2001); the Gliese 417 system comprised of G0 V and L4.5 components with a projected separation of 2000 AU (Kirkpatrick et al. 2001); the Gliese 618.1 system comprised of M0 V and L2.5 components with a projected separation of 1000 AU (Wilson et al. 2001); the HD 89744 system comprised of F7 IV-V and L0 components with a projected separation of 2500 AU (Wilson et al. 2001); and the HD 2057 system comprised of F8 and L4 components with a projected separation of 7000-9000 AU (Cruz et al. 2007). Each of these systems, however, has a more massive primary than the one discussed here. Assuming that LHS 302 has a mass of  $\sim 0.2 M_{\odot}$  in concert with other M5 dwarfs (see López-Morales 2007), then our projected separation of 4500 AU falls well outside the  $\Delta_{max} = 10^{3.33M_{tot}+1.1} = 58$  AU stability limit suggested empirically by Reid et al. (2001). This suggests that WISE 1122+2550 and LHS 302 are either physically unbound while sharing a common proper motion or are totally unassociated.

#### **N. WISEPC J115013.88+630240.7 ( $J=17.7$ mag, $W2=13.4$ mag)**

Our distance estimate places this T8 dwarf 9.6 pc from the Sun.

#### **O. WISEPC J121756.91+162640.2 ( $J=17.8$ mag, $W2=13.1$ mag)**

Our distance estimate places this T9 dwarf 6.7 pc from the Sun. Our measurement of  $\mu=1.765\pm0.388$  arcsec/yr, based on astrometry covering only 0.7 yr, may also indicate a high proper motion, but the uncertainty in this value is very large.

#### **P. WISEPC J131141.91+362925.2 ( $J=15.5$ mag, $W2=13.1$ mag)**

The near-infrared spectrum of this source is an excellent match to the L5 standard at  $J$  band. At longer wavelengths, however, the spectrum is considerably bluer, as shown in Figure A8. There is no evidence in the  $J$ -band that this source has a low-metallicity, and therefore that the  $H$  and  $K$  bands are being suppressed by the relatively stronger collision-induced absorption by  $H_2$  one would expect in a metal-starved atmosphere. The notch near  $1.62 \mu\text{m}$  in the top of the  $H$  band peak is very similar to the interesting feature noted by

Burgasser (2007) in the spectrum of SDSS J080531.84+481233.0, which those authors claim is an unresolved mid-L + mid-T binary. The  $H$ -band notch is also seen by Burgasser et al. (2011) in the spectrum of 2MASS J1315–2649, which those authors have successfully split, via high-resolution imaging and spectroscopy, into an L5 + T7 double. We classify WISE 1311+3629 as an “L5 blue” and note that its peculiar features may be caused by unresolved binarity as well. Our formal fits to synthetic binaries (see Burgasser 2007 for details) show that the most likely spectral types of the two components are  $L3.5\pm0.7$  and  $T2\pm0.5$  with estimated relative magnitudes of  $\Delta J = 1.4\pm0.2$ ,  $\Delta H = 1.7\pm0.3$ , and  $\Delta K = 2.2\pm0.3$  mag. This object would be an excellent target for high-resolution imaging. We note that this object was also identified as a brown dwarf candidate by Zhang et al. (2009) and given the designation SDSS J131142.11+362923.9.

**Q. WISEPC J140518.40+553421.4 ( $J=20.2$  mag,  $W2=14.1$  mag)**

This object is tentatively classified as Y0 (pec?) by Cushing et al. (accepted), who describe its spectral features and derived physical parameters. We estimate a distance of 8.6 pc and find a high proper motion of  $2.693\pm0.398$  arcsec/yr and high tangential velocity of  $109.8\pm16.2$  km/s. As with most of the other Y dwarf discoveries, this object is detected by WISE only in bands W2 and W3 and not in W1 or W4 (Table 2).

**R. WISEPA J143602.19–181421.8 ( $J$ =unknown,  $W2=14.7$  mag)**

The  $J$ -band spectrum of this object best fits the T8 standard, but there are discrepancies at  $Y$  and  $K$  bands. At  $Y$  band the spectrum of WISE 1436–1814 shows excess flux relative to the standard, and at  $K$  band the spectrum shows less flux relative to the standard (Figure A9). We therefore classify this object as a “T8 pec”. The physical cause, as discussed above for several other objects, may be low metal content.

**S. WISEPC J150649.97+702736.0 ( $J=13.6$  mag,  $W2=11.3$  mag)**

This T6 dwarf is estimated to fall only 4.9 pc from the Sun. Its large motion ( $\mu = 1.388\pm0.131$  arcsec/yr) placed it nearly in front of a star, now to the southeast, of similar near-infrared brightness during the 2MASS survey (see Figure 4.12), and this confusion led to the source having been missed in photometric searches of the 2MASS Point Source Catalog.

**T. WISEPA J154151.66–225025.2 ( $J=21.2$  mag,  $W2=14.0$  mag)**

The near-infrared spectrum of this object, discussed in Cushing et al. (accepted), is classified as Y0 because of its similarity to the spectrum of the Y0 near-infrared standard, WISE 1738+2732. As with most of the other Y dwarf discoveries, this object is detected by WISE only in bands W2 and W3 and not in W1 or W4 (Table 2). In contrast to our crude spectrophotometric distance estimate from Table 6 of 8.2 pc, we measure a trigonometric parallax placing it at  $2.8^{+1.3}_{-0.6}$  pc (Table 7), along with a proper motion of  $\mu = 0.81 \pm 0.34$  arcsec/yr. This parallax result is significant only at the  $3\sigma$  level and is measured only over a 1.2yr baseline, so it should be treated as preliminary only. Nonetheless, if confirmed, this distance would place WISE 1541–2250 as the seventh closest stellar system to the Sun after the  $\alpha$  Centauri system ( $d=1.3$  pc, van Leeuwen 2007), Barnard’s Star ( $d=1.8$  pc, van Leeuwen 2007), Wolf 359 ( $d=2.4$  pc, van Altena et al. 2001), Lalande 21185 ( $d=2.5$  pc, van Leeuwen 2007), Sirius AB ( $d=2.6$  pc, van Leeuwen 2007), and L 726-8 AB (also known as BL Ceti and UV Ceti;  $d=2.7$  pc, van Altena et al. 2001). The measured distance implies absolute magnitudes of  $M_J = 23.9 \pm 0.8$  and  $M_H = 23.8 \pm 0.9$  mag on the MKO filter system and  $M_{W2} = 16.7 \pm 0.7$  mag. This indicates a rapid dimming at those wavelengths in just a single spectral subclass from T9 to Y0 (see, e.g., Figure 29 and Figure 31).

**U. WISEPA J164715.59+563208.2 ( $J=16.6$  mag,  $W2=13.1$  mag)**

The  $J$ -band spectrum of this object best fits the L9 standard, but there is excess flux at  $H$  and particularly  $K$  relative to the standard itself (Figure A10). We therefore classify this object as an “L9 pec (red)”. This object adds to a growing list of red L dwarfs whose red colors cannot obviously be attributed to low gravity. It becomes the seventh example of this class, which now includes 2MASS J21481633+4003594 and 2MASS J18212815+1414010 from Looper et al. (2008); 2MASS J13313310+3407583, 2MASS J23174712–4838501, and 2MASS J23512200+3010540 from Kirkpatrick et al. (2010); and WISE 0206+2640 from above. As mentioned in Kirkpatrick et al. (2010), the kinematics of the first five examples suggest that these objects derive from an old population, making them distinct from the red L dwarfs that have low-gravity spectral signatures and young kinematics. We note, however, that this object has a low tangential velocity of only  $28.1 \pm 1.2$  km/s. However, this velocity assumes our spectrophotometric distance estimate of 20.2 pc, and our preliminary astrometric measurements over an 11.8yr baseline indicate a closer distance of  $8.6^{+2.9}_{-1.7}$  pc, along with a motion of  $\mu = 0.293 \pm 0.012$  arcsec/yr. Continued astrometric monitoring of this object is needed to see if this closer distance is confirmed, as this would provide another clue in deciphering the physical nature of this rare class of red (non low- $g$ ) L dwarfs.



**V. WISEPA J173835.53+273258.9 ( $J=19.5$  mag,  $W2=14.5$  mag)**

Cushing et al. (accepted) propose this object as the Y0 spectroscopic standard. It is the only one of our Y dwarfs detected in all three short-wavelength bands of WISE (W1, W2, and W3). Our spectrophotometric distance estimate places it at 10.5 pc; the available astrometry for this Y0 dwarf spans barely six months (Table 6), so we are not yet able to derive proper motion or parallax.

**W. WISEPA J174124.26+255319.5 ( $J=16.5$  mag,  $W2=12.3$  mag)**

This nearby dwarf of near-infrared spectral type T9 is detected in the 2MASS and SDSS surveys but was overlooked because of its weak detection in both. Using a 10.4yr baseline, we find a high proper motion of  $\mu = 1.555 \pm 0.023$  arcsec/yr and estimate a distance of 4.7 pc. Our preliminary trigonometric parallax measurement places it at  $5.5^{+1.4}_{-1.0}$  pc (Table 7). This object has identical optical and near-infrared types to another nearby object, UGPS J072227.51–054031.2, whose trigonometric parallax from Lucas et al. (2010) places it at a distance of 4.1 pc. Gelino et al. (2011) note that WISE 1741+2553 appears single in near-infrared imaging observations with laser guide star adaptive optics.

**X. WISEPA J180435.40+311706.1 ( $J=18.7$  mag,  $W2=14.7$  mag)**

The near-infrared spectrum of this object is classified as T9.5: because of its similarity to the spectrum of the T9.5 dwarf WISE 0148–7202. Although noisy, the narrowness of the J-band peaks falls intermediate between that of the T9 standard UGPS J072227.51–054031.2 and the Y0 standard WISE 1738+2732. We estimate that this object falls at a distance of 13.0 pc. The WISE detections for this object are very similar to those seen for Y dwarfs; namely, the object is detected only in bands W2 and W3 and not in W1 or W4 (Table 2).

**Y. WISEPA J182831.08+265037.8 ( $J=23.6$  mag,  $W2=14.3$  mag)**

This object, with a tentative classification of  $>Y0$  from Cushing et al. (accepted), is the latest object so far found with WISE. The spectrum is unique among late-T and Y dwarfs in that the  $J$ - and  $H$ -band peaks, in units of  $f_\lambda$ , are nearly the same height (Figure 25). This reddening of the near-infrared colors ( $J-H = 0.72 \pm 0.42$  mag; Table 3) is predicted by model atmosphere calculations to occur at effective temperatures below 300-400K (Burrows et al.

2003). This effect is due to the fact that the Wien tail of the spectral energy distribution becomes the overwhelming effect shaping the spectrum at those wavelengths, and this may be even more dramatically illustrated by the extremely red  $J - W2$  and  $H - W2$  colors measured for this object (Figure 7 and Figure 8). Our spectrophotometric distance estimate of  $<9.4$  pc implies exceedingly dim absolute magnitudes of  $M_J > 23.7$  and  $M_H > 23.0$  mag, on the MKO filter system. These values agree with expectations that WISE 1828+2650 should be dimmer at these wavelengths than the presumably warmer WISE 1541–2250, which also has exceedingly dim  $J$  and  $H$  magnitudes (Table 7).

### **Z. WISEPC J205628.90+145953.3 ( $J=19.2$ mag, $W2=13.9$ mag)**

This Y0 dwarf, discussed in Cushing et al. (accepted), is estimated to lie at a distance of 7.7 pc. As with several other Y dwarf discoveries, this object is detected by WISE only in bands W2 and W3 and not in W1 or W4 (Table 2).

### **AA. WISEPA J213456.73–713743.6 ( $J=19.8$ mag, $W2=13.9$ mag)**

The  $J$ -band spectrum of this object best fits the T9 standard, but there are discrepancies at  $Y$  and  $K$  bands. At  $Y$  band the spectrum of WISE 2134–7137 shows excess flux relative to the standard, and at  $K$  band the spectrum shows less flux relative to the standard (Figure A11). We therefore classify this object as a “T9 pec”. The physical cause, as discussed above for several other objects, may be low metal content.

### **BB. WISEPC J232519.54–410534.9 ( $J=19.7$ mag, $W2=14.1$ mag)**

As with the previous object, the  $J$ -band spectrum best fits the T9 standard, but there are discrepancies at  $Y$  and  $K$  bands. At  $Y$  band the spectrum of WISE 2325–4105 shows excess flux relative to the T9 standard, and at  $K$  band the spectrum shows less flux relative to the T9 standard (Figure A12). We therefore classify this object as a “T9 pec”. The physical cause, as discussed above for other objects, may be low metal content.

### **CC. WISEPC J232728.75–273056.5 ( $J=16.7$ mag, $W2=13.2$ mag)**

This object has the near-infrared spectrum of a normal L9 dwarf, but its WISE color of  $W1-W2 = 0.825 \pm 0.046$  is markedly redder than the other L9 dwarfs on Figure 1. The *Spitzer*/IRAC color of  $ch1-ch2 = 0.247 \pm 0.025$  is redder than all other L and early-T dwarfs in Figure 11. Effects such as low-gravity or low-metallicity would cause the near-infrared spectrum of this object to appear unusually red or unusually blue, respectively, in the near-infrared (Kirkpatrick et al. 2010), and this is not seen. One hypothesis is that this object is an unresolved L+T binary, but not one with such a warm T dwarf that the near-infrared

spectrum of the composite shows itself to be peculiar. We can test this as follows. The W1-W2 color of WISE 2327–2730 is  $\sim 0.23$  mag redder than the mean W1-W2 for other L9 dwarfs. Using the absolute W2 versus spectral type plot of Figure 29 along with the trend of W1-W2 color with spectral type in Figure 1, we estimate that the type of the hypothesized companion would have to be roughly T6.5. However, as Figure 4 of Burgasser (2007) shows, an object with a composite type of  $\sim$ L9 and secondary of  $\sim$ T6.5 would have a noticeably peculiar near-infrared spectrum which would distinguish it from a normal L9. Hence, binarity appears not to be the cause of the redder W1-W2 and ch1-ch2 colors. The reason for this color peculiarity remains unexplained.

## REFERENCES

- Albert, L., Artigau, É., Delorme, P., Reyl  , C., Forveille, T., Delfosse, X., & Willott, C. J. 2011, *AJ*, 141, 203
- Artigau,   ., Radigan, J., Folkes, S., Jayawardhana, R., Kurtev, R., Lafreni  re, D., Doyon, R., & Borissova, J. 2010, *ApJ*, 718, L38
- Artigau,   ., Doyon, R., Lafreni  re, D., Nadeau, D., Robert, J., & Albert, L. 2006, *ApJ*, 651, L57
- Baraffe, I., Chabrier, G., Allard, F., & Hauschildt, P. 2003, *Brown Dwarfs*, 211, 41
- Barman, T. S., Hauschildt, P. H., & Allard, F. 2005, *ApJ*, 632, 1132
- Bate, M. R., & Bonnell, I. A. 2005, *MNRAS*, 356, 1201
- Becklin, E. E., & Zuckerman, B. 1988, *Nature*, 336, 656
- Bertin, E., & Arnouts, S. 1996, *A&AS*, 117, 393
- Bessell, M. S. 2005, *ARA&A*, 43, 293
- Bessell, M. S., & Brett, J. M. 1988, *PASP*, 100, 1134
- Bloom, J. S., Starr, D. L., Blake, C. H., Skrutskie, M. F., & Falco, E. E. 2006, *Astronomical Data Analysis Software and Systems XV*, 351, 751
- Boss, A. P. 2004, *MNRAS*, 350, L57
- Bouvier, J., Kendall, T., & Meeus, G. 2009, *American Institute of Physics Conference Series*, 1094, 497

- Bouy, H., Brandner, W., Martín, E. L., Delfosse, X., Allard, F., & Basri, G. 2003, *AJ*, 126, 1526
- Bowler, B. P., Liu, M. C., & Dupuy, T. J. 2010, *ApJ*, 710, 45
- Boyd, D. F. A., & Whitworth, A. P. 2005, *A&A*, 430, 1059
- Burgasser, A. J., Sitarski, B. N., Gelino, C. R., Logsdon, S. E., & Perrin, M. D. 2011, arXiv:1107.1484
- Burgasser, A. J., et al. 2011, arXiv:1104.2537
- Burgasser, A. J., et al. 2010, *ApJ*, 725, 1405
- Burgasser, A. J., Looper, D., & Rayner, J. T. 2010, *AJ*, 139, 2448
- Burgasser, A. J. 2008, 14th Cambridge Workshop on Cool Stars, Stellar Systems, and the Sun, 384, 126
- Burgasser, A. J., Looper, D. L., Kirkpatrick, J. D., Cruz, K. L., & Swift, B. J. 2008, *ApJ*, 674, 451
- Burgasser, A. J. 2007, *AJ*, 134, 1330
- Burgasser, A. J., Geballe, T. R., Leggett, S. K., Kirkpatrick, J. D., & Golimowski, D. A. 2006, *ApJ*, 637, 1067
- Burgasser, A. J., Burrows, A., & Kirkpatrick, J. D. 2006, *ApJ*, 639, 1095
- Burgasser, A. J. 2004, *ApJS*, 155, 191
- Burgasser, A. J., McElwain, M. W., Kirkpatrick, J. D., Cruz, K. L., Tinney, C. G., & Reid, I. N. 2004, *AJ*, 127, 2856
- Burgasser, A. J., Kirkpatrick, J. D., Liebert, J., & Burrows, A. 2003, *ApJ*, 594, 510
- Burgasser, A. J., Kirkpatrick, J. D., McElwain, M. W., Cutri, R. M., Burgasser, A. J., & Skrutskie, M. F. 2003, *AJ*, 125, 850
- Burgasser, A. J., McElwain, M. W., & Kirkpatrick, J. D. 2003, *AJ*, 126, 2487
- Burgasser, A. J., et al. 2002, *ApJ*, 564, 421
- Burgasser, A. J., et al. 2000, *AJ*, 120, 1100

- Burgasser, A. J., et al. 2000, *ApJ*, 531, L57
- Burgasser, A. J., et al. 1999, *ApJ*, 522, L65
- Burningham, B., et al. 2011, *MNRAS*, 414, L90
- Burningham, B., et al. 2011, *MNRAS*, L259
- Burningham, B., et al. 2010, *MNRAS*, 406, 1885
- Burningham, B., et al. 2010, *MNRAS*, 404, 1952
- Burningham, B., et al. 2009, *MNRAS*, 395, 1237
- Burningham, B., et al. 2008, *MNRAS*, 391, 320
- Burrows, A., Sudarsky, D., & Lunine, J. I. 2003, *ApJ*, 596, 587
- Chiu, K., Fan, X., Leggett, S. K., Golimowski, D. A., Zheng, W., Geballe, T. R., Schneider, D. P., & Brinkmann, J. 2006, *AJ*, 131, 2722
- Costa, E., Méndez, R. A., Jao, W.-C., Henry, T. J., Subasavage, J. P., & Ianna, P. A. 2006, *AJ*, 132, 1234
- Cruz, K. L., et al. 2007, *AJ*, 133, 439
- Cruz, K. L., Burgasser, A. J., Reid, I. N., & Liebert, J. 2004, *ApJ*, 604, L61
- Cruz, K. L., Reid, I. N., Liebert, J., Kirkpatrick, J. D., & Lowrance, P. J. 2003, *AJ*, 126, 2421
- Cushing, M. C., Vacca, W. D., & Rayner, J. T. 2004, *PASP*, 116, 362
- Dahn, C. C., et al. 2002, *AJ*, 124, 117
- Dahn, C. C., et al. 1988, *AJ*, 95, 237
- Deacon, N. R., Hambly, N. C., King, R. R., & McCaughrean, M. J. 2009, *MNRAS*, 394, 857
- Deacon, N. R., Hambly, N. C., & Cooke, J. A. 2005, *A&A*, 435, 363
- Delfosse, X., Tinney, C. G., Forveille, T., Epchtein, N., Borsenberger, J., Fouqué, P., Kimeswenger, S., & Tiphène, D. 1999, *A&AS*, 135, 41
- Delfosse, X., et al. 1997, *A&A*, 327, L25

- Delorme, P., et al. 2010, *A&A*, 518, A39
- Delorme, P., et al. 2008, *A&A*, 482, 961
- Eddington, A. S., Sir 1940, *MNRAS*, 100, 354
- Eddington, A. S. 1913, *MNRAS*, 73, 359
- Eisenhardt, P. R. M., et al. 2010, *AJ*, 139, 2455
- Ellis, S. C., Tinney, C. G., Burgasser, A. J., Kirkpatrick, J. D., & McElwain, M. W. 2005, *AJ*, 130, 2347
- Faherty, J. K., Burgasser, A. J., Cruz, K. L., Shara, M. M., Walter, F. M., & Gelino, C. R. 2009, *AJ*, 137, 1
- Fan, X., et al. 2000, *AJ*, 119, 928
- Fazio, G. G., et al. 2004, *ApJS*, 154, 10
- Fortney, J. J., Marley, M. S., Lodders, K., Saumon, D., & Freedman, R. 2005, *ApJ*, 627, L69
- Geballe, T. R., et al. 2002, *ApJ*, 564, 466
- Gelino, C. R., et al. 2011, *AJ*, 142, 57
- Giclas, H. L., Burnham, R., & Thomas, N. G. 1971, Flagstaff, Arizona: Lowell Observatory, 1971,
- Gizis, J. E. 2002, *ApJ*, 575, 484
- Gizis, J. E., Monet, D. G., Reid, I. N., Kirkpatrick, J. D., Liebert, J., & Williams, R. J. 2000, *AJ*, 120, 1085
- Goldman, B., Marsat, S., Henning, T., Clemens, C., & Greiner, J. 2010, *MNRAS*, 405, 1140
- Hall, P. B. 2002, *ApJ*, 564, L89
- Hamuy, M., Suntzeff, N. B., Heathcote, S. R., Walker, A. R., Gigoux, P., & Phillips, M. M. 1994, *PASP*, 106, 566
- Hanisch, R. J., Farris, A., Greisen, E. W., Pence, W. D., Schlesinger, B. M., Teuben, P. J., Thompson, R. W., & Warnock, A., III 2001, *A&A*, 376, 359
- Hawkins, M. R. S., & Bessell, M. S. 1988, *MNRAS*, 234, 177

- Hawley, S. L., et al. 2002, *AJ*, 123, 3409
- Hayashi, C., & Nakano, T. 1963, *Progress of Theoretical Physics*, 30, 460
- Herter, T. L., et al. 2008, *Proc. SPIE*, 7014,
- Horne, K. 1986, *PASP*, 98, 609
- Kanneganti, S., Park, C., Skrutskie, M. F., Wilson, J. C., Nelson, M. J., Smith, A. W., & Lam, C. R. 2009, *PASP*, 121, 885
- Kendall, T. R., Jones, H. R. A., Pinfield, D. J., Pokorny, R. S., Folkes, S., Weights, D., Jenkins, J. S., & Maun, N. 2007, *MNRAS*, 374, 445
- Kirkpatrick, J. D., et al. 2010, *ApJS*, 190, 100
- Kirkpatrick, J. D. 2008, 14th Cambridge Workshop on Cool Stars, Stellar Systems, and the Sun, 384, 85
- Kirkpatrick, J. D., et al. 2008, *ApJ*, 689, 1295
- Kirkpatrick, J. D., Barman, T. S., Burgasser, A. J., McGovern, M. R., McLean, I. S., Tinney, C. G., & Lowrance, P. J. 2006, *ApJ*, 639, 1120
- Kirkpatrick, J. D. 2005, *ARA&A*, 43, 195
- Kirkpatrick, J. D., Dahn, C. C., Monet, D. G., Reid, I. N., Gizis, J. E., Liebert, J., & Burgasser, A. J. 2001, *AJ*, 121, 3235
- Kirkpatrick, J. D. 2000, *From Giant Planets to Cool Stars*, 212, 20
- Kirkpatrick, J. D., et al. 2000, *AJ*, 120, 447
- Kirkpatrick, J. D., et al. 1999, *ApJ*, 519, 802
- Kirkpatrick, J. D., Beichman, C. A., & Skrutskie, M. F. 1997, *ApJ*, 476, 311
- Kirkpatrick, J. D., & McCarthy, D. W., Jr. 1994, *AJ*, 107, 333
- Kirkpatrick, J. D., McGraw, J. T., Hess, T. R., Liebert, J., & McCarthy, D. W., Jr. 1994, *ApJS*, 94, 749
- Knapp, G. R., et al. 2004, *AJ*, 127, 3553

- Koekemoer, A. M., Fruchter, A. S., Hook, R. N., & Hack, W. 2002, The 2002 HST Calibration Workshop : Hubble after the Installation of the ACS and the NICMOS Cooling System, 337
- Kouzuma, S., & Yamaoka, H. 2010, A&A, 509, A64
- Kumar, S. S. 1963, ApJ, 137, 1121
- Kümmel, M., Walsh, J. R., Pirzkal, N., Kuntschner, H., & Pasquali, A. 2009, PASP, 121, 59
- Lawrence, A., et al. 2007, MNRAS, 379, 1599
- Leggett, S. K., et al. 2010, ApJ, 710, 1627
- Leggett, S. K., et al. 2009, ApJ, 695, 1517
- Leggett, S. K., et al. 2000, ApJ, 536, L35
- Lépine, S., & Shara, M. M. 2005, AJ, 129, 1483
- Liebert, J., Kirkpatrick, J. D., Cruz, K. L., Reid, I. N., Burgasser, A., Tinney, C. G., & Gizis, J. E. 2003, AJ, 125, 343
- Liu, M. C., et al. 2011, arXiv:1103.0014
- Lodieu, N., Scholz, R.-D., & McCaughrean, M. J. 2002, A&A, 389, L20
- Loh, E. D., Biel, J. D., Chen, J.-J., Davis, M., Laporte, R., & Loh, O. Y. 2004, Proc. SPIE, 5492, 1644
- Looper, D. L., et al. 2008, ApJ, 686, 528
- Looper, D. L., Kirkpatrick, J. D., & Burgasser, A. J. 2007, AJ, 134, 1162
- López-Morales, M. 2007, ApJ, 660, 732
- Lucas, P. W., et al. 2010, MNRAS, 408, L56
- Lucas, P. W., Weights, D. J., Roche, P. F., & Riddick, F. C. 2006, MNRAS, 373, L60
- Luhman, K. L., Burgasser, A. J., & Bochanski, J. J. 2011, ApJ, 730, L9
- Luhman, K. L., et al. 2007, ApJ, 654, 570
- Luhman, K. L. 2007, ApJS, 173, 104



- Luhman, K. L., Rieke, G. H., Young, E. T., Cotera, A. S., Chen, H., Rieke, M. J., Schneider, G., & Thompson, R. I. 2000, *ApJ*, 540, 1016
- Lutz, T. E., & Kelker, D. H. 1973, *PASP*, 85, 573
- Luyten, W. J. 1980, *NLTT Catalogue. Volume III. 0<sup>+</sup> to -30<sup>-</sup>*, by Luyten, W. J.. Published by University of Minnesota, Minneapolis, Minnesota, USA, 283 p.,
- Luyten, W. J. 1979, Minneapolis: University of Minnesota, 1979, 2nd ed.,
- Luyten, W. J. 1979, *New Luyten Catalogue of stars with proper motions larger than two tenths of an arcsecond*, 1, 0 (1979), 0
- Luyten, W. J. 1979, *New Luyten Catalogue of stars with proper motions larger than two tenths of an arcsecond*, 2, 0 (1979), 0
- Luyten, W. J., & Kowal, C. T. 1975, *Proper motion survey with the forty-eight inch Schmidt telescope. XLIII. One hundred and six faint stars with large proper motions.*, by Luyten, W. J.; Kowal, C. T.. Separate print Univ. Minnesota, Minneapolis, Minnesota, 2 p., 43, 1
- Luyten, W. J. 1974, *Proper Motion Survey with the forty-eight inch Schmidt telescope. XXXVII. Proper motions for 4483 faint stars.*, by Luyten, W. J.. Separate print Univ. Minnesota, Minneapolis, Minnesota, 44 p., 37, 1
- Luyten, W. J. 1974, *Proper Motion Survey with the forty-eight inch Schmidt telescope. XXXVI. Proper motions for 6955 faint stars.*, by Luyten, W. J.. Separate print Univ. Minnesota, Minneapolis, Minnesota, 64 p., 36, 1
- Luyten, W. J. 1972, *Proper Motion Survey with the forty-eight inch Schmidt telescope. XXXI. Proper motions for 2520 faint stars.*, by Luyten, W. J.. Separate print Univ. Minnesota, Minneapolis, Minnesota, 24 p., 31, 1
- Mainzer, A., et al. 2011, *ApJ*, 726, 30
- Malmquist, K. G. 1920, *Medd. Lund Astron. Obs. Ser.*, 2., No. 22
- Marocco, F., et al. 2010, *A&A*, 524, A38
- Marois, C., Macintosh, B., Barman, T., Zuckerman, B., Song, I., Patience, J., Lafrenière, D., & Doyon, R. 2008, *Science*, 322, 1348
- Martín, E. L., et al. 2010, *A&A*, 517, A53

- Martini, P., Persson, S. E., Murphy, D. C., Birk, C., Shectman, S. A., Gunnels, S. M., & Koch, E. 2004, *Proc. SPIE*, 5492, 1653
- Metchev, S. A., Kirkpatrick, J. D., Berriman, G. B., & Looper, D. 2008, *ApJ*, 676, 1281
- McLean, I. S., McGovern, M. R., Burgasser, A. J., Kirkpatrick, J. D., Prato, L., & Kim, S. S. 2003, *ApJ*, 596, 561
- McLean, I. S., Graham, J. R., Becklin, E. E., Figer, D. F., Larkin, J. E., Levenson, N. A., & Teplitz, H. I. 2000, *Proc. SPIE*, 4008, 1048
- McLean, I. S., et al. 1998, *Proc. SPIE*, 3354, 566
- McLean, I. S., et al. 1994, *Proc. SPIE*, 2198, 457
- Milligan, S., Cranton, B. W., & Skrutskie, M. F. 1996, *Proc. SPIE*, 2863, 2
- Monet, D. G., et al. 2003, *AJ*, 125, 984
- Muench, A. A., Lada, E. A., Lada, C. J., & Alves, J. 2002, *ApJ*, 573, 366
- Noll, K. S., Geballe, T. R., Leggett, S. K., & Marley, M. S. 2000, *ApJ*, 541, L75
- Oke, J. B., et al. 1995, *PASP*, 107, 375
- Padoan, P., Kritsuk, A., Michael, Norman, L., & Nordlund, Å. 2005, *Mem. Soc. Astron. Italiana*, 76, 187
- Patten, B. M., et al. 2006, *ApJ*, 651, 502
- Perryman, M. A. C., et al. 1997, *A&A*, 323, L49
- Phan-Bao, N., et al. 2008, *MNRAS*, 383, 831
- Pinfield, D. J., et al. 2008, *MNRAS*, 390, 304
- Rayner, J. T., Toomey, D. W., Onaka, P. M., Denault, A. J., Stahlberger, W. E., Vacca, W. D., Cushing, M. C., & Wang, S. 2003, *PASP*, 115, 362
- Reid, I. N., Cruz, K. L., Kirkpatrick, J. D., Allen, P. R., Mungall, F., Liebert, J., Lowrance, P., & Sweet, A. 2008, *AJ*, 136, 1290
- Reid, I. N., Kirkpatrick, J. D., Liebert, J., Gizis, J. E., Dahn, C. C., & Monet, D. G. 2002, *AJ*, 124, 519

- Reid, I. N., Gizis, J. E., Kirkpatrick, J. D., & Koerner, D. W. 2001, *AJ*, 121, 489
- Reid, I. N., Kirkpatrick, J. D., Gizis, J. E., Dahn, C. C., Monet, D. G., Williams, R. J., Liebert, J., & Burgasser, A. J. 2000, *AJ*, 119, 369
- Reipurth, B., & Clarke, C. 2001, *AJ*, 122, 432
- Reyl , C., et al. 2010, *A&A*, 522, A112
- Rodr guez, D. R., Zuckerman, B., Melis, C., & Song, I. 2011, *ApJ*, 732, L29
- Ross, F. E. 1928, *AJ*, 38, 117
- Ruiz, M. T., Leggett, S. K., & Allard, F. 1997, *ApJ*, 491, L107
- Ruiz, M. T., Takamiya, M. Y., & Roth, M. 1991, *ApJ*, 367, L59
- Schilbach, E., R ser, S., & Scholz, R.-D. 2009, *A&A*, 493, L27
- Schmidt, M. 1968, *ApJ*, 151, 393
- Schmidt, S. J., West, A. A., Burgasser, A. J., Bochanski, J. J., & Hawley, S. L. 2010, *AJ*, 139, 1045
- Schneider, D. P., et al. 2002, *AJ*, 123, 458
- Scholz, R.-D. 2010, *A&A*, 510, L8
- Scholz, R.-D. 2010, *A&A*, 515, A92
- Scholz, R.-D., McCaughrean, M. J., Lodieu, N., & Kuhlbrodt, B. 2003, *A&A*, 398, L29
- Sheppard, S. S., & Cushing, M. C. 2009, *AJ*, 137, 304
- Simcoe, R. A., et al. 2010, *Proc. SPIE*, 7735,
- Simcoe, R. A., et al. 2008, *Proc. SPIE*, 7014,
- Skrutskie, M. F., et al. 2006, *AJ*, 131, 1163
- Smith, J. D. T., et al. 2007, *PASP*, 119, 1133
- Stephens, D. C., & Leggett, S. K. 2004, *PASP*, 116, 9
- Stern, D., et al. 2007, *ApJ*, 663, 677
- Strauss, M. A., et al. 1999, *ApJ*, 522, L61

- Sutherland, I. E. & Hodgman, G. .W., 1974, Communications of the Association for Computing Machinery, 17
- Swaters, R. A., Valdes, F., & Dickinson, M. E. 2009, Astronomical Data Analysis Software and Systems XVIII, 411, 506
- Teerikorpi, P. 2004, A&A, 424, 73
- Tinney, C. G., Burgasser, A. J., Kirkpatrick, J. D., & McElwain, M. W. 2005, AJ, 130, 2326
- Tinney, C. G., Burgasser, A. J., & Kirkpatrick, J. D. 2003, AJ, 126, 975
- Tinney, C. G. 1993, AJ, 105, 1169
- Tody, D. 1986, Proc. SPIE, 627, 733
- Tokunaga, A. T., Simons, D. A., & Vacca, W. D. 2002, PASP, 114, 180
- Tsvetanov, Z. I., et al. 2000, ApJ, 531, L61
- Vacca, W. D., Cushing, M. C., & Rayner, J. T. 2003, PASP, 115, 389
- van Altena, W. F., Lee, J. T., & Hoffleit, E. D. 2001, VizieR Online Data Catalog, 1238, 0
- van Altena, W. F., Lee, J. T., & Hoffleit, D. 1995, VizieR Online Data Catalog, 1174, 0
- van Dam, M. A., et al. 2006, PASP, 118, 310
- van Leeuwen, F. 2007, A&A, 474, 653
- Vrba, F. J., et al. 2004, AJ, 127, 2948
- Warren, S. J., et al. 2007, MNRAS, 381, 1400
- Werner, M. W., et al. 2004, ApJS, 154, 1
- West, A. A., Hawley, S. L., Bochanski, J. J., Covey, K. R., Reid, I. N., Dhital, S., Hilton, E. J., & Masuda, M. 2008, AJ, 135, 785
- Whitworth, A. P., & Zinnecker, H. 2004, A&A, 427, 299
- Wilson, J. C., et al. 2003, Proc. SPIE, 4841, 451
- Wilson, J. C., Miller, N. A., Gizis, J. E., Skrutskie, M. F., Houck, J. R., Kirkpatrick, J. D., Burgasser, A. J., & Monet, D. G. 2003, Brown Dwarfs, 211, 197

- Wilson, J. C., Kirkpatrick, J. D., Gizis, J. E., Skrutskie, M. F., Monet, D. G., & Houck, J. R. 2001, *AJ*, 122, 1989
- Wizinowich, P. L., et al. 2006, *PASP*, 118, 297
- Wright, E. L., et al. 2010, *AJ*, 140, 1868
- Wright, E. L., Mainzer, A., Gelino, C., & Kirkpatrick, D. 2010, arXiv:1104.2569
- Wroblewski, H., & Torres, C. 1991, *A&AS*, 91, 129
- York, D. G., et al. 2000, *AJ*, 120, 1579
- Zhang, Z. H., et al. 2009, *A&A*, 497, 619

Table 1. WISE and Near-infrared Photometry for Known M, L, and T Dwarfs

WISE Designation <sup>a</sup>	Other Designation	Dis. Ref.	W1 (mag)	W2 (mag)	W3 (mag)	W4 (mag)	J (mag)	H (mag)	K <sub>s</sub> (mag)	Spec. Typ. <sup>b</sup>
(1)	(2)	(3)	(4)	(5)	(6)	(7)	(8)	(9)	(10)	(11)
T Dwarfs:										
WISEPC J003402.80-005207.4	ULAS J003402.77-005206.7	1	17.320±0.249	14.465±0.076	>11.801	>9.224	18.150±0.030	18.490±0.040	18.480±0.050	T8.5
WISEPC J005021.03-332229.2	2MASS J00501994-3322402	2	15.506±0.050	13.526±0.036	11.957±0.236	>8.989	15.928±0.070	15.838±0.191	15.241±0.185	T7
WISEPC J005911.09-011400.6	CFBDS J005910.90-011401.3	3	17.003±0.169	13.668±0.044	12.355±0.424	>9.290	18.060±0.030	18.270±0.050	18.630±0.050	T9
WISEPC J013657.45+093347.0	IPMS J013656.57+093347.3	4	11.967±0.025	10.962±0.022	9.671±0.047	9.002±0.442	13.455±0.030	12.771±0.032	12.562±0.024	T2.5
WISEPA J015024.39+135924.3	ULAS J015024.37+135924.0	5	17.392±0.265	15.186±0.131	>12.108	>8.942	17.730±0.020	18.110±0.020	17.840±0.160	T7.5
WISEPA J015142.21+124429.6	SDSS J015141.69+124429.6	6	14.595±0.039	13.823±0.053	12.246±0.445	8.563±0.383	16.566±0.129	15.603±0.112	15.183±0.189	T1
WISEPC J020742.96+000056.9	SDSS J020742.48+000056.2	6	16.403±0.097	15.035±0.100	>12.618	>9.231	16.799±0.156	>16.396	>15.412	T4.5
WISEPC J024313.48-245331.5	2MASS J0243137-245329	7	14.680±0.035	12.929±0.030	11.285±0.131	9.367±0.535	15.381±0.050	15.137±0.109	15.216±0.168	T6
WISEPA J024749.98-163111.4	SDSS J024749.90-163112.6	8	15.197±0.045	14.197±0.054	12.679±0.528	>9.114	17.186±0.183	16.170±0.139	15.616±0.193	T2:
WISEPA J032553.11+042540.6	SDSS J032553.17+042540.1	8	15.893±0.069	13.783±0.045	12.446±0.443	>9.091	16.254±0.137	>16.080	>16.525	T5.5
WISEPC J034807.34-602234.9	2MASS J03480772-6022270	9	15.019±0.047	12.571±0.027	11.095±0.141	>8.875	15.318±0.050	15.559±0.143	15.602±0.230	T7
WISEPA J035104.53+481046.5	SDSS J035104.37+481046.8	8	14.570±0.044	13.897±0.051	12.312±0.349	>8.827	16.466±0.130	15.566±0.136	14.996±0.121	T1:
WISEPA J040708.95+151455.4	2MASS J04070885+1514565	10	15.475±0.058	13.895±0.052	12.048±0.343	>8.868	16.055±0.092	16.017±0.209	15.922±0.261	T5
WISEPA J041521.20-093500.6	2MASS J0415195-093506	7	15.095±0.042	12.240±0.026	11.038±0.112	>8.712	15.695±0.058	15.537±0.113	15.429±0.201	T8
WISEPA J042348.32-041402.5	SDSSp J042348.57-041403.5	6	12.182±0.025	11.569±0.025	10.535±0.081	>8.462	14.465±0.027	13.463±0.035	12.929±0.034	T0
WISEPA J043038.81+130956.8	CFHT-Hy-20	11	15.602±0.056	14.652±0.085	>11.837	>8.722	—	—	>16.080	T2
WISEPA J051035.35-420809.2	2MASS J05103520-4208140	12	15.604±0.035	13.975±0.032	11.860±0.117	8.853±0.235	16.222±0.087	16.237±0.157	15.996±0.283	T5
WISEPA J051609.28-044552.4	2MASS J05160945-0445499	9	15.456±0.051	13.602±0.039	12.651±0.460	>9.010	15.984±0.079	15.721±0.165	15.486±0.204	T5.5
WISEPA J051859.89-282840.2	2MASS J05185995-2828372	13	13.412±0.026	12.822±0.026	11.730±0.166	>8.798	15.978±0.097	14.830±0.073	14.162±0.072	T1p
WISEPA J055919.58-140452.6	2MASS J05591914-1404488	14	13.388±0.027	11.896±0.023	10.561±0.074	>8.666	13.802±0.024	13.679±0.044	13.577±0.052	T4.5
WISEPA J060206.60+404356.8	2MASS J06020638+4043588	12	15.236±0.057	13.541±0.043	>12.678	>9.123	15.544±0.067	15.592±0.137	15.166±0.162	T4.5
WISEPA J072227.27-054029.9	UGPS J072227.51-054031.2	15	15.147±0.051	12.171±0.026	10.177±0.059	>8.637	16.489±0.128	16.147±0.205	—	T9
WISEPA J072719.13+170952.0	2MASS J0727182+171001	7	15.232±0.048	12.930±0.032	11.620±0.221	>8.200	15.600±0.061	15.756±0.171	15.556±0.194	T7
WISEPA J072859.49-395346.7	2MASS J07290002-3954043	12	15.247±0.052	12.947±0.026	11.339±0.097	>9.022	15.920±0.077	15.979±0.183	>15.290	T8spec
WISEPA J073922.43+661502.5	SDSS J073922.26+661503.5	8	15.505±0.048	14.534±0.057	>12.456	>9.180	16.823±0.128	15.998±0.098	15.831±0.183	T1.5:
WISEPA J074148.97+235124.0	SDSS J074149.15+235127.5	16	15.833±0.065	14.110±0.052	>12.002	>8.450	16.158±0.101	15.838±0.185	>15.847	T5
WISEPA J074201.00+205517.1	SDSS J074201.41+205520.5	16	15.533±0.055	13.706±0.044	>11.982	>8.973	16.193±0.091	15.911±0.181	>15.225	T5
WISEPA J075547.93+221214.4	2MASS J0755480+221218	7	15.432±0.057	13.502±0.038	12.513±0.471	>9.107	15.728±0.064	15.669±0.145	15.753±0.207	T5
WISEPA J075840.16+324721.0	SDSS J075840.33+324723.4	16	13.110±0.027	12.169±0.026	10.673±0.093	>8.612	14.947±0.044	14.111±0.042	13.879±0.057	T2
WISEPA J081729.74-615504.1	DENIS J081730.0-615520	17	12.971±0.021	11.237±0.017	9.612±0.031	9.006±0.219	13.613±0.024	13.526±0.031	13.520±0.043	T6
WISEPA J083048.90+012826.9	SDSS J083048.80+012831.1	16	15.753±0.062	14.045±0.051	12.583±0.504	>8.602	16.289±0.111	16.140±0.213	>16.358	T4.5
WISEPA J083717.18-000021.2	SDSSp J083717.22-000018.3	18	15.393±0.047	14.678±0.071	>12.770	>9.163	17.101±0.214	15.988±0.173	>15.674	T1
WISEPA J085834.06+325628.2	SDSS J085834.42+325627.7	8	14.046±0.032	13.463±0.041	12.264±0.338	>9.243	16.453±0.115	15.382±0.101	14.756±0.095	T1
WISEPA J085910.62+101013.8	ULAS J085910.69+101017.1	19	17.330±0.252	15.408±0.165	>12.442	>9.372	17.880±0.060	18.580±0.060	18.260±0.150	T7
WISEPA J090900.49+652526.5	SDSS J090900.73+652527.2	8	14.470±0.044	13.424±0.050	—	> null	16.034±0.086	15.214±0.097	15.171±0.151	T1.5
WISEPA J092012.04+351740.1	2MASSW J0920122+351742	20	13.279±0.029	12.791±0.029	12.461±0.443	>9.200	15.625±0.063	14.673±0.057	13.979±0.061	T0p
WISEPA J092615.39+584718.8	SDSSp J092615.38+584720.9	6	15.237±0.039	13.656±0.035	12.732±0.431	>9.209	15.897±0.065	15.307±0.095	15.450±0.186	T4.5
WISEPC J092624.75+071138.3	ULAS J092624.76+071140.7	5	16.950±0.160	15.014±0.104	>12.683	>9.451	17.480±0.020	17.410±0.020	17.880±0.060	T3.5
WISEPC J093735.61+293127.7	2MASS J0937347+293142	7	14.074±0.030	11.652±0.023	10.686±0.089	>8.651	14.648±0.036	14.703±0.068	15.267±0.130	T6p
WISEPC J094908.57-154548.5	2MASS J09490860-1545485	2	14.881±0.043	14.004±0.068	12.516±0.529	>9.128	16.149±0.117	15.262±0.114	15.227±0.168	T2
WISEPC J100732.94-455512.9	2MASS J10073369-4555147	12	15.633±0.061	13.806±0.042	12.660±0.450	>9.276	15.653±0.068	15.686±0.122	15.560±0.229	T5
WISEPC J102109.57-030421.5	SDSS J102109.69-030420.1	18	14.814±0.037	13.773±0.041	12.249±0.324	>8.850	16.253±0.091	15.346±0.101	15.126±0.173	T3
WISEPC J103931.34+325624.7	SDSS J103931.35+325625.5	8	14.279±0.032	13.427±0.037	11.946±0.283	>8.699	16.405±0.148	15.335±0.111	15.151±0.159	T1
WISEPC J104829.08+091939.4	SDSS J104829.21+091937.8	8	15.303±0.047	14.276±0.060	12.543±0.503	9.362±0.482	16.594±0.151	15.898±0.159	>16.365	T2.5
WISEPC J105213.53+442254.6	SDSS J105213.51+442255.7	8	13.700±0.028	13.092±0.029	12.484±0.325	>8.957	15.958±0.098	15.161±0.098	14.568±0.094	T0.5:
WISEPC J105951.63+304159.0	2MASS J10595185+3042059	21	15.805±0.064	14.237±0.058	12.360±0.426	>9.090	16.195±0.088	15.766±0.118	15.560±0.181	T4
WISEPC J110611.72+275417.5	2MASS J11061197+2754225	12	13.181±0.028	12.333±0.027	11.551±0.174	>8.718	14.824±0.043	14.150±0.054	13.801±0.051	T2.5
WISEPC J111009.86+011608.7	SDSSp J111010.01+011613.1	6	15.586±0.055	13.989±0.048	11.891±0.253	>9.296	16.343±0.115	15.924±0.144	>15.129	T5.5

Table 1—Continued

WISE Designation <sup>a</sup>	Other Designation	Dis. Ref. (3)	W1 (mag) (4)	W2 (mag) (5)	W3 (mag) (6)	W4 (mag) (7)	J (mag) (8)	H (mag) (9)	K <sub>s</sub> (mag) (10)	Spec. Typ. <sup>b</sup> (11)
WISEPC J111448.80-261828.2	2MASS J11145133-2618235	2	15.346±0.048	12.235±0.025	11.171±0.134	>9.463	15.858±0.083	15.734±0.123	>16.109	T7.5
WISEPC J112208.14-351239.7	2MASS J11220826-3512363	2	13.926±0.030	12.766±0.028	11.716±0.195	>8.824	15.019±0.039	14.358±0.050	14.383±0.066	T2
WISEPC J115323.23-014828.0	ULAS J115338.74-014724.1	5	16.903±0.158	15.129±0.115	12.607±0.541	8.922±0.446	17.590±0.020	17.970±0.020	17.830±0.020	T6
WISEPC J115700.56+061103.2	SDSS J115700.50+061105.2	16	15.373±0.051	14.519±0.069	>12.312	>9.229	16.926±0.200	16.038±0.166	>15.251	T1.5
WISEPC J120257.02+090158.1	ULAS J120257.05+090158.8	5	16.844±0.141	14.905±0.088	>12.041	>8.744	16.710±0.030	16.910±0.020	16.940±0.020	T5
WISEPC J120602.54+281328.2	SDSS J120602.51+281328.7	8	15.246±0.049	13.971±0.049	>12.080	>9.519	16.541±0.109	15.815±0.126	>15.817	T3
WISEPC J120746.83+024426.3	SDSS J120747.17+024424.8	22	13.414±0.028	12.779±0.030	11.549±0.210	>8.884	15.580±0.071	14.561±0.065	13.986±0.059	T0
WISEPC J120956.33-100405.8	2MASS J12095613-1004008	10	14.636±0.037	13.492±0.040	11.759±0.249	>9.012	15.914±0.074	15.329±0.092	15.062±0.141	T3
WISEPC J121441.14+631643.6	SDSS J121440.95+631643.4	8	14.921±0.035	13.742±0.035	12.173±0.221	>9.636	16.586±0.119	15.779±0.162	15.877±0.233	T3.5:
WISEPC J121544.12+342103.9	2MASS J12154432-3420591	12	16.014±0.077	14.378±0.064	>12.327	>9.062	16.236±0.134	15.809±0.187	>16.317	T4.5:
WISEPC J121710.30-031113.2	2MASS J121710-031113	23	15.383±0.050	13.195±0.035	11.588±0.205	>9.372	15.860±0.061	15.748±0.119	>15.887	T7.5
WISEPC J122554.67-273954.0	2MASS J12255432-2739466	23	14.658±0.037	12.692±0.030	11.161±0.131	9.175±0.438	15.260±0.047	15.098±0.081	15.073±0.148	T6
WISEPC J123146.73+084722.3	2MASS J12314753+0847331	10	15.023±0.049	13.022±0.038	11.679±0.274	>8.781	15.570±0.072	15.309±0.112	15.220±0.195	T5.5
WISEPC J123737.39+652608.2	2MASS J12373919+6526148	23	15.427±0.046	12.922±0.028	11.935±0.212	>9.343	16.053±0.086	15.739±0.145	>16.058	T6.5
WISEPC J123828.37+095352.5	ULAS J123828.51+095351.3	24	>17.806	15.205±0.127	>12.453	>8.620	18.950±0.020	19.200±0.020	—	T8.5
WISEPC J125011.60+392547.8	SDSS J125011.65+392553.9	8	15.868±0.061	14.477±0.060	>12.404	>9.303	16.540±0.112	16.183±0.179	16.057±0.247	T4
WISEPC J125453.57-012245.8	SDSSp J125453.90-012247.4	18	13.328±0.029	12.399±0.026	10.886±0.111	8.757±0.295	14.891±0.035	14.090±0.025	13.837±0.054	T2
WISEPC J130041.65+122114.6	Ross 485C	25	16.121±0.096	13.706±0.042	11.654±0.200	>9.257	16.690±0.010	17.010±0.040	16.900±0.060	T8
WISEPC J130217.09+130850.7	ULAS J130217.21+130851.2	5	17.942±0.383	14.903±0.091	>11.958	>8.611	18.110±0.040	18.600±0.060	18.280±0.030	T8.5
WISEPC J132434.95+635827.5	2MASS J13243559+6358284	12	13.150±0.025	12.284±0.023	10.791±0.064	>9.671	15.596±0.067	14.576±0.056	14.058±0.059	T2:pec
WISEPC J133553.41+113004.7	ULAS J133553.45+113005.2	24	16.885±0.153	13.839±0.046	12.209±0.354	>9.027	17.900±0.010	18.250±0.010	18.280±0.030	T9
WISEPA J134646.09-003151.4	SDSSp J134646.45-003150.4	26	15.410±0.054	13.558±0.042	11.992±0.322	>8.456	16.000±0.102	15.459±0.118	15.772±0.274	T6.5
WISEPC J135852.69+374708.7	SDSS J135852.68+374711.9	8	16.122±0.080	14.122±0.052	12.373±0.373	>9.251	16.460±0.088	16.142±0.170	>16.099	T4.5:
WISEPA J140255.66+080053.9	SDSS J140255.66+080055.2	8	14.927±0.041	14.197±0.060	>12.570	>8.834	16.839±0.178	15.966±0.164	15.594±0.258	T1.5
WISEPA J140449.73-315933.0	2MASS J14044941-3159329	12	13.819±0.030	12.908±0.032	11.636±0.193	>9.045	15.577±0.062	14.955±0.067	14.538±0.095	T2.5
WISEPC J141530.10+572426.1	SDSS J141530.05+572428.7	8	14.830±0.033	13.925±0.037	12.386±0.268	>9.617	16.734±0.156	>15.821	>15.544	T3:
WISEPC J142950.87+333011.5	IRAC J142950.8+333011	27	16.541±0.109	14.981±0.096	>12.039	>9.256	>16.880	—	>16.990	T4.5
WISEPA J143553.29+112949.3	SDSS J143553.25+112948.6	8	15.260±0.047	14.168±0.058	>12.090	>9.090	17.137±0.232	>16.150	>16.906	T2:
WISEPA J143945.75+304219.2	SDSS J143945.86+304220.6	8	15.751±0.061	14.723±0.079	>12.466	>9.152	17.223±0.228	>16.280	>15.881	T2.5
WISEPA J145715.84-212207.5	Gliese 570D	28	14.959±0.063	12.106±0.029	10.687±0.119	>8.577	15.324±0.048	15.268±0.089	15.242±0.156	T7.5
WISEPA J145829.35+101341.8	CFBDSIR J145829+101343	29	>17.883	15.488±0.147	>12.421	>9.057	19.660±0.020	20.120±0.130	20.600±0.370	T8+
WISEPA J150319.70+252525.4	2MASS J15031961+2525196	30	13.455±0.034	11.685±0.027	10.766±0.116	>9.031	13.937±0.024	13.856±0.031	13.963±0.059	T5
WISEPA J150411.81+102717.4	SDSS J150411.63+102718.4	8	16.303±0.093	14.116±0.051	12.132±0.331	>9.073	17.032±0.231	>16.909	>17.023	T7
WISEPA J151114.49+060740.9	SDSS J151114.66+060742.9	8	13.676±0.028	13.154±0.033	12.542±0.492	>9.165	16.016±0.079	14.955±0.075	14.544±0.100	T0.:
WISEPA J151603.01+025927.6	SDSS J151603.03+025928.9	16	14.648±0.041	14.025±0.063	—	> null	17.230±0.203	15.997±0.146	15.433±0.178	T0:
WISEPA J151642.98+305344.3	SDSS J151643.01+305344.4	8	14.120±0.031	13.317±0.034	12.078±0.264	>9.119	16.848±0.154	15.868±0.161	15.081±0.091	T0.5:
WISEPA J152040.02+354617.2	SDSS J152039.82+354619.8	8	13.440±0.028	12.888±0.029	11.863±0.215	>9.011	15.540±0.058	14.579±0.053	14.000±0.054	T0:
WISEPA J152103.14+013144.1	SDSS J152103.24+013142.7	16	14.921±0.034	13.946±0.043	12.177±0.266	>8.884	16.399±0.102	15.576±0.099	15.347±0.171	T2:
WISEPA J153417.03+161547.0	SDSS J153417.05+161546.1AB	8	15.439±0.042	14.408±0.051	>12.517	>9.542	16.753±0.133	16.078±0.159	>16.411	T3.5
WISEPA J153449.98-295230.8	2MASS J1534498-295227	7	13.939±0.032	12.562±0.029	11.585±0.226	>9.064	14.900±0.054	14.866±0.102	14.843±0.114	T5.5
WISEPA J154614.83+493204.7	2MASS J15461461+4932114	31	14.489±0.031	13.446±0.031	12.076±0.220	>8.915	15.902±0.069	15.135±0.087	>14.900	T2.5:
WISEPA J154627.30-332508.0	2MASS J1546291-332511	7	15.238±0.070	13.434±0.044	>12.306	>8.664	15.631±0.051	15.446±0.092	15.485±0.181	T5.5
WISEPA J155301.94+153238.6	2MASS J1553022+153236	7	15.284±0.047	13.023±0.032	12.023±0.288	>9.204	15.825±0.071	15.939±0.163	15.507±0.182	T7
WISEPA J161504.36+134004.2	2MASS J16150413+1340079	12	16.077±0.073	14.109±0.049	12.633±0.456	>9.302	16.350±0.092	16.489±0.254	>15.859	T6
WISEPA J162414.09+002916.0	SDSSp J162414.37+002915.6	32	15.075±0.043	13.073±0.032	12.012±0.291	>9.103	15.494±0.054	15.524±0.100	>15.518	T6
WISEPA J162838.99+230818.1	SDSS J162838.77+230821.1	8	16.156±0.071	13.923±0.042	11.878±0.234	>9.163	16.458±0.104	16.107±0.151	15.872±0.240	T7
WISEPC J163022.92+081819.8	SDSS J163022.92+081822.0	8	16.151±0.083	14.348±0.062	>12.210	>9.418	16.396±0.113	16.332±0.291	>16.611	T5.5
WISEPA J163239.30+415002.9	SDSS J163239.34+415004.3	16	16.094±0.065	15.283±0.092	>12.713	>9.455	17.078±0.215	16.114±0.208	>15.748	T1:
WISEPA J175023.81+422239.0	SDSS J175024.01+422237.8	16	14.784±0.033	13.967±0.039	12.998±0.488	>9.424	16.467±0.101	15.415±0.088	15.482±0.168	T2

Table 1—Continued

WISE Designation <sup>a</sup>	Other Designation	Dis. Ref.	W1 (mag)	W2 (mag)	W3 (mag)	W4 (mag)	J (mag)	H (mag)	K <sub>s</sub> (mag)	Spec. Typ. <sup>b</sup>
(1)	(2)	(3)	(4)	(5)	(6)	(7)	(8)	(9)	(10)	(11)
WISEPA J175033.07+175905.5	SDSSp J175032.96+175903.9	6	15.826±0.068	14.424±0.059	>12.742	>8.905	16.340±0.101	15.952±0.132	15.478±0.189	T3.5
WISEPA J175805.46+463317.5	SDSS J175805.46+463311.9	16	15.662±0.041	13.790±0.031	12.543±0.282	>9.305	16.152±0.088	16.254±0.218	15.465±0.191	T6.5
WISEPA J182835.97-484903.0	2MASS J18283572-4849046	10	14.518±0.043	12.710±0.029	11.455±0.181	>8.970	15.175±0.056	14.908±0.067	15.181±0.144	T5.5
WISEPA J190106.18+471818.4	2MASS J19010601+4718136	10	15.301±0.042	13.579±0.032	12.462±0.258	>9.618	15.856±0.071	15.468±0.092	15.641±0.286	T5
WISEPC J205235.45-160928.7	SDSS J205235.31-160929.8	8	14.220±0.032	13.547±0.041	>12.366	>9.194	16.334±0.118	15.414±0.115	15.123±0.150	T1:
WISEPC J212414.00+010002.6	SDSS J212413.89+010000.3	16	15.607±0.050	14.142±0.049	>12.493	>9.238	16.031±0.074	16.183±0.200	>16.144	T5
WISEPC J213927.09+022023.7	2MASS J21392676+0220226	33	12.746±0.026	11.936±0.025	10.490±0.080	>9.018	15.264±0.049	14.165±0.053	13.582±0.045	T1.5
WISEPC J214428.77+144606.2	HN Peg B	34	13.291±0.029	12.574±0.029	11.670±0.179	>9.123	15.860±0.030	15.400±0.030	15.120±0.030	T2.5
WISEPC J215138.86-485356.2	2MASS J21513839-4853542	35	14.945±0.041	13.630±0.041	12.203±0.338	>9.432	15.730±0.074	15.168±0.096	15.431±0.184	T4
WISEPC J215432.94+594213.7	2MASS J21543318+5942187	12	15.732±0.074	13.599±0.035	>13.013	>9.678	15.661±0.070	15.765±0.168	>15.338	T5
WISEPC J220415.66-564723.5	eps Indi Bab	36	10.633±0.022	9.443±0.020	8.347±0.022	7.977±0.167	12.290±0.020	11.510±0.020	11.350±0.020	T2.5
WISEPC J222829.00-431029.4	2MASS J22282889-4310262	9	15.183±0.044	13.286±0.033	11.631±0.184	>8.937	15.662±0.073	15.363±0.117	15.296±0.206	T6
WISEPC J225418.97+312352.2	2MASSI J2254188+312349	7	14.627±0.035	13.246±0.031	11.995±0.237	>9.383	15.262±0.047	15.018±0.081	14.902±0.147	T4
WISEPC J230600.99+130225.2	ULAS J230601.02+130225.0	5	>17.793	15.001±0.090	>12.801	>8.841	17.570±0.020	18.000±0.020	18.030±0.030	T6.5
WISEPC J231557.68+132255.6	ULAS J231557.61+132256.2	5	17.951±0.369	15.414±0.134	>12.458	>9.301	17.710±0.050	18.160±0.050	18.140±0.030	T6.5
WISEPC J232035.36+144830.2	ULAS J232035.28+144829.8	37	16.609±0.111	14.302±0.056	>12.633	>9.266	16.790±0.020	17.140±0.020	17.400±0.020	T5
WISEPC J232123.83+135453.5	ULAS J232123.79+135454.9	37	17.186±0.202	14.060±0.053	>12.394	>9.435	16.720±0.030	17.150±0.030	17.160±0.010	T7.5
WISEPC J232802.12+134545.2	ULAS J232802.03+134544.8	5	18.194±0.522	15.111±0.111	>12.617	>8.758	17.750±0.020	18.170±0.020	18.290±0.020	T7
WISEPC J233123.87-471828.0	2MASS J23312378-4718274	10	14.793±0.040	13.361±0.037	11.558±0.223	9.020±0.512	15.659±0.068	15.510±0.149	15.389±0.196	T5
WISEPC J233910.51+135218.8	2MASSI J2339101+135230	7	15.136±0.043	13.746±0.042	>12.215	>9.248	16.239±0.109	15.822±0.151	16.147±0.307	T5
WISEPC J235654.40-155318.5	2MASSI J2356547-155310	7	15.532±0.054	13.641±0.041	12.012±0.293	>9.508	15.824±0.057	15.630±0.100	15.771±0.183	T5.5
L Dwarfs:										
WISEPC J001544.82+351600.0	2MASSW J0015447+351603	20	11.790±0.024	11.538±0.024	10.912±0.097	>8.985	13.878±0.030	12.892±0.036	12.264±0.024	L2
WISEPC J003043.78+313931.8	2MASSW J0030438+313932	38	13.485±0.030	13.129±0.036	11.956±0.326	>9.239	15.480±0.054	14.617±0.057	14.027±0.048	L2
WISEPA J012912.38+351757.4	2MASSW J0129122+351758	38	14.089±0.032	13.677±0.042	12.117±0.308	>9.283	16.779±0.159	15.343±0.093	14.696±0.080	L4
WISEPA J013118.73+380155.0	2MASS J01311838+3801554	39	12.544±0.017	12.214±0.018	11.975±0.275	>9.171	14.679±0.034	13.696±0.034	13.054±0.034	L4:
WISEPC J013535.83+120517.7	2MASSW J0135358+120522	20	12.510±0.025	12.258±0.025	11.717±0.254	>8.987	14.412±0.032	13.527±0.032	12.918±0.029	L1.5
WISEPC J014435.67-071616.3	2MASS J01443536-0716142	40	11.630±0.026	11.356±0.023	10.812±0.099	>8.841	14.191±0.026	13.008±0.029	12.268±0.023	L5
WISEPA J014733.46+345310.5	2MASSW J0147334+345311	38	13.178±0.026	12.863±0.031	11.679±0.190	>9.194	14.946±0.039	14.162±0.041	13.574±0.038	L0.5
WISEPC J020333.45-010813.4	SDSS J020333.26-010812.5	16	15.414±0.058	14.760±0.096	>12.479	>8.700	>16.858	16.516±0.243	16.076±0.323	L9.5 (IR)
WISEPA J020503.70+125142.2	2MASSW J0205034+125142	20	12.920±0.026	12.526±0.027	11.440±0.207	>8.764	15.679±0.056	14.449±0.047	13.671±0.036	L5
WISEPC J020529.69-115929.1	DENIS-P J0205.4-1159	41	12.219±0.027	11.768±0.025	10.865±0.119	>8.651	14.587±0.030	13.568±0.037	12.998±0.030	L7
WISEPA J020735.76+135554.4	SDSS J020735.60+135556.3	22	13.478±0.029	13.228±0.037	>12.495	>8.958	15.462±0.049	14.474±0.043	13.808±0.046	L3
WISEPA J020818.65+254253.0	2MASSW J0208183+254253	20	12.193±0.026	11.924±0.026	11.326±0.328	—	13.989±0.026	13.107±0.030	12.588±0.027	L1
WISEPA J020823.82+273738.7	2MASSW J0208236+273740	20	13.268±0.028	12.955±0.038	12.065±0.407	>8.526	15.714±0.060	14.560±0.059	13.872±0.051	L5
WISEPA J020854.98+250049.0	2MASSW J0208549+250048	20	13.656±0.032	13.251±0.048	>11.418	>8.106	16.206±0.093	14.974±0.080	14.405±0.069	L5
WISEPC J021828.98-313324.1	2MASSI J0218291-313322	42	12.610±0.026	12.292±0.025	12.153±0.288	>9.474	14.728±0.040	13.808±0.037	13.154±0.035	L3
WISEPC J021928.20-193842.7	SSSPM J0219-1939	43	12.552±0.026	12.332±0.027	12.309±0.365	>8.868	14.110±0.027	13.339±0.028	12.910±0.034	L1
WISEPC J022710.62-162450.7	2MASS J02271036-1624479	33	11.793±0.025	11.548±0.023	11.163±0.126	>8.842	13.573±0.023	12.630±0.024	12.143±0.030	L1
WISEPA J022811.20+253737.8	2MASSW J0228110+253738	44	12.123±0.024	11.889±0.024	11.392±0.174	>9.240	13.839±0.027	12.993±0.024	12.471±0.025	L0:
WISEPA J023015.66+270405.9	2MASS J02301551+2704061	39	12.642±0.025	12.378±0.027	11.909±0.287	>9.023	14.294±0.027	13.478±0.029	12.986±0.023	L0:
WISEPA J023547.53-084919.7	SDSS J023547.56-084919.8	22	13.762±0.031	13.493±0.039	>12.048	>9.076	15.571±0.055	14.812±0.056	14.191±0.067	L2
WISEPA J023618.01+004852.8	SDSSp J023617.93+004855.0	6	13.806±0.029	13.360±0.036	12.362±0.393	>9.050	16.098±0.077	15.265±0.066	14.666±0.091	L6
WISEPA J023942.48-173548.3	2MASSI J0239424-173547	42	12.705±0.025	12.407±0.026	11.717±0.227	>8.598	14.291±0.029	13.525±0.034	13.039±0.030	L0
WISEPA J024153.91-124107.5	2MASSI J0241536-124106	42	13.603±0.028	13.271±0.032	12.675±0.493	>9.295	15.605±0.068	14.646±0.062	13.931±0.063	L2:
WISEPA J024243.68+160737.6	2MASSW J0242435+160739	38	13.897±0.030	13.495±0.040	>12.324	>9.075	15.776±0.053	14.998±0.054	14.349±0.058	L1.5
WISEPA J025601.91+011046.3	SDSS J025601.86+011047.2	22	14.919±0.042	14.526±0.078	>12.464	>9.080	16.212±0.102	15.696±0.184	15.216±0.175	L0
WISEPA J030136.57+002057.0	SDSSp J030136.53+002057.9	45	15.512±0.052	15.215±0.113	>12.585	>9.167	16.882±0.190	16.326±0.278	>15.619	L1:



Table 1—Continued

WISE Designation <sup>a</sup>	Other Designation	Dis. Ref.	W1 (mag)	W2 (mag)	W3 (mag)	W4 (mag)	J (mag)	H (mag)	K <sub>s</sub> (mag)	Spec. Typ. <sup>b</sup>
(1)	(2)	(3)	(4)	(5)	(6)	(7)	(8)	(9)	(10)	(11)
WISEPA J030321.24-000938.0	SDSSp J030321.24-000938.2	45	14.645±0.036	14.215±0.057	12.451±0.436	>8.742	16.120±0.072	15.609±0.128	14.880±0.103	L0
WISEPA J030909.04-194939.0	2MASSW J0309088-194938	20	13.380±0.027	13.071±0.028	12.746±0.361	>9.444	15.752±0.056	14.656±0.062	14.057±0.065	L4.5
WISEPA J031013.90-275645.8	2MASS J03101401-2756452	39	13.183±0.026	12.820±0.029	12.336±0.357	>9.008	15.795±0.071	14.662±0.049	13.959±0.061	L5
WISEPA J031645.21-284852.8	2MASSI J0316451-284852	42	12.681±0.025	12.315±0.025	11.928±0.226	>9.191	14.570±0.040	13.770±0.030	13.110±0.030	L0:
WISEPA J031854.37-342128.7	2MASS J03185403-3421292	46	12.622±0.025	12.123±0.024	11.157±0.104	>9.214	15.569±0.055	14.346±0.044	13.507±0.039	L7
WISEPA J033703.73-175806.6	2MASSW J0337036-175807	20	12.832±0.026	12.445±0.027	11.866±0.228	>9.151	15.621±0.058	14.412±0.050	13.581±0.041	L4.5
WISEPA J035822.59-411605.0	2MASS J03582255-4116060	33	12.900±0.026	12.430±0.024	11.658±0.150	>9.419	15.846±0.087	14.608±0.057	13.838±0.049	L5
WISEPA J065219.57-253449.5	DENIS-P J0652197-253450	47	11.125±0.024	10.792±0.022	10.355±0.059	>8.784	12.759±0.023	12.020±0.021	11.516±0.021	L0
WISEPA J065230.58+471036.3	2MASSI J0652307+471034	42	10.874±0.024	10.505±0.020	9.860±0.048	8.978±0.496	13.511±0.023	12.384±0.024	11.694±0.020	L4.5
WISEPA J071716.22+570543.6	2MASSW J0717163+570543	44	12.303±0.025	11.935±0.024	11.340±0.152	>8.907	14.636±0.032	13.593±0.030	12.945±0.026	L3
WISEPC J071932.08-505141.5	2MASS J07193188-5051410	33	12.441±0.026	12.213±0.025	11.579±0.135	>9.190	14.094±0.032	13.282±0.035	12.773±0.027	L0
WISEPA J072314.69+572705.6	2MASS J07231462+5727081	33	12.291±0.026	12.046±0.023	11.668±0.191	>8.427	13.970±0.026	13.156±0.030	12.613±0.030	L1
WISEPA J074642.23+200032.5	2MASSI J0746425+200032	48	10.133±0.024	9.866±0.022	9.383±0.039	>8.985	11.759±0.020	11.007±0.022	10.468±0.022	L0.5
WISEPA J075259.41+413634.6	SDSS J075259.43+413634.6	22	14.919±0.040	14.749±0.079	>12.600	>8.969	16.356±0.131	15.601±0.160	>15.191	L0
WISEPA J075332.07+291710.3	2MASSI J0753321+291711	20	13.319±0.028	13.002±0.031	>11.874	>8.419	15.516±0.048	14.527±0.040	13.849±0.043	L2
WISEPA J075515.18+293445.0	SDSS J075515.26+293445.4	16	15.151±0.047	14.817±0.097	>12.325	>9.073	17.229±0.194	16.231±0.175	15.638±0.198	L3.5: (IR)
WISEPA J075625.28+124454.2	2MASSI J0756252+124456	20	14.190±0.032	13.577±0.036	>12.032	>8.803	16.659±0.139	15.758±0.150	14.730±0.115	L6
WISEPA J075656.43+231455.4	SDSS J075656.54+231458.5	16	14.179±0.034	13.830±0.047	>11.893	>9.174	16.773±0.145	15.552±0.145	14.994±0.101	L3.5: (IR)
WISEPA J080048.13+465825.8	SDSS J080048.13+465825.5	22	13.806±0.028	13.547±0.038	>12.307	>9.124	15.513±0.070	14.549±0.058	14.315±0.078	L2
WISEPA J080140.31+462845.8	2MASSW J0801405+462850	20	13.937±0.030	13.674±0.038	>12.846	>9.310	16.275±0.134	15.452±0.142	14.536±0.100	L6.5
WISEPA J080322.74+123845.2	SDSS J080322.77+123845.3	49	14.625±0.036	14.313±0.062	>12.339	>8.947	16.308±0.083	15.436±0.075	15.227±0.114	L2.5
WISEPA J080531.37+481233.7	SDSS J080531.84+481233.0	22	12.886±0.026	12.429±0.025	11.971±0.257	>8.829	14.734±0.036	13.917±0.041	13.444±0.041	L4
WISEPA J080958.86+443419.5	SDSS J080959.01+443422.2	16	13.340±0.027	12.802±0.028	11.601±0.183	>9.002	16.437±0.114	15.184±0.098	14.417±0.059	L6 (IR)
WISEPC J081231.81-244443.9	DENIS-P J0812316-244442	47	12.046±0.025	11.817±0.023	11.351±0.134	>9.100	13.817±0.029	12.929±0.027	12.391±0.024	L2.5+/-1
WISEPA J082029.82+450027.4	2MASSW J0820299+450031	20	13.512±0.026	13.174±0.033	12.221±0.324	>8.996	16.279±0.108	15.000±0.087	14.218±0.066	L5
WISEPA J082030.08+103736.8	SDSS J082030.12+103737.0	8	14.703±0.038	14.171±0.060	12.083±0.347	>8.911	16.980±0.185	16.079±0.191	15.538±0.190	L9.5: (IR)
WISEPA J082307.65+612518.5	2MASS J08230838+6125208	33	12.747±0.026	12.407±0.025	12.502±0.381	>8.989	14.820±0.036	13.814±0.037	13.196±0.029	L2:
WISEPA J082348.05+242858.2	2MASS J08234818+2428577	33	12.812±0.026	12.478±0.027	12.034±0.265	>9.070	14.986±0.043	14.060±0.044	13.377±0.030	L3
WISEPA J082906.58+145619.6	2MASSW J0829066+145622	20	12.817±0.026	12.519±0.029	>12.156	>8.997	14.750±0.030	13.801±0.036	13.166±0.033	L2
WISEPA J082957.00+265509.4	2MASSW J0829570+265510	20	13.897±0.031	13.391±0.038	>12.625	>9.089	17.109±0.186	15.807±0.129	14.959±0.095	L6.5
WISEPA J083204.55-012835.8	2MASSW J0832045-012835	20	12.408±0.026	12.160±0.026	11.627±0.220	>9.026	14.128±0.030	13.318±0.023	12.712±0.027	L1.5
WISEPA J083506.10+195303.6	SDSS J083506.16+195304.4	8	13.609±0.029	13.166±0.040	>11.939	>8.618	16.094±0.075	14.889±0.057	14.319±0.049	L4.5 (IR)
WISEPA J083558.21+054830.5	2MASS J08355829+0548308	33	12.715±0.026	12.388±0.027	11.997±0.287	>8.443	14.533±0.036	13.683±0.037	13.168±0.034	L2:
WISEPA J084016.40+543001.4	SDSS J084016.42+543002.1	49	14.758±0.035	14.365±0.057	12.772±0.499	>9.106	16.393±0.117	15.512±0.127	15.347±0.153	L1
WISEPC J084728.84-153239.4	2MASSI J0847287-153237	42	11.710±0.026	11.452±0.023	10.925±0.089	>9.052	13.513±0.026	12.629±0.027	12.061±0.023	L2
WISEPA J085234.85+472031.0	SDSS J085234.90+472035.0	16	13.762±0.029	13.183±0.031	11.738±0.185	>9.056	16.182±0.109	15.419±0.146	14.718±0.116	L9.5: (IR)
WISEPA J085757.95+570847.5	SDSSp J085758.45+570851.4	6	12.026±0.026	11.416±0.022	10.298±0.058	8.768±0.351	15.038±0.040	13.790±0.042	12.962±0.030	L8
WISEPA J085938.38+634130.4	2MASS J08593854+6341355	33	12.000±0.026	11.753±0.022	11.434±0.133	>9.135	13.701±0.029	12.890±0.030	12.387±0.026	L0
WISEPC J090347.54+011445.2	SDSS J090347.55+011446.0	49	14.555±0.034	14.235±0.051	>12.855	>9.400	16.449±0.139	15.603±0.105	14.887±0.128	L2
WISEPA J090546.55+562312.9	2MASS J09054654+5623117	33	12.995±0.027	12.643±0.027	12.172±0.277	>9.113	15.395±0.052	14.284±0.041	13.730±0.037	L5
WISEPA J090837.56+503203.6	2MASSI J0908380+503208	42	12.100±0.024	11.635±0.024	10.709±0.093	>9.153	14.549±0.023	13.477±0.030	12.945±0.027	L5
WISEPC J090957.35-065818.4	DENIS-P J0909-0658	50	12.218±0.024	11.965±0.024	11.188±0.136	>8.466	13.890±0.024	13.090±0.021	12.539±0.026	L0
WISEPA J091112.50+740106.6	2MASS J09111297+7401081	33	11.344±0.025	11.019±0.021	10.543±0.062	>8.896	12.921±0.027	12.205±0.029	11.748±0.026	L0
WISEPC J091303.23+184147.9	2MASSW J0913032+184150	38	13.756±0.030	13.417±0.038	>12.600	>9.136	15.966±0.055	14.844±0.048	14.279±0.052	L3
WISEPC J091534.08+042205.1	2MASS J09153413+0422045	33	12.077±0.024	11.704±0.022	10.952±0.119	>9.502	14.548±0.030	13.531±0.032	13.011±0.041	L7
WISEPA J091714.75+314824.1	SDSS J091714.76+314824.8	49	14.760±0.037	14.494±0.071	>11.971	>8.955	16.297±0.103	15.731±0.135	15.011±0.130	L2
WISEPC J091838.44+213404.1	2MASSW J0918382+213406	38	13.377±0.027	13.067±0.033	12.534±0.517	9.153±0.526	15.662±0.061	>14.580	13.903±0.043	L2.5
WISEPA J092757.41+602746.0	SDSS J092757.46+602746.3	22	13.851±0.028	13.547±0.034	>12.380	>9.218	15.520±0.055	14.743±0.055	14.231±0.056	L1
WISEPC J092933.44+342951.8	2MASSW J0929336+342952	20	13.868±0.031	13.253±0.033	12.093±0.292	>9.158	16.601±0.125	15.440±0.103	14.644±0.104	L8

Table 1—Continued

WISE Designation <sup>a</sup>	Other Designation	Dis. Ref.	W1 (mag)	W2 (mag)	W3 (mag)	W4 (mag)	J (mag)	H (mag)	K <sub>s</sub> (mag)	Spec. Typ. <sup>b</sup>
(1)	(2)	(3)	(4)	(5)	(6)	(7)	(8)	(9)	(10)	(11)
WISEPC J094402.83+313132.1	2MASSW J0944027+313132	20	13.576±0.027	13.265±0.034	12.745±0.526	>8.614	15.495±0.048	14.629±0.047	14.007±0.042	L2
WISEPC J102214.76+411425.6	HD 89744B	51	13.055±0.025	12.759±0.029	>12.021	>8.766	14.901±0.037	14.022±0.033	13.608±0.039	L0
WISEPC J102552.58+321231.5	SDSS J102552.43+321234.0	8	14.396±0.031	14.033±0.045	12.509±0.396	>9.395	>15.913	15.593±0.167	15.072±0.184	L7.5: (IR)
WISEPC J102947.62+483411.8	SDSS J102947.68+483412.2	49	15.240±0.044	15.063±0.101	12.773±0.539	9.128±0.462	16.764±0.193	16.039±0.212	15.585±0.238	L0
WISEPC J103322.01+400547.8	SDSS J103321.92+400549.5	8	14.846±0.036	14.568±0.066	>12.258	>8.967	16.644±0.162	15.874±0.181	>15.408	L6 (IR)
WISEPC J103602.46+372447.4	SDSS J103602.44+372448.5	49	14.896±0.037	14.603±0.067	>12.351	>9.434	16.420±0.116	15.541±0.132	14.993±0.114	L0
WISEPC J105118.71+561305.5	2MASS J10511900+5613086	33	11.517±0.024	11.257±0.023	10.758±0.080	>9.098	13.244±0.026	12.423±0.032	11.905±0.024	L2
WISEPC J110009.49+495745.4	2MASS J11000965+4957470	33	12.960±0.027	12.610±0.025	12.172±0.255	>8.801	15.282±0.043	14.192±0.041	13.474±0.033	L3.5
WISEPA J110830.33+683014.8	2MASSW J1108307+683017	52	11.123±0.026	10.759±0.021	10.151±0.045	>9.464	13.123±0.024	12.235±0.021	11.583±0.019	L1
WISEPC J113833.15+674038.8	SDSS J113833.10+674040.3	22	13.630±0.028	13.336±0.032	>12.553	>9.527	15.215±0.041	14.482±0.050	13.950±0.046	L0
WISEPC J115442.09-340038.8	2MASS J11544223-3400390	53	12.363±0.025	12.051±0.025	11.552±0.172	>9.502	14.195±0.033	13.331±0.028	12.851±0.033	L0
WISEPC J120703.54-315130.5	2MASS J12070374-3151298	33	13.584±0.029	13.237±0.033	>12.420	>9.059	15.850±0.066	14.719±0.052	13.997±0.057	L3:
WISEPC J120737.92-390904.6	2MASS J12073804-3909050	33	12.886±0.028	12.540±0.025	12.238±0.281	>9.048	16.689±0.040	13.817±0.027	13.244±0.038	L2:
WISEPC J122815.35-154736.4	DENIS-P J1228.2-1547	41	12.009±0.023	11.670±0.024	10.995±0.124	>9.162	14.378±0.030	13.347±0.032	12.767±0.030	L5
WISEPC J125656.74+014615.9	2MASS J12565688+0146163	33	12.332±0.025	12.043±0.024	11.523±0.197	>9.018	14.480±0.030	13.516±0.031	12.791±0.030	L2:
WISEPC J125737.34-011336.5	SDSSp J125737.26-011336.1	6	13.488±0.028	13.183±0.036	>11.856	>8.969	15.941±0.084	14.722±0.057	14.123±0.070	L4
WISEPC J130154.60-151023.0	2MASS J13015465-1510223	33	12.794±0.028	12.520±0.028	11.961±0.297	>9.196	14.538±0.037	13.665±0.027	13.098±0.030	L1
WISEPA J130539.94-254106.1	Kelu-1Aab	54	11.248±0.025	10.909±0.024	10.372±0.077	>9.051	13.414±0.026	12.392±0.025	11.747±0.023	L2
WISEPA J131530.35-264954.6	2MASSI J1315309-264951	55	12.733±0.025	12.280±0.025	11.870±0.275	>8.957	15.195±0.051	14.058±0.035	13.462±0.043	L5.5
WISEPA J132619.81-272937.2	2MASSW J1326201-272937	56	12.863±0.026	12.329±0.026	11.275±0.166	>8.560	15.847±0.071	14.741±0.058	13.852±0.054	L5
WISEPC J132629.66-003832.6	SDSSp J132629.82-003831.5	57	13.267±0.027	12.718±0.030	11.824±0.270	>9.150	16.103±0.071	15.050±0.060	14.208±0.067	L8:
WISEPC J133406.18+194036.4	2MASSW J1334062+194034	38	13.678±0.029	13.388±0.035	12.207±0.322	>9.170	15.477±0.060	14.833±0.066	14.001±0.054	L1.5
WISEPA J134111.63-305252.1	2MASS J13411160-3052505	33	12.736±0.026	12.386±0.026	11.952±0.288	>9.039	14.607±0.033	13.725±0.033	13.081±0.026	L2::
WISEPC J134203.12+134022.4	SDSS J134203.11+134022.2	8	14.523±0.084	13.874±0.130	>11.353	>7.451	16.756±0.144	15.708±0.110	15.109±0.142	L5.5 (IR)
WISEPA J135955.14-403503.3	2MASS J13595510-4034582	33	12.179±0.024	11.885±0.023	11.342±0.141	>9.241	13.645±0.026	13.034±0.028	12.566±0.029	L1
WISEPA J140231.60+014830.1	SDSS J140231.75+014830.3	22	13.806±0.031	13.435±0.039	12.310±0.452	>9.046	15.451±0.063	14.653±0.070	14.176±0.071	L1
WISEPA J140441.70+023547.5	SDSS J140441.68+023550.1	22	14.188±0.032	13.889±0.050	>11.891	>8.882	15.601±0.058	14.908±0.067	14.530±0.103	L1
WISEPA J140753.39+124111.0	2MASS J14075361+1241099	33	13.048±0.026	12.734±0.028	11.915±0.262	>9.028	15.378±0.055	14.344±0.052	13.598±0.043	L1::
WISEPA J140903.19-335755.8	2MASS J14090310-3357565	46	12.569±0.026	12.278±0.028	12.001±0.289	>9.098	14.248±0.026	13.424±0.033	12.865±0.029	L2
WISEPA J141011.08+132900.8	SDSS J141011.14+132900.8	49	15.166±0.048	15.019±0.110	>12.196	>8.902	16.846±0.141	15.894±0.146	15.531±0.187	L4
WISEPA J141224.51+163310.5	2MASSW J1412244+163312	20	12.172±0.027	11.895±0.024	11.429±0.182	>8.828	13.888±0.029	13.150±0.036	12.521±0.029	L0.5
WISEPA J142227.23+221558.3	SDSS J142227.25+221557.1	8	14.930±0.038	14.649±0.073	>12.830	>9.104	17.064±0.181	16.032±0.156	15.642±0.172	L6.5: (IR)
WISEPA J142438.96+091709.8	GD 165B	58	13.214±0.027	13.010±0.032	>12.466	>9.095	15.687±0.078	14.781±0.070	14.169±0.095	L4
WISEPA J143043.42+291542.1	2MASSI J1430435+291540	44	12.328±0.025	12.002±0.025	11.201±0.136	>8.465	14.273±0.028	13.439±0.027	12.771±0.025	L2
WISEPA J143055.92+001351.8	SDSS J143055.90+001352.1	22	14.663±0.036	14.320±0.063	>12.506	>8.435	16.290±0.114	15.375±0.081	14.981±0.133	L0
WISEPA J143130.64+143653.0	2MASS J14313097+1436539	21	13.715±0.029	13.360±0.037	12.556±0.520	>9.140	15.151±0.041	14.501±0.048	14.125±0.062	L2
WISEPA J143517.22-004612.6	SDSS J143517.20-004612.9	22	15.071±0.046	14.744±0.091	>12.107	>8.924	16.484±0.097	15.613±0.115	15.321±0.175	L0
WISEPA J143535.75-004347.4	SDSS J143535.72-004347.0	22	14.896±0.044	14.694±0.091	>12.450	>8.405	16.488±0.116	15.664±0.116	15.025±0.137	L3
WISEPA J143855.11-130910.8	2MASSW J1438549-130910	20	13.288±0.027	12.930±0.034	11.747±0.280	>8.250	15.490±0.057	14.504±0.045	13.863±0.053	L3:
WISEPA J143940.90+182637.7	2MASSW J1439409+182637	38	14.331±0.034	13.970±0.054	>12.224	8.792±0.463	16.220±0.104	15.454±0.107	14.542±0.103	L1
WISEPA J144001.75+002146.7	SDSSp J144001.82+002145.8	57	14.100±0.030	13.835±0.046	>12.625	>9.056	15.948±0.078	15.080±0.090	14.598±0.092	L1
WISEPA J144016.21+002639.5	SDSS J144016.20+002638.9	22	14.280±0.032	13.955±0.050	>12.115	>9.024	16.069±0.114	15.414±0.123	14.815±0.143	L3
WISEPA J144600.73+002451.2	SDSSp J144600.60+002452.0	6	13.253±0.027	12.900±0.032	11.946±0.300	>8.712	15.894±0.082	14.514±0.035	13.935±0.053	L6
WISEPC J144938.12+235536.3	2MASSW J1449378+235537	20	14.241±0.032	14.528±0.095	>12.473	9.216±0.311	15.818±0.075	15.004±0.087	14.311±0.085	L0
WISEPA J151136.27+353511.5	SDSS J151136.24+353511.4	49	14.618±0.035	14.236±0.055	>12.632	>9.139	16.294±0.099	15.621±0.114	14.946±0.117	L1
WISEPA J151506.18+443648.1	SDSS J151506.11+443648.3	8	13.982±0.029	13.465±0.033	12.331±0.300	>8.848	16.583±0.152	15.636±0.158	14.757±0.137	L7.5: (IR)
WISEPA J152322.73+301454.3	Gl 584C	59	13.555±0.034	12.994±0.035	11.919±0.262	>9.187	16.056±0.099	14.928±0.081	14.348±0.067	L8
WISEPA J152613.85+204337.0	2MASSI J1526140+204341	20	13.147±0.027	12.794±0.029	12.180±0.305	>8.734	15.586±0.055	14.497±0.044	13.922±0.052	L7
WISEPA J154009.25+374227.7	SDSS J154009.36+374230.3	8	13.999±0.030	13.568±0.037	12.113±0.279	>9.053	16.558±0.138	15.348±0.101	14.739±0.081	L9: (IR)

Table 1—Continued

WISE Designation <sup>a</sup>	Other Designation	Dis. Ref.	W1 (mag)	W2 (mag)	W3 (mag)	W4 (mag)	J (mag)	H (mag)	K <sub>s</sub> (mag)	Spec. Typ. <sup>b</sup>
(1)	(2)	(3)	(4)	(5)	(6)	(7)	(8)	(9)	(10)	(11)
WISEPA J154508.84+355528.5	SDSS J154508.93+355527.3	8	14.587±0.033	14.116±0.047	>12.566	>9.099	16.834±0.167	15.997±0.190	15.427±0.158	L7.5
WISEPA J161542.46+495321.3	2MASS J16154255+4953211	39	13.221±0.027	12.598±0.025	12.428±0.261	>8.862	16.789±0.138	15.332±0.098	14.306±0.070	L4
WISEPA J163229.39+190439.9	2MASSW J1632291+190441	38	13.143±0.027	12.620±0.026	11.703±0.187	>9.398	15.867±0.070	14.612±0.038	14.003±0.047	L8
WISEPC J171714.33+652620.9	SDSS J171714.10+652622.2	22	12.540±0.024	12.212±0.023	11.553±0.109	>9.827	14.950±0.041	13.840±0.035	13.177±0.031	L4
WISEPA J172006.70+615536.5	SDSS J172006.69+615537.7	49	15.366±0.036	15.252±0.067	>13.442	>9.372	—	—	—	L3
WISEPA J180715.97+501530.2	2MASSI J1807159+501531	42	11.249±0.025	10.966±0.022	10.483±0.049	>8.967	12.934±0.024	12.127±0.031	11.602±0.025	L1.5
WISEPA J184108.66+311728.3	2MASSW J1841086+311727	20	13.612±0.031	13.235±0.033	12.762±0.371	>9.017	16.158±0.091	14.971±0.066	14.220±0.070	L4pec
WISEPA J190908.18-193749.6	DENIS-P J1909081-193748	47	12.464±0.030	12.156±0.050	—	> null	14.520±0.029	13.543±0.027	12.915±0.029	L1+/-1
WISEPA J200250.64-052153.6	2MASS J20025073-0521524	39	12.531±0.024	12.068±0.026	11.088±0.144	>8.553	15.316±0.051	14.278±0.050	13.417±0.036	L6
WISEPC J202820.42+005226.6	SDSS J202820.32+005226.5	22	12.301±0.024	12.018±0.024	11.273±0.160	8.929±0.447	14.298±0.035	13.377±0.031	12.793±0.030	L3
WISEPC J203437.63+082656.0	2MASS J20343769+0827009	33	12.749±0.027	12.557±0.031	11.773±0.298	>8.225	14.464±0.034	13.593±0.035	13.080±0.031	L1
WISEPC J203603.08+105127.8	2MASS J20360316+1051295	33	11.900±0.024	11.600±0.025	11.044±0.137	>8.995	13.950±0.026	13.018±0.022	12.447±0.027	L3
WISEPA J204142.87-350645.8	2MASS J20414283-3506442	39	12.866±0.027	12.555±0.027	12.203±0.336	>8.779	14.887±0.033	13.987±0.021	13.401±0.037	L2:
WISEPC J204317.70-155104.0	SDSS J204317.69-155103.4	8	14.775±0.039	14.160±0.056	11.769±0.246	9.297±0.469	16.625±0.162	16.054±0.197	15.402±0.214	L9 (IR)
WISEPC J205754.09-025230.9	2MASSI J2057540-025230	42	11.281±0.023	10.985±0.020	10.343±0.076	>9.101	13.121±0.024	12.268±0.024	11.724±0.025	L1.5
WISEPA J210754.20-454406.2	2MASS J21075409-4544064	33	12.942±0.027	12.628±0.027	12.814±0.543	>9.137	14.915±0.032	13.953±0.038	13.380±0.034	L0:
WISEPC J220645.11-421723.1	2MASSW J2206450-421721	20	12.855±0.026	12.371±0.026	11.840±0.229	>9.392	15.555±0.066	14.447±0.061	13.609±0.055	L2
WISEPC J224316.94-593223.0	2MASS J22431696-5932206	60	12.480±0.025	12.262±0.026	11.429±0.197	>8.359	14.074±0.030	13.386±0.031	12.837±0.029	L0:
M Dwarfs:										L7
WISEPC J002127.85-635108.6	F 079-18 <sup>h</sup>	80	9.909±0.024	9.655±0.021	9.381±0.031	9.418±0.510	11.021±0.021	10.483±0.027	10.108±0.023	M9.5 V
WISEPC J003519.14+280715.5	CTI 003439.1+280309	62	12.021±0.024	11.852±0.022	11.401±0.146	>8.950	13.015±0.017	12.458±0.024	12.163±0.019	M4 V
WISEPC J004324.51+280543.7	CTI 004244.4+280140	62	14.040±0.031	13.815±0.040	>12.893	>9.414	15.217±0.053	14.641±0.061	14.288±0.060	M6 V
WISEPC J004446.85+280741.8	CTI 004406.7+280336	62	12.544±0.027	12.413±0.025	12.000±0.248	8.935±0.368	13.533±0.018	12.915±0.018	12.710±0.025	M1.5 V
WISEPC J004605.87+280841.3	CTI 004525.7+280437	62	13.481±0.031	13.202±0.034	12.077±0.319	>8.900	14.544±0.029	13.959±0.032	13.673±0.045	M4.5 V
WISEPC J010412.78+280634.3	CTI 010332.0+280234	62	11.938±0.024	11.746±0.024	11.537±0.191	>9.029	12.909±0.019	12.315±0.022	12.069±0.020	M3.5 V
WISEPC J011749.92+280245.3	CTI 011708.6+275850	62	13.446±0.027	13.261±0.035	>12.704	>9.258	14.420±0.026	13.793±0.028	13.574±0.042	M3.5 V
WISEPA J011908.43+280910.9	CTI 011826.7+280514	62	13.579±0.029	13.333±0.038	>12.223	>9.154	14.817±0.036	14.189±0.041	13.822±0.047	M6 V
WISEPA J012559.40+280640.4	CTI 012517.7+280247	62	13.776±0.031	13.738±0.045	>12.079	>9.103	14.767±0.035	14.075±0.042	13.888±0.058	M0 V
WISEPA J012739.04+280552.3	CTI 012657.5+280202	62	12.482±0.027	12.206±0.027	11.932±0.294	>8.992	14.044±0.027	13.357±0.029	12.856±0.030	M8.5 V
WISEPC J012821.03+021116.5	LHS 1252	70	11.596±0.026	11.323±0.026	11.131±0.197	>8.673	12.674±0.023	12.110±0.025	11.758±0.023	M6 V
WISEPA J013825.39+280943.7	CTI 013743.0+280553:	62	13.852±0.031	13.462±0.040	>12.595	>8.570	14.790±0.035	14.265±0.051	14.073±0.053	M4.5 V
WISEPA J015158.49+280838.4	CTI 015115.8+280458	62	11.596±0.024	11.435±0.022	11.529±0.223	>8.240	12.745±0.022	12.138±0.026	11.842±0.023	M3.5 V
WISEPA J015209.72+340034.1	2MASP J0152096+340037	67	13.607±0.028	13.242±0.036	12.541±0.446	>8.935	14.729±0.032	14.254±0.037	13.793±0.043	M6.5 V
WISEPA J015421.12+280414.9	CTI 015338.5+280036	62	14.746±0.040	14.456±0.078	>12.085	>8.708	15.771±0.057	15.179±0.090	14.766±0.114	M3.5 V
WISEPA J015748.95+280854.5	CTI 015705.9+280519	62	14.073±0.032	13.818±0.051	>12.348	>8.557	15.077±0.035	14.573±0.057	14.398±0.078	M4.5 V
WISEPA J015908.24+280457.8	CTI 015825.4+280120	62	12.629±0.026	12.587±0.033	—	>7.048	13.636±0.020	12.917±0.026	12.774±0.026	M1.5 V
WISEPA J020215.77+102011.1	LHS 1326	70	8.698±0.024	8.488±0.021	8.256±0.025	7.952±0.210	9.842±0.019	9.254±0.024	8.928±0.023	M5.5 V
WISEPA J021816.35-274049.1	LP 885-45	68	12.348±0.025	12.129±0.025	12.032±0.256	>9.391	13.338±0.026	12.838±0.025	12.529±0.024	M4.5 V
WISEPA J022537.02+240833.8	LP 353-59	72	12.341±0.024	12.140±0.027	11.694±0.254	>8.217	13.449±0.021	12.837±0.027	12.547±0.025	M4.5 V
WISEPA J024840.95-165124.8	LP 771-21	68	11.186±0.025	10.983±0.022	10.619±0.084	>8.671	12.551±0.018	11.872±0.020	11.422±0.019	M8 V
WISEPA J025226.18+005621.5	TVLM 832-10443	66	11.657±0.025	11.387±0.025	10.964±0.134	>8.603	13.126±0.019	12.441±0.022	11.963±0.017	M8 V
WISEPA J031547.91+280600.1	CTI 031502.6+280315	62	12.359±0.027	12.164±0.026	11.707±0.243	>9.090	13.383±0.021	12.788±0.024	12.551±0.023	M3.5 V
WISEPA J032059.95+185420.3	LP 412-31	63	10.360±0.024	10.146±0.021	9.873±0.052	>8.461	11.759±0.017	11.066±0.020	10.639±0.016	M8 V
WISEPA J032527.98+280636.0	CTI 032442.5+280400	62	12.098±0.025	11.957±0.025	11.475±0.187	>8.965	13.203±0.019	12.492±0.022	12.263±0.020	M4 V
WISEPA J032744.93+280146.3	CTI 032659.6+275912	62	11.428±0.025	11.204±0.023	10.838±0.108	>9.044	12.547±0.021	11.832±0.031	11.553±0.019	M4.5 V
WISEPA J033935.48-352541.0	LP 944-20	69	9.141±0.024	8.796±0.019	8.242±0.022	7.964±0.134	10.725±0.018	10.017±0.020	9.548±0.021	M9 V
WISEPA J065038.51+280347.1	CTI 064951.4+280442	62	14.062±0.036	13.943±0.053	12.100±0.353	>9.055	15.188±0.038	14.522±0.046	14.292±0.056	M5.5 V
WISEPA J065237.89+280214.3	CTI 065150.8+280311	62	14.663±0.048	14.658±0.092	>12.280	>8.617	15.661±0.054	15.283±0.087	14.735±0.083	M5.5 V

Table 1—Continued

WISE Designation <sup>a</sup>	Other Designation	Dis. Ref.	W1 (mag)	W2 (mag)	W3 (mag)	W4 (mag)	J (mag)	H (mag)	K <sub>s</sub> (mag)	Spec. Typ. <sup>b</sup>
(1)	(2)	(3)	(4)	(5)	(6)	(7)	(8)	(9)	(10)	(11)
WISEPA J065757.51+621913.9	LHS 1885	70	7.448±0.025	7.278±0.021	7.108±0.019	7.071±0.069	8.585±0.007	7.988±0.011	7.690±0.007	M4.5 V
WISEPA J070037.46+280122.5	CTI 065950.5+280228	62	14.499±0.035	14.272±0.059	12.433±0.493	>8.496	15.638±0.046	14.942±0.052	14.602±0.060	M4.5 V
WISEPA J070753.25-490046.2	ESO 207-61	74	11.835±0.025	11.549±0.022	11.206±0.090	>9.515	13.228±0.023	12.538±0.029	12.105±0.024	M8.5 V
WISEPA J071931.60+324944.9	GI 270 <sup>g</sup>	70	6.300±0.036	6.244±0.023	6.165±0.018	6.172±0.050	7.184±0.011	6.541±0.031	6.376±0.013	M0 V
WISEPA J073625.27+070440.0	G 89-32	75	7.118±0.029	6.895±0.021	6.746±0.018	6.518±0.063	8.180±0.013	7.611±0.029	7.282±0.013	M4.5 V
WISEPA J075059.51+280415.4	CTI 075013.2+280613	62	14.422±0.033	14.097±0.053	>12.435	>9.115	15.366±0.047	14.855±0.064	14.654±0.091	M4.5 V
WISEPA J075353.10+085359.9	LHS 5129	70	11.587±0.025	11.313±0.023	11.090±0.129	>9.134	12.627±0.021	12.139±0.031	11.806±0.023	M6 V
WISEPA J075809.36+280329.2	CTI 075723.2+280533	62	13.900±0.032	13.846±0.049	>12.587	>9.150	14.977±0.034	14.301±0.036	13.983±0.048	M4 V
WISEPA J083618.33-192040.1	LP 785-18	68	9.383±0.024	9.247±0.021	9.115±0.030	9.221±0.464	10.341±0.021	9.802±0.026	9.535±0.019	M3 V
WISEPA J085335.80-032934.2	LHS 2065	64	9.623±0.019	9.385±0.020	8.941±0.030	9.236±0.483	11.212±0.023	10.469±0.024	9.942±0.023	M9 V
WISEPA J090205.32+280138.2	CTI 090120.6+280439	62	13.736±0.028	13.558±0.041	12.461±0.430	>8.844	14.967±0.043	14.361±0.052	13.923±0.051	M5.5 V
WISEPA J090206.59+003318.5	LHS 5142	70	10.947±0.022	10.700±0.021	10.433±0.074	>8.858	12.106±0.021	11.538±0.021	11.161±0.019	M6 V
WISEPC J091800.96+280220.5	CTI 091716.8+280531	62	14.161±0.031	13.859±0.044	>12.380	>9.414	15.411±0.057	14.798±0.078	14.493±0.087	M6 V
WISEPA J092416.05+351644.1	G 117-B15 B	75	10.711±0.025	10.525±0.022	10.404±0.072	>8.871	11.729±0.013	11.156±0.015	10.917±0.015	M3.5 V
WISEPC J092507.00+275727.8	CTI 092423.0+280044	62	11.776±0.024	11.620±0.022	11.575±0.183	>9.344	12.692±0.018	12.126±0.021	11.897±0.015	M3 V
WISEPC J092623.81+275700.9	CTI 092539.9+280018	62	14.109±0.030	13.904±0.047	>11.995	>9.000	15.324±0.049	14.558±0.057	14.269±0.062	M6.5 V
WISEPC J093714.90+275913.2	CTI 093631.3+280237	62	11.225±0.014	11.093±0.013	10.959±0.115	>9.289	12.237±0.021	11.600±0.028	11.347±0.020	M3 V
WISEPC J094222.68+424533.4	TVLM 262-111511	66	12.788±0.028	12.472±0.027	12.195±0.324	>9.281	14.197±0.026	13.512±0.029	13.095±0.036	M8.5 V
WISEPC J095147.80+423348.7	TVLM 262-70502	66	12.902±0.027	12.654±0.027	12.241±0.301	>9.274	14.183±0.027	13.473±0.025	13.093±0.032	M6.5 V
WISEPC J095723.93+263250.6	LP 315-11	72	12.450±0.026	12.210±0.025	11.614±0.191	>8.564	13.485±0.021	13.006±0.032	12.632±0.021	M4.5 V
WISEPC J100203.26+454456.3	LP 166-56	71	12.337±0.024	12.129±0.024	11.661±0.190	>9.261	13.477±0.019	12.895±0.019	12.565±0.023	M4.5 V
WISEPC J100743.69+113429.3	LSPM J1007+1134 <sup>c</sup>	78	12.668±0.026	12.426±0.026	11.946±0.241	>9.389	13.705±0.029	13.137±0.027	12.867±0.033	M4.5 V
WISEPC J101634.54+275144.1	LHS 2243	65	10.715±0.023	10.517±0.020	10.242±0.065	9.034±0.458	11.987±0.015	11.331±0.020	10.955±0.016	M8 V
WISEPC J102236.87+301657.6	PSS 1022+3016 <sup>f</sup>	80	11.578±0.025	11.369±0.022	11.009±0.123	>9.192	12.743±0.018	12.116±0.018	11.771±0.018	M6 V
WISEPC J102921.73+275937.9	CTI 102840.1+280330	62	13.904±0.021	13.727±0.035	12.573±0.435	>9.564	15.129±0.032	14.463±0.037	14.075±0.042	M5.5 V
WISEPC J103042.10+280040.4	CTI 103000.3+280432	62	14.194±0.034	13.956±0.053	>11.871	>8.676	15.391±0.041	14.698±0.040	14.442±0.052	M5.5 V
WISEPA J133100.85-453507.2	WT 426	79	8.536±0.024	8.316±0.020	8.183±0.022	8.121±0.196	9.469±0.018	8.950±0.025	8.702±0.024	M3.5 V
WISEPC J135421.74+280041.2	LP 324-30	72	12.638±0.026	12.444±0.026	11.989±0.245	>8.710	13.778±0.024	13.195±0.023	12.892±0.036	M6 V
WISEPA J135620.19-280350.7	LHS 2826	70	9.374±0.023	9.218±0.020	9.003±0.032	>8.644	10.480±0.023	9.875±0.022	9.565±0.017	M4.5 V
WISEPA J135644.07-173014.0	LP 799-3	68	13.975±0.033	13.730±0.051	>12.042	>8.553	14.988±0.041	14.542±0.061	14.244±0.086	M4.5: V
WISEPA J135910.02-195005.4	LHS 2836	70	7.292±0.027	7.114±0.021	6.955±0.020	6.808±0.080	8.334±0.033	7.761±0.059	7.445±0.021	M4.5 V
WISEPC J141107.82+275826.3	CTI 141034.2+280158	62	12.222±0.023	12.032±0.024	11.999±0.248	>9.092	13.295±0.021	12.676±0.031	12.422±0.021	M4.5 V
WISEPC J141144.97+275808.2	LP 325-1	72	13.283±0.028	13.059±0.031	12.528±0.383	>9.388	14.412±0.032	13.763±0.032	13.436±0.038	M5.5 V
WISEPC J141311.37+280226.4	CTI 141237.7+280557	62	12.230±0.024	12.077±0.024	11.906±0.211	>9.411	13.289±0.024	12.697±0.013	12.392±0.023	M3 V
WISEPC J141403.20+275801.0	CTI 141329.8+280131	62	12.266±0.025	12.112±0.023	12.167±0.267	>9.524	13.273±0.020	12.647±0.022	12.388±0.020	M2.5 V
WISEPA J145824.46+283953.3	2MASS J14582453+2839580 <sup>e</sup>	33	11.617±0.027	11.394±0.024	11.239±0.139	>8.876	13.083±0.015	12.309±0.019	11.849±0.022	M8.5 V
WISEPA J150108.17+225001.4	TVLM 513-46546	66	10.368±0.023	10.059±0.021	9.552±0.040	8.986±0.445	11.866±0.018	11.181±0.029	10.706±0.022	M8.5 V
WISEPA J150618.61+275824.0	CTI 150546.8+280117	62	15.223±0.042	14.994±0.086	>12.177	>9.038	16.451±0.127	16.044±0.189	>14.941	M5.5 V
WISEPA J151016.58-024107.6	TVLM 868-110639	66	10.957±0.024	10.667±0.021	10.212±0.073	>9.004	12.614±0.019	11.842±0.020	11.347±0.019	M9 V
WISEPA J151420.46+234104.1	TVLM 513-8328	66	12.653±0.026	12.351±0.026	12.175±0.301	>9.224	14.087±0.025	13.422±0.023	12.961±0.030	M8 V
WISEPA J151943.12+260936.2	2MASP J1519431+260937	80	14.090±0.031	13.782±0.042	12.504±0.430	>9.146	15.428±0.058	14.758±0.080	14.257±0.068	M8 V
WISEPA J152047.56+300208.5	SDSS J152047.63+300209.0 <sup>d</sup>	76	13.645±0.028	13.293±0.037	12.540±0.532	>8.405	15.024±0.039	14.365±0.044	14.041±0.064	M8.5 V
WISEPA J152424.72+292525.2	2MASP J1524248+292535	77	9.935±0.026	9.720±0.023	9.422±0.036	8.726±0.369	11.206±0.018	10.535±0.019	10.155±0.013	M7.5 V
WISEPA J153946.68+275951.0	CTI 153915.5+280214	62	15.566±0.052	15.190±0.096	>12.229	>9.307	16.521±0.143	>17.395	15.701±0.197	M4: V
WISEPA J153946.73+280222.3	CTI 153915.6+280445	62	14.371±0.031	14.168±0.048	>12.351	>9.298	15.493±0.054	15.002±0.096	14.580±0.075	M6.5 V
WISEPA J154016.16+280010.2	CTI 153945.1+280233	62	11.846±0.024	11.794±0.023	11.816±0.197	>9.146	12.849±0.019	12.182±0.028	11.946±0.018	M1.5 V
WISEPA J154019.25+280058.3	CTI 153948.1+280322	62	12.447±0.023	12.349±0.025	11.984±0.231	>8.954	13.506±0.026	12.871±0.034	12.573±0.025	M2 V
WISEPA J154302.42+280139.5	CTI 154231.3+280401	62	13.544±0.028	13.359±0.032	>12.092	>9.047	14.700±0.038	14.076±0.043	13.794±0.052	M5.5 V
WISEPA J183436.70+400724.3	LP 229-17	71	6.166±0.038	6.011±0.022	5.929±0.018	5.855±0.034	7.184±0.009	6.530±0.011	>7.104	M4 V

Table 1—Continued

WISE Designation <sup>a</sup>	Other Designation	Dis. Ref.	W1 (mag)	W2 (mag)	W3 (mag)	W4 (mag)	J (mag)	H (mag)	K <sub>s</sub> (mag)	Spec. Typ. <sup>b</sup>
(1)	(2)	(3)	(4)	(5)	(6)	(7)	(8)	(9)	(10)	(11)
WISEPA J184110.13+244715.5	GJ 1230 B	70	6.348±0.040	6.199±0.025	6.105±0.019	6.018±0.058	7.528±0.007	6.912±0.035	6.616±0.017	M4.5 V
WISEPA J185848.03+280147.8	CTI 185818.3+280045	62	11.633±0.026	11.566±0.022	11.519±0.188	>8.873	12.645±0.019	11.993±0.019	11.763±0.018	M2.5 V
WISEPA J190705.22+205313.4	GI 745 A	61	6.414±0.037	6.204±0.021	6.145±0.017	6.092±0.039	7.295±0.011	6.726±0.059	6.521±0.015	M3 V
WISEPA J190712.86+205233.9	GI 745 B	61	6.388±0.036	6.181±0.023	6.128±0.018	6.078±0.043	7.278±0.013	6.752±0.049	6.517±0.017	M2 V
WISEPA J191246.79+280346.1	CTI 191216.9+280228	62	14.320±0.045	14.163±0.062	>12.568	>9.035	15.351±0.051	14.673±0.057	14.594±0.076	M4 V
WISEPA J192033.38-073945.4	GI 754.1 B	68	7.089±0.029	6.975±0.021	6.871±0.018	6.655±0.070	8.221±0.023	7.661±0.021	7.414±0.013	M3 V
WISEPA J193238.07+003439.3	GI 761.2	72	6.741±0.033	6.737±0.020	6.648±0.020	6.564±0.061	7.635±0.017	7.045±0.037	6.808±0.019	M0.5 V
WISEPA J194932.81-624921.4	LHS 3487	70	11.509±0.023	11.359±0.021	11.427±0.103	>8.996	12.319±0.018	11.812±0.023	11.628±0.018	M0 V
WISEPA J201916.77-562123.2	LHS 3538	70	10.379±0.026	10.163±0.023	10.036±0.052	>8.456	11.314±0.018	10.807±0.025	10.536±0.019	M4 V
WISEPC J202948.79+094121.5	GI 791.2AB	70	7.180±0.027	6.949±0.021	6.783±0.018	6.742±0.059	8.228±0.011	7.666±0.033	7.307±0.019	M4.5 V
WISEPA J211832.15-450557.1	HB 2115-4518	73	12.060±0.026	11.762±0.025	11.206±0.141	>8.837	13.425±0.022	12.768±0.025	12.368±0.029	M8.5 V
WISEPC J212310.80+641415.3	LP 75-10	72	10.196±0.021	10.021±0.021	9.826±0.036	>9.220	11.119±0.019	10.536±0.028	10.316±0.020	M2.5 V
WISEPC J212726.25-421519.7	HB 2124-4228	73	11.922±0.025	11.651±0.022	11.275±0.188	>8.602	13.321±0.019	12.665±0.024	12.186±0.021	M7.5 V
WISEPC J213008.67-444632.2	HB 2126-4459	73	12.943±0.026	12.686±0.029	>12.137	>8.797	14.315±0.028	13.604±0.022	13.163±0.028	M8.5 V

Note. — The quoted photometric limits for non-detections are two-sigma lower limits, as defined in [http://wise2.ipac.caltech.edu/docs/release/prelim/expsup/sec4\\_5c.html#upperlimits](http://wise2.ipac.caltech.edu/docs/release/prelim/expsup/sec4_5c.html#upperlimits).

Note. — Discovery references: (1) Warren et al. 2007, (2) Tinney et al. 2005, (3) Delorme et al. 2008, (4) Artigau et al. 2006, (5) Burningham et al. 2010, (6) Geballe et al. 2002, (7) Burgasser et al. 2002, (8) Chiu et al. 2006, (9) Burgasser et al. 2003, (10) Burgasser et al. 2004, (11) Bouvier et al. 2009, (12) Looper et al. 2007, (13) Cruz et al. 2004, (14) Burgasser et al. 2000, (15) Lucas et al. 2010, (16) Knapp et al. 2004, (17) Artigau et al. 2010, (18) Leggett et al. 2000, (19) Pinfield et al. 2008, (20) Kirkpatrick et al. 2000, (21) Sheppard & Cushing 2009, (22) Hawley et al. 2002, (23) Burgasser et al. 1999, (24) Burningham et al. 2008, (25) Goldman et al. 2010, (26) Tsvetanov et al. 2000, (27) Stern et al. 2007, (28) Burgasser et al. 2000, (29) Delorme et al. 2010, (30) Burgasser et al. 2003, (31) Metchev et al. 2008, (32) Strauss et al. 1999, (33) Reid et al. 2008, (34) Luhman et al. 2007, (35) Ellis et al. 2005, (36) Scholz et al. 2003, (37) Scholz 2010, (38) Kirkpatrick et al. 1999, (39) Cruz et al. 2007, (40) Liebert et al. 2003, (41) Delfosse et al. 1997, (42) Cruz et al. 2003, (43) Lodieu et al. 2002, (44) Wilson et al. 2003, (45) Schneider et al. 2002, (46) Kirkpatrick et al. 2008, (47) Phan-Bao et al. 2008, (48) Reid et al. 2000, (49) Zhang et al. 2009, (50) Delfosse et al. 1999, (51) Wilson et al. 2001, (52) Gizis et al. 2000, (53) Bouy et al. 2003, (54) Ruiz et al. 1997, (55) Hall 2002, (56) Gizis 2002, (57) Fan et al. 2000, (58) Becklin & Zuckerman 1988, (59) Kirkpatrick et al. 2001, (60) Kendall et al. 2007, (61) Ross 1928, (62) Kirkpatrick et al. 1994, (63) Luyten 1974, (64) Luyten 1972, (65) Luyten 1974, (66) Tinney 1993, (67) Kirkpatrick et al. 1997, (68) Luyten 1980, (69) Luyten & Kowal 1975, (70) Luyten 1979, (71) Luyten 1979, (72) Luyten 1979, (73) Hawkins & Bessell 1988, (74) Ruiz et al. 1991, (75) Giclas et al. 1971, (76) West et al. 2008, (77) Reid et al. 2002, (78) Lépine & Shara 2005, (79) Wroblewski & Torres 1991, (80) this paper.

<sup>a</sup>WISE sources are given designations as follows. The prefix is “WISE” followed by either “PC” for sources taken from the first-pass precessing operations coadd Source Working Database, or “PA” for objects drawn from the preliminary release Atlas Tile Source Working Database. The suffix is the J2000 position of the source in the format Jhhmmss.ss±ddmmss.s. As stated in section 5.2, the positions measured in first-pass WISE processing and used to derive these designations should not be used for astrometric purposes.

<sup>b</sup>Special symbols on spectral types: “:” indicates an uncertain type; “::” indicates a highly uncertain type; “+” indicates that the spectrum is likely later than the type given.

<sup>c</sup>Previously identified, though unpublished, in 2MASS Prototype Camera Data as 2MASP J1007435+113432.

<sup>d</sup>Previously identified, though unpublished, in 2MASS Prototype Camera Data as 2MASP J1520477+300210.

<sup>e</sup>Also known as PSS 1458+2839 (Kennefick, priv. comm.).

<sup>f</sup>Object from Kennefick (priv. comm.).

<sup>g</sup>Luyten (1979) quotes the discoverer as Hertzsprung.

<sup>h</sup>Object from Kunkel (priv. comm.).

Table 2. WISE Photometry for WISE Brown Dwarf Discoveries

Object Name <sup>a</sup>	Disc. Ref.	<i>b</i> (deg)	W1 (mag)	W2 (mag)	W3 (mag)	W4 (mag)	W1-W2 (mag)	W2-W3 (mag)	No. of WISE Coverages
(1)	(2)	(3)	(4)	(5)	(6)	(7)	(8)	(9)	(10)
WISEPC J000849.76−173922.6	1	−76.3	16.593±0.114	14.543±0.072	>12.235	8.928±0.381	2.050±0.135	<2.308	13
WISEPC J003119.76−384036.4 <sup>b</sup>	1	−77.7	12.433±0.026	12.028±0.024	11.455±0.160	>8.763	0.405±0.035	0.574±0.162	12
WISEPC J004928.48+044100.1	1	−58.1	13.448±0.028	12.942±0.030	12.237±0.359	8.677±0.286	0.506±0.041	0.705±0.360	14
WISEPC J010637.07+151852.8 <sup>c</sup>	1	−47.3	13.088±0.030	12.687±0.028	12.110±0.313	9.105±0.465	0.401±0.041	0.577±0.314	13
WISEPA J012333.21+414203.9	1	−20.7	17.123±0.168	14.848±0.086	>12.339	>8.839	2.275±0.189	<2.509	13
WISEPC J013836.59−032221.2	1	−63.7	14.427±0.034	13.359±0.034	11.910±0.252	>8.957	1.068±0.048	1.449±0.254	14
WISEPC J014807.25−720258.7	1,5	−44.4	18.812±0.529	14.584±0.051	>12.579	>9.521	4.228±0.531	<2.005	24
WISEPA J015010.86+382724.3	1	−22.9	13.619±0.028	12.984±0.036	11.933±0.305	>8.779	0.635±0.046	1.051±0.307	10
WISEPA J020625.26+264023.6	1	−33.2	13.401±0.028	12.805±0.035	11.596±0.230	>9.144	0.596±0.045	1.209±0.233	11
WISEPA J022105.94+384202.9	1	−20.9	16.715±0.130	14.621±0.075	>12.087	>8.685	2.094±0.150	<2.534	12
WISEPC J022322.39−293258.1	1	−69.6	16.928±0.138	13.992±0.044	12.838±0.504	>9.544	2.936±0.145	1.154±0.506	15
WISEPA J022623.98−021142.8	1	−56.2	17.635±0.291	14.543±0.069	>12.285	>8.998	3.092±0.299	<2.258	13
WISEPA J025409.45+022359.1	1	−48.2	15.743±0.070	12.707±0.031	11.042±0.131	>9.067	3.036±0.077	1.665±0.135	11
WISEPA J030533.54+395434.4	1	−16.0	16.815±0.143	14.643±0.073	>12.243	>9.169	2.172±0.161	<2.400	13
WISEPA J030724.57+290447.6	1	−25.0	17.438±0.285	14.882±0.103	>12.339	>8.977	2.556±0.303	<2.543	11
WISEPA J031325.96+780744.2	1	17.2	16.087±0.070	13.234±0.034	11.854±0.282	>8.760	2.853±0.078	1.380±0.284	16
WISEPC J032337.53−602554.9	1	−47.9	17.504±0.190	14.466±0.054	12.807±0.430	>9.287	3.038±0.198	1.659±0.433	17
WISEPC J033349.34−585618.7	1	−47.6	14.024±0.028	13.247±0.029	12.114±0.212	>9.746	0.777±0.040	1.133±0.214	20
WISEPA J041022.71+150248.5	1	−25.9	>18.101	14.190±0.059	12.472±0.482	>8.923	>3.911	1.718±0.486	12
WISEPA J041054.48+141131.6	1	−26.3	17.103±0.186	15.021±0.102	>12.001	>9.069	2.082±0.212	<3.020	12
WISEPA J044853.29−193548.5	1	−35.4	16.483±0.086	14.189±0.046	13.042±0.528	>8.950	2.294±0.098	1.147±0.530	19
WISEPA J045853.89+643452.9	2	13.3	16.370±0.088	13.003±0.030	12.029±0.256	>9.260	3.367±0.093	0.974±0.258	15
WISEPA J050003.05−122343.2	1	−30.2	17.762±0.276	13.973±0.046	>12.500	>8.845	3.789±0.280	<1.473	16
WISEPA J051317.28+060814.7	1	−18.5	15.856±0.079	13.834±0.047	>12.374	>9.118	2.022±0.092	<1.460	11
WISEPA J052536.33+673952.3	1	17.3	17.920±0.330	14.899±0.083	>12.727	>9.128	3.021±0.340	<2.172	16
WISEPA J052844.51−330823.9	1	−30.8	17.632±0.219	14.534±0.055	12.461±0.316	>9.312	3.098±0.226	2.073±0.321	18
WISEPA J053957.02−103436.5	1	−20.6	16.845±0.134	14.764±0.077	>12.743	>9.202	2.081±0.155	<2.021	14
WISEPA J054231.26−162829.1	1	−22.4	16.385±0.087	13.907±0.043	>12.071	>9.068	2.478±0.097	<1.836	15
WISEPA J061135.13−041024.0	1	−10.7	13.554±0.029	12.891±0.030	12.054±0.286	>8.818	0.663±0.042	0.837±0.288	13
WISEPA J061213.93−303612.7	1	−21.2	16.586±0.147	14.044±0.045	>12.468	>8.954	2.542±0.154	<1.576	18
WISEPA J061208.69−492023.8	1	−26.4	15.349±0.036	14.075±0.034	12.572±0.234	>9.720	1.274±0.050	1.503±0.236	44
WISEPA J061407.49+391236.4	1	10.1	16.338±0.110	13.633±0.039	>11.968	>8.960	2.705±0.117	<1.665	13
WISEPA J062309.94−045624.6	1	−8.5	17.036±0.177	13.781±0.043	12.510±0.394	>8.661	3.255±0.182	1.271±0.396	16
WISEPA J062542.21+564625.5	1	19.0	16.558±0.102	14.321±0.056	12.624±0.423	>8.886	2.237±0.116	1.697±0.427	15
WISEPA J062720.07−111428.8	1	−10.4	14.897±0.038	13.227±0.029	11.510±0.145	>9.206	1.670±0.048	1.717±0.148	26
WISEPA J065609.60+420531.0	1	18.6	14.318±0.032	13.226±0.033	11.786±0.240	>8.846	1.092±0.046	1.440±0.242	14
WISEPA J074457.15+562821.8	1	29.5	17.136±0.168	14.492±0.059	12.603±0.414	>9.091	2.644±0.178	1.889±0.418	15
WISEPA J075003.84+272544.8	1	24.2	>18.338	14.483±0.070	>12.658	>8.765	>3.855	<1.825	12
WISEPA J075108.79−763449.6	1	−22.9	17.129±0.102	14.465±0.040	11.837±0.121	>9.306	2.664±0.110	2.628±0.127	45
WISEPC J075946.98−490454.0	1	−9.9	17.680±0.276	13.808±0.038	13.030±0.503	>9.120	3.872±0.279	0.778±0.504	19
WISEPA J081958.05−033529.0	1	17.8	14.356±0.034	13.066±0.034	11.938±0.284	>8.926	1.290±0.048	1.128±0.286	13
WISEPA J082131.63+144319.3	1	26.4	16.438±0.114	14.283±0.064	>12.572	>8.893	2.155±0.131	<1.711	10
WISEPC J083641.12−185947.2	1	12.9	18.405±0.520	15.024±0.085	>12.755	>9.156	3.381±0.527	<2.269	15
WISEPA J085716.25+560407.6	1	39.6	17.068±0.153	14.031±0.046	>12.291	>9.270	3.037±0.160	<1.740	15
WISEPA J090649.36+473538.6	1	42.1	17.342±0.209	14.595±0.071	12.551±0.461	>8.746	2.747±0.221	2.044±0.466	12
WISEPC J092906.77+040957.9	1	36.6	16.550±0.122	14.111±0.056	12.129±0.369	>9.140	2.439±0.134	1.982±0.373	10
WISEPC J095259.29+195507.3	1	48.7	17.249±0.228	14.385±0.067	>12.468	>9.183	2.864±0.238	<1.917	11
WISEPC J101808.05−244557.7	1	26.2	17.001±0.159	14.088±0.047	>12.222	>8.771	2.913±0.166	<1.866	14
WISEPA J101905.63+652954.2	1	44.8	16.285±0.073	13.941±0.040	12.679±0.411	>9.147	2.344±0.083	1.262±0.413	18

Table 2—Continued

Object Name <sup>a</sup>	Disc. Ref.	$b$ (deg)	W1 (mag)	W2 (mag)	W3 (mag)	W4 (mag)	W1-W2 (mag)	W2-W3 (mag)	No. of WISE Coverages
(1)	(2)	(3)	(4)	(5)	(6)	(7)	(8)	(9)	(10)
WISEPC J104245.23−384238.3	1	17.6	>18.496	14.515±0.060	>12.746	>9.099	>3.981	<1.769	14
WISEPC J112254.73+255021.5	1	70.1	16.051±0.084	13.965±0.052	>12.317	>9.429	2.086±0.099	<1.648	9
WISEPC J115013.88+630240.7	1	52.7	16.993±0.133	13.425±0.034	12.147±0.253	>8.831	3.568±0.137	1.278±0.255	16
WISEPC J121756.91+162640.2	1	76.7	16.591±0.118	13.074±0.034	11.929±0.277	>8.710	3.517±0.123	1.145±0.279	11
WISEPC J131106.24+012252.4	1	63.8	18.064±0.431	14.733±0.080	>12.110	>9.287	3.331±0.438	<2.623	12
WISEPC J131141.91+362925.2	1	79.7	13.496±0.027	13.067±0.030	12.516±0.373	>8.830	0.429±0.040	0.551±0.374	15
WISEPC J132004.16+603426.2	1	56.2	16.609±0.121	14.489±0.070	>12.046	>9.087	2.120±0.140	<2.443	9
WISEPA J132233.66−234017.1	1,4	38.6	17.192±0.222	13.876±0.052	>12.017	8.594±0.340	3.316±0.228	<1.859	9
WISEPC J134806.99+660327.8	1	50.0	14.441±0.030	13.754±0.036	12.724±0.393	>9.760	0.687±0.047	1.030±0.395	18
WISEPC J140518.40+553421.4	1,5	58.5	>17.989	14.085±0.041	12.312±0.252	>9.115	>3.904	1.773±0.255	21
WISEPA J143602.19−181421.8	1	38.0	16.904±0.159	14.650±0.082	12.467±0.491	>8.799	2.254±0.179	2.183±0.498	12
WISEPC J145715.03+581510.2	1	51.9	16.541±0.086	14.380±0.050	12.615±0.355	>9.558	2.161±0.099	1.765±0.359	18
WISEPC J150649.97+702736.0	1	42.6	13.390±0.025	11.277±0.020	10.171±0.043	9.889±0.498	2.113±0.032	1.106±0.047	25
WISEPC J151906.64+700931.5	1	42.0	17.594±0.160	14.064±0.035	13.064±0.418	>10.043	3.530±0.164	1.000±0.419	29
WISEPA J154151.66−225025.2	1,5	25.2	>17.018	13.982±0.112	12.134±0.443	>9.064	>3.036	1.848±0.457	11
WISEPA J161215.94−342027.1	1	12.3	>16.881	14.085±0.077	>12.150	>8.744	>2.796	<1.935	13
WISEPA J161441.45+173936.7	1,4	42.3	18.333±0.503	14.229±0.053	>12.318	>9.151	4.104±0.506	<1.911	14
WISEPA J161705.75+180714.3	3	42.0	16.831±0.117	14.039±0.046	12.241±0.312	>9.255	2.792±0.126	1.798±0.315	16
WISEPA J162208.94−095934.6	1	26.8	16.251±0.102	14.016±0.054	>11.958	>8.760	2.235±0.115	<2.058	11
WISEPA J162725.64+325525.5	1,4	43.3	16.303±0.077	13.613±0.036	12.967±0.532	>9.197	2.690±0.085	0.646±0.533	18
WISEPA J164715.59+563208.2	1	39.3	13.603±0.026	13.068±0.026	12.204±0.171	>9.208	0.535±0.037	0.864±0.173	41
WISEPA J165311.05+444423.9	1,4	39.2	16.580±0.089	13.817±0.036	12.238±0.249	>9.517	2.763±0.096	1.579±0.252	23
WISEPA J171104.60+350036.8	1	34.8	18.267±0.367	14.611±0.056	12.715±0.381	>9.454	3.656±0.371	1.896±0.385	21
WISEPA J171717.02+612859.3	1	34.7	18.436±0.334	14.958±0.056	13.267±0.505	>9.142	3.478±0.339	1.691±0.508	36
WISEPA J172844.93+571643.6	1	33.6	17.368±0.106	14.918±0.049	13.409±0.462	>9.899	2.450±0.117	1.509±0.465	52
WISEPA J173835.53+273258.9	1,5	27.2	18.155±0.362	14.535±0.057	12.536±0.350	>9.182	3.620±0.366	1.999±0.355	18
WISEPA J174124.26+255319.5	1,4	26.1	15.228±0.040	12.312±0.025	10.675±0.075	>8.580	2.916±0.047	1.637±0.079	17
WISEPA J180435.40+311706.1	1	23.0	>18.423	14.709±0.062	12.854±0.468	>9.391	>3.714	1.855±0.472	19
WISEPA J181210.85+272144.3	3	20.1	17.238±0.173	14.181±0.050	>12.369	>9.284	3.057±0.180	<1.812	15
WISEPA J182831.08+265037.8	1,5	16.5	>18.452	14.276±0.050	12.320±0.291	9.147±0.438	>4.176	1.956±0.295	18
WISEPA J183058.57+454257.9	1	22.4	14.759±0.029	14.094±0.034	>12.833	>9.286	0.665±0.045	<1.261	42
WISEPA J184124.74+700038.0	1,4	26.2	16.485±0.050	14.309±0.032	13.045±0.265	>9.424	2.176±0.059	1.264±0.267	77
WISEPA J185215.78+353716.3	1	15.2	16.261±0.087	14.162±0.044	12.167±0.228	9.405±0.489	2.099±0.097	1.995±0.232	21
WISEPA J190624.75+450808.2	1	16.3	15.978±0.052	13.819±0.033	12.703±0.317	>9.480	2.159±0.062	1.116±0.319	30
WISEPA J195246.66+724000.8	1	21.4	14.201±0.027	12.995±0.025	11.924±0.128	>9.141	1.206±0.037	1.071±0.130	47
WISEPA J195905.66−333833.7	1	−27.9	16.419±0.135	13.818±0.048	>12.287	>8.789	2.601±0.143	<1.531	13
WISEPA J201824.96−742325.9	3	−31.8	16.609±0.115	13.719±0.041	12.513±0.501	>8.977	2.890±0.122	1.206±0.503	12
WISEPC J205628.90+145953.3	1,5	−19.1	>17.742	13.852±0.043	11.791±0.222	>8.646	>3.890	2.061±0.226	12
WISEPA J213456.73−713743.6	1	−38.0	18.124±0.404	13.944±0.045	12.242±0.299	>8.830	4.180±0.406	1.702±0.302	13
WISEPC J215751.38+265931.4	1	−21.6	16.956±0.193	14.553±0.088	>11.927	>8.441	2.403±0.212	<2.626	8
WISEPC J220922.10−273439.5	1	−54.1	16.473±0.113	13.786±0.048	>11.861	>9.124	2.687±0.123	<1.925	10
WISEPC J221354.69+091139.4	1	−37.3	16.635±0.111	14.508±0.064	>12.329	>9.155	2.127±0.128	<2.179	14
WISEPC J222623.05+044003.9	1	−42.6	17.410±0.255	14.625±0.082	>11.992	>9.075	2.785±0.268	<2.633	11
WISEPC J223729.53−061434.2	1	−51.9	17.527±0.297	14.660±0.088	>12.460	>8.854	2.867±0.310	<2.200	10
WISEPC J223937.55+161716.2	1	−36.0	14.621±0.034	13.437±0.035	12.105±0.295	>9.173	1.184±0.049	1.332±0.297	12
WISEPC J225540.74−311841.8	1	−64.4	16.617±0.129	14.080±0.055	>11.975	>9.165	2.537±0.140	<2.105	10
WISEPA J231336.40−803700.3	3	−35.5	16.187±0.063	13.677±0.034	12.354±0.275	>9.312	2.510±0.072	1.323±0.277	22
WISEPC J231939.13−184404.3	1	−67.3	17.043±0.187	13.733±0.051	12.076±0.341	8.971±0.467	3.310±0.194	1.657±0.345	11
WISEPC J232519.54−410534.9	1	−67.4	17.499±0.242	14.112±0.051	>12.061	>9.251	3.387±0.247	<2.051	12

Table 2—Continued

Object Name <sup>a</sup>	Disc. Ref.	$b$ (deg)	W1 (mag)	W2 (mag)	W3 (mag)	W4 (mag)	W1-W2 (mag)	W2-W3 (mag)	No. of WISE Coverages
(1)	(2)	(3)	(4)	(5)	(6)	(7)	(8)	(9)	(10)
WISEPC J232728.75−273056.5	1	−71.3	14.031±0.031	13.206±0.034	11.687±0.203	>9.283	0.825±0.046	1.519±0.206	12
WISEPC J234026.62−074507.2	1	−64.3	15.951±0.070	13.558±0.037	>11.977	>9.477	2.393±0.079	<1.581	11
WISEPA J234351.20−741847.0	1	−42.0	15.710±0.050	13.689±0.035	12.634±0.364	>9.405	2.021±0.061	1.055±0.366	19
WISEPC J234446.25+103415.8	1	−48.9	>17.949	14.895±0.105	>12.429	>8.543	>3.054	<2.466	10
WISEPC J234841.10−102844.4	1	−67.7	16.570±0.114	14.268±0.057	>11.958	>9.525	2.302±0.127	<2.310	13
WISEPA J235941.07−733504.8	3	−43.0	15.166±0.039	13.269±0.031	11.482±0.129	>9.446	1.897±0.050	1.787±0.133	18

Note. — Discovery Reference: (1) this paper, (2) Mainzer et al. 2011, (3) Burgasser et al. 2011, (4) Gelino et al., submitted, (5) Cushing et al., accepted

<sup>a</sup>WISE sources are given designations as follows. The prefix is “WISE” followed by either “PC” for sources taken from the first-pass precessing operations coadd Source Working Database, or “PA” for objects drawn from the preliminary release Atlas Tile Source Working Database. The suffix is the J2000 position of the source in the format Jhhmmss.ss±ddmmss.s. As stated in section 5.2, the positions measured in first-pass WISE processing and used to derive these designations should not be used for astrometric purposes. Instead, refer to the re-measured astrometry given in Table 6.

<sup>b</sup>Identified as a high-motion object by Deacon et al. (2005) and classified in the optical as an early-L dwarf by Martín et al. (2010). Alternate name is SIPS J0031−3840.

<sup>c</sup>Identified as a high-motion object by Deacon et al. (2009). Alternate name is ULAS2MASS J0106+1518.

<sup>d</sup>Identified as a brown dwarf candidate by Zhang et al. (2009). Alternate name is SDSS J131142.11+362923.9.



Table 3. Follow-up Photometry of WISE Brown Dwarf Discoveries

Object Name	Obs. Ref.	Y (mag)	Two Micron All-Sky Survey filter system			Mauna Kea Observatories filter system			Spitzer/IRAC observations		
			J (mag)	H (mag)	K <sub>s</sub> (mag)	J (mag)	H (mag)	K <sub>s</sub> (mag)	ch1 (mag)	ch2 (mag)	ch1-ch2 (mag)
(1)	(2)	(3)	(4)	(5)	(6)	(7)	(8)	(9)	(10)	(11)	(12)
WISE J0008−1739	4	—	17.03±0.06	17.77±0.13	>17.0	—	—	—	16.044±0.030	14.867±0.021	1.177±0.037
WISE J0031−3840	1	—	14.101±0.032	13.399±0.023	12.924±0.034	—	—	—	extant	—	—
WISE J0049+0441	1	—	15.854±0.067	14.674±0.068	14.170±0.066	—	—	—	12.977±0.017	12.950±0.017	0.027±0.024
	3	—	15.85±0.05	14.77±0.07	14.17±0.04	—	—	—	—	—	—
WISE J0106+1518	1	—	14.358±0.031	13.815±0.033	13.434±0.053	—	—	—	12.862±0.017	12.716±0.017	0.146±0.024
	10	15.095±0.004	—	—	—	14.277±0.003	13.867±0.004	13.363±0.004	—	—	—
WISE J0123+4142	3	—	17.38±0.11	17.20±0.13	18.37±0.37	—	—	—	16.125±0.032	14.845±0.021	1.280±0.038
WISE J0138−0322	1	—	16.389±0.096	15.801±0.147	15.198±0.129	—	—	—	13.888±0.018	13.426±0.018	0.461±0.026
	3	—	16.36±0.07	15.65±0.05	15.30±0.08	—	—	—	—	—	—
WISE J0148−7202	8	—	—	—	—	18.96±0.07	19.22±0.04	—	16.844±0.045	14.650±0.020	2.194±0.050
WISE J0150+3827	1	—	16.111±0.077	15.018±0.080	14.477±0.070	—	—	—	13.236±0.017	13.117±0.017	0.119±0.025
	5	—	16.12±0.06	15.03±0.06	—	—	—	—	—	—	—
	4	—	16.070±0.054	14.973±0.074	14.376±0.067	—	—	—	—	—	—
WISE J0206+2640	1	—	16.530±0.114	15.096±0.077	14.523±0.076	—	—	—	13.075±0.017	12.867±0.017	0.208±0.024
WISE J0221+3842	3	—	17.59±0.12	17.45±0.15	16.95±0.17	—	—	—	15.931±0.029	14.863±0.021	1.068±0.036
WISE J0223−2932	4	—	17.341±0.153	16.850±0.163	>16.94	17.100±0.050	17.304±0.114	—	15.810±0.028	14.015±0.019	1.795±0.033
WISE J0226−0211	5	—	18.94±0.12	>19.10	—	—	—	—	16.599±0.040	14.675±0.021	1.924±0.045
WISE J0254+0223	1	—	16.557±0.156	15.884±0.199	>16.006	—	—	—	14.692±0.021	12.710±0.017	1.982±0.027
	7	—	—	—	—	15.91±0.03	16.29±0.04	—	—	—	—
WISE J0305+3954	3	—	17.13±0.09	17.08±0.12	16.93±0.17	—	—	—	15.981±0.030	14.542±0.020	1.440±0.036
WISE J0307+2904	3	—	17.78±0.11	17.70±0.14	17.78±0.21	—	—	—	16.385±0.036	14.967±0.022	1.419±0.043
	10	—	—	—	—	—	—	18.084±0.122	—	—	—
WISE J0313+7807	6	18.27±0.05	17.65±0.07	17.63±0.06	—	—	—	—	15.310±0.024	13.268±0.017	2.042±0.029
WISE J0323−6025	8	—	—	—	—	18.15±0.10	18.40±0.02	—	16.572±0.039	14.506±0.020	2.066±0.043
WISE J0333−5856	1	—	15.997±0.083	15.418±0.120	14.639±0.097	—	—	—	13.590±0.018	13.297±0.017	0.293±0.025
WISE J0410+1502	7	—	—	—	—	19.25±0.5	19.05±0.09	—	16.642±0.042	14.183±0.019	2.459±0.046
WISE J0410+1411	3	—	17.16±0.09	17.26±0.12	16.98±0.18	—	—	—	16.099±0.032	15.001±0.022	1.098±0.039
	10	—	—	—	—	—	—	17.823±0.196	—	—	—
WISE J0448−1935	2	—	17.016±0.172	16.821±0.309	>15.858	—	—	—	—	—	—
	2	—	16.986±0.173	16.392±0.188	>16.556	—	—	—	—	—	—
WISE J0458+6434	6	18.34±0.07	17.47±0.05	17.41±0.06	—	—	—	—	15.080±0.022	12.985±0.017	2.094±0.028
WISE J0500−1223	9	—	—	—	—	17.782±0.496	18.132±0.121	—	15.947±0.029	13.999±0.019	1.948±0.035
WISE J0513+0608	1	—	16.205±0.094	>16.890	>15.936	—	—	—	15.108±0.022	13.949±0.018	1.160±0.029
	3	—	16.21±0.06	16.13±0.08	16.05±0.11	—	—	—	—	—	—
WISE J0525+6739	7	—	—	—	—	17.49±0.04	17.87±0.05	—	16.404±0.036	14.881±0.021	1.522±0.042
WISE J0528−3308	9	—	—	—	—	16.666±0.087	16.970±0.141	17.119±0.153	16.308±0.034	14.593±0.020	1.716±0.040
WISE J0539−1034	3	—	17.71±0.11	17.82±0.15	18.40±0.31	—	—	—	16.145±0.032	15.008±0.021	1.137±0.038
WISE J0542−1628	1	—	16.577±0.135	>15.887	>15.934	—	—	—	15.265±0.023	13.968±0.018	1.297±0.030
	3	—	16.64±0.08	16.57±0.10	16.63±0.14	—	—	—	—	—	—
WISE J0611−0410	1	—	15.489±0.055	14.645±0.048	14.221±0.070	—	—	—	13.069±0.017	12.924±0.017	0.145±0.024
WISE J0612−3036	2	—	17.096±0.191	>15.808	>15.781	—	—	—	15.588±0.026	14.033±0.019	1.555±0.032
	3	—	17.00±0.09	17.06±0.11	17.34±0.21	—	—	—	—	—	—
WISE J0612−4920	-	—	—	—	—	—	—	—	14.732±0.021	14.130±0.019	0.602±0.028
WISE J0614+3912	2	—	16.933±0.163	16.356±0.246	>16.283	—	—	—	15.190±0.023	13.599±0.018	1.591±0.029
WISE J0623−0456	3	—	17.51±0.10	17.31±0.11	17.80±0.22	—	—	—	15.494±0.025	13.736±0.018	1.759±0.031
WISE J0625+5646	1	—	16.783±0.151	16.233±0.248	>15.771	—	—	—	15.470±0.025	14.414±0.019	1.056±0.031
	3	—	17.10±0.10	16.90±0.10	16.84±0.15	—	—	—	—	—	—
WISE J0627−1114	1	—	15.487±0.052	15.441±0.075	15.432±0.181	—	—	—	14.272±0.019	13.326±0.018	0.946±0.026

Table 3—Continued

Object Name	Obs. Ref.	Y (mag)	Two Micron All-Sky Survey filter system			Mauna Kea Observatories filter system			Spitzer/IRAC observations		
			J (mag)	H (mag)	K <sub>s</sub> (mag)	J (mag)	H (mag)	K <sub>s</sub> (mag)	ch1 (mag)	ch2 (mag)	ch1-ch2 (mag)
(1)	(2)	(3)	(4)	(5)	(6)	(7)	(8)	(9)	(10)	(11)	(12)
WISE J0656+4205	1	—	15.446±0.049	14.874±0.049	14.831±0.096	—	—	—	—	—	—
WISE J0744+5628	3	—	17.68±0.11	17.59±0.12	17.57±0.20	—	—	—	—	—	—
WISE J0750+2725	4	—	>18.57	>17.92	>16.91	—	—	—	16.679±0.042	14.486±0.020	2.194±0.046
	3	—	19.02 ±0.21	>19.49	>18.63	—	—	—	—	—	—
	7	—	—	—	—	18.69±0.04	19.00±0.06	—	—	—	—
	10	—	—	—	—	18.744±0.053	—	—	—	—	—
WISE J0751−7634	9	—	—	—	—	19.342±0.048	>19.02	—	16.432±0.036	14.621±0.020	1.811±0.041
WISE J0759−4904	-	—	—	—	—	—	—	—	15.623±0.026	13.761±0.018	1.862±0.032
WISE J0819−0335	1	—	14.991±0.044	14.638±0.057	14.586±0.105	—	—	—	13.608±0.018	13.071±0.017	0.537±0.025
WISE J0821+1443	1	—	16.825±0.155	16.515±0.240	>17.089	—	—	—	—	—	—
	3	—	16.78±0.07	16.59±0.08	16.58±0.12	—	—	—	—	—	—
WISE J0836−1859	-	—	—	—	—	—	—	—	16.884±0.047	15.091±0.022	1.793±0.052
WISE J0857+5604	3	—	17.65±0.12	17.49±0.14	17.69±0.22	—	—	—	16.026±0.030	14.137±0.019	1.889±0.035
WISE J0906+4735	4	—	18.126±0.134	>18.33	>17.36	—	—	—	16.474±0.037	14.554±0.020	1.920±0.042
	3	—	18.16±0.16	17.81±0.16	18.54±0.34	—	—	—	—	—	—
WISE J0929+0409	4	—	17.214±0.056	>18.26	>17.37	—	—	—	15.717±0.027	14.238±0.019	1.479±0.033
	10	—	—	—	—	—	17.373±0.067	17.395±0.087	—	—	—
WISE J0952+1955	2	—	17.293±0.179	>17.166	>16.447	—	—	—	15.815±0.028	14.499±0.020	1.316±0.035
	4	—	17.126±0.062	17.223±0.100	>17.337	—	—	—	—	—	—
WISE J1018−2445	-	—	—	—	—	—	—	—	16.132±0.032	14.137±0.019	1.994±0.037
WISE J1019+6529	1	—	16.554±0.149	>16.328	>17.016	—	—	—	15.313±0.024	14.004±0.019	1.309±0.030
	4	—	16.589±0.055	16.517±0.115	16.457±0.179	—	—	—	—	—	—
WISE J1042−3842	-	—	—	—	—	—	—	—	16.771±0.043	14.572±0.020	2.198±0.048
WISE J1122+2550	1	—	16.376±0.130	>16.062	>16.824	—	—	—	15.374±0.024	14.062±0.019	1.312±0.031
	3	—	16.67±0.09	16.64±0.11	16.55±0.12	—	—	—	—	—	—
WISE J1150+6302	4	—	17.72±0.08	>18.01	>16.65	—	—	—	15.614±0.026	13.429±0.018	2.185±0.031
WISE J1217+1626	4	—	>18.52	>17.50	>16.64	—	—	—	15.437±0.024	13.105±0.017	2.332±0.030
	7	—	—	—	—	17.83±0.02	18.18±0.05	—	—	—	—
WISE J1311+0122	7	—	—	—	—	19.16±0.12	—	—	16.817±0.045	14.676±0.020	2.142±0.049
WISE J1311+3629	1	—	15.545±0.053	14.752±0.056	14.140±0.049	—	—	—	13.164±0.017	13.191±0.017	−0.027±0.025
WISE J1320+6034	2	—	16.789±0.188	>16.806	>15.622	—	—	—	15.833±0.028	14.496±0.020	1.336±0.034
	2	—	17.189±0.257	>15.759	>16.921	—	—	—	—	—	—
	4	—	16.496±0.092	16.724±0.149	16.396±0.213	—	—	—	—	—	—
	4	—	16.947±0.084	16.564±0.128	17.431±0.427	—	—	—	—	—	—
WISE J1322−2340	4	—	17.006±0.105	16.605±0.141	16.991±0.399	—	—	—	15.666±0.026	13.892±0.018	1.775±0.032
WISE J1348+6603	1	—	16.943±0.191	15.909±0.155	15.259±0.152	—	—	—	13.953±0.018	13.821±0.018	0.131±0.026
	4	—	17.109±0.128	15.700±0.110	15.052±0.126	—	—	—	—	—	—
	4	—	17.174±0.070	15.841±0.072	15.551±0.109	—	—	—	—	—	—
	7	—	—	—	—	20.20±0.13	21.45±0.41	—	16.884±0.047	14.061±0.019	2.823±0.050
WISE J1405+5534	-	—	—	—	—	—	—	—	15.990±0.030	14.718±0.021	1.272±0.036
WISE J1436−1814	-	—	—	—	—	—	—	—	15.853±0.028	14.443±0.019	1.411±0.034
WISE J1457+5815	2	—	17.137±0.261	>17.636	>17.320	—	—	—	—	—	—
	2	—	16.954±0.218	>16.725	>15.464	—	—	—	—	—	—
	2	—	16.825±0.169	16.638±0.287	>16.704	—	—	—	—	—	—
	4	—	>17.48	>16.42	>15.03	—	—	—	—	—	—
WISE J1506+7027	7	—	—	—	—	13.56±0.05	13.91±0.04	—	12.629±0.017	11.315±0.016	1.314±0.023
	4	—	14.328±0.095	14.150±0.203	14.048±0.136	—	—	—	—	—	—
WISE J1519+7009	4	—	>17.58	>16.82	—	—	—	—	16.194±0.033	14.088±0.019	2.105±0.038
	7	—	—	—	—	17.88±0.03	18.28±0.07	—	—	—	—

Table 3—Continued

Object Name	Obs. Ref.	Y (mag)	Two Micron All-Sky Survey filter system			Mauna Kea Observatories filter system			Spitzer/IRAC observations		
			J (mag)	H (mag)	K <sub>s</sub> (mag)	J (mag)	H (mag)	K <sub>s</sub> (mag)	ch1 (mag)	ch2 (mag)	ch1-ch2 (mag)
(1)	(2)	(3)	(4)	(5)	(6)	(7)	(8)	(9)	(10)	(11)	(12)
WISE J1541−2250	12	—	—	—	—	21.16±0.36	20.99±0.52	—	16.725±0.044	14.230±0.020	2.495±0.048
WISE J1612−3420	-	—	—	—	—	—	—	—	15.445±0.025	13.856±0.018	1.589±0.031
WISE J1614+1739	6	19.43±0.10	—	—	—	—	—	—	16.426±0.036	14.218±0.019	2.209±0.041
	9	—	—	—	—	19.084±0.059	18.471±0.216	—	—	—	—
WISE J1617+1807	6	18.71±0.04	—	—	—	—	—	—	15.964±0.029	14.097±0.019	1.868±0.035
	9	—	—	—	—	17.659±0.080	18.234±0.078	—	—	—	—
WISE J1622−0959	1	—	16.398±0.118	>16.615	15.737±0.257	—	—	—	15.363±0.024	14.146±0.019	1.217±0.031
	4	—	16.44±0.03	16.05±0.05	16.07±0.11	—	—	—	—	—	—
WISE J1627+3255	1	—	16.720±0.128	16.558±0.251	>17.362	—	—	—	15.219±0.023	13.618±0.018	1.601±0.029
	4	—	16.48±0.04	16.40±0.05	—	—	—	—	—	—	—
	6	17.49±0.02	16.61±0.02	—	—	—	—	—	—	—	—
WISE J1647+5632	1	—	16.911±0.180	15.259±0.084	14.611±0.087	—	—	—	13.253±0.017	13.128±0.017	0.125±0.025
	4	—	16.590±0.062	15.336±0.060	14.483±0.072	—	—	—	—	—	—
WISE J1653+4444	6	18.11±0.02	17.59±0.03	17.53±0.05	—	—	—	—	15.671±0.026	13.869±0.018	1.802±0.032
WISE J1711+3500	4	—	17.886±0.130	>18.12	—	—	—	—	16.459±0.037	14.623±0.020	1.836±0.042
WISE J1717+6129	7	—	—	—	—	18.49±0.04	18.91±0.09	—	17.063±0.052	15.134±0.022	1.929±0.057
	4	—	>18.93	>18.17	>16.75	—	—	—	—	—	—
WISE J1728+5716	6	18.59±0.05	17.68±0.05	17.88±0.07	—	—	—	—	16.469±0.037	14.986±0.021	1.484±0.042
WISE J1738+2732	7	—	—	—	—	19.47±0.08	20.66±0.38	—	17.097±0.053	14.476±0.019	2.621±0.057
WISE J1741+2553	1	—	16.451±0.099	16.356±0.216	>16.785	—	—	—	14.428±0.020	12.388±0.017	2.040±0.026
	4	—	16.48±0.02	16.24±0.04	16.89±0.20	—	—	—	—	—	—
	6	17.23±0.02	16.53±0.02	16.63±0.03	—	—	—	—	—	—	—
WISE J1804+3117	7	—	—	—	—	18.70±0.05	19.21±0.11	—	16.616±0.039	14.602±0.020	2.014±0.044
	4	—	>18.88	>18.24	>16.86	—	—	—	—	—	—
WISE J1812+2721	7	—	—	—	—	18.19±0.06	18.83±0.16	—	—	—	—
	4	—	>18.58	>17.77	>17.03	—	—	—	—	—	—
WISE J1828+2650	11	—	—	—	—	23.57±0.35	22.85±0.24	—	16.917±0.020	14.322±0.020	2.595±0.028
WISE J1830+4542	2	—	>18.752	16.082±0.179	15.369±0.183	—	—	—	—	—	—
WISE J1841+7000	2	—	17.211±0.250	16.544±0.241	>15.626	—	—	—	15.630±0.026	14.331±0.019	1.299±0.032
	7	—	—	—	—	16.64±0.03	16.99±0.04	—	—	—	—
	4	—	16.800±0.035	16.912±0.082	—	—	—	—	—	—	—
WISE J1852+3537	1	—	16.501±0.116	>17.407	>17.076	—	—	—	15.587±0.026	14.188±0.019	1.399±0.032
	4	—	>16.70	>15.88	—	—	—	—	—	—	—
WISE J1906+4508	1	—	16.320±0.108	16.129±0.214	>16.107	—	—	—	—	—	—
	3	—	16.36±0.09	16.32±0.09	16.83±0.19	—	—	—	—	—	—
WISE J1952+7240	4	—	15.086±0.045	14.728±0.077	14.650±0.078	—	—	—	14.048±0.019	13.196±0.017	0.852±0.026
WISE J1959−3338	1	—	16.866±0.145	>16.077	>16.227	—	—	—	—	—	—
	9	—	—	—	—	16.714±0.069	17.178±0.054	—	—	—	—
WISE J2018−7423	-	—	—	—	—	—	—	—	—	—	—
WISE J2056+1459	7	—	—	—	—	19.31±0.12	>19.5	—	16.036±0.030	13.924±0.018	2.112±0.036
	4	—	>17.6	>17.1	—	—	—	—	—	—	—
	11	—	—	—	—	19.21±0.07	19.56±0.18	—	—	—	—
WISE J2134−7131	8	—	—	—	—	19.8±0.1	19.7±0.15	—	16.179±0.032	13.958±0.018	2.221±0.037
WISE J2157+2659	5	—	17.31±0.03	17.45±0.04	—	—	—	—	16.012±0.030	14.438±0.019	1.574±0.035
WISE J2209−2734	1	—	16.809±0.152	>16.408	>16.903	—	—	—	15.478±0.025	13.900±0.018	1.577±0.031
WISE J2213+0911	2	—	17.044±0.219	>16.046	>16.092	—	—	—	15.795±0.028	14.565±0.020	1.229±0.034
	2	—	16.834±0.187	>16.071	>17.175	—	—	—	—	—	—
	4	—	16.98±0.05	17.09±0.11	>16.2	—	—	—	—	—	—

Table 3—Continued

Object Name	Obs. Ref.	Y (mag)	Two Micron All-Sky Survey filter system			Mauna Kea Observatories filter system			Spitzer/IRAC observations		
			J (mag)	H (mag)	K <sub>s</sub> (mag)	J (mag)	H (mag)	K <sub>s</sub> (mag)	ch1 (mag)	ch2 (mag)	ch1-ch2 (mag)
(1)	(2)	(3)	(4)	(5)	(6)	(7)	(8)	(9)	(10)	(11)	(12)
	3	—	17.13±0.10	17.32±0.14	16.99±0.20	—	—	—	—	—	—
WISE J2226+0440	4	—	17.02±0.08	>17.3	—	—	—	—	16.124±0.031	14.545±0.020	1.579±0.037
WISE J2237−0614	2	—	17.182±0.191	>16.009	>17.054	—	—	—	16.164±0.032	14.927±0.021	1.236±0.038
	4	—	17.40±0.05	17.40±0.11	>16.8	—	—	—	—	—	—
WISE J2239+1617	1	—	16.079±0.077	15.416±0.091	>14.890	—	—	—	14.147±0.019	13.553±0.018	0.594±0.026
	3	—	16.18±0.07	15.50±0.07	15.36±0.10	—	—	—	—	—	—
WISE J2255−3118	7	—	—	—	—	17.34±0.03	17.70±0.11	—	15.915±0.029	14.210±0.019	1.706±0.035
	4	—	17.29±0.07	>17.7	>16.4	—	—	—	—	—	—
WISE J2313−8037	2	—	16.974±0.236	>16.192	>16.358	—	—	—	—	—	—
WISE J2319−1844	2	—	17.433±0.229	>17.225	>16.009	—	—	—	15.924±0.029	13.949±0.018	1.974±0.034
	7	—	—	—	—	17.56±0.02	17.95±0.05	—	—	—	—
WISE J2325−4105	9	—	—	—	—	19.745±0.050	19.216±0.114	—	16.265±0.033	14.087±0.019	2.178±0.038
WISE J2327−2730	1	—	16.681±0.145	15.481±0.103	14.756±0.096	—	—	—	13.584±0.018	13.337±0.018	0.247±0.025
WISE J2340−0745	1	—	16.540±0.104	16.212±0.193	>16.271	—	—	—	15.199±0.023	13.627±0.018	1.572±0.029
	4	—	16.15±0.03	16.19±0.06	>16.3	—	—	—	—	—	—
WISE J2343−7418	1	—	16.132±0.091	>16.142	15.906±0.311	—	—	—	—	—	—
WISE J2344+1034	7	—	—	—	—	18.78±0.06	19.07±0.11	—	16.734±0.042	14.908±0.021	1.826±0.047
WISE J2348−1028	1	—	16.546±0.118	>16.441	>15.977	—	—	—	15.869±0.028	14.357±0.019	1.512±0.034
	4	—	16.913±0.047	17.099±0.116	>16.443	—	—	—	—	—	—
	3	—	17.01±0.10	16.93±0.12	16.71±0.18	—	—	—	—	—	—
WISE J2359−7335	-	—	16.160±0.105	15.912±0.194	>15.159	—	—	—	14.475±0.020	13.383±0.018	1.092±0.026

Note. — Ref. for JHK instrument or catalog: 2MASS filter system: (1) 2MASS All-Sky Point Source Catalog, (2) 2MASS Reject Table, (3) Bigelow/2MASS, (4) PAIRITEL, (5) Shane/Gemini, (6) FanMt./FanCam; MKO filter system: (7) Palomar/WIRC, (8) Magellan/PANIC, (9) SOAR/SpartanIRC, (10) UKIDSS, (11) Keck/NIRC2. (12) CTIO-4m/NEWFIRM

Table 4. Follow-up Spectroscopy of WISE Brown Dwarf Discoveries

Object Name and J2000 Coordinates (1)	Opt. Sp. Type <sup>c</sup> (2)	NIR Sp. Type <sup>c</sup> (3)	Spectrograph (4)	Int. Time (s) (5)	Tell. Corr. Star <sup>e</sup> (6)	Obs. Date (UT) (7)
WISE J0008–1739	—	T6	Keck/NIRSPEC-J	1200	HD 13936	2010 Dec 18
WISE J0031–3840	—	L2 pec (blue)	IRTF/SpeX	720	HD 4065	2010 Nov 17
WISE J0049+0441	—	L9	IRTF/SpeX	1200	HD 7215	2010 Sep 14
WISE J0106+1518	—	M8 pec	IRTF/SpeX	960	HD 7215	2010 Sep 14
WISE J0123+4142	—	T7	Keck/NIRSPEC-J	600	HD 13936	2010 Dec 19
WISE J0138–0322	—	T3	IRTF/SpeX	960	HD 13936	2010 Aug 17
WISE J0148–7202	—	T9.5	Magellan/FIRE	960	HD 1881	2010 Sep 18
WISE J0150+3827	—	T0	IRTF/SpeX	1920	HD 19600	2010 Sep 12
WISE J0206+2640	—	L9 pec (red)	IRTF/SpeX	1680	HD 19600	2010 Sep 12
WISE J0221+3842	—	T6.5	Palomar/TSpec	1200	HD 19600	2011 Jan 22
WISE J0223–2932	—	T7	Keck/NIRSPEC-H	1200	HD 25792	2010 Jul 18
	—	T7.5	IRTF/SpeX	1560	HD 20423	2010 Aug 17
WISE J0226–0211	—	T7	Keck/NIRSPEC-H	1200	HD 21875	2010 Jul 19
WISE J0254+0223	—	T8	IRTF/SpeX	960	HD 21379	2010 Jul 14
WISE J0305+3954	—	T6	Palomar/TSpec	1200	HD 19600	2011 Jan 22
WISE J0307+2904	—	T6.5	IRTF/SpeX	720	HD 19600	2010 Dec 17
WISE J0313+7807	—	T8.5	Palomar/TSpec	1800	HD 210501	2010 Nov 16
WISE J0323–6025	—	T8.5	Magellan/FIRE	1268	HD 62762	2010 Dec 24
WISE J0333–5856	—	T3	SOAR/OSIRIS	1080	HD 16636	2010 Dec 28
WISE J0410+1502	—	Y0	Magellan/FIRE	600	HD 18620	2010 Nov 18
WISE J0410+1411	—	T6	IRTF/SpeX	600	HD 25175	2010 Dec 18
WISE J0448–1935	—	T5 pec	IRTF/SpeX	240	HD 29433	2010 Aug 17
WISE J0458+6434	—	T8.5	— <sup>a</sup>	— <sup>a</sup>	— <sup>a</sup>	— <sup>a</sup>
WISE J0500–1223	—	T8	IRTF/SpeX	960	HD 31743	2010 Oct 29
WISE J0513+0608	—	T6.5	Palomar/TSpec	1200	HD 40686	2010 Nov 15
WISE J0525+6739	—	T6 pec	IRTF/SpeX	3240	HD 38831	2010 Nov 17
WISE J0528–3308	—	T7 pec	Palomar/TSpec	2400	HD 38056	2010 Nov 16
WISE J0539–1034	—	T5.5	Palomar/TSpec	2400	HD 38386	2011 Jan 22
WISE J0542–1628	—	T6.5	Palomar/TSpec	2400	HD 21127	2010 Nov 16
WISE J0611–0410	—	T0	IRTF/SpeX	360	HD 56525	2010 Dec 18
WISE J0612–3036	—	T6	Palomar/TSpec	1800	HD 32855	2010 Nov 16
WISE J0612–4920	—	T3.5	SOAR/OSIRIS	1080	HD 48169	2010 Dec 28
WISE J0614+3912	—	T6	Palomar/TSpec	1800	HD 56385	2010 Nov 15
WISE J0623–0456	—	T8	IRTF/SpeX	900	HD 45137	2010 Dec 17
WISE J0625+5646	—	T6	Palomar/TSpec	1200	HD 38831	2011 Jan 22
WISE J0627–1114	—	T6	IRTF/SpeX	720	HD 56525	2010 Dec 18
WISE J0656+4205	—	T3	IRTF/SpeX	240	HD 56525	2010 Dec 18
WISE J0744+5628	—	T8	Palomar/TSpec	2400	HD 45105	2011 Jan 22
WISE J0750+2725	—	T8.5	Keck/NIRSPEC-J	1800	HD 71906	2010 Dec 24
	—	T8.5	Keck/NIRSPEC-H	3000	HD 71906	2010 Dec 24/25
WISE J0751–7634	—	T9	Magellan/FIRE	760	HD 98671	2010 Apr 03
WISE J0759–4904	—	T8	Magellan/FIRE	760	CPD-44 2691	2011 Mar 25
WISE J0819–0335	—	T4	IRTF/SpeX	360	HD 65241	2010 Dec 18
WISE J0821+1443	—	T5.5	IRTF/SpeX	720	HD 65241	2010 Dec 18

Table 4—Continued

Object Name and J2000 Coordinates (1)	Opt. Sp. Type <sup>c</sup> (2)	NIR Sp. Type <sup>c</sup> (3)	Spectrograph (4)	Int. Time (s) (5)	Tell. Corr. Star <sup>e</sup> (6)	Obs. Date (UT) (7)
WISE J0836–1859	—	T8 pec	Magellan/FIRE	1522	HD 75159	2011 Mar 27
WISE J0857+5604	—	T8	Palomar/TSpec	2400	HD 45105	2011 Jan 22
WISE J0906+4735	—	T8	Palomar/TSpec	3600	HD 82191	2010 Jun 04
WISE J0929+0409	—	T6.5	Palomar/TSpec	1200	HD 121409	2011 Jan 22
WISE J0952+1955	—	T6	IRTF/Spex	1800	HD 89239	2011 Mar 09
WISE J1018–2445	—	T8	Magellan/FIRE	507	HD 90738	2011 Mar 27
WISE J1019+6529	—	T6	IRTF/Spex	1680	HD 143187	2010 May 27
	—	T6	Palomar/TSpec	2400	SAO 15429	2010 May 30
	T <sub>o</sub> 7	—	Keck/LRIS	3000	HD 151506	2010 Jun 18
WISE J1042–3842	—	T8.5	Magellan/FIRE	1014	HD 90738	2011 Mar 27
WISE J1122+2550	—	T6	IRTF/Spex	1440	HD 99966	2010 Jul 14
WISE J1150+6302	—	T8	Palomar/TSpec	2400	HD 121409	2011 Jan 22
WISE J1217+1626	—	T9	Palomar/TSpec	2400	HD 19600	2011 Jan 22
WISE J1311+0122	—	T9:	Keck/NIRSPEC-H	900	HD 71906	2010 Dec 25
WISE J1311+3629	—	L5 pec (blue)	IRTF/Spex	1200	HD 109615	2011 Jan 26
WISE J1320+6034	—	T6.5	IRTF/Spex	720	HD 118214	2010 Jul 02
WISE J1322–2340	—	T8	IRTF/Spex	1920	HD 114345	2010 May 24
WISE J1348+6603	—	L9	IRTF/Spex	1200	HD 71906	2011 Jan 26
WISE J1405+5534	—	Y0 (pec?)	HST/WFC3	2212	—	2011 Mar 14
WISE J1436–1814	—	T8 pec	Magellan/FIRE	507	HD 130755	2011 Mar 27
WISE J1457+5815	—	T7	IRTF/Spex	960	HD 143187	2010 Jul 14
	T <sub>o</sub> 8	—	Keck/LRIS	3600	HD 238493	2010 Jul 17
WISE J1506+7027	—	T6	Keck/NIRSPEC-H	960	HD 25792 <sup>d</sup>	2010 Oct 20
	—	T6	Palomar/TSpec	960	HD 145454	2011 Jan 22
WISE J1519+7009	—	T8	Palomar/TSpec	2400	HD 145454	2010 Jun 04
WISE J1541–2250	—	Y0	Magellan/FIRE	1522	HD 130755	2011 Mar 27
WISE J1612–3420	—	T6.5	Keck/NIRSPEC-H	1200	HD 152384	2010 Jul 19
WISE J1614+1739	—	T9	Magellan/FIRE	600	HD 98671	2010 Apr 03
WISE J1617+1807	—	T8	— <sup>b</sup>	— <sup>b</sup>	— <sup>b</sup>	— <sup>b</sup>
	T <sub>o</sub> 8	—	Keck/LRIS	3600	BD+18 3241	2010 Jul 17
WISE J1622–0959	—	T6	IRTF/Spex	1200	HD 148968	2010 Apr 23
WISE J1627+3255	—	T6	Keck/NIRSPEC-H	2400	HD 145647	2010 Feb 24
	—	T6	IRTF/Spex	4080	HD 145647	2010 Feb 28
WISE J1647+5632	—	L9 pec (red)	IRTF/Spex	960	HD 179933	2010 Aug 17
WISE J1653+4444	—	T8	IRTF/Spex	1440	HD 143187	2010 Apr 21
	T <sub>o</sub> 8	—	Keck/LRIS	2400	HD 159518	2010 Jul 17
WISE J1711+3500	—	T8	IRTF/Spex	1440	HD 165029	2010 Jul 13
WISE J1717+6129	—	T8	Keck/NIRSPEC-J	1200	HD 179933	2010 Jul 19
	—	T8	Keck/NIRSPEC-H	1200	HD 179933	2010 Jul 19
WISE J1728+5716	—	T6	IRTF/Spex	3120	HD 143187	2010 Apr 21
WISE J1738+2732	—	Y0	HST/WFC3	2012	—	2011 May 12
WISE J1741+2553	—	T9	Magellan/FIRE	1800	HD 98671	2010 Apr 03
	T <sub>o</sub> 9	—	Keck/LRIS	3900	HD 335701	2010 Jun 18
WISE J1804+3117	—	T9.5:	Keck/NIRSPEC-H	1200	HD 171623	2010 Jul 19

Table 4—Continued

Object Name and J2000 Coordinates (1)	Opt. Sp. Type <sup>c</sup> (2)	NIR Sp. Type <sup>c</sup> (3)	Spectrograph (4)	Int. Time (s) (5)	Tell. Corr. Star <sup>e</sup> (6)	Obs. Date (UT) (7)
WISE J1812+2721	—	T8.5:	— <sup>b</sup>	— <sup>b</sup>	— <sup>b</sup>	— <sup>b</sup>
WISE J1828+2650	—	>Y0	HST/WFC3	2012	—	2011 May 09
WISE J1830+4542	—	L9	IRTF/Spex	1920	HD 178207	2010 Sep 12
WISE J1841+7000	—	T5	Palomar/TSpec	2400	HD 179933	2010 Jun 04
	T <sub>o</sub> 5	—	Keck/LRIS	3600	BD+70 1059	2010 Jul 17
WISE J1852+3537	—	T7	IRTF/Spex	1680	HD 174567	2010 May 25
WISE J1906+4508	—	T6	IRTF/Spex	1200	HD 174567	2010 Nov 17
WISE J1952+7240	—	T4	Palomar/TSpec	1200	HD 18187	2010 Nov 16
WISE J1959–3338	—	T8	Palomar/TSpec	3600	HD 194272	2010 Jun 04
WISE J2018–7423	—	T7	— <sup>b</sup>	— <sup>b</sup>		
WISE J2056+1459	—	Y0	Keck/NIRSPEC-J	2400	HD 198070	2010 Oct 21
	—	Y0	Keck/NIRSPEC-H	1800	HD 198069	2010 Nov 22
WISE J2134–7137	—	T9 pec	Magellan/FIRE	600	HD 223296	2010 Sep 18
WISE J2157+2659	—	T7	Palomar/TSpec	1200	HD 208108	2010 Sep 29
WISE J2209–2734	—	T7	Keck/NIRSPEC-H	600	HD 212643	2010 Jul 18
WISE J2213+0911	—	T7	IRTF/Spex	2400	HD 210501	2010 Aug 04
WISE J2226+0440	—	T8.5	Keck/NIRSPEC-J	1200	HD 190807	2010 Jul 18
	—	T8	Keck/NIRSPEC-H	1200	HD 190807	2010 Jul 18
	—	T8	IRTF/Spex	1920	HD 210501	2010 Aug 04
WISE J2237–0614	—	T5	IRTF/Spex	1200	HD 219833	2010 Jul 14
WISE J2239+1617	—	T3	IRTF/Spex	1200	HD 210501	2010 Aug 17
WISE J2255–3118	—	T8	Keck/NIRSPEC-H	1200	HD 202941	2010 Jul 19
	—	T8	IRTF/Spex	2400	HD 202025	2010 Sep 10
WISE J2313–8037	—	T8	— <sup>b</sup>	— <sup>b</sup>	— <sup>b</sup>	— <sup>b</sup>
WISE J2319–1844	—	T7.5	IRTF/Spex	2880	HD 222332	2010 Aug 17
WISE J2325–4105	—	T9 pec	Magellan/FIRE	960	HD 221805	2010 Sep 18
WISE J2327–2730	—	L9	IRTF/Spex	1200	HD 219290	2010 Sep 12
WISE J2340–0745	—	T7	IRTF/Spex	960	HD 219833	2010 Jul 14
	T <sub>o</sub> 7	—	Keck/LRIS	2400	HD 1920	2010 Jul 17
WISE J2343–7418	—	T6	Magellan/FIRE	634	HD 223296	2010 Dec 24
WISE J2344+1034	—	T9	Keck/NIRSPEC-J	1200	HD 198070	2010 Oct 21
WISE J2348–1028	—	T7	IRTF/Spex	960	HD 219833	2010 Jul 14
WISE J2359–7335	—	T5.5	— <sup>b</sup>	— <sup>b</sup>	— <sup>b</sup>	— <sup>b</sup>

<sup>a</sup>See Mainzer et al. (2010) for details on spectroscopic follow-up.

<sup>b</sup>See Burgasser et al. (submitted) for details on spectroscopic follow-up. A newer spectrum of this object from Magellan/FIRE supports a type of T6.5 rather than T5.5 as originally assigned by Burgasser et al. (submitted).

<sup>c</sup>Spectral types are accurate to  $\pm 0.5$  type unless indicated by a “:” symbol to indicate a more uncertain assignment.

<sup>d</sup>Due to closing of the telescope due to fog, no A0 V star was taken on this night so an A0 V observation from an earlier run on 2010 Jul 18 was used.

<sup>e</sup>Telluric corrector stars for optical spectral are G0 dwarfs; those for near-infrared spectra are A0 dwarfs.

Table 5. L and T Dwarfs with Measured Trigonometric Parallaxes

Object Name	$\pi_{trig}$ (mas)	Ref.	NIR Sp. Type	W2 (mag)	$H$ (mag)
(1)	(2)	(3)	(4)	(5)	(6)
a) Objects not known to be binary					
UGPS J072227.51–054031.2	246±33	2	T9	12.197±0.027	16.147±0.205
DENIS J081730.0–615520	203±13	3	T6	11.237±0.017	13.526±0.031
DENIS-P J0255–4700	201.37±3.89	4	L8	10.190±0.021	12.204±0.024
2MASS J0415195–093506	174.34±2.76	5	T8	12.232±0.026	15.537±0.113
Gliese 570D	169.3±1.7	6	T7.5	12.105±0.026	15.268±0.089
2MASS J0937347+293142	163.39±1.76	7	T6	11.652±0.023	14.703±0.068
2MASSW J1507476–162738	136.4±0.6	8	L5	10.367±0.022	11.895±0.024
2MASSW J0036159+182110	114.2±0.8	8	L3.5	10.239±0.020	11.588±0.029
2MASS J0727182+171001	110.14±2.34	5	T7	12.969±0.033	15.756±0.171
CFBDS J005910.90–011401.3	108.2±5.0	1	T8.5	13.668±0.044	18.270±0.050
2MASS J05591914–1404488	97.7±1.3	8	T4.5	11.891±0.023	13.679±0.044
ULAS J133553.45+113005.2	96.7±3.2	1	T8.5	13.839±0.046	18.250±0.010
2MASS J12373919+6526148	96.07±4.78	5	T6.5	12.922±0.028	15.739±0.145
2MASS J0825196+211552	93.8±1.0	8	L7.5	11.574±0.022	13.792±0.032
2MASS J0243137–245329	93.62±3.63	5	T6	12.929±0.030	15.137±0.109
SDSSp J162414.37+002915.6	90.9±1.2	9	T6	13.077±0.032	15.524±0.100
2MASS J1217110–031113	90.8±2.2	9	T7.5	13.195±0.035	15.748±0.119
2MASS J1546291–332511	88.0±1.9	9	T5.5	13.439±0.039	15.446±0.092
SDSSp J125453.90012247.4	84.9±1.9	8	T2	12.391±0.037	14.090±0.025
ULAS J003402.77–005206.7	78.0±3.6	1	T8.5	14.465±0.076	18.490±0.040
SDSSp J053951.99–005902.0	76.12±2.17	5	L5	11.569±0.021	13.104±0.026
2MASSW J1439284+192915	69.6±0.5	8	L1	10.936±0.021	12.041±0.019
2MASS J2356547–155310	68.97±3.42	5	T5.5	13.641±0.041	15.630±0.100
SDSSp J134646.45–003150.4	68.3±2.3	9	T6.5	13.560±0.042	15.459±0.118
2MASSW J1632291+190441	65.6±2.1	8	L8	12.598±0.028	14.612±0.038
DENIS-P J1058.7–1548	57.7±1.0	8	L3	11.758±0.023	13.226±0.025
2MASSW J1658037+702701	53.9±0.7	8	L1	11.388±0.022	12.470±0.032
Gliese 584C	53.70±1.24	6	L8	12.996±0.033	14.928±0.081
SDSSp J132629.82–003831.5	49.98±6.33	5	L8	12.718±0.030	15.050±0.060
SDSS J015141.69+124429.6	46.73±3.37	5	T1	13.823±0.053	15.603±0.112
SDSSp J144600.60+002452.0	45.46±3.25	5	L6	12.882±0.034	14.514±0.035
SDSSp J175032.96+175903.9	36.24±4.53	5	T3.5	14.414±0.057	15.952±0.132
2MASSW J0030300–145033	37.42±4.50	5	L7	13.241±0.034	15.273±0.100
2MASS J1711457+223204	33.11±4.81	5	L6.5	13.802±0.040	15.797±0.109
GD 165B <sup>a</sup>	31.7±2.5	10	L4	13.042±0.032	14.781±0.070
2MASSW J1328550+211449	31.0±3.8	8	L5	13.383±0.036	15.002±0.081
2MASSW J0326137+295015	31.0±1.5	8	L3.5	12.746±0.029	14.395±0.050
SDSSp J003259.36+141036.6	30.14±5.16	5	L8	13.600±0.041	15.648±0.142
SDSS J020742.48+000056.2	29.3±4.0	1	T4.5	15.035±0.100	>16.396
ULAS J082707.67–020408.2	26.0±3.1	1	T5.5	15.290±0.142	17.440±0.050
HD 89744B	25.65±0.70	6	L0	12.759±0.029	14.022±0.033
SDSSp J225529.09–003433.4	16.19±2.59	5	L0	13.715±0.052	14.756±0.058



Table 5—Continued

Object Name	$\pi_{trig}$ (mas)	Ref.	NIR Sp. Type	W2 (mag)	$H$ (mag)
(1)	(2)	(3)	(4)	(5)	(6)
b) Known binaries/multiples:					
$\epsilon$ Ind Bab	275.76 $\pm$ 0.69	6	T1	9.443 $\pm$ 0.020	11.510 $\pm$ 0.020
2MASS J0746425+200032	81.9 $\pm$ 0.3	8	L0.5	9.889 $\pm$ 0.022	11.007 $\pm$ 0.022
2MASS J12255432–2739466	75.1 $\pm$ 2.5	9	T6	12.692 $\pm$ 0.030	15.098 $\pm$ 0.081
2MASS J1534498–295227	73.6 $\pm$ 1.2	9	T5.5	12.592 $\pm$ 0.029	14.866 $\pm$ 0.102
SDSSp J042348.57–041403.5	65.93 $\pm$ 1.70	5	T0	11.559 $\pm$ 0.025	13.463 $\pm$ 0.035
HN Peg B	54.37 $\pm$ 0.85	6	T2.5	12.574 $\pm$ 0.029	15.400 $\pm$ 0.030
Kelu-1AB	53.6 $\pm$ 2.0	8	L2	10.918 $\pm$ 0.025	12.392 $\pm$ 0.025
DENIS-P J0205.4–1159	50.6 $\pm$ 1.5	8	L7	11.724 $\pm$ 0.030	13.568 $\pm$ 0.037
DENIS-P J1228.2–1547	49.4 $\pm$ 1.9	8	L5	11.675 $\pm$ 0.034	13.347 $\pm$ 0.032
Gliese 417BC	46.04 $\pm$ 0.90	6	L4.5	11.616 $\pm$ 0.023	13.499 $\pm$ 0.032
2MASSW J1728114+394859	41.49 $\pm$ 3.26	5	L7	12.597 $\pm$ 0.017	14.756 $\pm$ 0.066
G 124-62B	36.39 $\pm$ 3.57	4	L0.5	12.077 $\pm$ 0.026	13.190 $\pm$ 0.031
SDSS J102109.69–030420.1	34.4 $\pm$ 4.6	9	T3	13.773 $\pm$ 0.041	15.346 $\pm$ 0.101
2MASSW J2101154+175658	30.14 $\pm$ 3.42	5	L7.5	13.512 $\pm$ 0.036	15.861 $\pm$ 0.182

Note. — References: (1) Marocco et al. (2010); (2) Lucas et al. (2010); (3) Artigau et al. (2010); (4) Costa et al. (2006); (5) Vrba et al. (2004); (6) Perryman et al. (1997); (7) Schilbach et al. (2009); (8) Dahn et al. (2002); (9) Tinney et al. (2003); (10) van Altena et al. (1995);

<sup>a</sup>It is assumed that most of the W2 flux comes from the L dwarf companion and not the white dwarf primary.

Table 6. Astrometry for WISE Brown Dwarf Discoveries

Object Name	Dist. Est.	RA (J2000)	Dec (J2000)	RA err	Dec err	Reference	MJD	$\mu_\alpha$	$\mu_\delta$	$\mu_{total}$	$v_{tan}$
(1)	(2)	(3)	(4)	(5)	(6)	(7)	(8)	arcsec/yr	arcsec/yr	arcsec/yr	km/s
WISE 0008-1739	22.0	2.2073557	-17.6563363	0.179	0.185	WISE epoch 1	55363.39	$-0.116 \pm 0.589$	$-1.108 \pm 0.532$		
		2.2073061	-17.6565639	0.279	0.293	WISE epoch 2	55542.36				
		2.2073379	-17.6564659	0.485	0.309	Spitzer	55571				
WISE 0031-3840	22.0	7.830238	-38.676575	0.06	0.07	2MASS PSC	51391.3054	$0.548 \pm 0.006$	$-0.049 \pm 0.007$	$0.550 \pm 0.009$	$57.4 \pm 1.0$
		7.8323524	-38.6766992	0.045	0.044	WISE epoch 1	55357.83				
		7.8324281	-38.6767498	0.046	0.044	WISE epoch 2	55535.75				
WISE 0049+0441	19.2	12.367782	4.682658	0.07	0.12	2MASS PSC	51768.4283	$0.315 \pm 0.008$	$0.228 \pm 0.012$	$0.389 \pm 0.014$	$35.4 \pm 1.3$
		12.3686648	4.6833142	0.053	0.053	WISE epoch 1	55382.38				
		12.3686625	4.6832837	0.066	0.062	WISE epoch 2	55560.23				
		12.3686292	4.6833140	0.206	0.260	Spitzer	55591				
WISE 0106+1518	43.8	16.655734	15.315453	0.06	0.06	2MASS PSC	50696.4341	$-0.349 \pm 0.005$	$-0.219 \pm 0.004$	$0.412 \pm 0.006$	$85.5 \pm 1.3$
		16.65554497	15.31529756	0.058	0.045	SDSS DR7	51464.3				
		16.6544791	15.3146837	0.048	0.047	WISE epoch 1	55298.38				
		16.6543939	15.3146032	0.053	0.052	WISE epoch 2	55567.30				
		16.6543859	15.3146712	0.157	0.351	Spitzer	55633				
WISE 0123+4142	21.9	20.8883990	41.7010723	0.301	0.309	WISE epoch 1	55217.30	$0.885 \pm 0.293$	$0.894 \pm 0.280$	$1.258 \pm 0.405$	$130.6 \pm 42.1$
		20.8885524	41.7010216	0.230	0.237	WISE epoch 2	55408.13				
		20.8886559	41.7012568	0.282	0.292	WISE epoch 3	55583.18				
		20.8887898	41.7012899	0.222	0.182	Spitzer	55646				
WISE 0138-0322	17.7	24.652009	-3.371703	0.18	0.17	2MASS PSC	51079.2142	$0.132 \pm 0.016$	$-0.276 \pm 0.015$	$0.306 \pm 0.022$	$25.7 \pm 1.8$
		24.6524238	-3.3725727	0.065	0.066	WISE epoch 1	55298.71				
		24.6524451	-3.3726575	0.080	0.081	WISE epoch 2	55570.43				
		24.6523636	-3.3726830	0.441	0.318	Spitzer	55624				
WISE 0148-7202	12.1	27.0301973	-72.0496466	0.179	0.166	WISE epoch 1	55324.30	$1.106 \pm 0.355$	$-0.073 \pm 0.332$		
		27.0306266	-72.0497359	0.158	0.149	WISE epoch 2	55504.92				
		27.0306647	-72.0496657	0.207	0.212	Spitzer epoch 1	55458				
		27.0308488	-72.0496856	0.188	0.177	Spitzer epoch 2	55580				
WISE 0150+3827	18.8	27.541553	38.457203	0.08	0.09	2MASS PSC	50771.1947	$0.858 \pm 0.007$	$-0.136 \pm 0.008$	$0.869 \pm 0.011$	$77.4 \pm 0.9$
		27.5452547	38.4567195	0.060	0.061	WISE epoch 1	55221.20				
		27.5454455	38.4567394	0.055	0.056	WISE epoch 2	55410.43				
		27.5455516	38.4566765	0.064	0.063	WISE epoch 3	55586.55				
		27.5457112	38.4567635	0.258	0.172	Spitzer	55646				
WISE 0206+2640	17.9	31.603883	26.673265	0.09	0.08	2MASS PSC	51506.2524	$0.433 \pm 0.009$	$-0.007 \pm 0.008$	$0.433 \pm 0.012$	$36.7 \pm 1.0$
		31.6052461	26.6732349	0.056	0.055	WISE epoch 1	55220.34				
		31.6053520	26.6732556	0.056	0.056	WISE epoch 2	55408.11				
		31.6053749	26.6732325	0.056	0.053	WISE epoch 3	55585.36				
		31.6053859	26.6732165	0.240	0.237	Spitzer	55646				
WISE 0221+3842	21.4	35.2747550	38.7009027	0.221	0.236	WISE epoch 1	55227.70	$0.152 \pm 0.258$	$0.378 \pm 0.246$		
		35.2750666	38.7008127	0.225	0.244	WISE epoch 2	55417.64				
		35.2749576	38.7007578	0.279	0.308	WISE epoch 3	55592.18				

Table 6—Continued

Object Name	Dist. Est. (pc)	RA (J2000) (deg)	Dec (J2000) (deg)	RA err (arcsec)	Dec err (arcsec)	Reference	MJD	$\mu_\alpha$ arcsec/yr	$\mu_\delta$ arcsec/yr	$\mu_{total}$ arcsec/yr	$v_{tan}$ km/s
(1)	(2)	(3)	(4)	(5)	(6)	(7)	(8)	(9)	(10)	(11)	(12)
		35.2747902	38.7010427	0.239	0.184	Spitzer	55651				
WISE 0223-2932	13.3	35.8432105	-29.5492102	0.114	0.120	WISE epoch 1	55298.25	0.464±0.250	-0.361±0.213		
		35.8432970	-29.5493427	0.155	0.161	WISE epoch 2	55570.15				
		35.8433178	-29.5492604	0.420	0.158	Spitzer epoch 1	55457				
		35.8434107	-29.5492880	0.543	0.153	Spitzer epoch 2	55586				
WISE 0226-0211	19.3	36.5998759	-2.1952331	0.214	0.228	WISE epoch 1	55217.31	0.204±0.300	0.198±0.311		
		36.5999766	-2.1951802	0.253	0.274	WISE epoch 2	55406.74				
		36.5999836	-2.1951423	0.240	0.252	WISE epoch 3	55580.86				
		36.5998761	-2.1955429	0.216	0.297	Spitzer epoch 1	55457				
		36.5997878	-2.1950815	0.609	0.498	Spitzer epoch 2	55620				
WISE 0254+0223	6.9	43.532860	2.398985	0.28	0.39	2MASS PSC	51808.4049	2.534±0.028	0.243±0.037	2.546±0.046	83.3±1.5
		43.5393853	2.3995999	0.078	0.079	WISE epoch 1	55222.06				
		43.5398386	2.3996419	0.077	0.076	WISE epoch 2	55412.34				
		43.5400634	2.3996809	0.089	0.084	WISE epoch 3	55588.27				
		43.5399385	2.3996560	0.270	0.275	Spitzer epoch 1	55457				
		43.5401933	2.3996251	0.138	0.218	Spitzer epoch 2	55623				
WISE 0305+3954	23.1	46.3897630	39.9095717	0.214	0.231	WISE epoch 1	55236.15	0.255±0.270	0.121±0.273		
		46.3898024	39.9096596	0.238	0.252	WISE epoch 2	55426.37				
		46.3898707	39.9096158	0.235	0.224	Spitzer	55666				
WISE 0307+2904	24.0	46.8524209	29.0798600	0.288	0.313	WISE epoch 1	55233.50	0.091±0.307	-0.079±0.312		
		46.8523979	29.0798509	0.339	0.363	WISE epoch 2	55423.59				
		46.8524465	29.0798329	0.229	0.213	Spitzer	55666				
WISE 0313+7807	8.1	48.3581817	78.1289629	0.078	0.081	WISE epoch 1	55256.85	0.147±0.151	-0.004±0.148		
		48.3584055	78.1289989	0.071	0.071	WISE epoch 2	55448.07				
		48.3587833	78.1290043	0.182	0.131	Spitzer epoch 1	55551				
		48.3585620	78.1289581	0.233	0.249	Spitzer epoch 2	55675				
WISE 0323-6025	15.5	50.9063954	-60.4318079	0.171	0.163	WISE epoch 1	55369.41	0.559±0.401	-0.041±0.396		
		50.9065228	-60.4318044	0.158	0.157	WISE epoch 2	55549.31				
		50.9066237	-60.4318259	0.288	0.170	Spitzer epoch 1	55457				
		50.9065579	-60.4319125	0.214	0.238	Spitzer epoch 2	55580				
WISE 0333-5856	16.8	53.456318	-58.936623	0.08	0.07	2MASS PSC	51484.2013	-0.126±0.008	-0.607±0.007	0.620±0.011	49.4±0.8
		53.4555971	-58.9383889	0.053	0.052	WISE epoch 1	55377.88				
		53.4555377	-58.9385002	0.054	0.053	WISE epoch 2	55554.87				
		53.4556255	-58.9385088	0.290	0.121	Spitzer	55550				
WISE 0410+1502	9.0	62.5946668	15.0468130	0.187	0.202	WISE epoch 1	55246.29	1.044±0.236	-2.193±0.237	2.429±0.334	103.6±14.3
		62.5949435	15.0465208	0.164	0.178	WISE epoch 2	55434.04				
		62.5949913	15.0464124	0.215	0.126	Spitzer epoch 1	55490				
		62.5950070	15.0461156	0.201	0.189	Spitzer epoch 2	55666				
WISE 0410+1411	27.5	62.7269959	14.1920334	0.285	0.319	WISE epoch 1	55246.20	0.019±0.302	-0.198±0.326		

Table 6—Continued

Object Name	Dist. Est. (pc)	RA (J2000) (deg)	Dec (J2000) (deg)	RA err (arcsec)	Dec err (arcsec)	Reference	MJD	$\mu_\alpha$ arcsec/yr	$\mu_\delta$ arcsec/yr	$\mu_{total}$ arcsec/yr	$v_{tan}$ km/s
(1)	(2)	(3)	(4)	(5)	(6)	(7)	(8)	(9)	(10)	(11)	(12)
		62.7269105	14.1920574	0.316	0.358	WISE epoch 2	55434.04				
		62.7269833	14.1919793	0.209	0.214	Spitzer	55666				
WISE 0448-1935	21.4	72.219501	-19.598743	0.24	0.22	2MASS Reject	51838.3186	0.907 $\pm$ 0.021	0.736 $\pm$ 0.020	1.168 $\pm$ 0.029	118.5 $\pm$ 2.9
		72.219098	-19.599138	0.34	0.32	2MASS Reject	51146.2679				
		72.2220593	-19.5968744	0.127	0.136	WISE epoch 1	55248.32				
		72.2221445	-19.5966820	0.139	0.147	WISE epoch 2	55439.14				
WISE 0458+6434	7.3 <sup>a</sup>	74.7245596	64.5812869	0.084	0.085	WISE epoch 1	55262.15	0.185 $\pm$ 0.141	0.118 $\pm$ 0.149		
		74.7247231	64.5813115	0.082	0.085	WISE epoch 2	55453.42				
		74.7248445	64.5812701	0.140	0.164	Spitzer epoch 1	55499				
		74.7247249	64.5813482	0.153	0.167	Spitzer epoch 2	55670				
WISE 0500-1223	12.4	75.0126995	-12.3953585	0.139	0.149	WISE epoch 1	55251.81	-0.646 $\pm$ 0.293	0.546 $\pm$ 0.322		
		75.0126275	-12.3952592	0.120	0.130	WISE epoch 2	55444.82				
		75.0126456	-12.3952697	0.162	0.195	Spitzer	55487				
WISE 0513+0608	14.8	78.321983	6.138618	0.13	0.14	2MASS PSC	51539.2078	0.006 $\pm$ 0.014	-0.427 $\pm$ 0.015	0.427 $\pm$ 0.021	30.0 $\pm$ 1.4
		78.3219766	6.1374197	0.114	0.122	WISE epoch 1	55259.05				
		78.3220117	6.1373744	0.110	0.118	WISE epoch 2	55450.18				
		78.3220245	6.1372354	0.175	0.187	Spitzer	55666				
WISE 0525+6739	25.6	81.4012734	67.6644117	0.211	0.236	WISE epoch 1	55266.05	0.072 $\pm$ 0.240	0.671 $\pm$ 0.258		
		81.4011703	67.6638300	0.169	0.189	WISE epoch 2	55457.33				
		81.4014639	67.6644615	0.165	0.142	Spitzer epoch 1	55499				
		81.4012915	67.6644678	0.168	0.173	Spitzer epoch 2	55670				
WISE 0528-3308	19.0	82.1854678	-33.1399839	0.171	0.186	WISE epoch 1	55259.30	0.037 $\pm$ 0.361	-0.162 $\pm$ 0.406		
		82.1855415	-33.1399867	0.149	0.161	WISE epoch 2	55450.45				
		82.1854770	-33.1400365	0.218	0.276	Spitzer	55505				
WISE 0539-1034	26.0	84.9875161	-10.5768926	0.235	0.261	WISE epoch 1	55264.73	0.069 $\pm$ 0.250	-0.831 $\pm$ 0.261		
		84.9874342	-10.5768627	0.241	0.268	WISE epoch 2	55456.07				
		84.9875164	-10.5771147	0.159	0.149	Spitzer	55669				
WISE 0542-1628	15.3	85.631043	-16.475651	0.16	0.15	2MASS PSC	51196.1551	-0.223 $\pm$ 0.015	0.282 $\pm$ 0.015	0.360 $\pm$ 0.021	26.1 $\pm$ 1.5
		85.6302683	-16.4747751	0.127	0.134	WISE epoch 1	55265.19				
		85.6303505	-16.4747098	0.128	0.136	WISE epoch 2	55456.47				
		85.6303011	-16.4747332	0.184	0.204	Spitzer epoch 1	55548				
		85.6302423	-16.4746955	0.183	0.203	Spitzer epoch 2	55671				
WISE 0611-0410	17.7	92.896153	-4.172446	0.06	0.07	2MASS PSC	51095.3441	0.082 $\pm$ 0.006	-0.283 $\pm$ 0.007	0.295 $\pm$ 0.009	24.7 $\pm$ 0.8
		92.8963777	-4.1733529	0.055	0.054	WISE epoch 1	55275.79				
		92.8964286	-4.1733818	0.052	0.053	WISE epoch 2	55467.18				
		92.8964138	-4.1734137	0.165	0.167	Spitzer	55669				
WISE 0612-3036	17.0	93.058322	-30.602640	0.23	0.22	2MASS Reject	51470.3267	-0.137 $\pm$ 0.022	-0.256 $\pm$ 0.021	0.290 $\pm$ 0.030	23.4 $\pm$ 2.5
		93.0578204	-30.6033715	0.113	0.119	WISE epoch 1	55276.30				
		93.0578414	-30.6033901	0.121	0.133	WISE epoch 2	55467.73				

Table 6—Continued

Object Name	Dist. Est. (pc)	RA (J2000) (deg)	Dec (J2000) (deg)	RA err (arcsec)	Dec err (arcsec)	Reference	MJD	$\mu_\alpha$ arcsec/yr	$\mu_\delta$ arcsec/yr	$\mu_{total}$ arcsec/yr	$v_{tan}$ km/s
(1)	(2)	(3)	(4)	(5)	(6)	(7)	(8)	(9)	(10)	(11)	(12)
WISE 0612-4920	29.2	93.0578281	-30.6034545	0.217	0.180	Spitzer epoch 1	55553	$-0.041 \pm 0.156$	$0.405 \pm 0.165$	$0.529 \pm 0.032$	$36.4 \pm 2.2$
		93.0577910	-30.6034781	0.243	0.167	Spitzer epoch 2	55675				
		93.0362290	-49.3400502	0.065	0.069	WISE epoch 1	55277.56				
		93.0362551	-49.3399726	0.063	0.066	WISE epoch 2	55469.23				
WISE 0614+3912	14.5	93.0362060	-49.3400468	0.212	0.223	Spitzer	55592	$-0.185 \pm 0.023$	$-0.496 \pm 0.022$	$0.529 \pm 0.032$	$36.4 \pm 2.2$
		93.531962	39.211395	0.24	0.23	2MASS Reject	51519.4327				
		93.5312108	39.2099957	0.112	0.119	WISE epoch 1	55275.58				
		93.5312727	39.2099085	0.111	0.118	WISE epoch 2	55466.94				
WISE 0623-0456	11.3	93.5312418	39.2098538	0.150	0.183	Spitzer epoch 1	55548	$-0.949 \pm 0.195$	$0.410 \pm 0.177$	$1.034 \pm 0.263$	$55.4 \pm 14.1$
		93.5311786	39.2098092	0.161	0.208	Spitzer epoch 2	55670				
		95.7913950	-4.9401879	0.120	0.130	WISE epoch 1	55277.49				
		95.7912970	-4.9400740	0.123	0.131	WISE epoch 2	55468.97				
WISE 0625+5646	19.9	95.7911133	-4.9400708	0.183	0.142	Spitzer	55675	$-0.039 \pm 0.027$	$-0.117 \pm 0.023$	$0.123 \pm 0.035$	$11.6 \pm 3.3$
		96.426281	56.774120	0.29	0.24	2MASS PSC	51448.4972				
		96.4258596	56.7737642	0.144	0.159	WISE epoch 1	55276.24				
		96.4261210	56.7737633	0.166	0.182	WISE epoch 2	55467.53				
WISE 0627-1114	12.0	96.4260484	56.7737822	0.184	0.209	Spitzer epoch 1	55551	$-0.013 \pm 0.009$	$-0.343 \pm 0.008$	$0.343 \pm 0.012$	$19.5 \pm 0.7$
		96.4260262	56.7737448	0.182	0.144	Spitzer epoch 2	55675				
		96.833665	-11.240032	0.10	0.08	2MASS PSC	51182.2328				
		96.8336050	-11.2411311	0.068	0.069	WISE epoch 1	55278.95				
WISE 0656+4205	16.6	96.8336478	-11.2411066	0.064	0.066	WISE epoch 2	55470.56	$0.334 \pm 0.009$	$0.168 \pm 0.007$	$0.374 \pm 0.011$	$29.4 \pm 0.9$
		96.8336096	-11.2411756	0.170	0.179	Spitzer	55671				
		104.038623	42.091709	0.09	0.07	2MASS PSC	51122.4585				
		104.0399904	42.0922078	0.063	0.067	WISE epoch 1	55280.98				
WISE 0744+5628	15.7	104.0401314	42.0922872	0.062	0.066	WISE epoch 2	55474.39	$0.413 \pm 0.489$	$-0.122 \pm 0.528$	$0.374 \pm 0.011$	$29.4 \pm 0.9$
		116.2384910	56.4725580	0.169	0.182	WISE epoch 1	55288.54				
		116.2386617	56.4725324	0.193	0.209	WISE epoch 2	55480.15				
		117.5157736	27.4293219	0.221	0.245	WISE epoch 1	55295.29				
WISE 0750+2725	14.1	117.5157144	27.4290782	0.220	0.250	WISE epoch 2	55486.76	$-0.869 \pm 0.424$	$-1.107 \pm 0.438$	$0.374 \pm 0.011$	$29.4 \pm 0.9$
		117.5156237	27.4291158	0.190	0.164	Spitzer	55540				
		117.7865794	-76.5804610	0.120	0.116	WISE epoch 1	55247.30				
		117.7864634	-76.5804277	0.117	0.111	WISE epoch 2	55427.39				
WISE 0751-7634	13.0	117.7868452	-76.5804157	0.187	0.178	Spitzer epoch 1	55465	$0.227 \pm 0.197$	$-0.063 \pm 0.187$	$0.374 \pm 0.011$	$29.4 \pm 0.9$
		117.7870092	-76.5804892	0.206	0.192	Spitzer epoch 2	55665				
		119.9457963	-49.0816846	0.117	0.123	WISE epoch 1	55327.64				
		119.9458493	-49.0817034	0.102	0.104	WISE epoch 2	55518.12				
WISE 0759-4904	11.5	119.9457564	-49.0816408	0.205	0.207	Spitzer	55563	$-0.171 \pm 0.269$	$0.143 \pm 0.279$	$0.374 \pm 0.011$	$29.4 \pm 0.9$
		124.992527	-3.590735	0.07	0.07	2MASS PSC	51158.3227				
WISE 0819-0335	14.1							$-0.190 \pm 0.007$	$-0.163 \pm 0.007$	$0.250 \pm 0.010$	$16.7 \pm 0.7$

Table 6—Continued

Object Name	Dist. Est. (pc)	RA (J2000) (deg)	Dec (J2000) (deg)	RA err (arcsec)	Dec err (arcsec)	Reference	MJD	$\mu_\alpha$ arcsec/yr	$\mu_\delta$ arcsec/yr	$\mu_{total}$ arcsec/yr	$v_{tan}$ km/s		
(1)	(2)	(3)	(4)	(5)	(6)	(7)	(8)	(9)	(10)	(11)	(12)		
		124.9918916	-3.5912481	0.065	0.068	WISE epoch 1	55309.51						
		124.9919050	-3.5912565	0.061	0.062	WISE epoch 2	55500.87						
		124.9918753	-3.5912920	0.177	0.134	Spitzer	55582						
WISE 0821+1443	20.9	125.382219	14.723092	0.27	0.27	2MASS PSC	50757.4660	-0.098±0.024	-0.300±0.024	0.316±0.034	31.3±3.4		
		125.3817907	14.7220453	0.182	0.202	WISE epoch 1	55304.68						
		125.3819009	14.7220247	0.189	0.212	WISE epoch 2	55495.78						
WISE 0836-1859	20.1	129.1713270	-18.9964194	0.300	0.335	WISE epoch 1	55319.57	0.946±0.530	0.523±0.539				
		129.1715540	-18.9964381	0.327	0.366	WISE epoch 2	55510.58						
		129.1715373	-18.9963358	0.188	0.132	Spitzer	55563						
WISE 0857+5604	13.0	134.3176838	56.0687846	0.139	0.154	WISE epoch 1	55299.85	-1.000±0.311	-0.008±0.326				
		134.3175161	56.0687720	0.132	0.143	WISE epoch 2	55494.98						
		134.3173712	56.0687644	0.231	0.202	Spitzer	55548						
WISE 0906+4735	16.3	136.7056493	47.5940957	0.240	0.262	WISE epoch 1	55306.35	-0.528±0.530	-0.649±0.558				
		136.7055665	47.5939434	0.233	0.247	WISE epoch 2	55497.55						
		136.7055675	47.5940058	0.349	0.337	Spitzer	55554						
WISE 0929+0409	16.8	142.2782394	4.1660918	0.158	0.171	WISE epoch 1	55324.92	0.105±0.374	-0.773±0.367				
		142.2782409	4.1659982	0.196	0.213	WISE epoch 2	55515.74						
		142.2783300	4.1659286	0.234	0.188	Spitzer	55563						
WISE 0952+1955	20.5	148.247322	19.919182	0.21	0.21	2MASS Reject	50836.4072	-0.062±0.020	-0.054±0.020				
		148.2470846	19.9189556	0.210	0.227	WISE epoch 1	55325.26						
		148.2471023	19.9190241	0.204	0.221	WISE epoch 2	55515.94						
		148.2470632	19.9189825	0.293	0.249	Spitzer	55563						
WISE 1018-2445	13.1	154.5335346	-24.7660780	0.148	0.158	WISE epoch 1	55349.86	-0.294±0.355	-0.520±0.353				
		154.5335261	-24.7661840	0.168	0.175	WISE epoch 2	55539.49						
		154.5335257	-24.7661780	0.241	0.204	Spitzer	55588						
WISE 1019+6529	16.6	154.773976	65.497971	0.20	0.19	2MASS PSC	51496.4619	-0.066±0.020	0.137±0.019	0.152±0.028	12.0±2.2		
		154.7734412	65.4984032	0.115	0.119	WISE epoch 1	55307.00						
		154.7734862	65.4983792	0.109	0.112	WISE epoch 2	55498.47						
		154.7735020	65.4983754	0.186	0.222	Spitzer	55540						
WISE 1042-3842	14.5	160.6884450	-38.7106301	0.200	0.213	WISE epoch 1	55364.71	0.337±0.335	-0.160±0.383				
		160.6887008	-38.7105165	0.229	0.236	WISE epoch 2	55554.90						
		160.6885579	-38.7107245	0.169	0.216	Spitzer	55649						
WISE 1122+2550	16.9	170.731266	25.840298	0.17	0.20	2MASS PSC	51324.1702	-0.954±0.016	-0.276±0.018	0.993±0.024	79.6±1.9		
		170.72963579	25.83988882	0.118	0.098	SDSS DR7	53387.5						
		170.7280297	25.8394998	0.128	0.137	WISE epoch 1	55344.11						
		170.7279454	25.8394037	0.156	0.165	WISE epoch 2	55534.13						
		170.7277844	25.8393187	0.231	0.311	Spitzer	55581						
WISE 1150+6302	9.6	177.5577364	63.0448752	0.092	0.093	WISE epoch 1	55322.30	0.221±0.256	-0.765±0.250				

Table 6—Continued

Object Name	Dist. Est. (pc)	RA (J2000) (deg)	Dec (J2000) (deg)	RA err (arcsec)	Dec err (arcsec)	Reference	MJD	$\mu_\alpha$ arcsec/yr	$\mu_\delta$ arcsec/yr	$\mu_{total}$ arcsec/yr	$v_{tan}$ km/s
(1)	(2)	(3)	(4)	(5)	(6)	(7)	(8)	(9)	(10)	(11)	(12)
WISE 1217+1626	6.7	177.5579005	63.0447128	0.106	0.104	WISE epoch 2	55513.36	0.935 $\pm$ 0.269	-1.497 $\pm$ 0.279	1.765 $\pm$ 0.388	56.1 $\pm$ 12.3
		177.5578860	63.0447494	0.336	0.284	Spitzer	55554				
		184.4871110	16.4446764	0.104	0.108	WISE epoch 1	55362.98				
		184.4873517	16.4444386	0.117	0.121	WISE epoch 2	55549.01				
WISE 1311+0122	14.4	184.4873182	16.4443118	0.274	0.287	Spitzer	55633	-0.068 $\pm$ 0.324	-0.827 $\pm$ 0.325	0.365 $\pm$ 0.009	45.7 $\pm$ 1.2
		197.7760031	1.3817110	0.218	0.240	WISE epoch 1	55293.42				
		197.7758861	1.3815585	0.315	0.322	WISE epoch 2	55568.13				
		197.7760406	1.3814727	0.249	0.215	Spitzer	55649				
WISE 1311+3629	26.4	197.926132	36.489887	0.08	0.06	2MASS PSC	50920.2820	-0.352 $\pm$ 0.007	0.096 $\pm$ 0.006	0.547 $\pm$ 0.023	51.8 $\pm$ 2.2
		197.9246218	36.4901989	0.051	0.052	WISE epoch 1	55363.90				
		197.9246197	36.4902302	0.056	0.058	WISE epoch 2	55554.11				
		197.9245666	36.4901695	0.168	0.169	Spitzer	55623				
WISE 1320+6034	20.0	200.020494	60.573997	0.29	0.26	2MASS Reject	51685.2443	-0.546 $\pm$ 0.016	-0.028 $\pm$ 0.017	0.547 $\pm$ 0.023	51.8 $\pm$ 2.2
		200.021008	60.573971	0.19	0.24	2MASS Reject	51237.5119				
		200.0173925	60.5739840	0.168	0.171	WISE epoch 1	55339.40				
		200.0174182	60.5738862	0.142	0.141	WISE epoch 2	55529.70				
WISE 1322-2340	11.9	200.0173022	60.5738479	0.151	0.101	Spitzer	55567	-0.299 $\pm$ 0.204	0.158 $\pm$ 0.225	0.307 $\pm$ 0.037	40.6 $\pm$ 4.9
		200.6401733	-23.6713770	0.128	0.134	WISE epoch 1	55303.81				
		200.6401337	-23.6713074	0.172	0.182	WISE epoch 2	55579.11				
		200.6401028	-23.6713742	0.184	0.220	Spitzer	55664				
WISE 1348+6603	27.9	207.028236	66.058762	0.30	0.29	2MASS PSC	51274.83561	0.136 $\pm$ 0.026	-0.275 $\pm$ 0.026	2.693 $\pm$ 0.398	109.8 $\pm$ 16.2
		207.0291320	66.0579122	0.060	0.061	WISE epoch 1	55334.60				
		207.0293434	66.0578476	0.068	0.070	WISE epoch 2	55525.60				
		207.0291262	66.0579238	0.281	0.269	Spitzer	55562				
WISE 1405+5534	8.6	211.3266880	55.5726255	0.132	0.135	WISE epoch 1	55355.75	-2.691 $\pm$ 0.292	0.095 $\pm$ 0.271	0.514 $\pm$ 0.028	43.1 $\pm$ 2.4
		211.3261242	55.5725614	0.149	0.150	WISE epoch 2	55545.11				
		211.3259057	55.5725984	0.147	0.108	Spitzer	55583				
WISE 1436-1814	16.8	219.0091232	-18.2394159	0.254	0.282	WISE epoch 1	55230.10	-0.006 $\pm$ 0.252	-0.127 $\pm$ 0.312	1.388 $\pm$ 0.131	32.2 $\pm$ 3.0
		219.0092676	-18.2394081	0.242	0.264	WISE epoch 2	55408.01				
		219.0091654	-18.2394558	0.187	0.257	Spitzer	55671				
WISE 1457+5815	17.7	224.315332	58.253193	0.29	0.34	2MASS Reject	51716.2127	-0.505 $\pm$ 0.019	-0.096 $\pm$ 0.021	0.514 $\pm$ 0.028	43.1 $\pm$ 2.4
		224.315344	58.253124	0.33	0.35	2MASS Reject	51699.2167				
		224.315402	58.252907	0.31	0.36	2MASS Reject	51592.4008				
		224.3127027	58.2528351	0.131	0.132	WISE epoch 1	55363.89				
		224.3124989	58.2527587	0.150	0.147	WISE epoch 2	55554.11				
		224.3124228	58.2527638	0.380	0.177	Spitzer	55586				
WISE 1506+7027	4.9	226.7082158	70.4600383	0.038	0.042	WISE epoch 1	55327.90	-0.996 $\pm$ 0.075	0.966 $\pm$ 0.107	1.388 $\pm$ 0.131	32.2 $\pm$ 3.0
		226.7078583	70.4600650	0.041	0.043	WISE epoch 2	55518.52				
		226.7077094	70.4600814	0.320	0.286	Spitzer epoch 1	55553				

Table 6—Continued

Object Name	Dist. Est. (pc)	RA (J2000) (deg)	Dec (J2000) (deg)	RA err (arcsec)	Dec err (arcsec)	Reference	MJD	$\mu_\alpha$ arcsec/yr	$\mu_\delta$ arcsec/yr	$\mu_{total}$ arcsec/yr	$v_{tan}$ km/s
(1)	(2)	(3)	(4)	(5)	(6)	(7)	(8)	(9)	(10)	(11)	(12)
		226.7075505	70.4602557	0.069	0.216	Spitzer epoch 2	55675				
WISE 1519+7009	12.9	229.7776851	70.1587724	0.100	0.097	WISE epoch 1	55332.47	0.301±0.244	-0.701±0.179		
		229.7778701	70.1585885	0.111	0.104	WISE epoch 2	55523.36				
		229.7775452	70.1586150	0.474	0.267	Spitzer epoch 1	55540				
		229.7778838	70.1585951	0.327	0.145	Spitzer epoch 2	55666				
WISE 1541-2250	8.2	235.4651859	-22.8404607	0.189	0.211	WISE epoch 1	55244.67	-0.780±0.234	-0.218±0.249		
		235.4648903	-22.8402853	0.167	0.186	WISE epoch 2	55424.68				
		235.4649058	-22.8405027	0.193	0.198	Spitzer	55665				
WISE 1612-3420	16.2	243.0664600	-34.3412500	0.149	0.165	WISE epoch 1	55252.92	-0.367±0.207	-0.462±0.218		
		243.0663368	-34.3412819	0.148	0.164	WISE epoch 2	55434.47				
		243.0663573	-34.3412643	0.183	0.184	Spitzer epoch 1	55458				
		243.0663181	-34.3414016	0.190	0.191	Spitzer epoch 2	55675				
WISE 1614+1739	11.3	243.6727451	17.6598663	0.170	0.186	WISE epoch 1	55243.86	0.759±0.211	-0.178±0.224		
		243.6728541	17.6598448	0.142	0.154	WISE epoch 2	55423.69				
		243.6728699	17.6598646	0.190	0.195	Spitzer epoch 1	55459				
		243.6730063	17.6598073	0.179	0.185	Spitzer epoch 2	55669				
WISE 1617+1807	12.7	244.2739640	18.1206173	0.134	0.148	WISE epoch 1	55244.39	-0.046±0.231	-0.089±0.174		
		244.2739204	18.1206136	0.115	0.120	WISE epoch 2	55424.22				
		244.2739060	18.1205622	0.197	0.142	Spitzer epoch 1	55459				
		244.2739485	18.1205905	0.264	0.140	Spitzer epoch 2	55669				
WISE 1622-0959	17.3	245.536974	-9.993136	0.26	0.29	2MASS PSC	51276.4110	0.085±0.023	0.054±0.026		
		245.5372651	-9.9929576	0.151	0.161	WISE epoch 1	55251.08				
		245.5372808	-9.9929933	0.154	0.166	WISE epoch 2	55432.49				
		245.5372360	-9.9929079	0.200	0.206	Spitzer epoch 1	55458				
		245.5372316	-9.9929665	0.131	0.141	Spitzer epoch 2	55669				
WISE 1627+3255	14.3	246.857210	32.924686	0.30	0.27	2MASS PSC	50908.4198	-0.0623±0.012	-0.350±0.012	0.356±0.017	24.1±1.2
		246.85704879	32.92431447	0.126	0.126	SDSS DR7	52402.2				
		246.85701573	32.92417129	0.114	0.114	SDSS DR7	52788.2				
		246.8568583	32.9235349	0.096	0.104	WISE epoch 1	55242.60				
		246.8568878	32.9234726	0.080	0.086	WISE epoch 2	55422.86				
		246.8568177	32.9234703	0.241	0.225	Spitzer epoch 1	55459				
		246.8568639	32.9234009	0.352	0.183	Spitzer epoch 2	55668				
WISE 1647+5632	20.2	251.815856	56.534924	0.10	0.08	2MASS PSC	51308.4127	-0.166±0.009	0.242±0.008	0.293±0.012	28.1±1.2
		251.8149734	56.5356318	0.048	0.048	WISE epoch 1	55226.51				
		251.8148281	56.5356748	0.045	0.046	WISE epoch 2	55406.42				
		251.8149394	56.5356781	0.054	0.055	WISE epoch 3	55592.29				
		251.8148690	56.5357524	0.112	0.173	Spitzer	55621				
WISE 1653+4444	11.2	253.2960324	44.7396889	0.098	0.104	WISE epoch 1	55245.44	-0.143±0.210	-0.533±0.249		
		253.2959638	44.7396403	0.076	0.079	WISE epoch 2	55425.41				
		253.2958575	44.7396392	0.256	0.209	Spitzer epoch 1	55459				



Table 6—Continued

Object Name	Dist. Est. (pc)	RA (J2000) (deg)	Dec (J2000) (deg)	RA err (arcsec)	Dec err (arcsec)	Reference	MJD	$\mu_\alpha$ arcsec/yr	$\mu_\delta$ arcsec/yr	$\mu_{total}$ arcsec/yr	$v_{tan}$ km/s
(1)	(2)	(3)	(4)	(5)	(6)	(7)	(8)	(9)	(10)	(11)	(12)
		253.2959160	44.7387647	0.340	1.476	Spitzer epoch 2	55667				
WISE 1711+3500	17.0	257.7691694	35.0102353	0.168	0.189	WISE epoch 1	55259.07	-0.071±0.251	-0.108±0.185		
		257.7691388	35.0102031	0.162	0.177	WISE epoch 2	55437.93				
		257.7691150	35.0102595	0.209	0.194	Spitzer epoch 1	55458				
		257.7691399	35.0101974	0.232	0.115	Spitzer epoch 2	55669				
WISE 1717+6129	19.6	259.3209221	61.4831687	0.219	0.226	WISE epoch 1	55228.46	0.073±0.272	-0.194±0.307		
		259.3209456	61.4831246	0.177	0.185	WISE epoch 2	55407.56				
		259.3213856	61.4830062	0.273	0.291	WISE epoch 3	55591.70				
		259.3206293	61.4832354	0.140	0.252	Spitzer epoch 1	55458				
		259.3207534	61.4831919	0.204	0.291	Spitzer epoch 2	55586				
WISE 1728+5716	25.1	262.1872683	57.2785228	0.152	0.165	WISE epoch 1	55250.60	0.037±0.256	0.210±0.299		
		262.1873665	57.2785841	0.181	0.199	WISE epoch 2	55431.66				
		262.1872315	57.2785926	0.214	0.237	Spitzer epoch 1	55458				
		262.1872521	57.2785553	0.225	0.287	Spitzer epoch 2	55621				
WISE 1738+2732	10.5	264.6480391	27.5497726	0.172	0.193	WISE epoch 1	55269.06	0.602±0.398	-0.969±0.456		
		264.6480755	27.5496620	0.165	0.182	WISE epoch 2	55451.22				
		264.6480850	27.5496349	0.140	0.179	Spitzer	55458				
WISE 1741+2553	4.7	265.352586	25.892878	0.26	0.29	2MASS PSC	51645.3888	-0.488±0.016	-1.476±0.016	1.555±0.023	34.6±0.5
		265.3517935	25.89105715	0.109	0.098	SDSS DR7	53264.1				
		265.3510834	25.8887959	0.060	0.060	WISE epoch 1	55270.05				
		265.3509014	25.8886009	0.057	0.056	WISE epoch 2	55451.80				
		265.3508910	25.8886468	0.189	0.190	Spitzer	55458				
WISE 1804+3117	13.0	271.1475485	31.2849339	0.165	0.185	WISE epoch 1	55277.66	-0.719±0.414	0.757±0.475		
		271.1474413	31.2849933	0.176	0.191	WISE epoch 2	55459.94				
		271.1473240	31.2851309	0.189	0.253	Spitzer	55465				
WISE 1812+2721	12.2	273.0452354	27.3623147	0.154	0.167	WISE epoch 1	55280.04	-0.319±0.407	-0.143±0.441		
		273.0451342	27.3622949	0.132	0.143	WISE epoch 2	55462.27				
WISE 1828+2650	<9.4	277.1295227	26.8438370	0.173	0.192	WISE epoch 1	55288.38	1.078±0.327	0.118±0.409		
		277.1295880	26.8438296	0.167	0.182	WISE epoch 2	55467.61				
		277.1296054	26.8438464	0.195	0.164	Spitzer epoch 1	55387				
		277.1296928	26.8438604	0.151	0.236	Spitzer epoch 2	55534				
WISE 1830+4542	32.8	277.743778	45.715626	0.26	0.26	2MASS Reject	50969.2963	0.056±0.022	0.107±0.022	0.121±0.031	18.8±4.8
		277.7440428	45.7159649	0.062	0.064	WISE epoch 1	55291.22				
		277.7440349	45.7159869	0.064	0.065	WISE epoch 2	55472.33				
WISE 1841+7000	22.4 <sup>b</sup>	280.354101	70.009018	0.28	0.31	2MASS Reject	51325.3783	-0.104±0.025	0.527±0.028	0.537±0.038	57.0±4.0
		280.3530928	70.0105747	0.086	0.085	WISE epoch 1	55226.23				
		280.3531427	70.0107065	0.122	0.119	WISE epoch 2	55590.80				
		280.3531553	70.0106363	0.263	0.201	Spitzer epoch 1	55459				
		280.3530727	70.0107399	0.233	0.239	Spitzer epoch 2	55586				

Table 6—Continued

Object Name	Dist. Est. (pc)	RA (J2000) (deg)	Dec (J2000) (deg)	RA err (arcsec)	Dec err (arcsec)	Reference	MJD	$\mu_\alpha$ arcsec/yr	$\mu_\delta$ arcsec/yr	$\mu_{total}$ arcsec/yr	$v_{tan}$ km/s
(1)	(2)	(3)	(4)	(5)	(6)	(7)	(8)	(9)	(10)	(11)	(12)
WISE 1852+3537	16.2	283.064682	35.622112	0.14	0.16	2MASS PSC	50925.4682	0.300 $\pm$ 0.013	-0.271 $\pm$ 0.014	0.404 $\pm$ 0.019	31.0 $\pm$ 1.5
		283.0659051	35.6212634	0.105	0.111	WISE epoch 1	55297.44				
		283.0659721	35.6211283	0.096	0.101	WISE epoch 2	55480.31				
		283.0656975	35.6211998	0.214	0.220	Spitzer	55465				
WISE 1906+4508	15.8	286.603188	45.136463	0.30	0.26	2MASS PSC	50972.2922	-0.021 $\pm$ 0.025	-0.347 $\pm$ 0.022	0.348 $\pm$ 0.033	26.0 $\pm$ 2.5
		286.6031075	45.1353261	0.085	0.086	WISE epoch 1	55307.23				
		286.6030488	45.1352444	0.087	0.090	WISE epoch 2	55489.38				
WISE 1952+7240	13.6	298.1944081	72.6669049	0.048	0.049	WISE epoch 1	55224.36	-0.220 $\pm$ 0.069	-0.347 $\pm$ 0.072	0.411 $\pm$ 0.100	26.5 $\pm$ 6.4
		298.1942123	72.6668797	0.050	0.051	WISE epoch 2	55416.38				
		298.1942250	72.6668371	0.053	0.055	WISE epoch 3	55590.99				
		298.1940345	72.6664128	0.115	0.197	Spitzer	55562				
WISE 1959-3338	11.6	299.773538	-33.642067	0.17	0.17	2MASS PSC	51348.2416	0.014 $\pm$ 0.017	-0.214 $\pm$ 0.017	0.214 $\pm$ 0.024	11.8 $\pm$ 1.3
		299.7736161	-33.6426513	0.123	0.132	WISE epoch 1	55301.80				
		299.7735368	-33.6427860	0.123	0.132	WISE epoch 2	55482.83				
WISE 2018-7423	13.3	304.6040683	-74.3909858	0.118	0.122	WISE epoch 1	55290.76	0.455 $\pm$ 0.312	-0.756 $\pm$ 0.323		
		304.6041586	-74.3911074	0.100	0.104	WISE epoch 2	55471.93				
WISE 2056+1459	7.7	314.1204202	14.9981500	0.167	0.175	WISE epoch 1	55329.26	0.604 $\pm$ 0.393	0.629 $\pm$ 0.378		
		314.1203454	14.9982440	0.171	0.176	WISE epoch 2	55511.01				
		314.1205276	14.9982240	0.194	0.145	Spitzer	55540				
WISE 2134-7137	10.1	323.7363420	-71.6290364	0.159	0.162	WISE epoch 1	55301.54	1.337 $\pm$ 0.367	-0.112 $\pm$ 0.363		
		323.7367230	-71.6290448	0.120	0.123	WISE epoch 2	55482.63				
		323.7370297	-71.6291393	0.227	0.187	Spitzer	55516				
WISE 2157+2659	19.1	329.4640457	26.9920831	0.203	0.215	WISE epoch 1	55351.02	-0.452 $\pm$ 0.448	-0.363 $\pm$ 0.502		
		329.4639163	26.9920130	0.187	0.203	WISE epoch 2	55530.32				
		329.4639525	26.9920269	0.165	0.224	Spitzer	55554				
WISE 2209-2734	13.4	332.344856	-27.576269	0.17	0.18	2MASS PSC	51119.0341	-0.785 $\pm$ 0.016	-0.448 $\pm$ 0.017	0.904 $\pm$ 0.023	57.4 $\pm$ 1.5
		332.3420794	-27.5776833	0.161	0.165	WISE epoch 1	55331.90				
		332.3418675	-27.5777599	0.137	0.145	WISE epoch 2	55512.35				
		332.3419420	-27.5778063	0.240	0.300	Spitzer	55540				
WISE 2213+0911	18.8	333.478168	9.194306	0.26	0.25	2MASS Reject	51738.3571	-0.109 $\pm$ 0.022	-0.043 $\pm$ 0.019	0.117 $\pm$ 0.029	10.4 $\pm$ 2.6
		333.478251	9.194472	0.28	0.23	2MASS Reject	51738.3621				
		333.4778840	9.1942733	0.169	0.180	WISE epoch 1	55348.46				
		333.4779537	9.1942974	0.212	0.222	WISE epoch 2	55526.69				
		333.4777956	9.1942456	0.224	0.160	Spitzer	55562				
WISE 2226+0440	16.7	336.5960623	4.6677288	0.279	0.301	WISE epoch 1	55346.85	-0.056 $\pm$ 0.584	-0.529 $\pm$ 0.596		
		336.5960856	4.6675165	0.210	0.220	WISE epoch 2	55527.75				
		336.5959869	4.6676643	0.229	0.190	Spitzer	55562				

Table 6—Continued

Object Name	Dist. Est. (pc)	RA (J2000) (deg)	Dec (J2000) (deg)	RA err (arcsec)	Dec err (arcsec)	Reference	MJD	$\mu_\alpha$ arcsec/yr	$\mu_\delta$ arcsec/yr	$\mu_{total}$ arcsec/yr	$v_{tan}$ km/s
(1)	(2)	(3)	(4)	(5)	(6)	(7)	(8)	(9)	(10)	(11)	(12)
WISE 2237-0614	16.4	339.372445	-6.243156	0.23	0.24	2MASS Reject	51087.1236	0.139 $\pm$ 0.023	0.086 $\pm$ 0.022	0.163 $\pm$ 0.032	12.7 $\pm$ 2.5
		339.3730006	-6.2428667	0.281	0.298	WISE epoch 1	55345.46				
		339.3728426	-6.2428775	0.304	0.323	WISE epoch 2	55526.42				
		339.3729068	-6.2428666	0.218	0.158	Spitzer	55562				
WISE 2239+1617	18.3	339.904942	16.286875	0.12	0.12	2MASS PSC	50711.2743	0.410 $\pm$ 0.010	0.255 $\pm$ 0.010	0.483 $\pm$ 0.014	41.9 $\pm$ 1.2
		339.9064502	16.2878008	0.071	0.072	WISE epoch 1	55356.91				
		339.9065291	16.2877786	0.080	0.080	WISE epoch 2	55534.89				
		339.9064381	16.2877837	0.216	0.230	Spitzer	55563				
WISE 2255-3118	13.0	343.9198262	-31.3116495	0.165	0.173	WISE epoch 1	55339.91	-0.155 $\pm$ 0.415	-0.231 $\pm$ 0.394		
		343.9197639	-31.3116969	0.154	0.159	WISE epoch 2	55521.06				
		343.9197363	-31.3117099	0.288	0.178	Spitzer	55548				
WISE 2313-8037	11.2	348.397355	-80.615623	0.25	0.29	2MASS Reject	51519.0917	0.237 $\pm$ 0.024	-0.401 $\pm$ 0.028	0.466 $\pm$ 0.037	24.7 $\pm$ 2.0
		348.4015688	-80.6167123	0.093	0.089	WISE epoch 1	55297.70				
		348.4018567	-80.6168599	0.086	0.084	WISE epoch 2	55480.40				
WISE 2319-1844	12.1	349.912834	-18.735308	0.26	0.28	2MASS Reject	51002.3174	0.069 $\pm$ 0.022	0.236 $\pm$ 0.025	0.246 $\pm$ 0.033	14.1 $\pm$ 1.9
		349.9130580	-18.7345555	0.144	0.152	WISE epoch 1	55351.15				
		349.9130362	-18.7344856	0.159	0.165	WISE epoch 2	55530.59				
		349.9130638	-18.7344989	0.141	0.302	Spitzer	55562				
WISE 2325-4105	10.9	351.3314055	-41.0930503	0.165	0.171	WISE epoch 1	55340.97	0.398 $\pm$ 0.450	0.212 $\pm$ 0.460		
		351.3314102	-41.0930321	0.173	0.175	WISE epoch 2	55522.12				
		351.3314778	-41.0930998	0.394	0.393	Spitzer	55548				
WISE 2327-2730	21.7	351.868790	-27.515934	0.09	0.08	2MASS PSC	51341.3803	0.283 $\pm$ 0.009	0.070 $\pm$ 0.008	0.292 $\pm$ 0.012	30.0 $\pm$ 1.2
		351.8697702	-27.5157049	0.061	0.063	WISE epoch 1	55349.70				
		351.8697700	-27.5157391	0.063	0.066	WISE epoch 2	55528.80				
		351.8698347	-27.5157046	0.268	0.215	Spitzer	55562				
WISE 2340-0745	12.1	355.110349	-7.751374	0.22	0.19	2MASS PSC	51098.1200	0.158 $\pm$ 0.020	-0.286 $\pm$ 0.017	0.327 $\pm$ 0.026	18.7 $\pm$ 1.5
		355.1109091	-7.7522765	0.120	0.122	WISE epoch 1	55361.14				
		355.1108439	-7.7523496	0.114	0.124	WISE epoch 2	55541.19				
		355.1109954	-7.7523579	0.267	0.306	Spitzer	55571				
WISE 2343-7418	14.9	355.960273	-74.313484	0.36	0.37	2MASS PSC	51774.2181	0.337 $\pm$ 0.036	0.166 $\pm$ 0.038	0.376 $\pm$ 0.052	26.5 $\pm$ 3.6
		355.9633757	-74.3130319	0.090	0.085	WISE epoch 1	55310.21				
		355.9637530	-74.3130163	0.089	0.086	WISE epoch 2	55492.35				
WISE 2344+1034	15.6	356.1926713	10.5710647	0.334	0.347	WISE epoch 1	55369.15	0.574 $\pm$ 0.667	-0.211 $\pm$ 0.668		
		356.1926410	10.5711379	0.381	0.385	WISE epoch 2	55548.91				
		356.1927398	10.5710142	0.196	0.169	Spitzer	55580				
WISE 2348-1028	16.8	357.169203	-10.479364	0.15	0.13	2MASS PSC	51105.0337	0.629 $\pm$ 0.016	0.144 $\pm$ 0.014	0.645 $\pm$ 0.021	51.4 $\pm$ 1.7
		357.1712843	-10.4788976	0.172	0.182	WISE epoch 1	55361.94				
		357.1713877	-10.4789185	0.189	0.194	WISE epoch 2	55541.59				
		357.1713313	-10.4788145	0.256	0.204	Spitzer	55571				

Table 6—Continued

Object Name	Dist. Est.	RA (J2000)	Dec (J2000)	RA err	Dec err	Reference	MJD	$\mu_\alpha$	$\mu_\delta$	$\mu_{total}$	$v_{tan}$
(1)	(pc)	(deg)	(deg)	(arcsec)	(arcsec)	(7)	(8)	arcsec/yr	arcsec/yr	arcsec/yr	km/s
	(2)	(3)	(4)	(5)	(6)			(9)	(10)	(11)	(12)
WISE 2359-7335	13.1	359.918122	-73.584862	0.19	0.23	2MASS PSC	51528.1013	0.281 $\pm$ 0.018	0.045 $\pm$ 0.022	0.285 $\pm$ 0.028	17.7 $\pm$ 1.8
		359.9211060	-73.5846766	0.073	0.070	WISE epoch 1	55316.75				
		359.9211513	-73.5847461	0.071	0.069	WISE epoch 2	55494.74				
		359.9212621	-73.5847480	0.260	0.222	Spitzer	55552				

<sup>a</sup>Gelino et al. (submitted) find this object to be a binary. Their revised distance to this system is 12.3 $\pm$ 2.3 pc.

<sup>b</sup>Gelino et al. (submitted) find this object to be a binary. Their revised distance to this system is 40.1 $\pm$ 3.0 pc.

Table 7. Preliminary Parallaxes and Absolute Magnitudes for WISE Brown Dwarf Discoveries

Object Name (1)	Near-infrared Spectral Type (2)	$\pi_{trig}$ (arcsec) (3)	Dist. Range ( $\pm 1\sigma$ ) (pc) (4)	$M_J^a$ (mag) (5)	$M_H^a$ (mag) (6)	$M_{W2}$ (mag) (7)
WISE 0254+0223	T8	0.165 $\pm$ 0.046	4.7-8.4	17.0 $\pm$ 0.6	17.4 $\pm$ 0.6	13.8 $\pm$ 0.6
WISE 1541-2250	Y0	0.351 $\pm$ 0.108	2.2-4.1	23.9 $\pm$ 0.8	23.7 $\pm$ 0.9	16.7 $\pm$ 0.7
WISE 1647+5632	L9 pec (red)	0.116 $\pm$ 0.029	6.9-11.5	16.9 $\pm$ 0.5	15.7 $\pm$ 0.5	13.4 $\pm$ 0.5
WISE 1741+2732	T9	0.182 $\pm$ 0.038	4.5-6.9	17.8 $\pm$ 0.5	17.9 $\pm$ 0.5	13.6 $\pm$ 0.5

<sup>a</sup>Absolute  $J$  and  $H$  magnitudes for WISE 0254+0223 and WISE 1541–2250 are on the MKO filter system; magnitudes for WISE 1647+5632 and WISE 1741+2732 are on the 2MASS filter system.

Table 8. Preliminary Space Densities for an All-sky, Volume-limited Sample of Late-T and Y Dwarfs

Spectral Type Range (1)	Approx. $T_{eff}$ Range (K) (2)	$d_{max}$ (pc) (3)	# from Previous Surveys (4)	# from WISE to date (5)	Total # to date (6)	Obs. Space Density ( $\#/pc^3$ ) (7)	$< V/V_{max} >$ (8)	# per 100K Bin w/in 10 pc (9)
T6-T6.5	900-1050	20	14	16	30	$>9.0e-4$	0.36	$>2.5$
T7-T7.5	750-900	20	13	12	25	$>7.5e-4$	0.34	$>2.1$
T8-T8.5	600-750	20	9	26	35	$>1.0e-3$	0.30	$>2.9$
T9-T9.5	450-600	15	1	9	10	$>7.1e-4$	0.40	$>2.0$
Y0	300-450	10	0	4	4	$>9.5e-4$	0.59	$>2.7$
$>Y0$	$<300$	10	0	1	1	$>2.4e-4$	0.83	$>0.7$

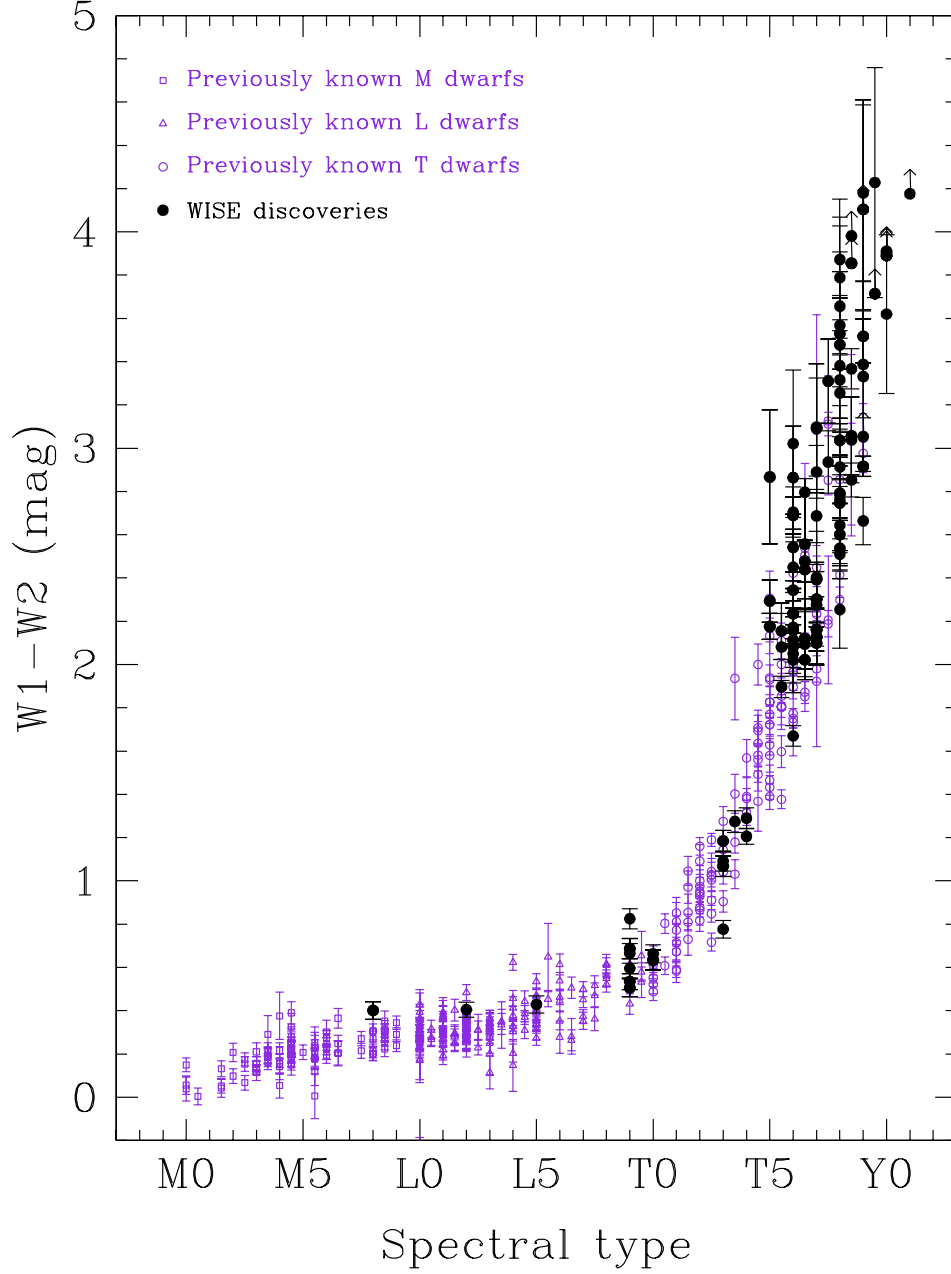


Fig. 1.— WISE W1-W2 color versus spectral type. The W1-W2 colors for a sample of previously known M (open squares), L (open triangles) and T (open circles) dwarfs from Table 1 are shown in blue violet. The colors of new WISE discoveries from Table 2 are shown by the solid, black circles. W1-W2 color limits are indicated by arrows.

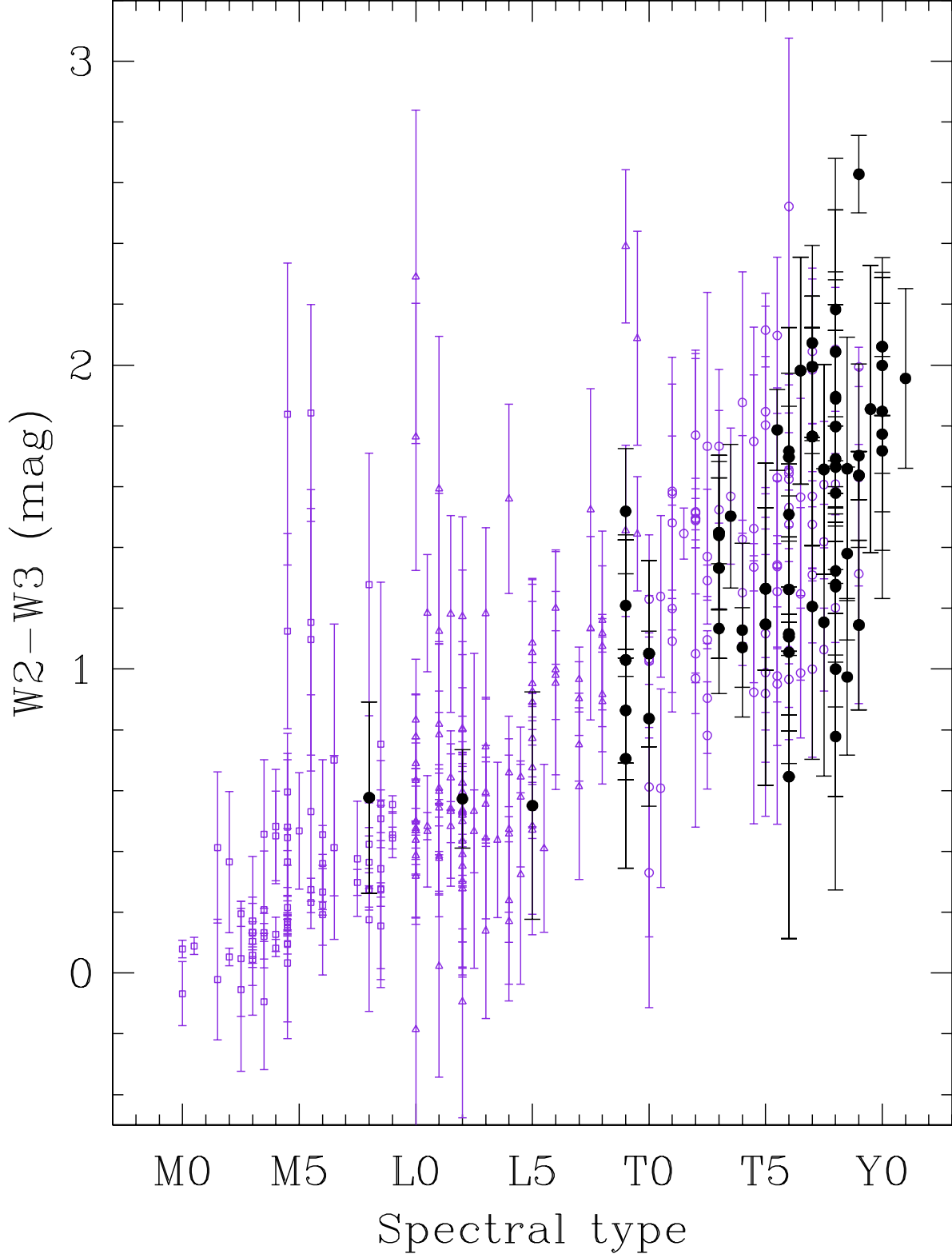


Fig. 2.— WISE W2-W3 color versus spectral type. The color scheme is identical to that of Figure 1. For clarity, only those objects with detections in both W2 and W3 are shown.



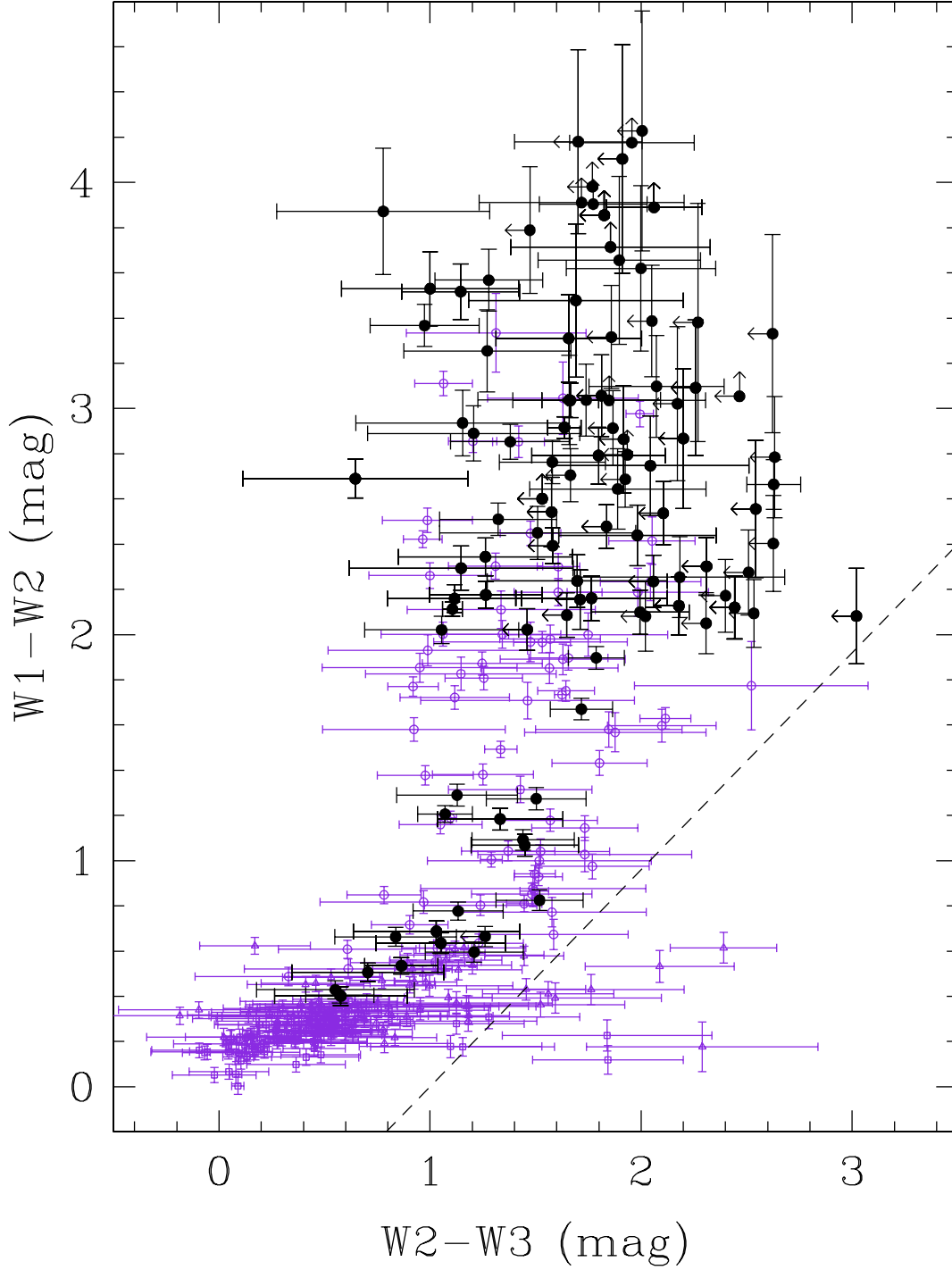


Fig. 3.— WISE color-color plot showing  $W1-W2$  versus  $W2-W3$ . Color coding is the same as in Figure 1. The dashed line indicates the criterion used, in search #2 (see section 2.2), to eliminate extragalactic sources to the right of the line from the bulk of the M, L, and T dwarfs to the left.

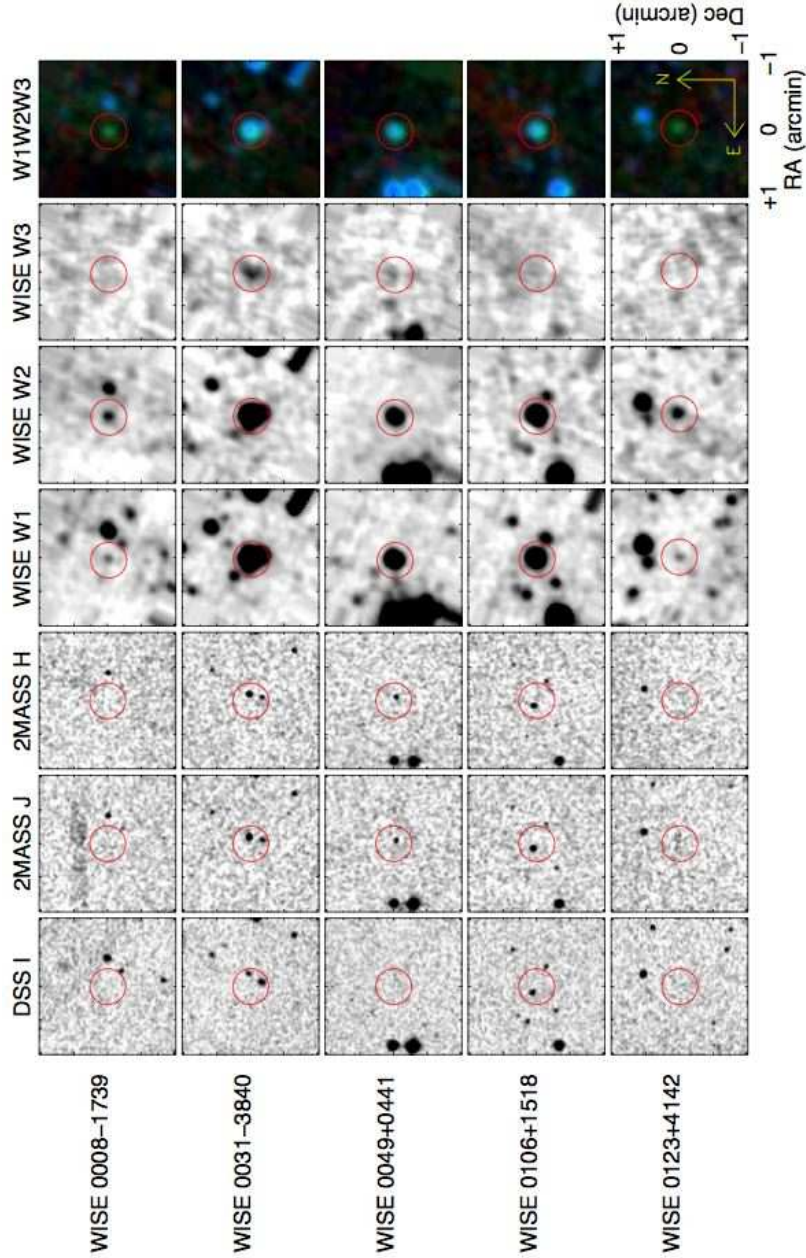


Fig. 4.1.— Finder charts for new WISE brown dwarf discoveries. Each row represents one object and shows a selection of  $2 \times 2$  arcmin cutouts from various all-sky surveys centered at the position (red circle) of the WISE source. From left to right, these cutouts are from the Digitized Sky Survey I band, the Two Micron All-Sky Survey J and H bands, the three shortest wavelength bands of WISE (W1, W2, and W3), and a three-color image made from these same three WISE bands (W1 encoded as blue, W2 as green, and W3 as red). In each cutout, north is oriented up and east is to the left. Images are not shown for sources already presented elsewhere – WISE 0458+6434 from Mainzer et al. (2011); WISE 1617+1807, WISE 1812+2721, WISE 2018-6423, WISE 2313-8037, and WISE 2359-7335 from Burgasser et al. (2011); and WISE 0148-7202, WISE 0410+1502, WISE 1405+5534, WISE 1541-2250, and WISE 2056+1459 from Cushing et al. (accepted).

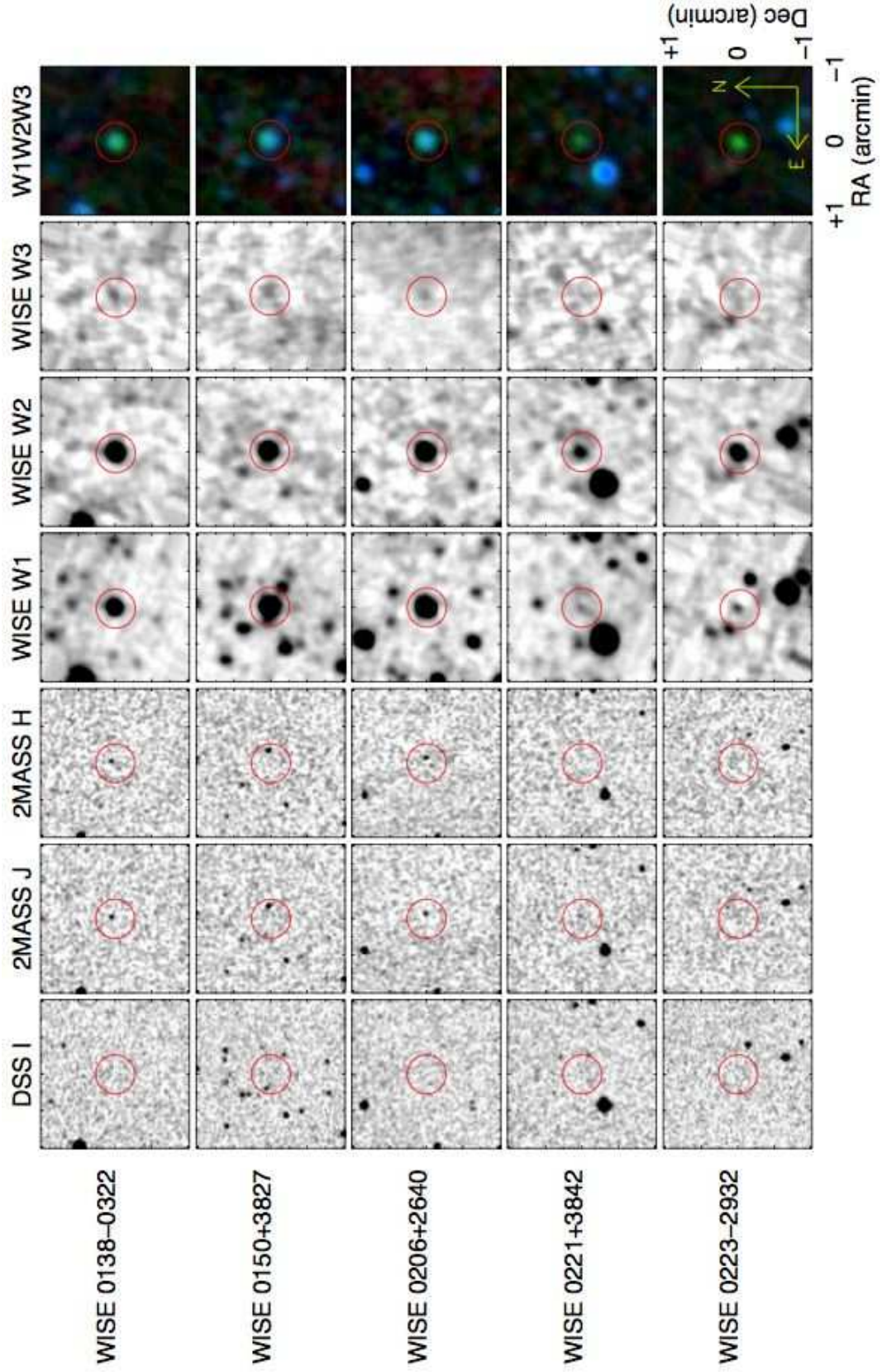


Fig. 4.2.— Continued.



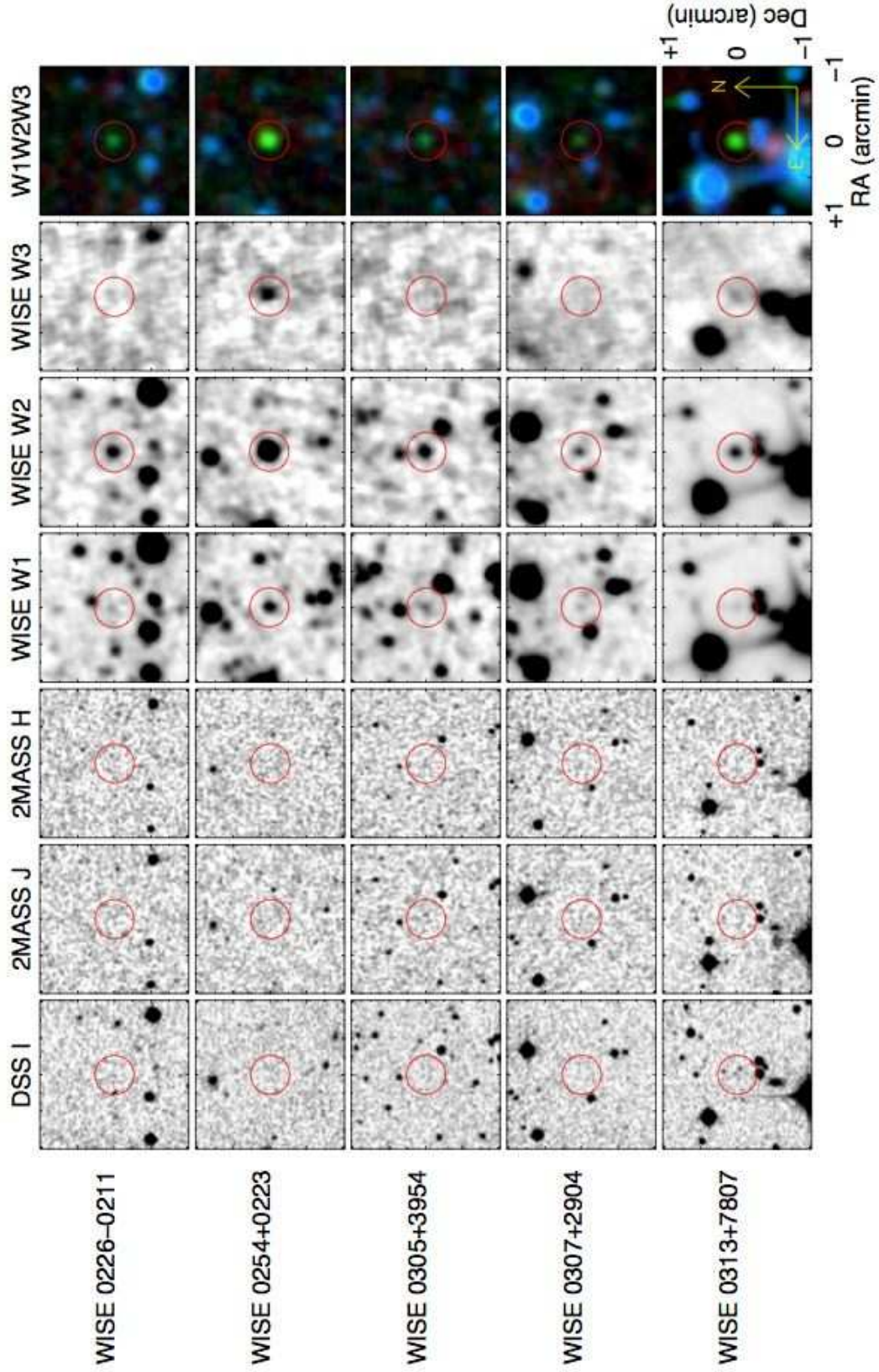


Fig. 4.3.— Continued.

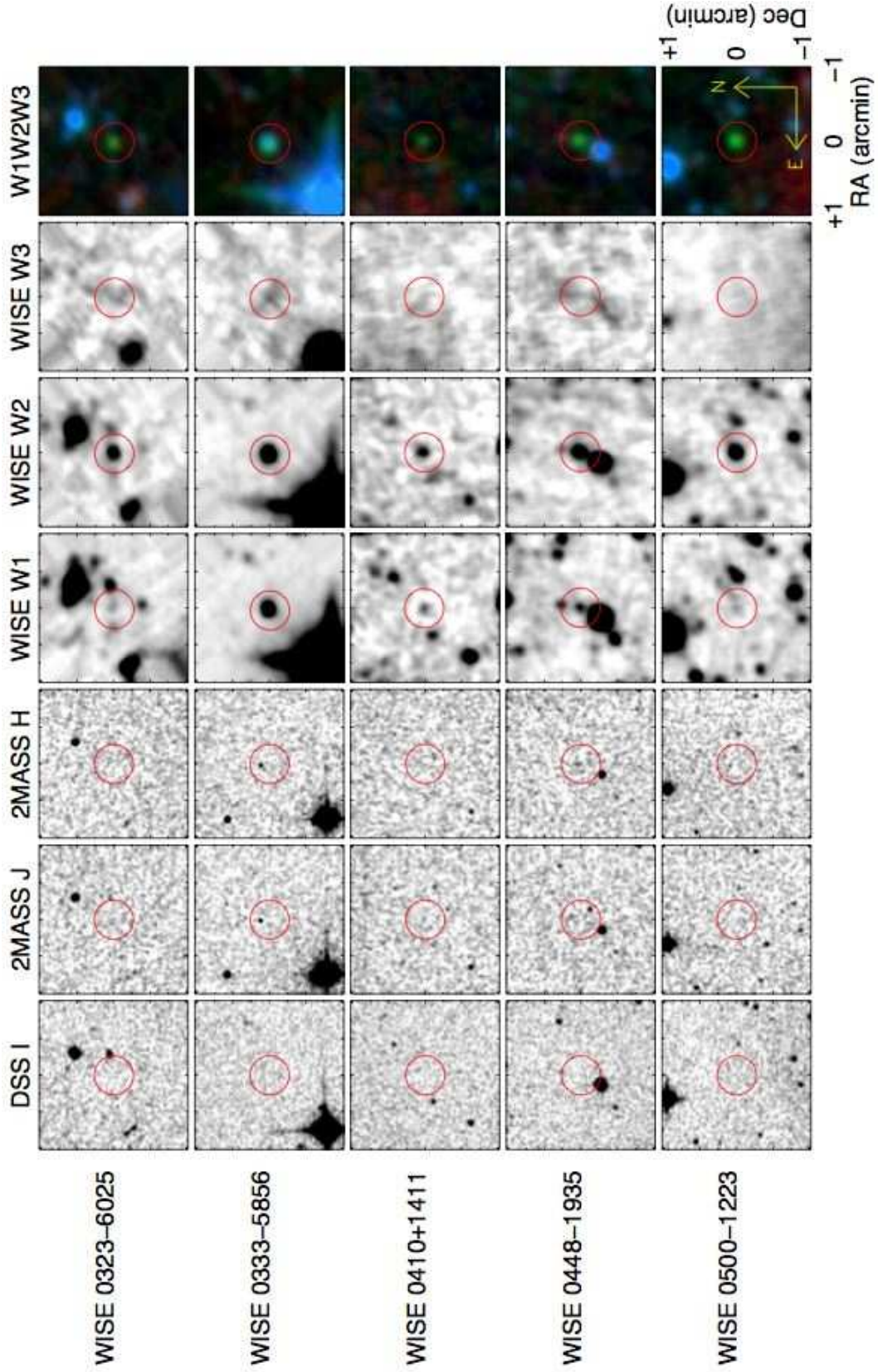


Fig. 4.4.— Continued.



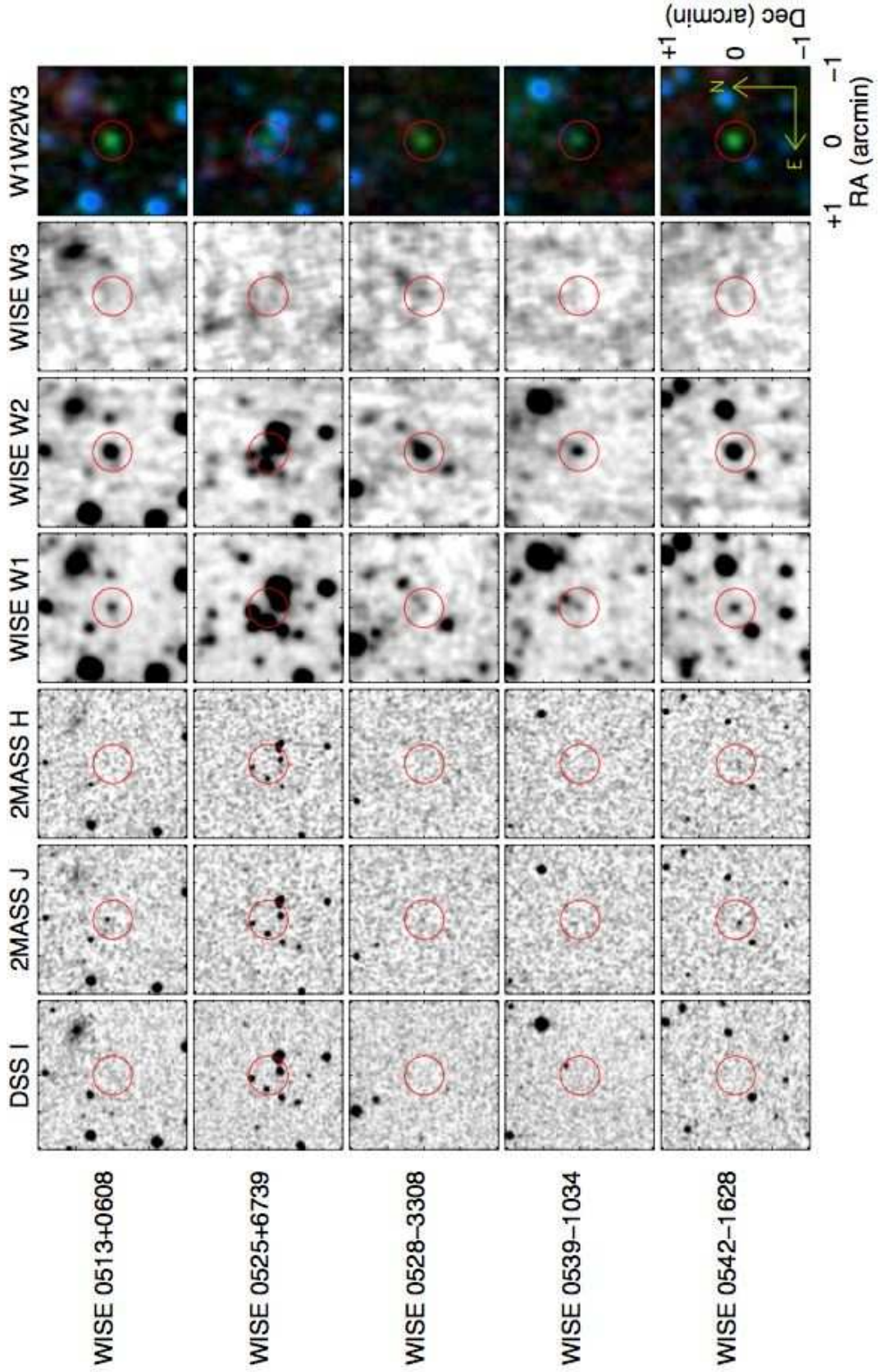


Fig. 4.5.— Continued.

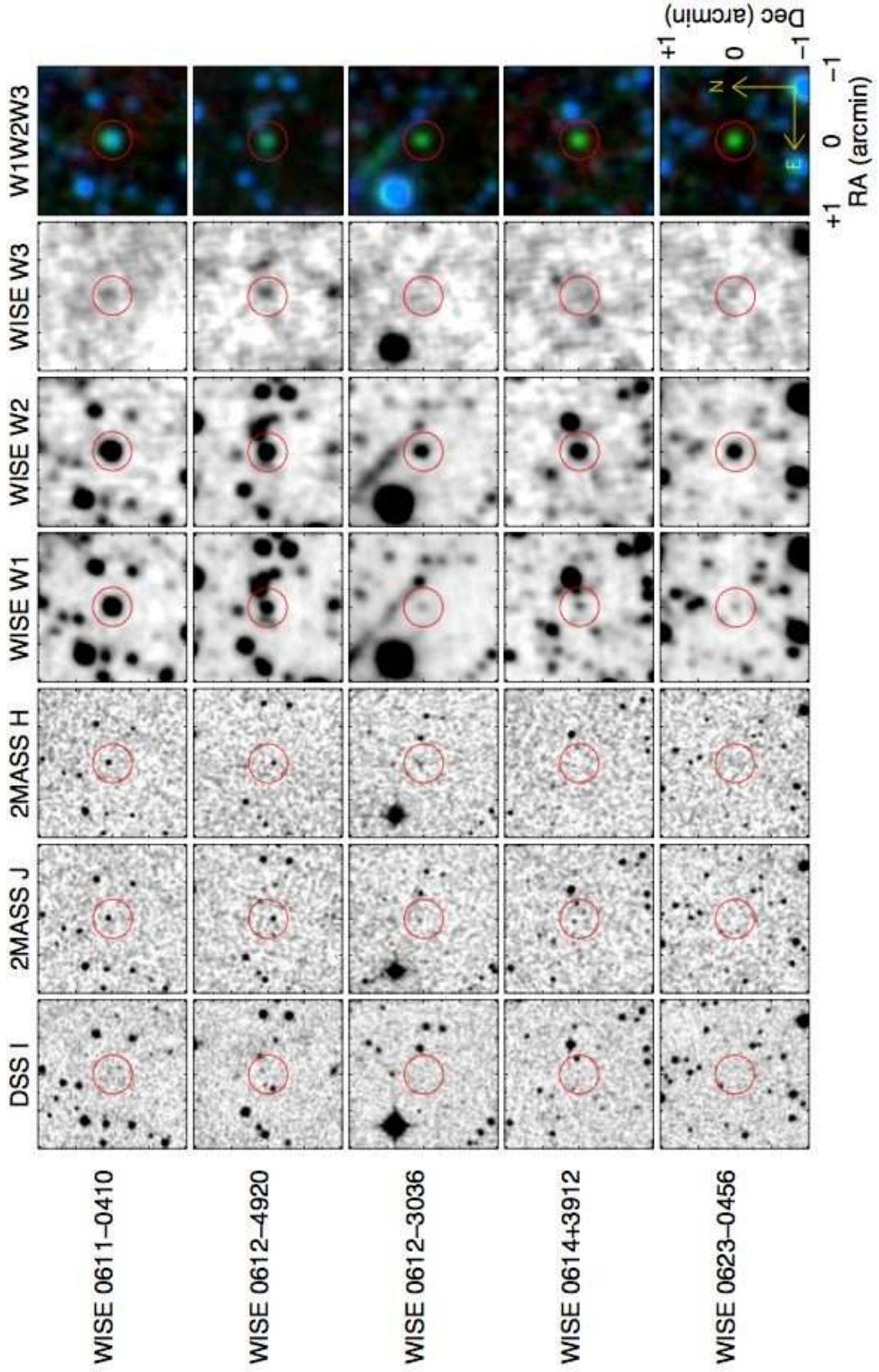


Fig. 4.6.— Continued.



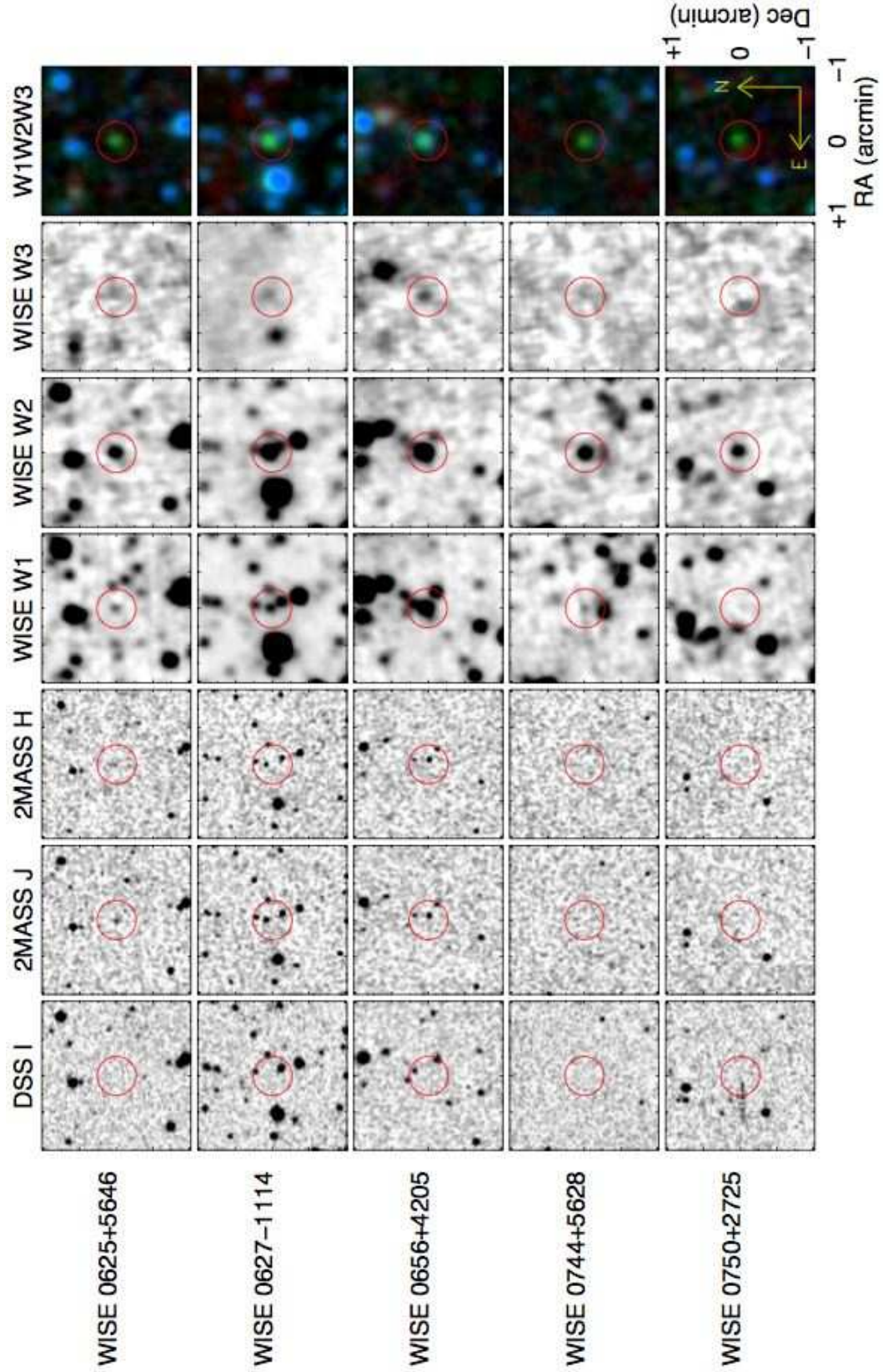


Fig. 4.7.— Continued.



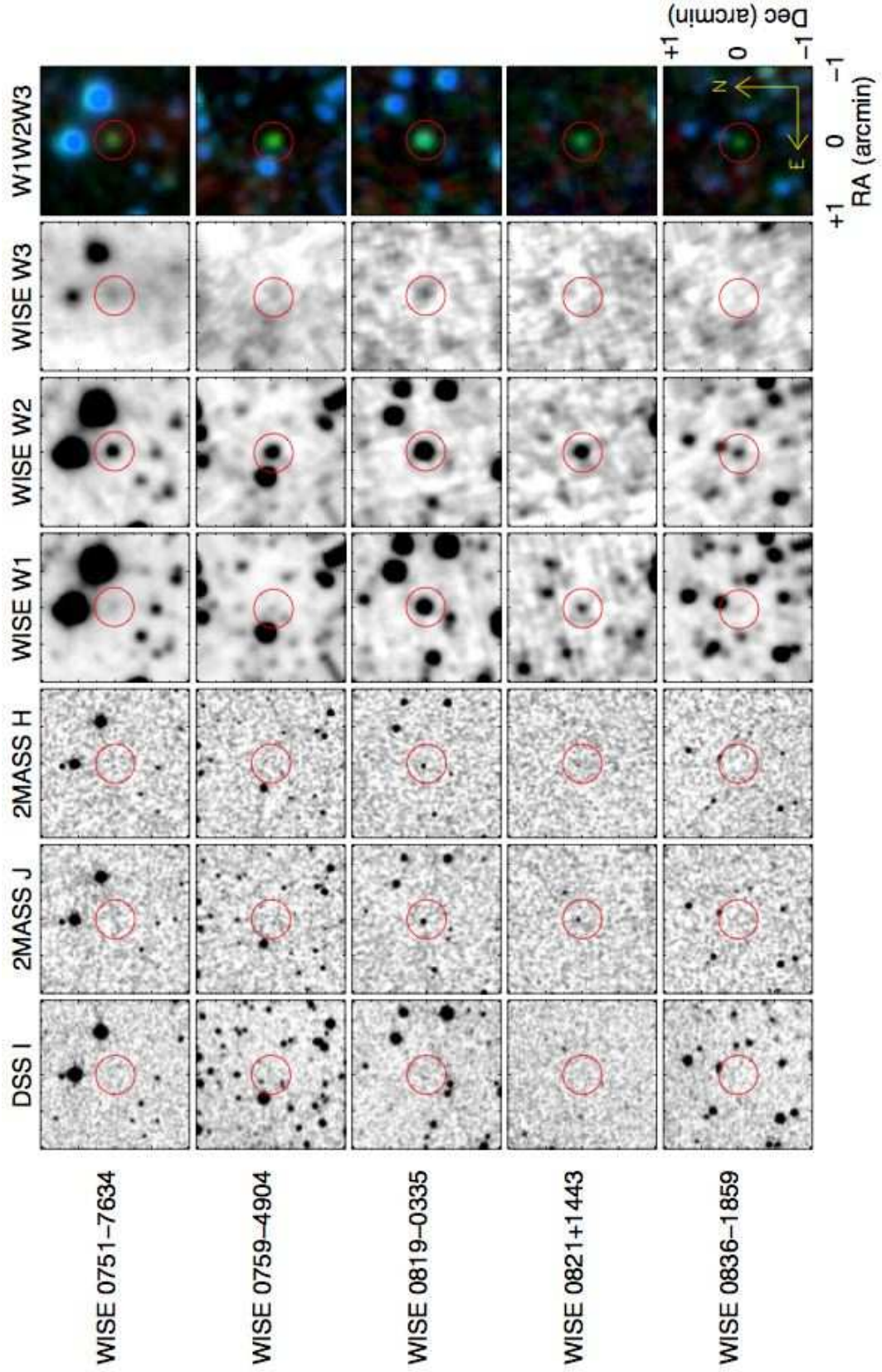


Fig. 4.8.— Continued.

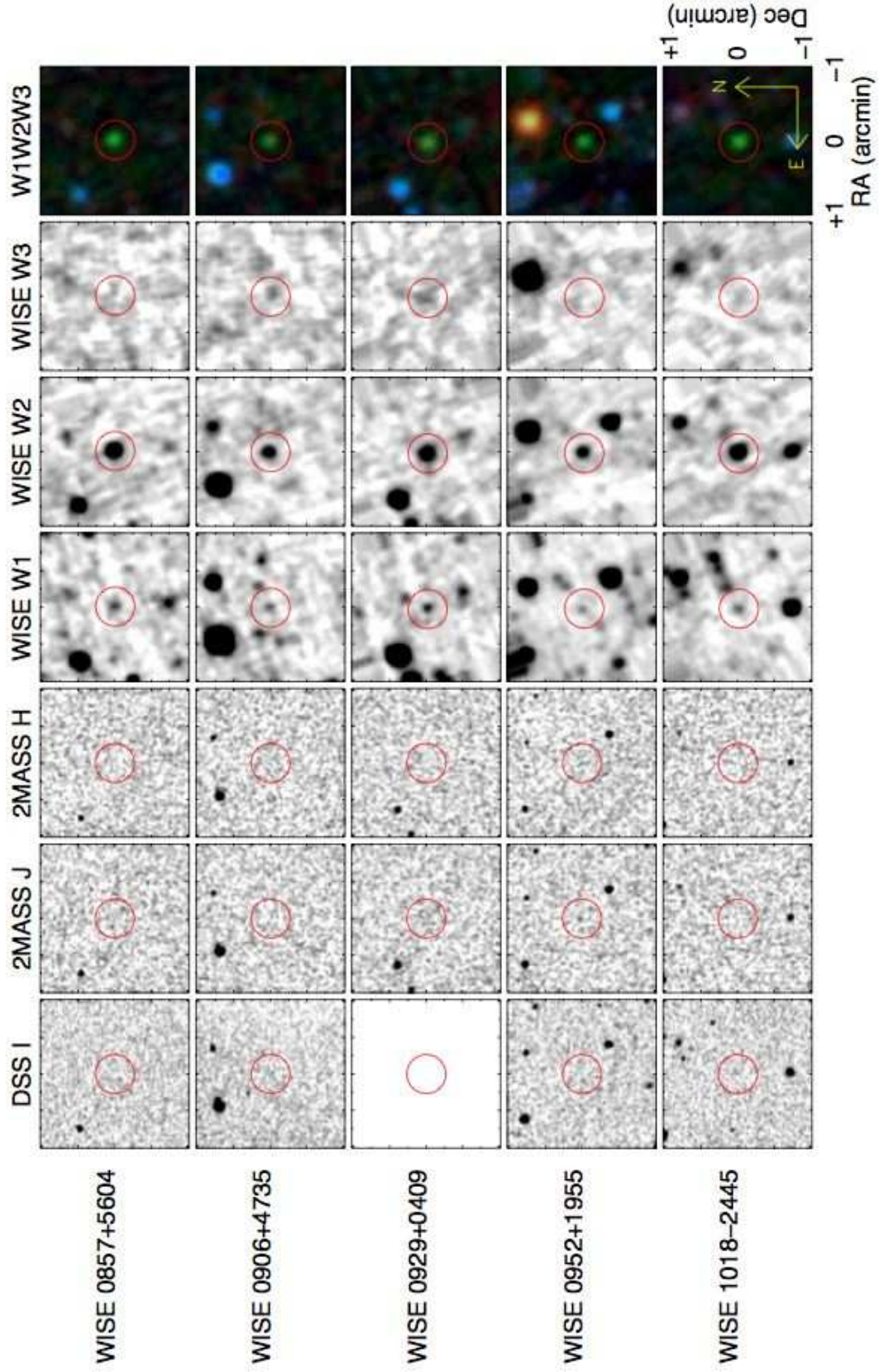


Fig. 4.9.— Continued.



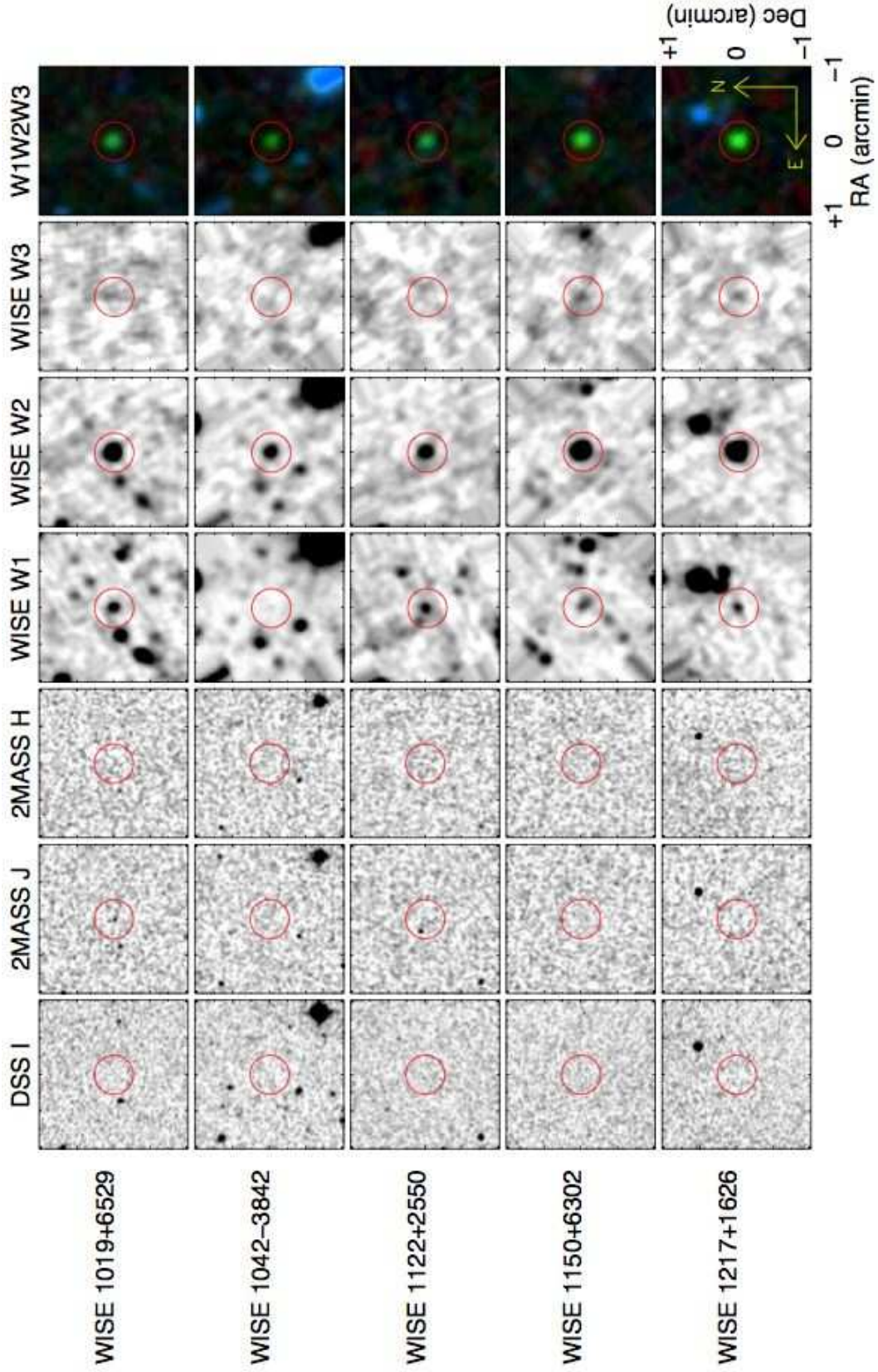


Fig. 4.10.— Continued.

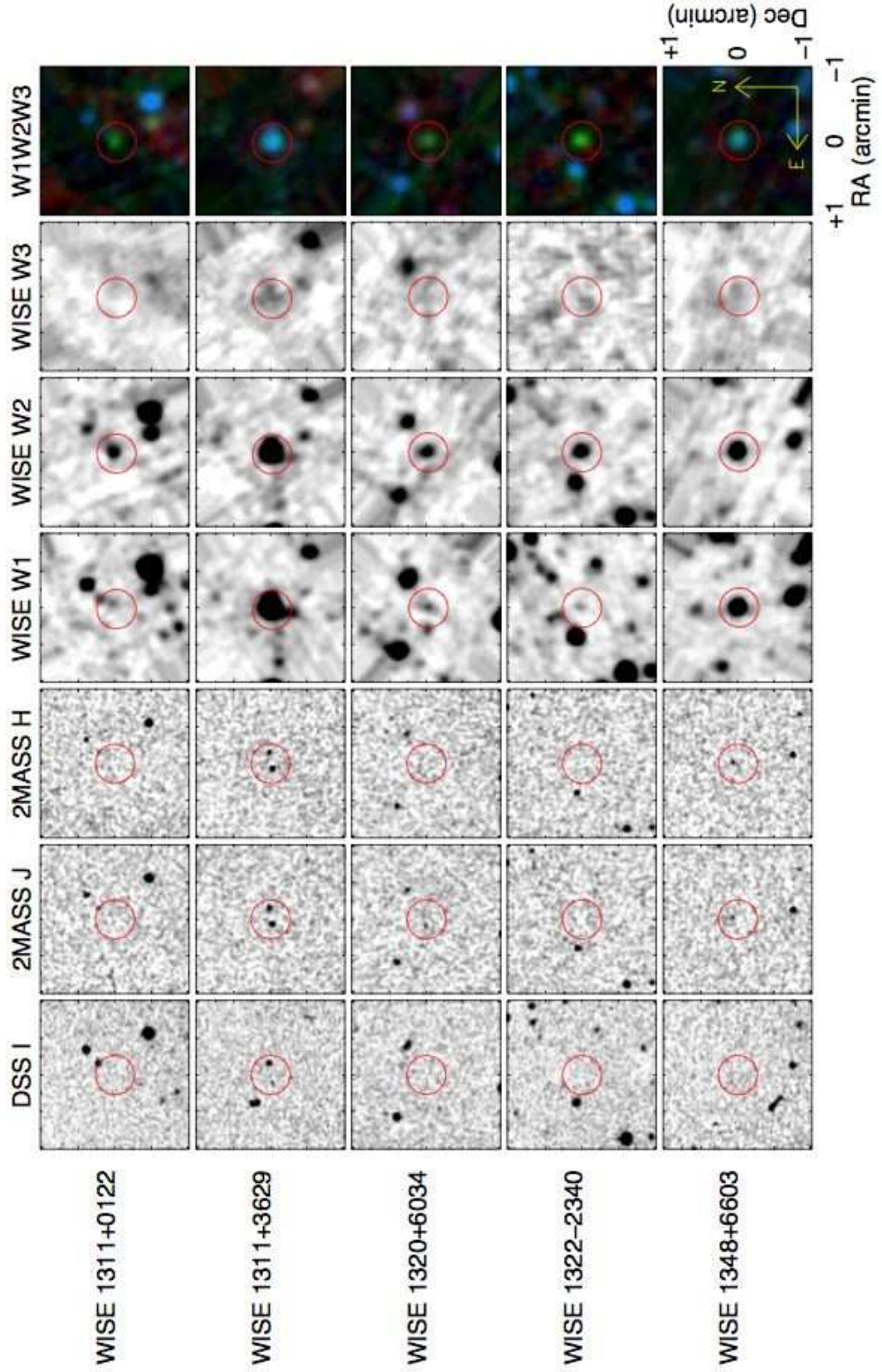


Fig. 4.11.— Continued.



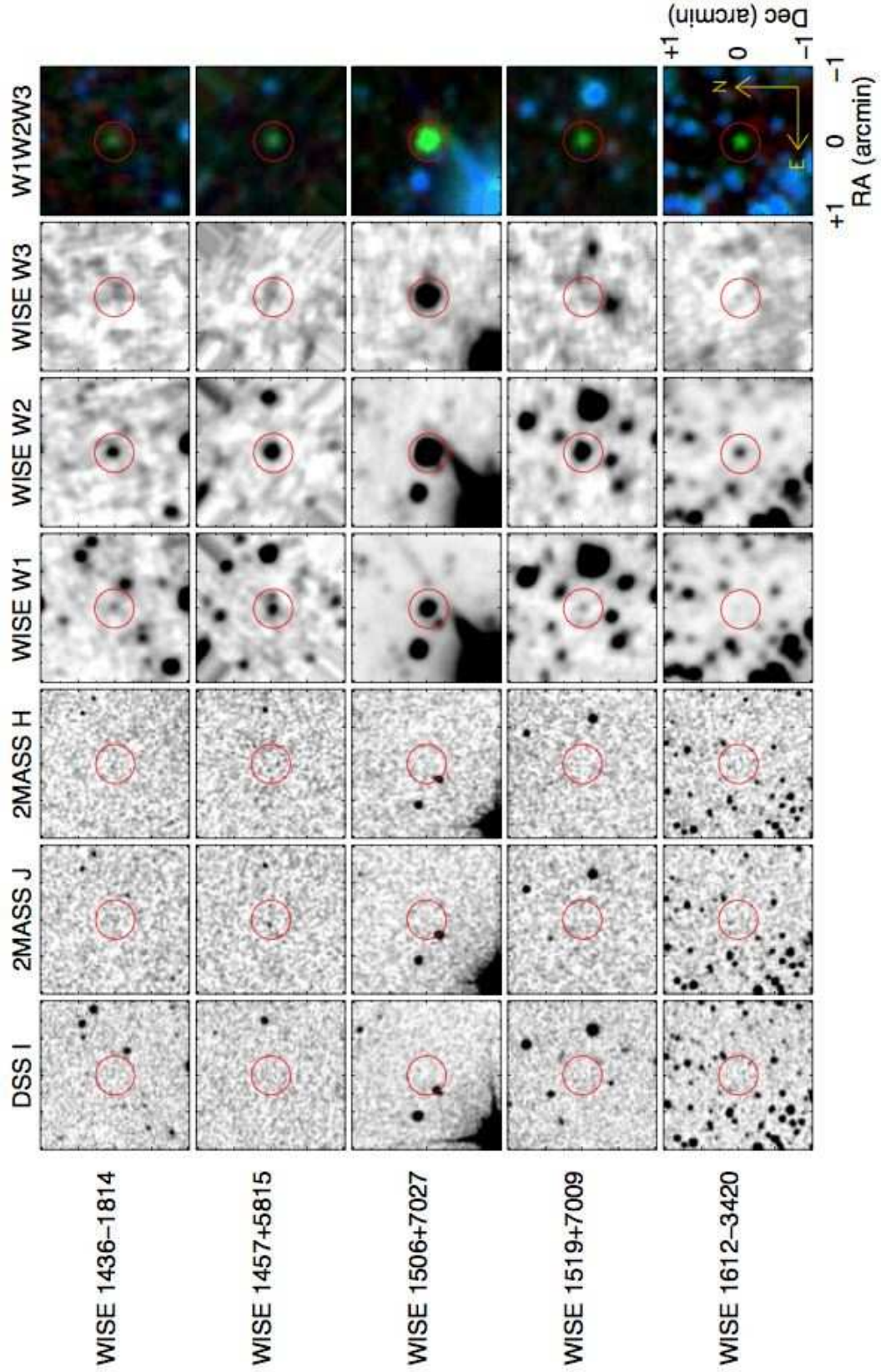


Fig. 4.12.— Continued.

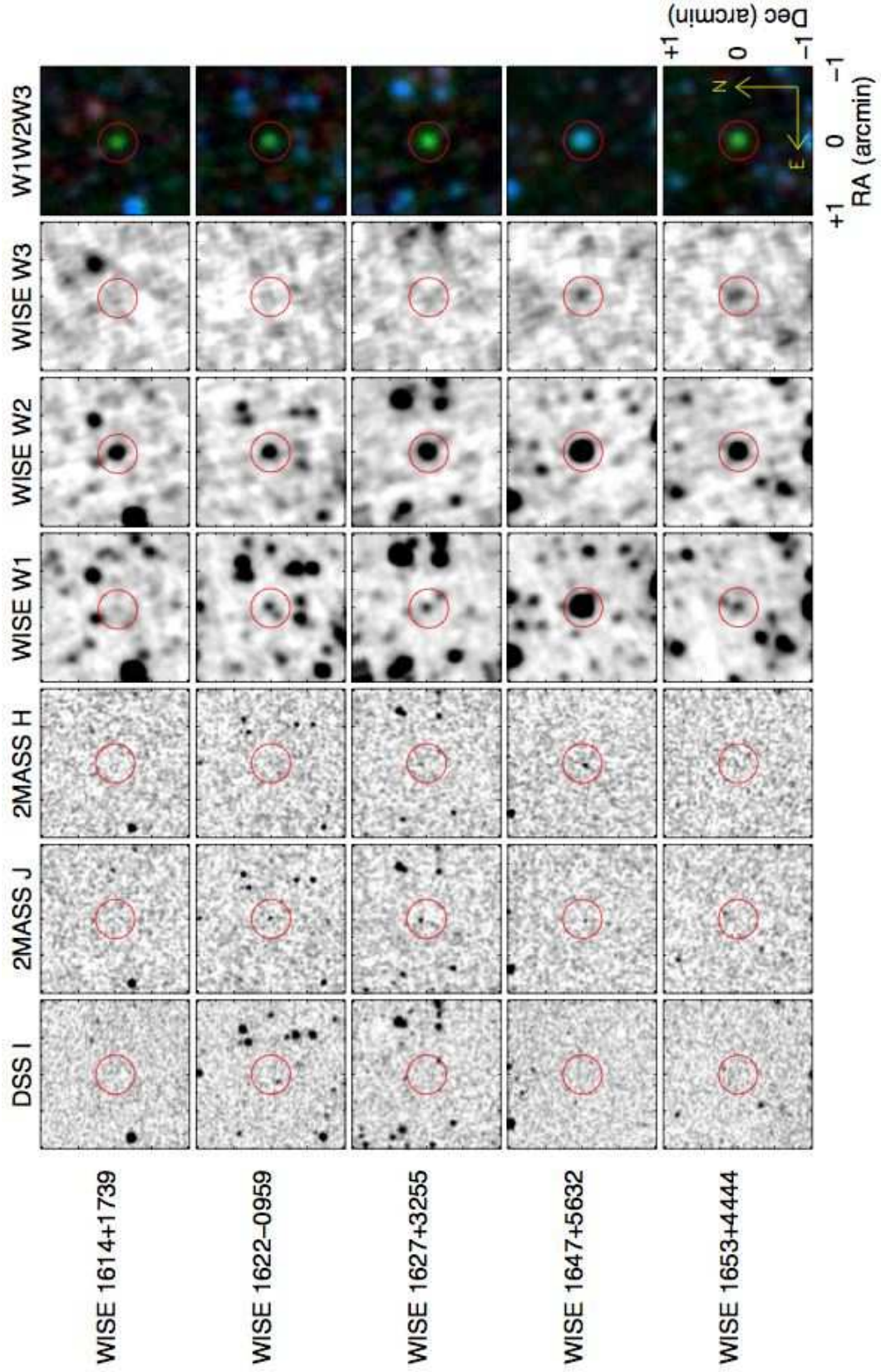


Fig. 4.13.— Continued.



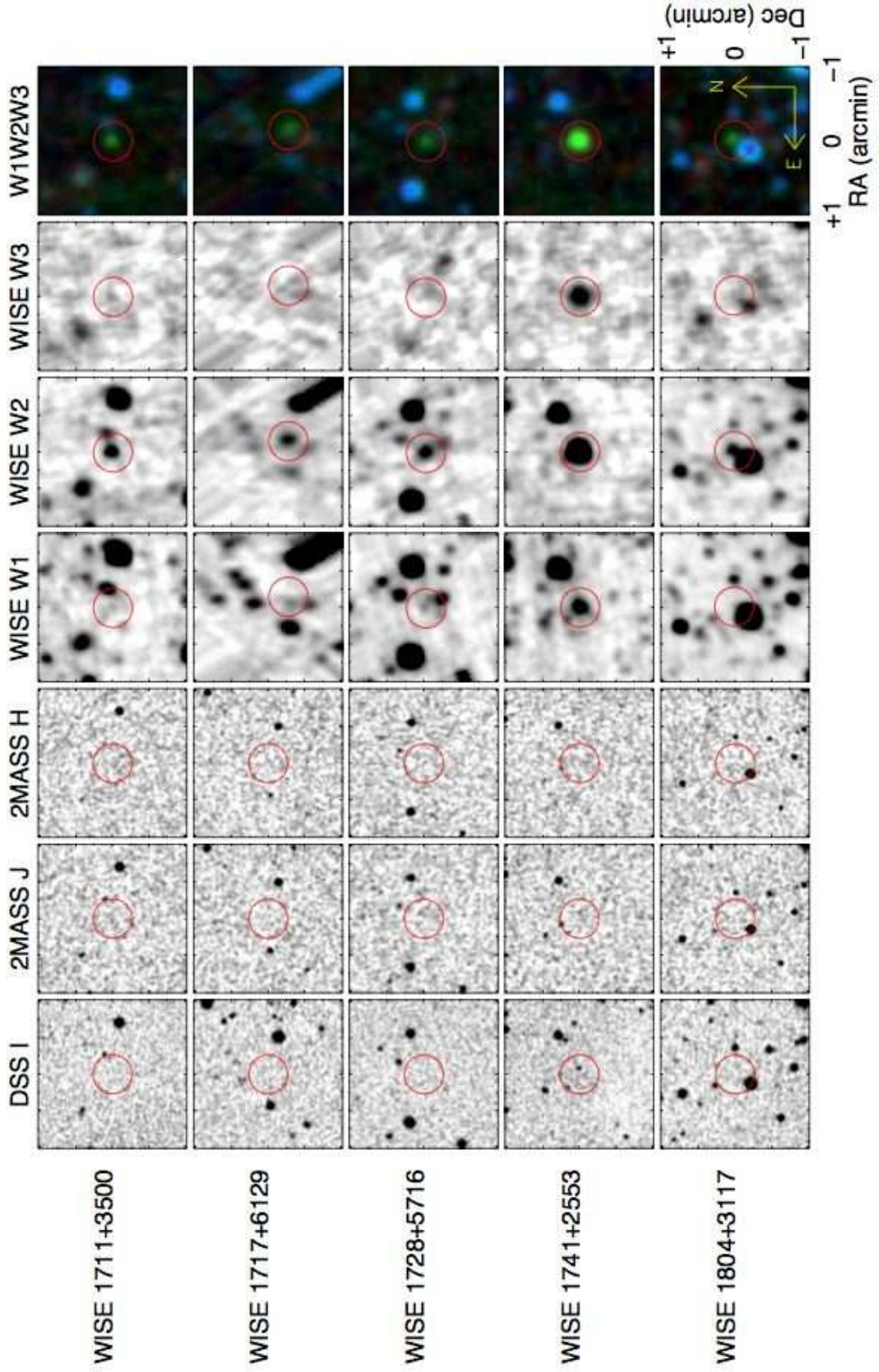


Fig. 4.14.— Continued.

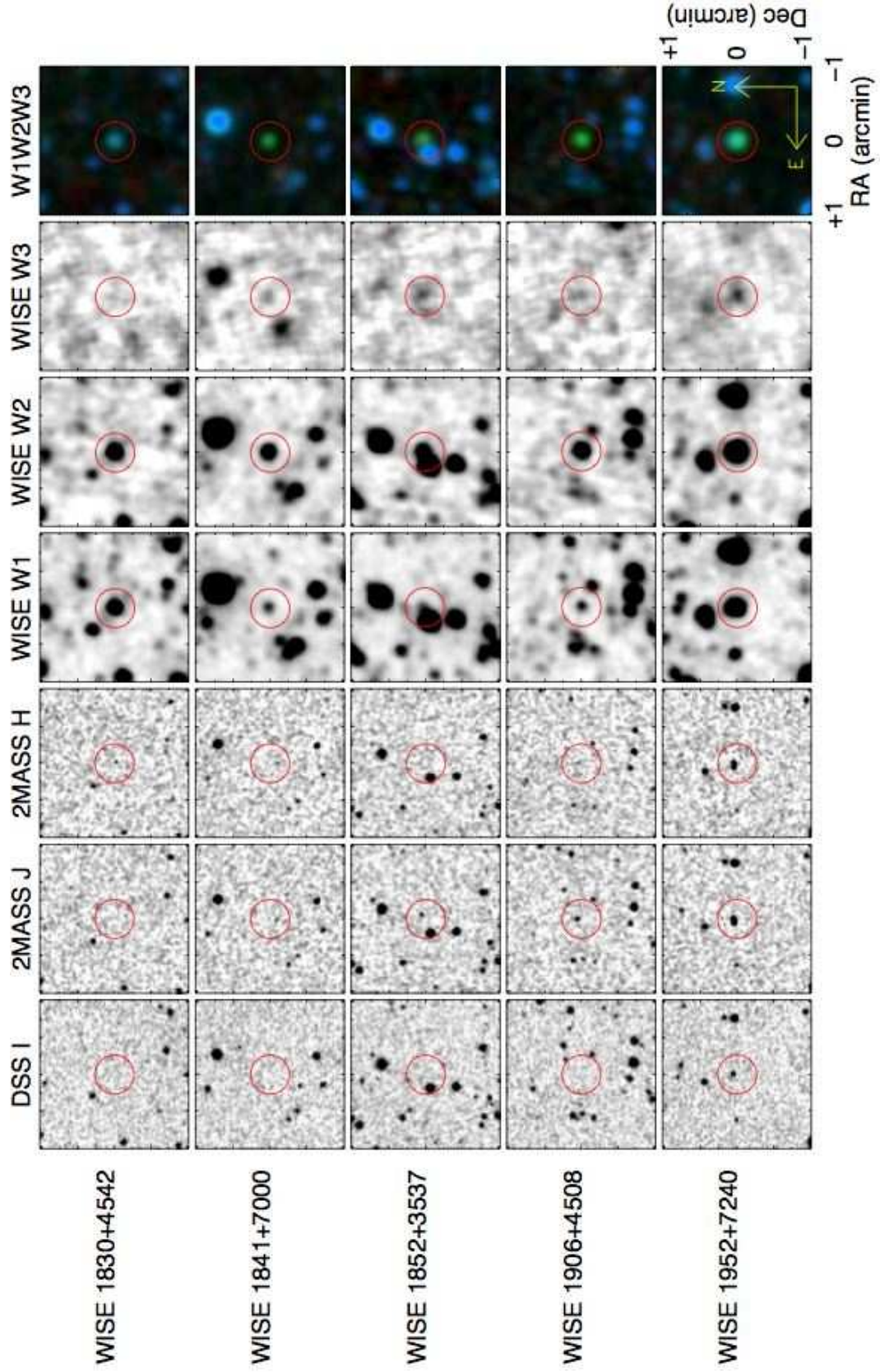


Fig. 4.15.— Continued.



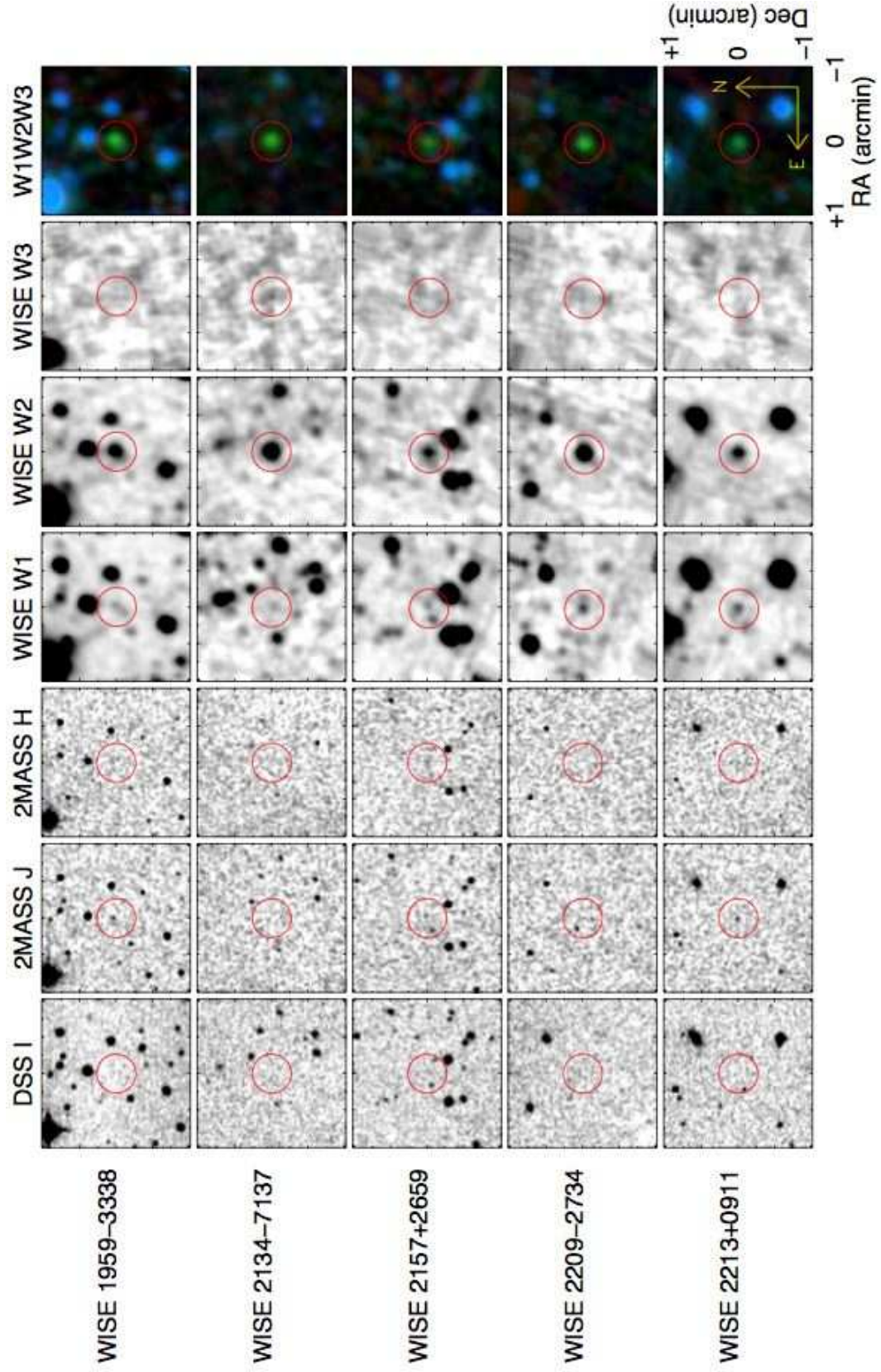


Fig. 4.16.— Continued.

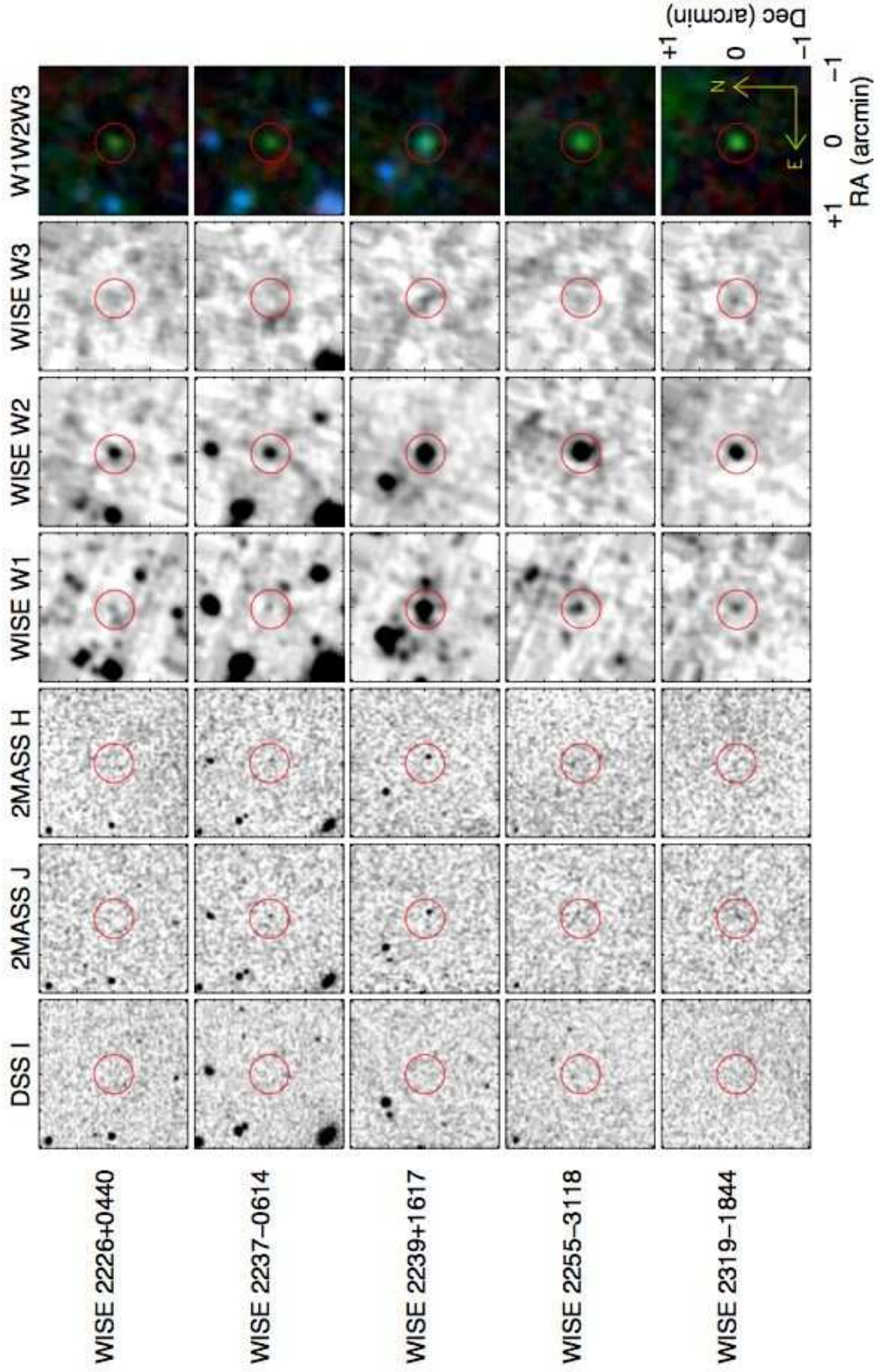


Fig. 4.17.— Continued.



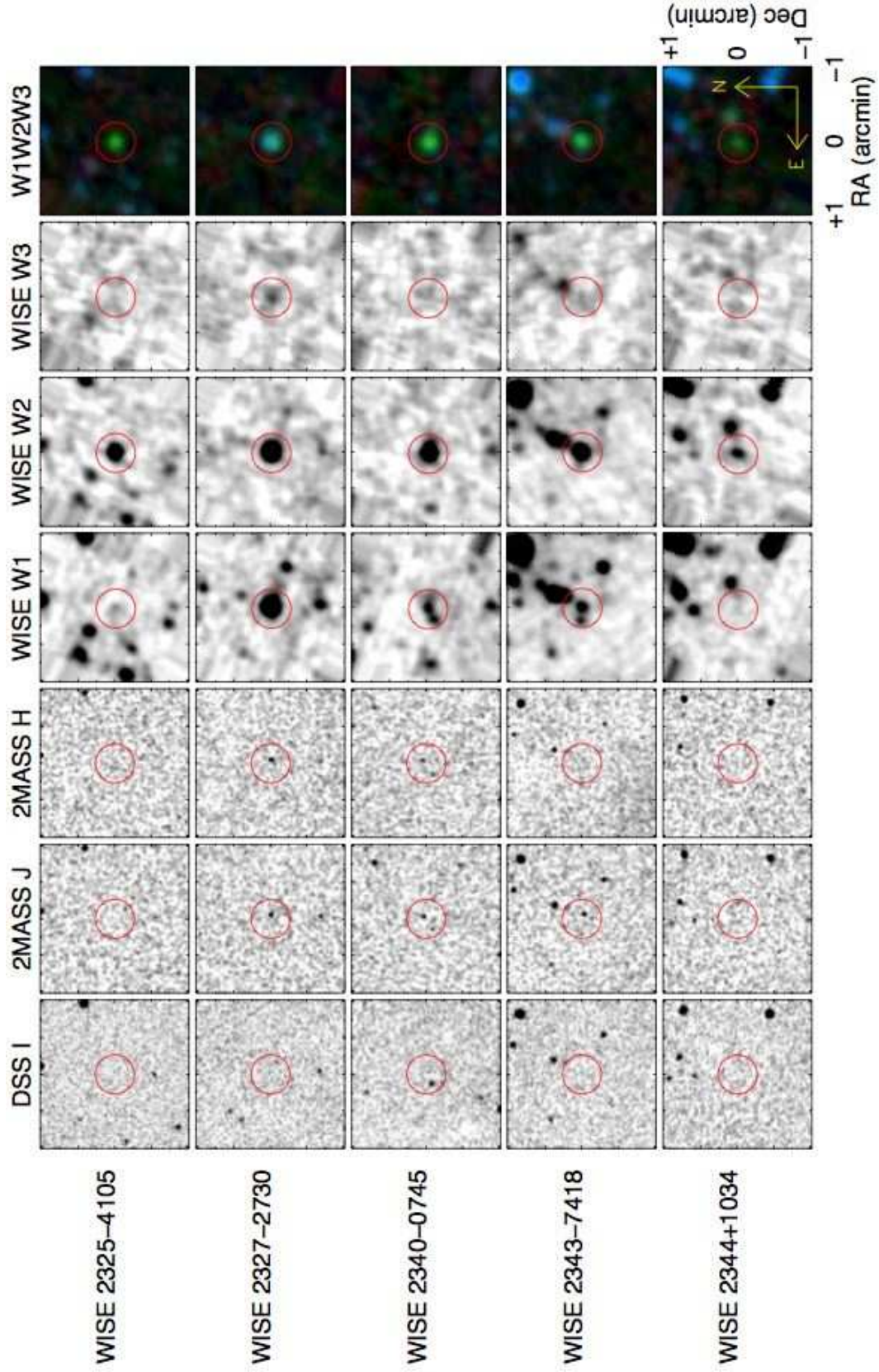


Fig. 4.18.— Continued.

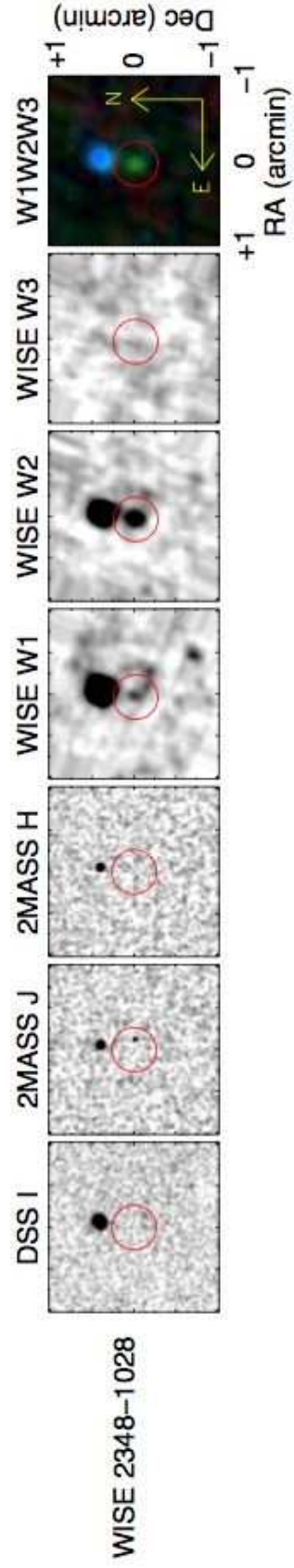


Fig. 4.19.— Continued.

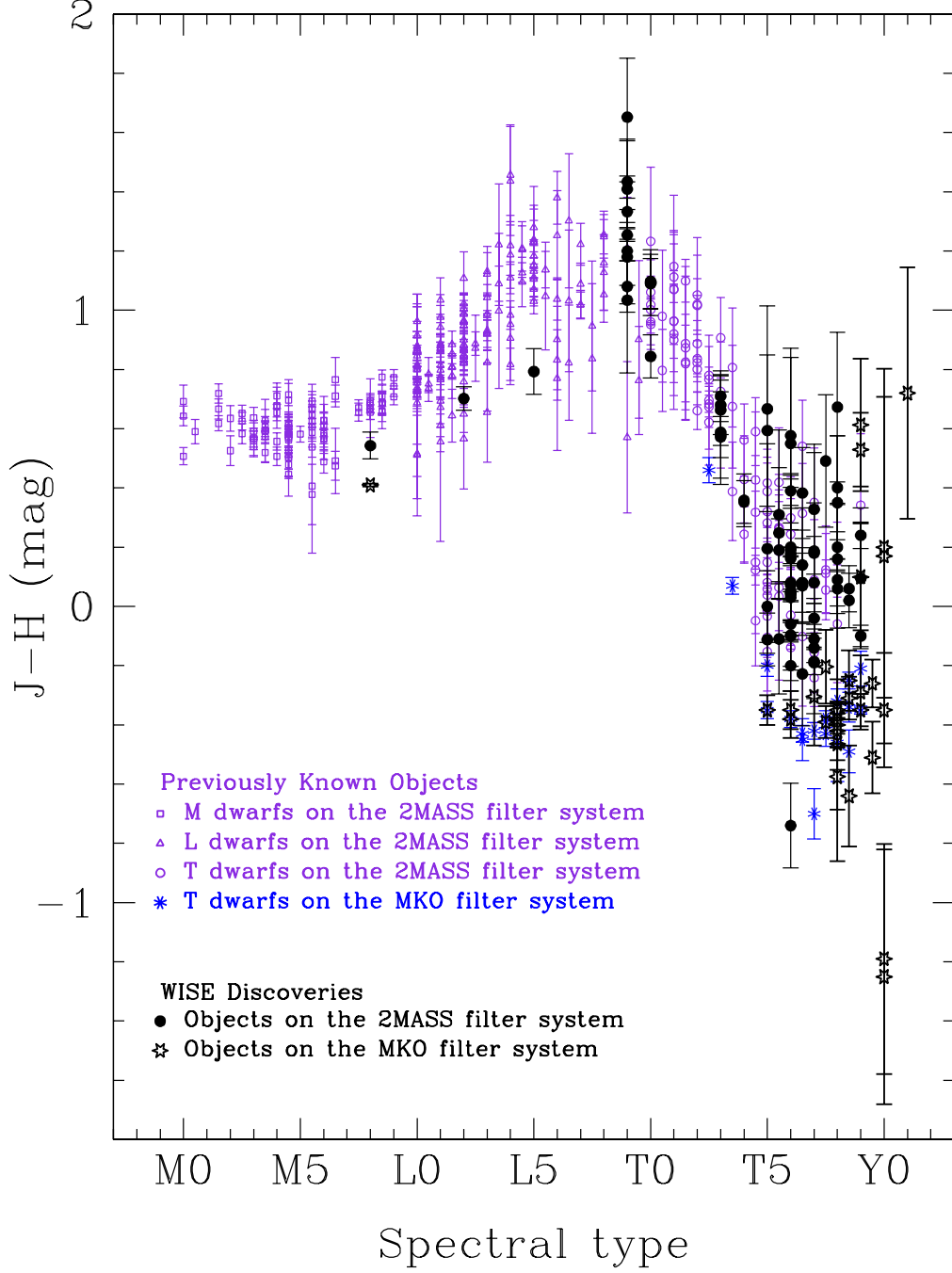


Fig. 5.—  $J - H$  color versus spectral type for objects with solid  $J - H$  colors (not limits). Color coding and symbol selection are explained in the legend.

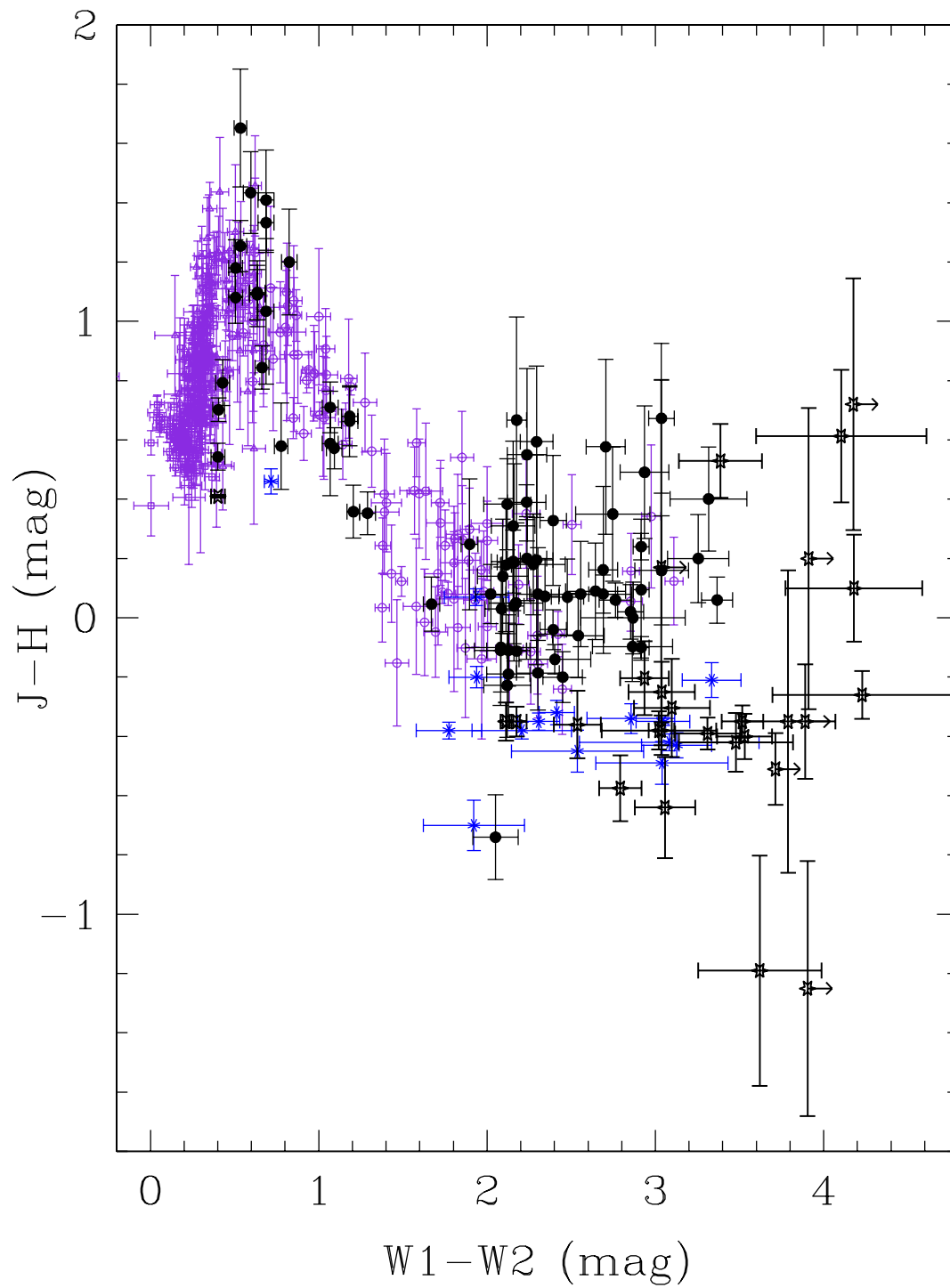


Fig. 6.—  $J - H$  color versus  $W1-W2$  color. Symbols are the same as in Figure 5.

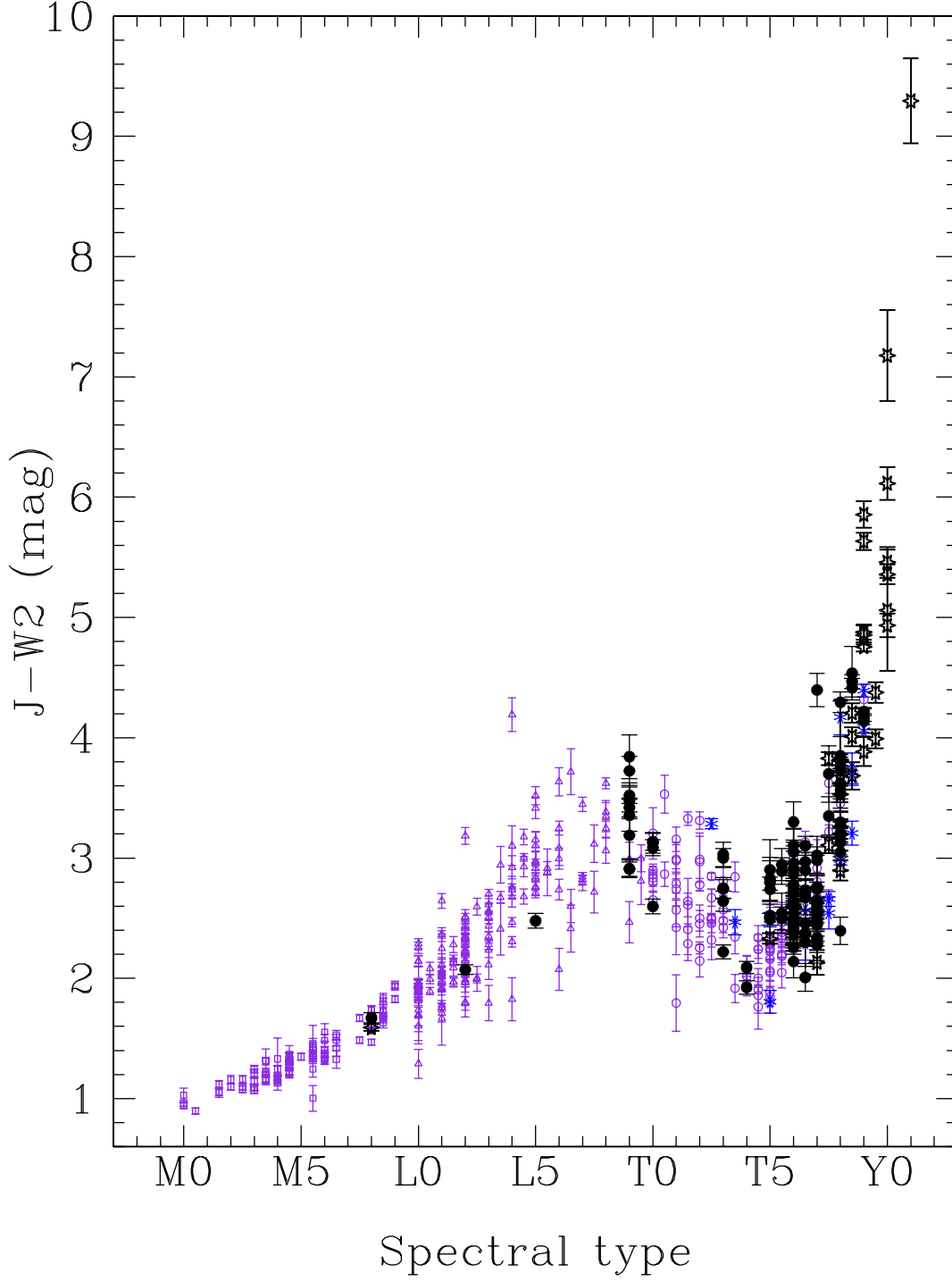


Fig. 7.—  $J-W2$  color versus spectral type. Color coding is the same as in Figure 5.

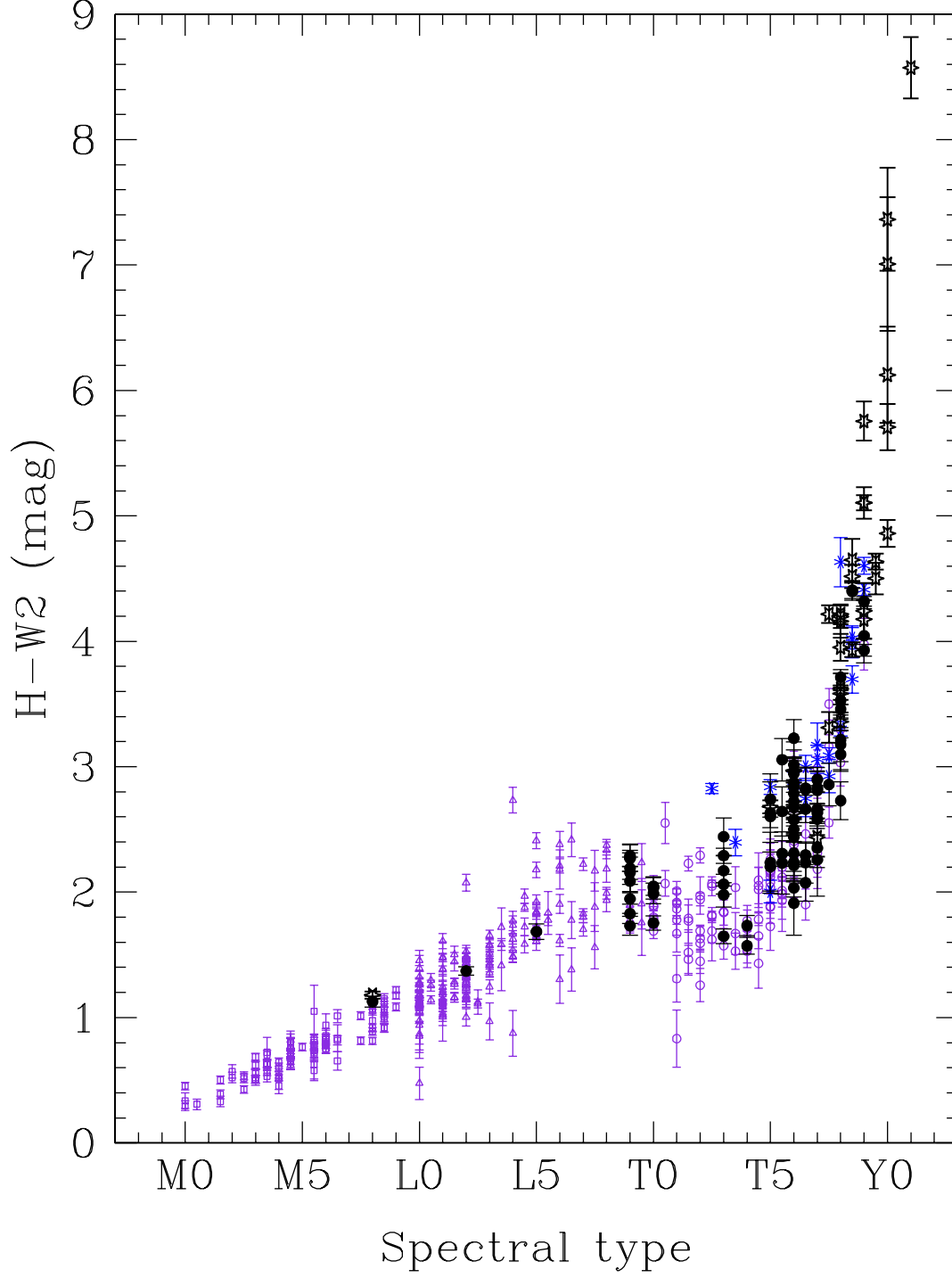


Fig. 8.—  $H$ - $W2$  color versus spectral type. Color coding is the same as in Figure 5.



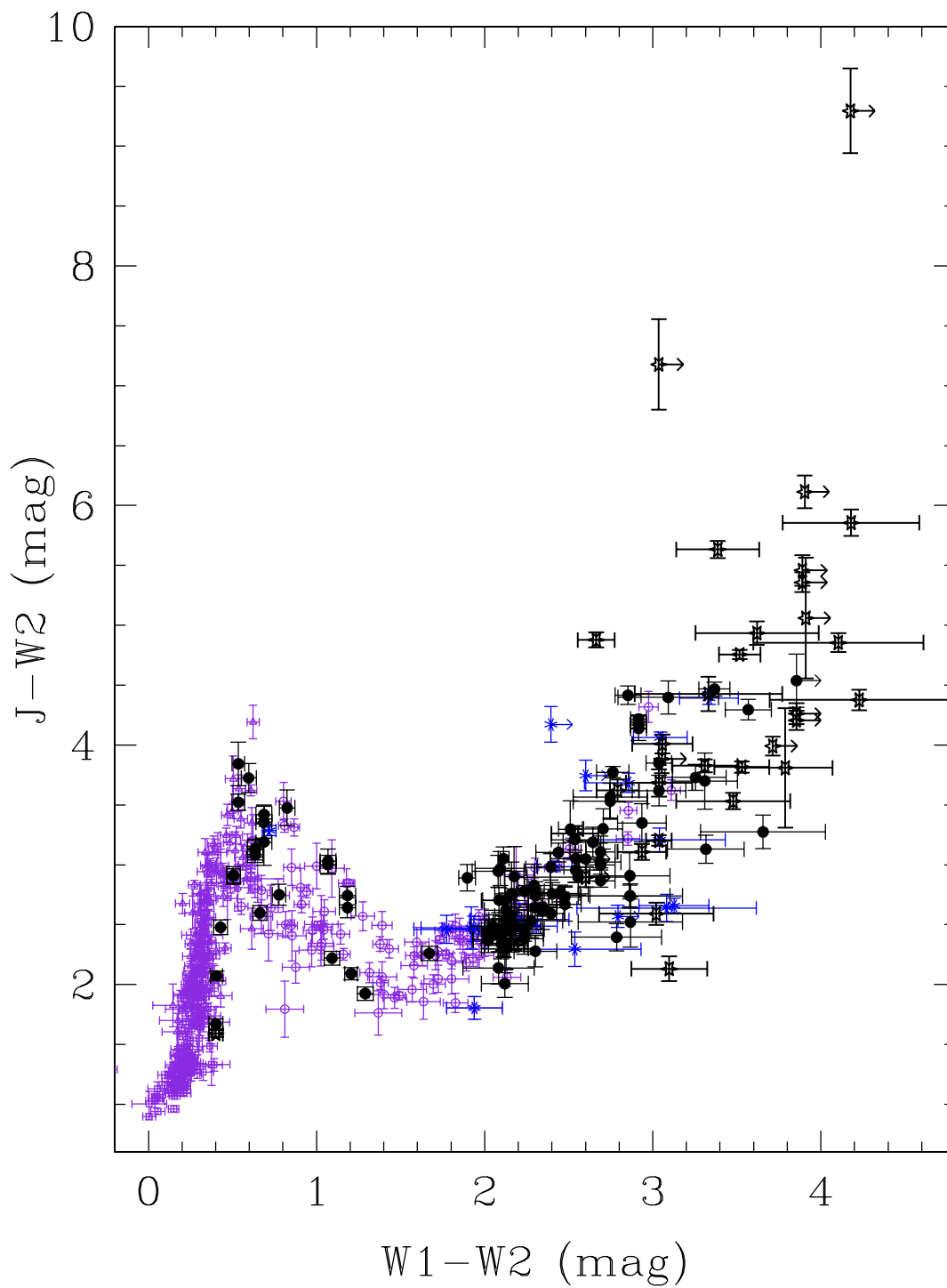


Fig. 9.—  $J-W2$  color plotted against  $W1-W2$  color. Color coding is the same as in Figure 5.

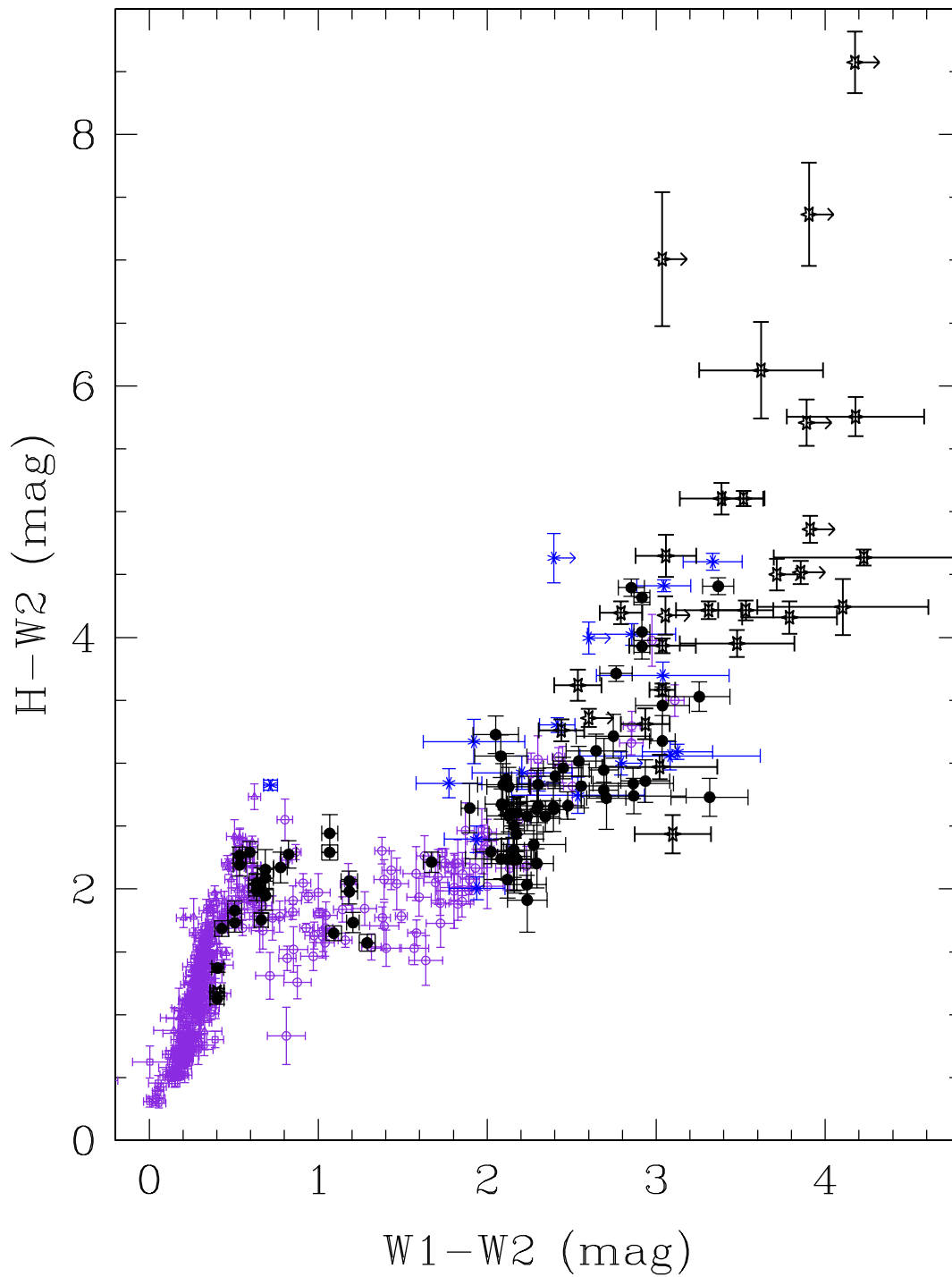


Fig. 10.—  $H-W2$  color plotted against  $W1-W2$  color. Color coding is the same as in Figure 5.

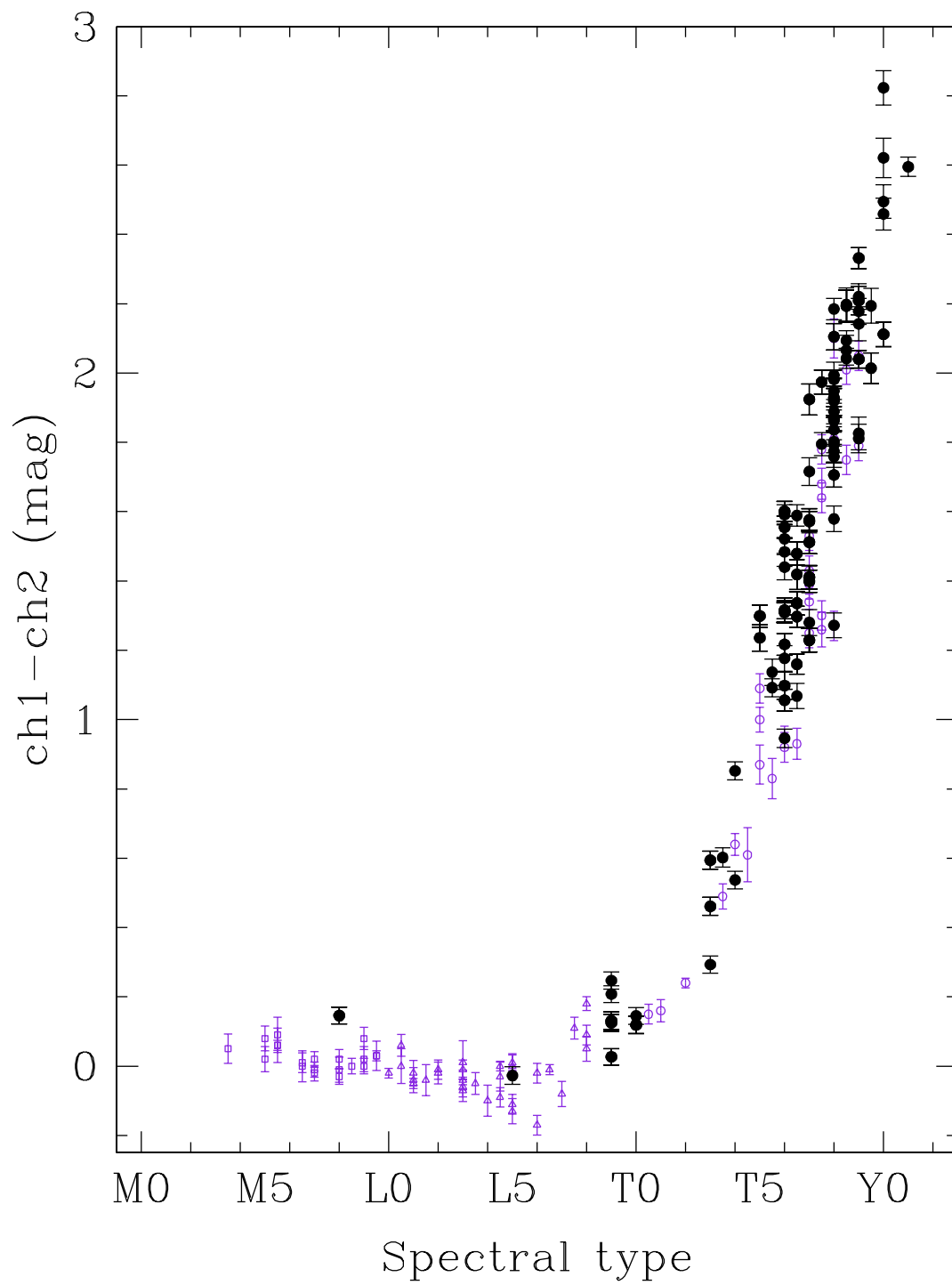


Fig. 11.— *Spitzer* IRAC  $ch1-ch2$  color as a function of spectral type. The color scheme is identical to that of Figure 1.

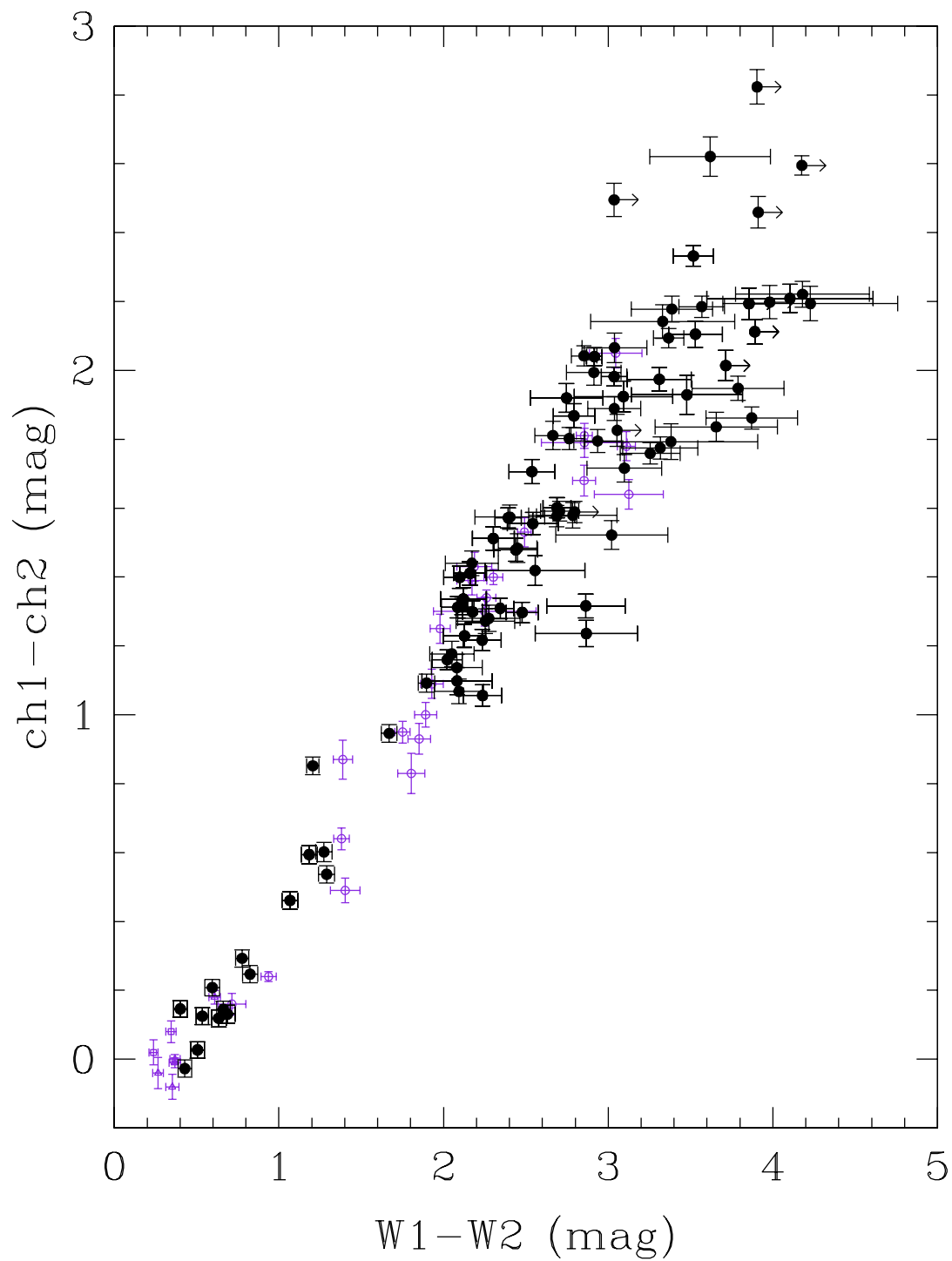


Fig. 12.— *Spitzer* IRAC ch1-ch2 color as a function of W1-W2 color. The color scheme is identical to that of Figure 1.

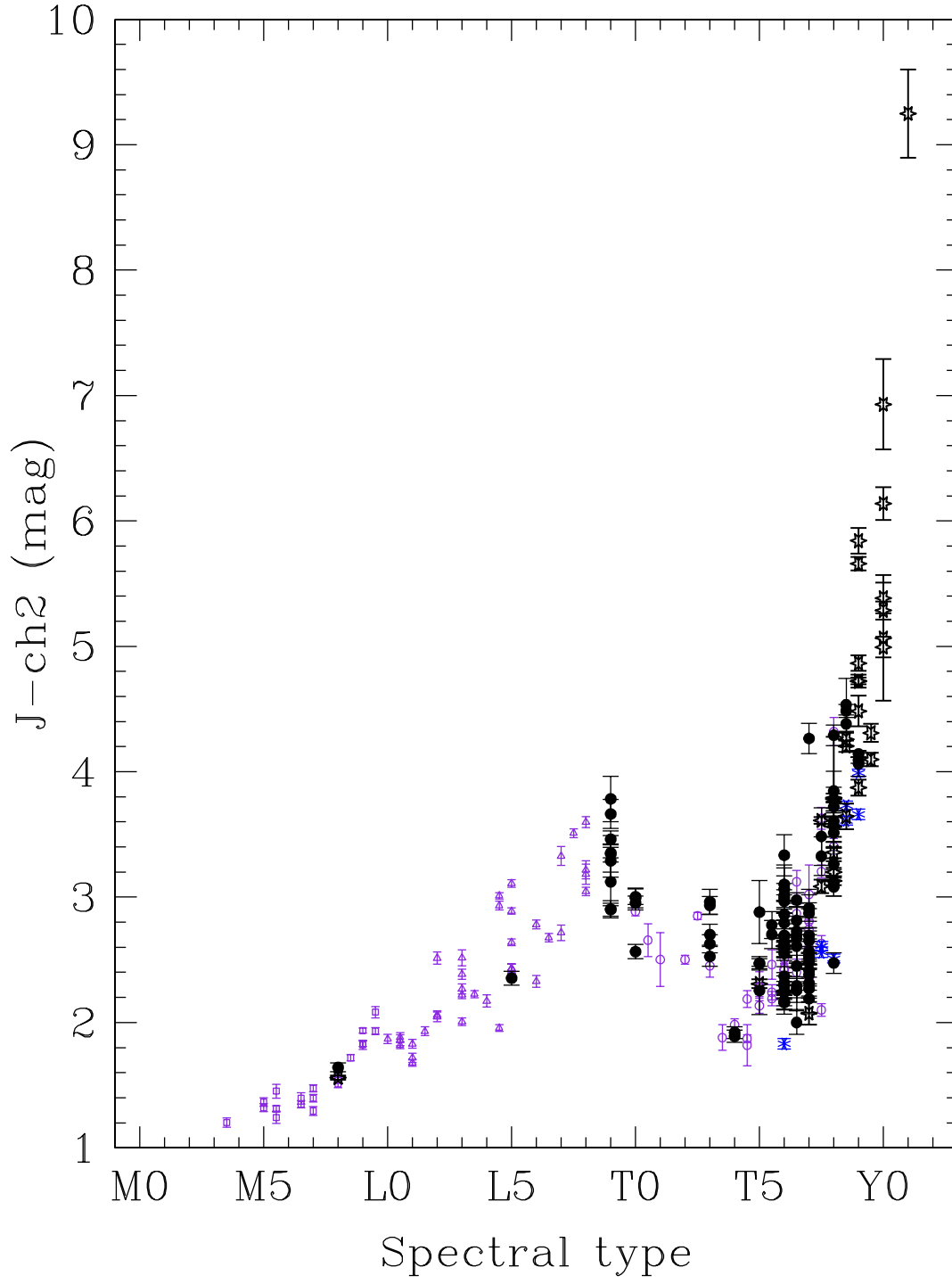


Fig. 13.—  $J$ -ch2 color as a function of spectral type. Color coding is the same as in Figure 5.

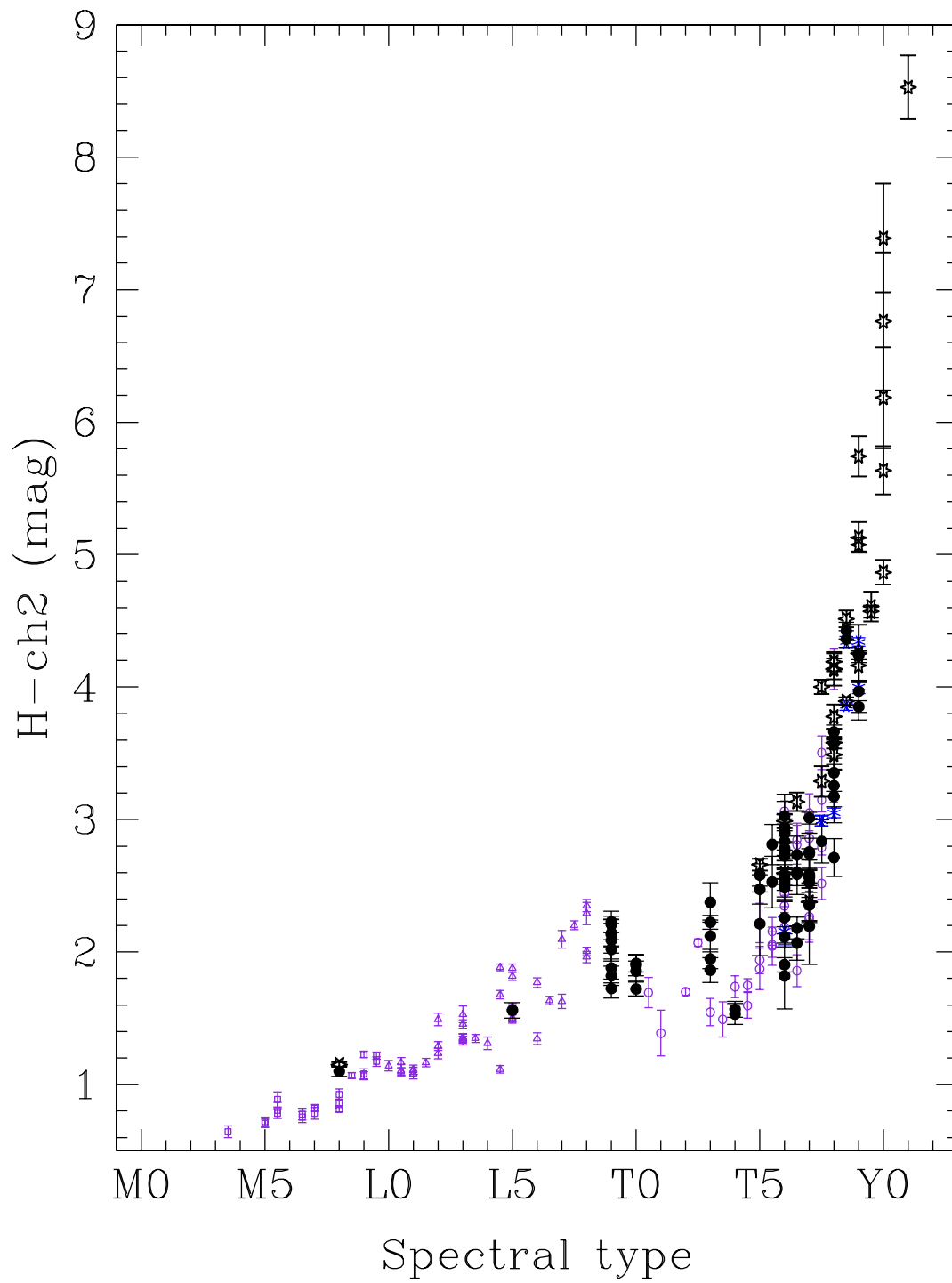


Fig. 14.—  $H$ -ch2 color as a function of spectral type. Color coding is the same as in Figure 5.

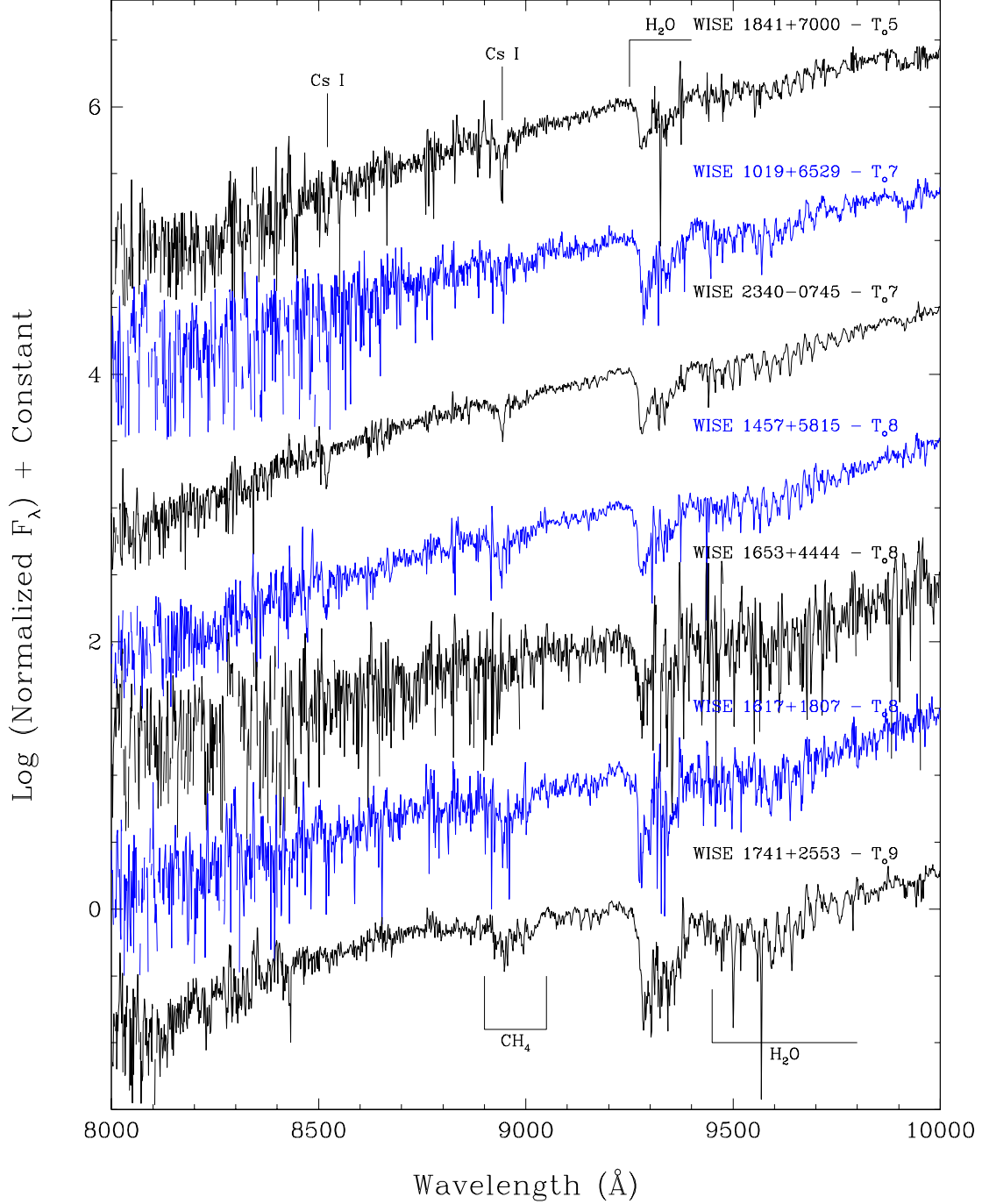


Fig. 15.— Spectra from 8000 to 10000  $\text{\AA}$  for seven WISE brown dwarf discoveries. Data have been corrected for telluric absorption and prominent spectral features are marked. All spectra have been normalized at 9200  $\text{\AA}$  and an integral offset added to the  $y$ -axis values to separate the spectra vertically.

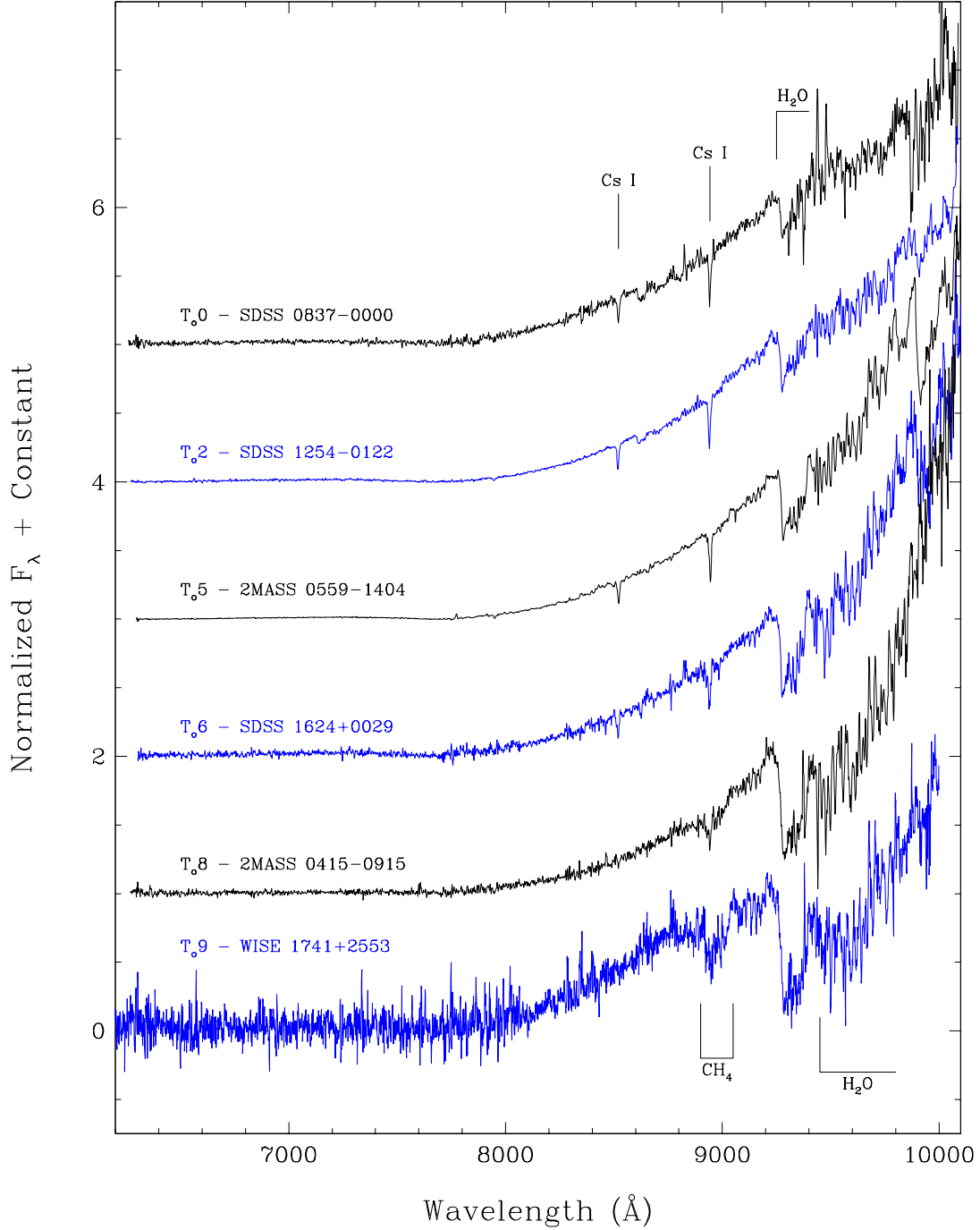


Fig. 16.— Spectra from 6200 to 10000 Å for the optical spectral standards from Burgasser et al. (2006) supplemented with the T<sub>0</sub> standard from Kirkpatrick et al. (2010) and the T<sub>9</sub> standard proposed here. Data have been corrected for telluric absorption and prominent spectral features are marked. All spectra have been normalized at 9200 Å and an integral offset added to the  $y$ -axis values to separate the spectra vertically.



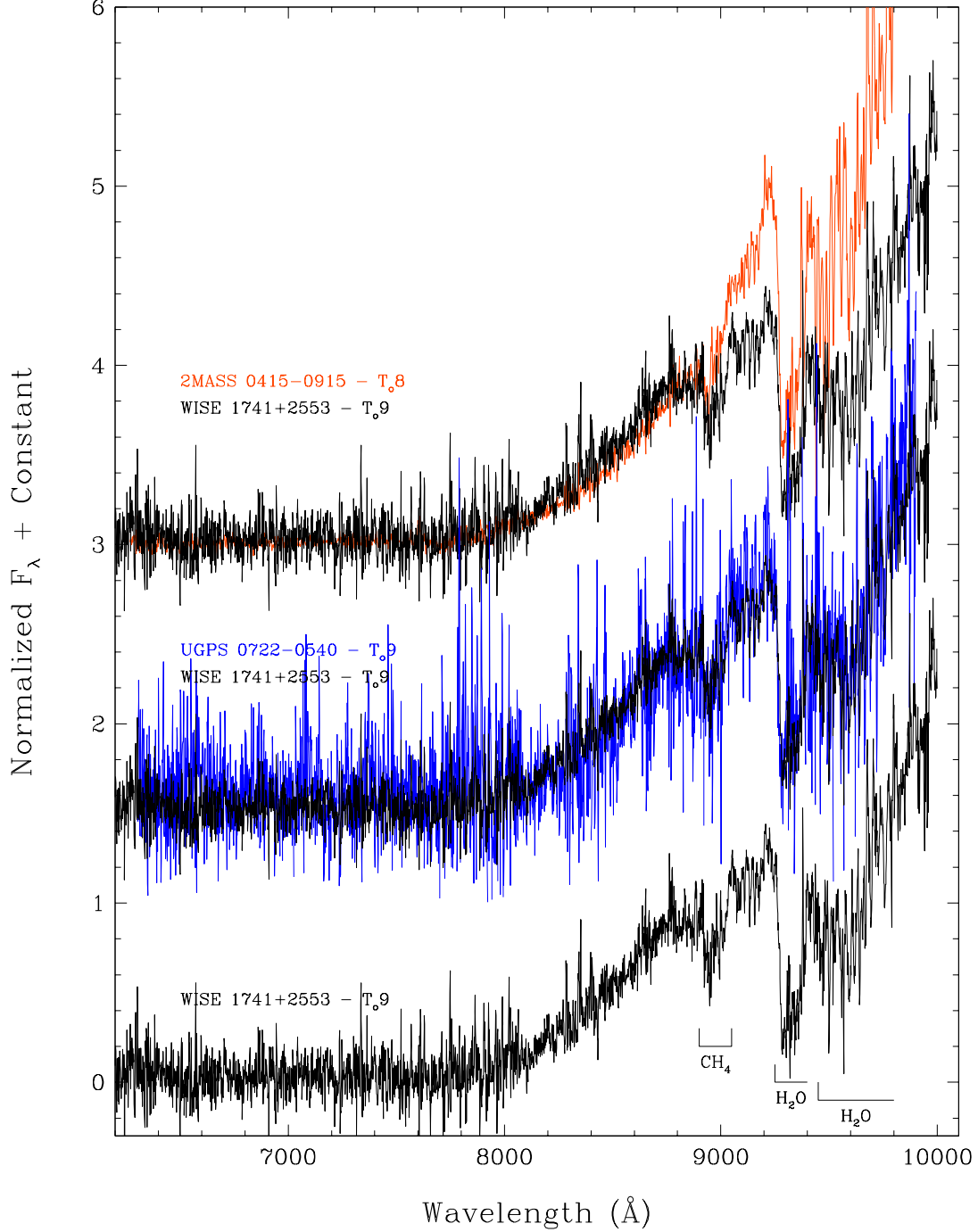


Fig. 17.— Spectra from 6200 to 10000 Å for three late-T dwarfs: the T<sub>8</sub> standard 2MASS J04151954–0935066 (orange red), the T<sub>9</sub> standard WISE 1741+2553 (black), and the T<sub>9</sub> dwarf UGPS J072227.51–054031.2 (blue violet). Data have been corrected for telluric absorption and prominent spectral features are marked. Spectra have been normalized at 8800 Å and offsets in increments of 1.5 added to the  $y$ -axis values to separate the spectra vertically except where overplotting was intended.

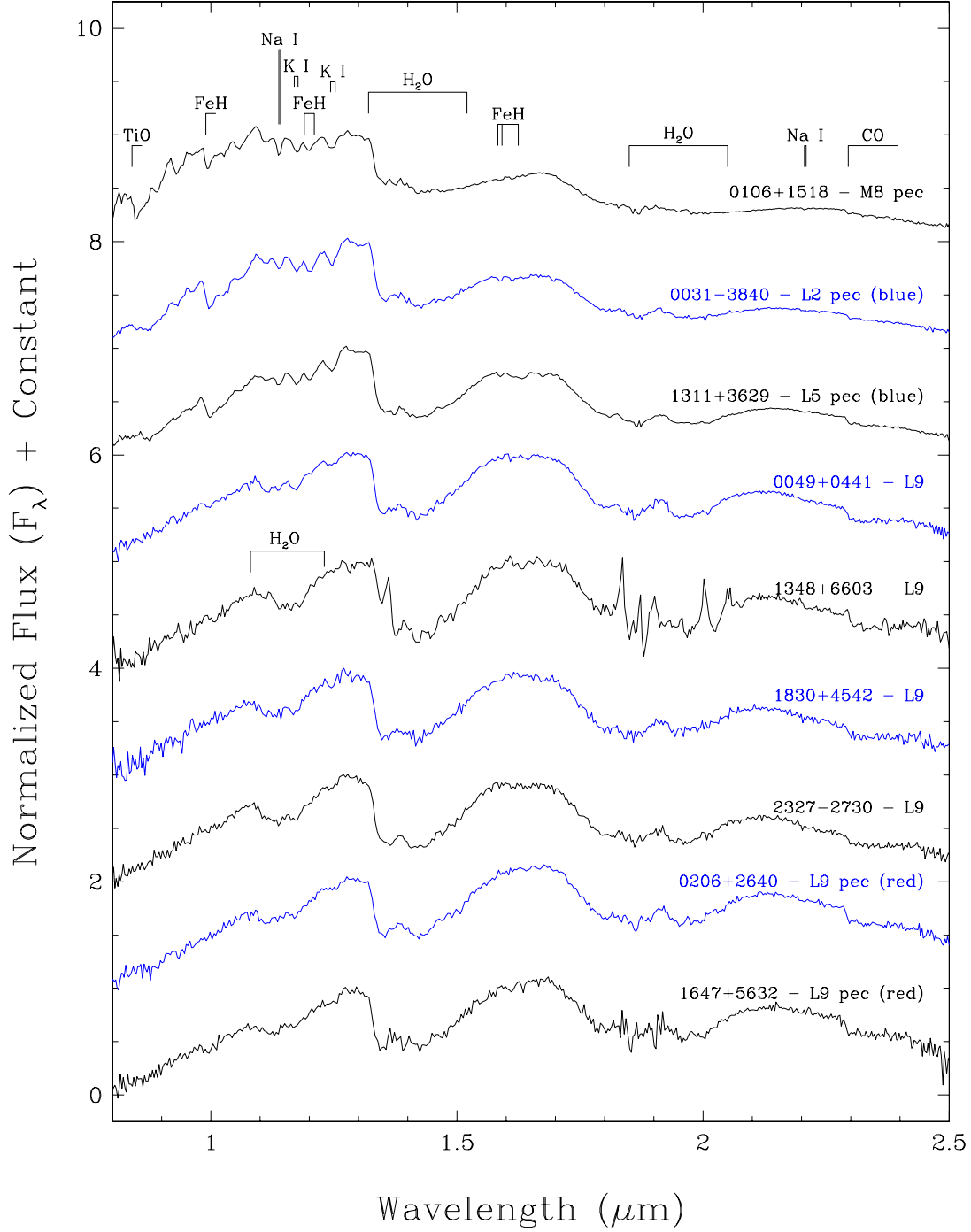


Fig. 18.— Near-infrared spectra of confirmed WISE brown dwarfs with spectral types earlier than T0. Spectra have been normalized to one around 1.28  $\mu\text{m}$  and integral offsets have been added to the  $y$ -axis values to separate the spectra vertically. Prominent spectral features are marked.

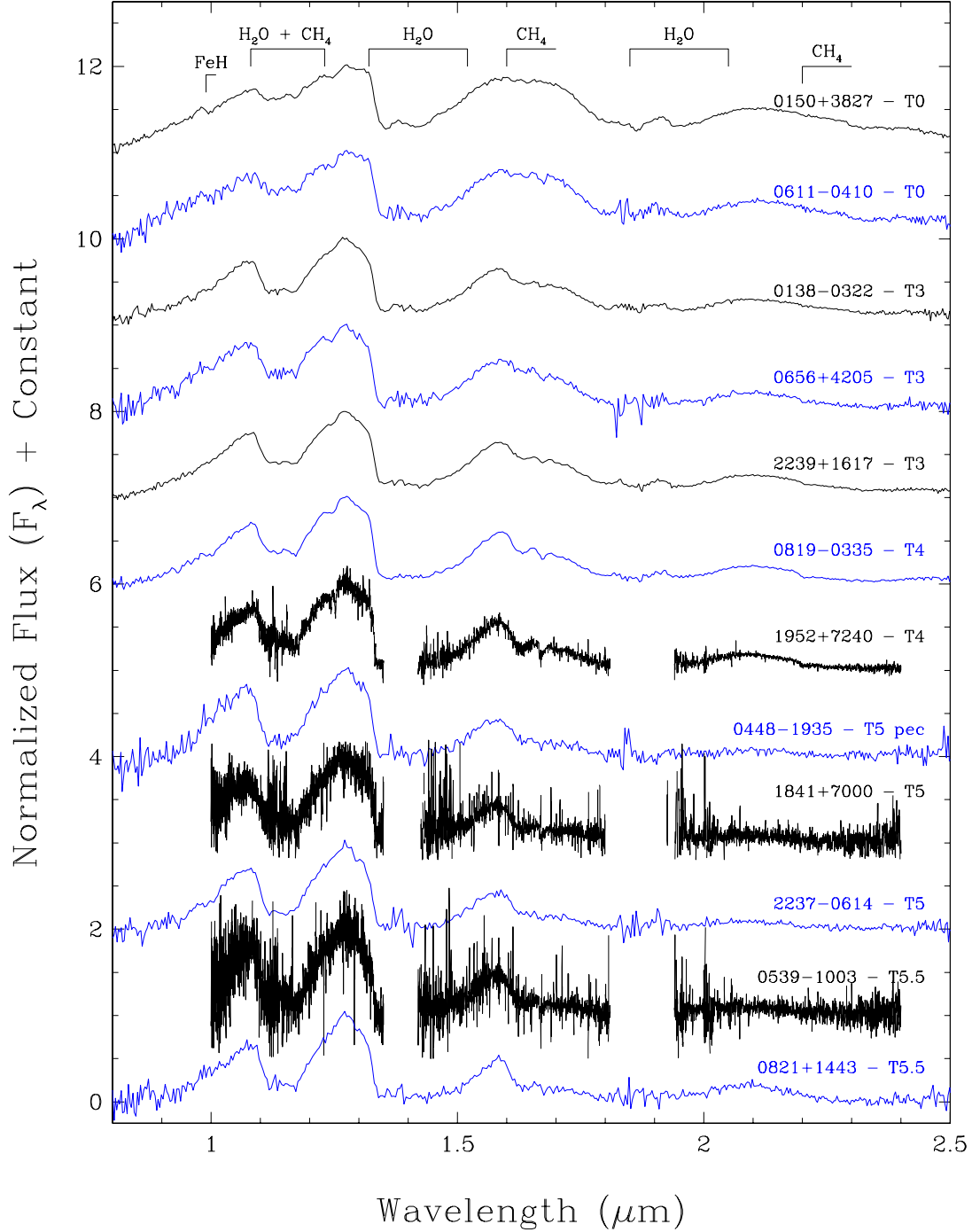


Fig. 19.— Near-infrared spectra of confirmed WISE brown dwarfs with spectral types from T0 to T5.5. Spectra have been normalized to one around  $1.28 \mu\text{m}$  and integral offsets have been added to the  $y$ -axis values to separate the spectra vertically. For some spectra, noisy data in the depths of the telluric water bands are not plotted. Prominent spectral features are marked.

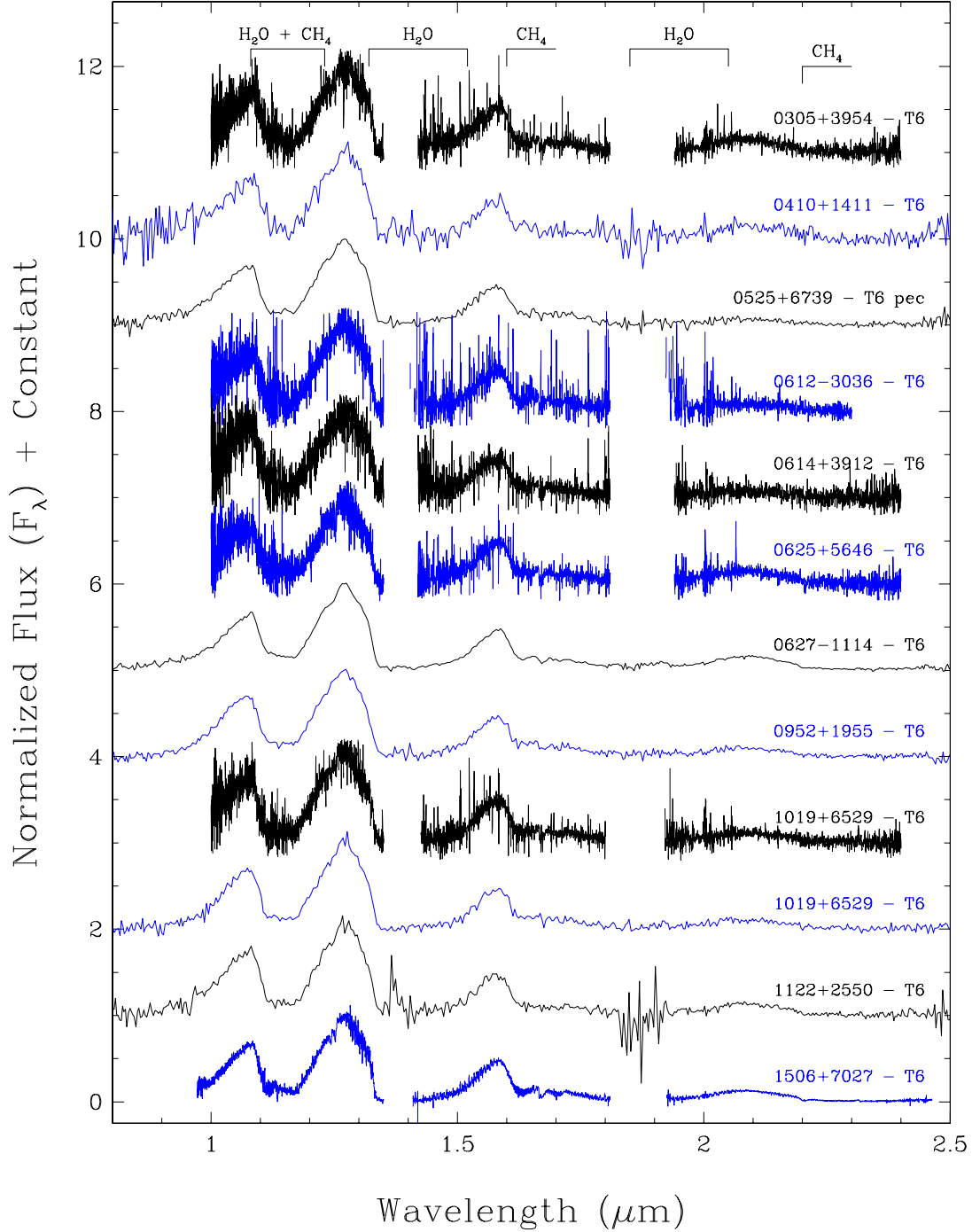


Fig. 20.— Near-infrared spectra of confirmed WISE brown dwarfs with spectral types of T6. (Additional T6 dwarfs are shown in Figure 21.) Spectra have been normalized to one around  $1.28 \mu\text{m}$  and integral offsets have been added to the  $y$ -axis values to separate the spectra vertically. For some spectra, noisy data in the depths of the telluric water bands are not plotted. Prominent spectral features are marked.

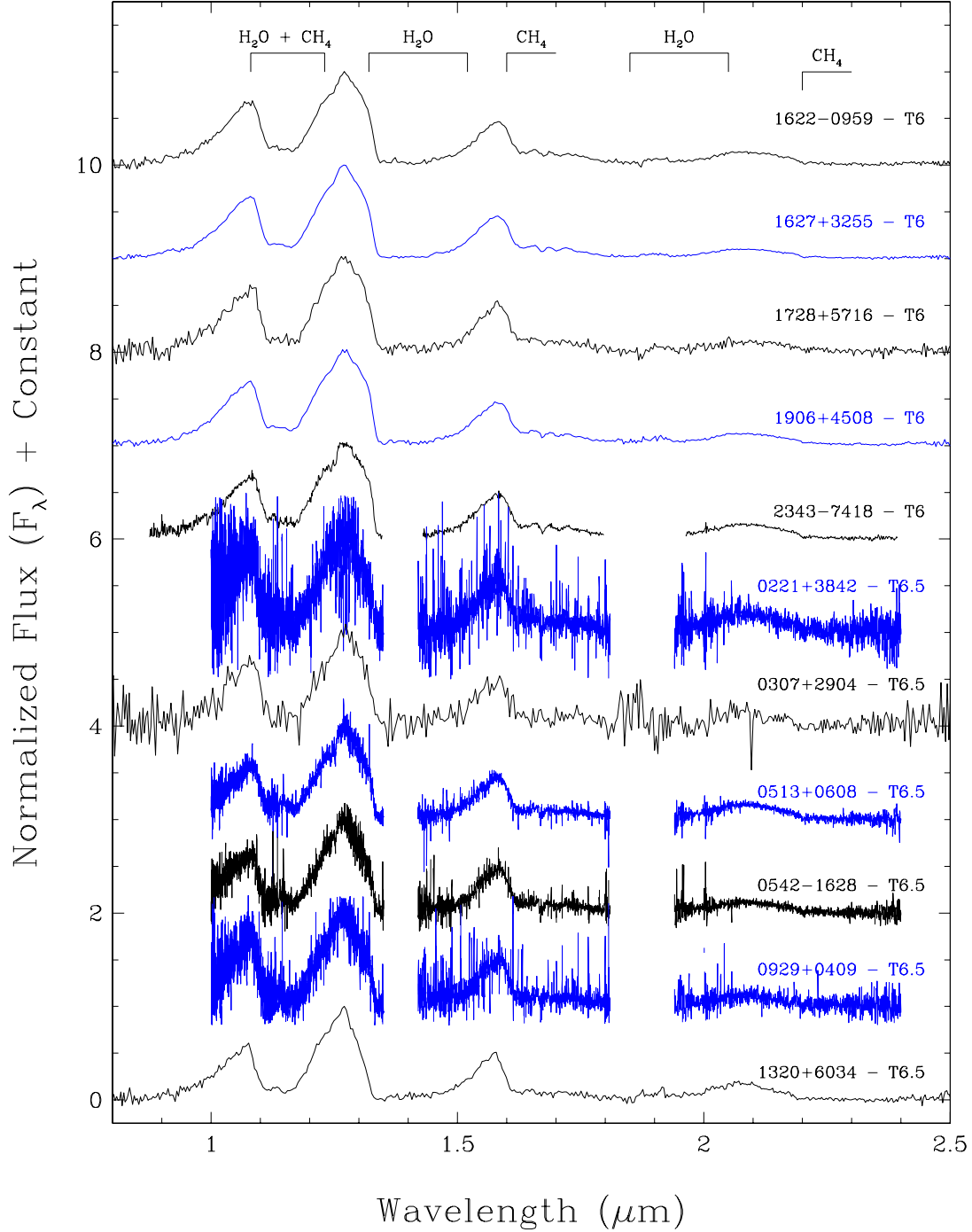


Fig. 21.— Near-infrared spectra of confirmed WISE brown dwarfs with spectral types from T6 (continued) to T6.5. Spectra have been normalized to one around  $1.28 \mu\text{m}$  and integral offsets have been added to the  $y$ -axis values to separate the spectra vertically. For some spectra, noisy data in the depths of the telluric water bands are not plotted. Prominent spectral features are marked.

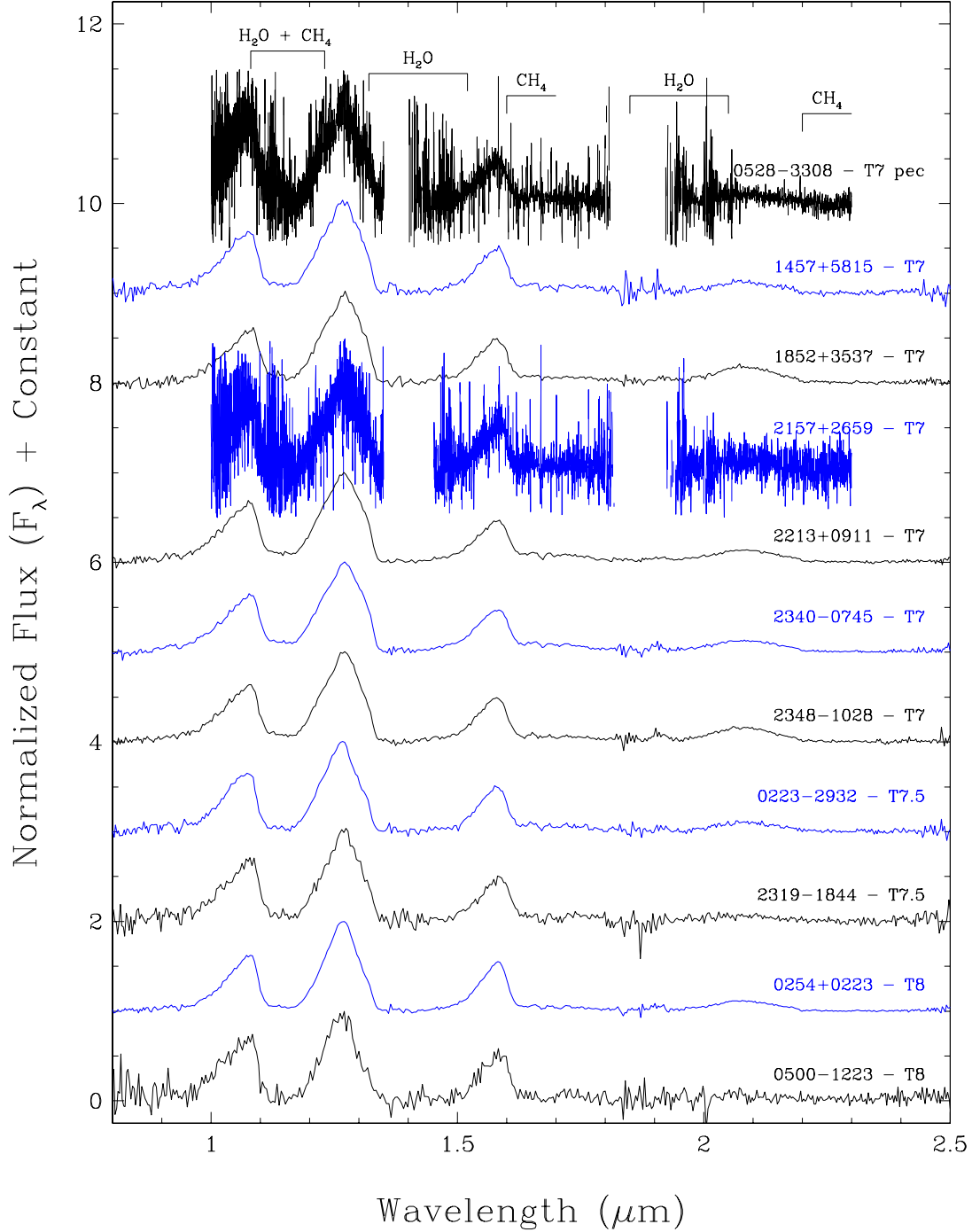


Fig. 22.— Near-infrared spectra of confirmed WISE brown dwarfs with spectral types from T7 to T8. (Additional T8 dwarfs are shown in Figure 23 and Figure 24.) Spectra have been normalized to one around  $1.28 \mu\text{m}$  and integral offsets have been added to the  $y$ -axis values to separate the spectra vertically. For some spectra, noisy data in the depths of the telluric water bands are not plotted. Prominent spectral features are marked.

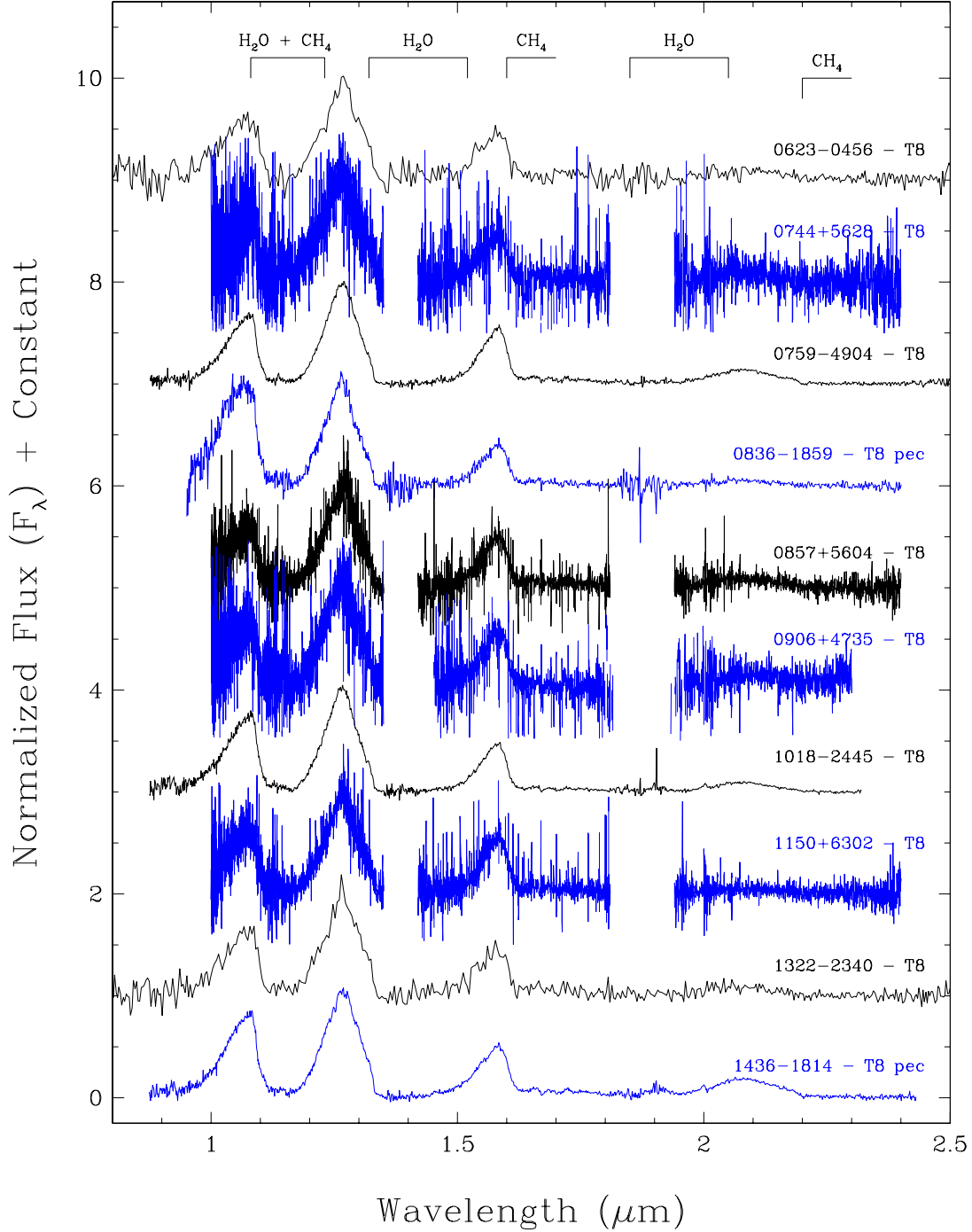


Fig. 23.— Near-infrared spectra of confirmed WISE brown dwarfs with spectral types of T8 (continued). Spectra have been normalized to one around 1.28  $\mu\text{m}$  and integral offsets have been added to the  $y$ -axis values to separate the spectra vertically. For some spectra, noisy data in the depths of the telluric water bands are not plotted. Prominent spectral features are marked.

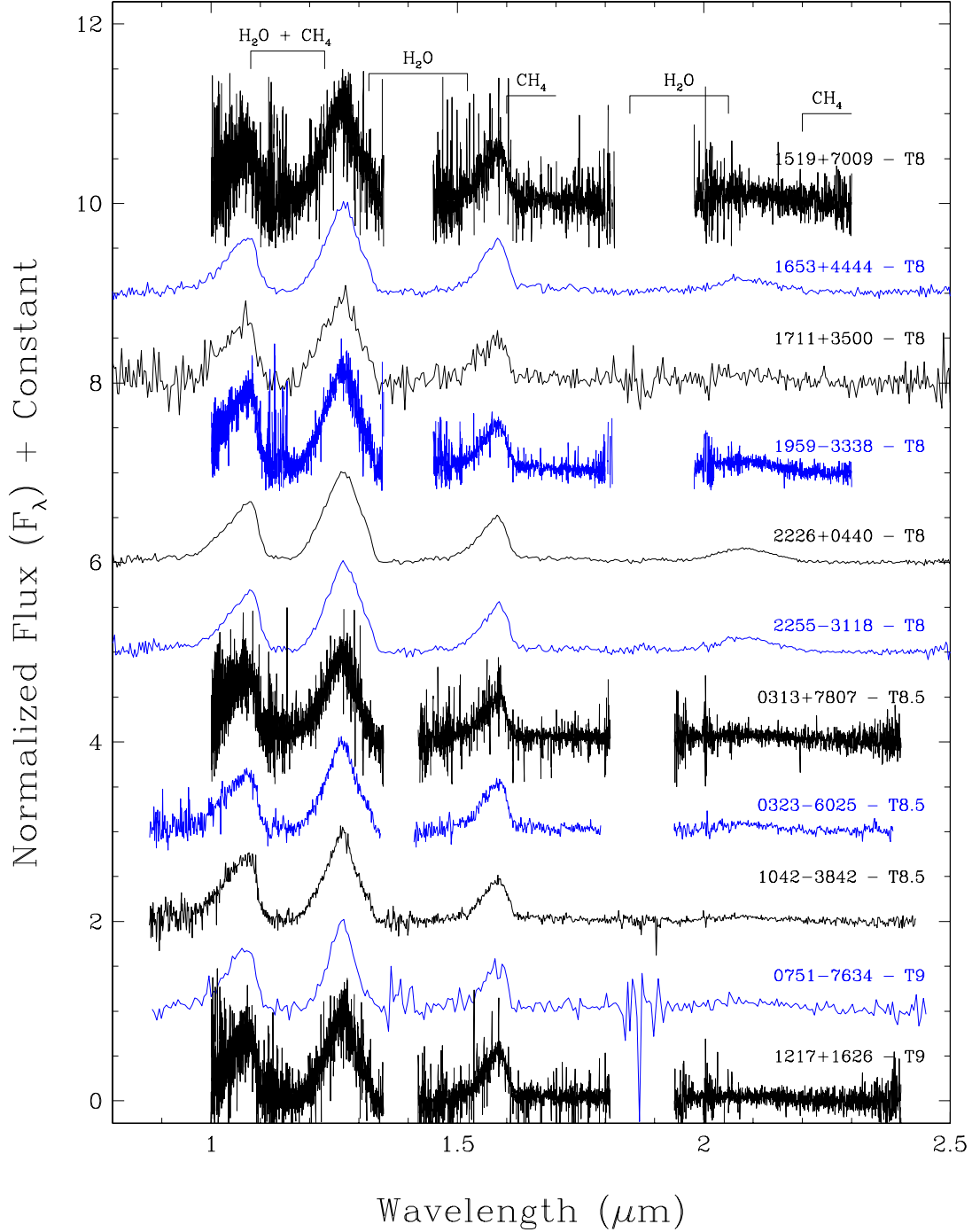


Fig. 24.— Near-infrared spectra of confirmed WISE brown dwarfs with spectral types from T8 (continued) to T9. (Additional T9 dwarfs are shown in Figure 25.) Spectra have been normalized to one around  $1.28 \mu\text{m}$  and integral offsets have been added to the  $y$ -axis values to separate the spectra vertically. For some spectra, noisy data in the depths of the telluric water bands are not plotted. Prominent spectral features are marked.



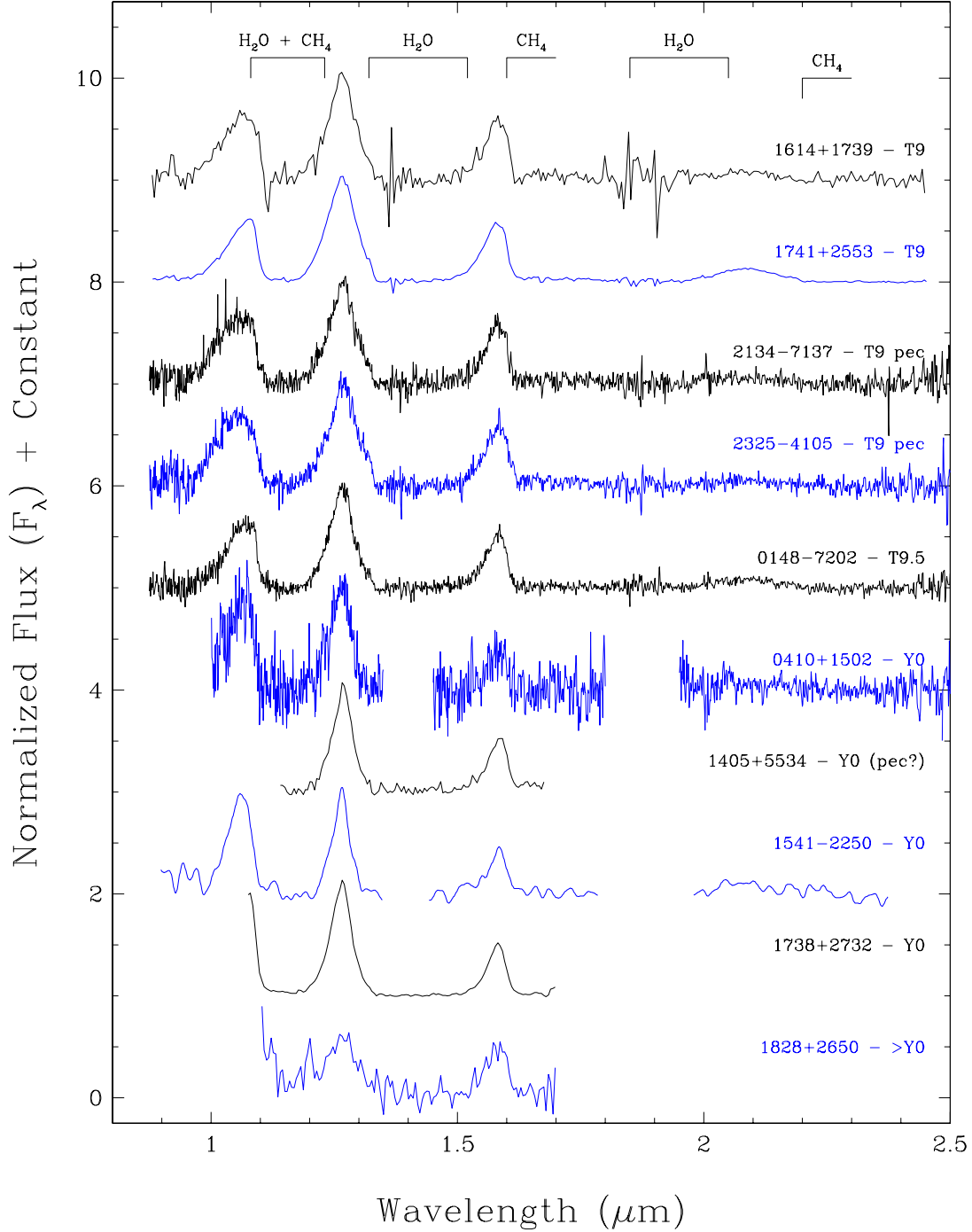


Fig. 25.— Near-infrared spectra of confirmed WISE brown dwarfs with spectral types from T9 to early Y. Spectra have been normalized to one around  $1.28 \mu\text{m}$  and integral offsets have been added to the  $y$ -axis values to separate the spectra vertically. For some spectra, noisy data in the depths of the telluric water bands are not plotted. Prominent spectral features are marked.

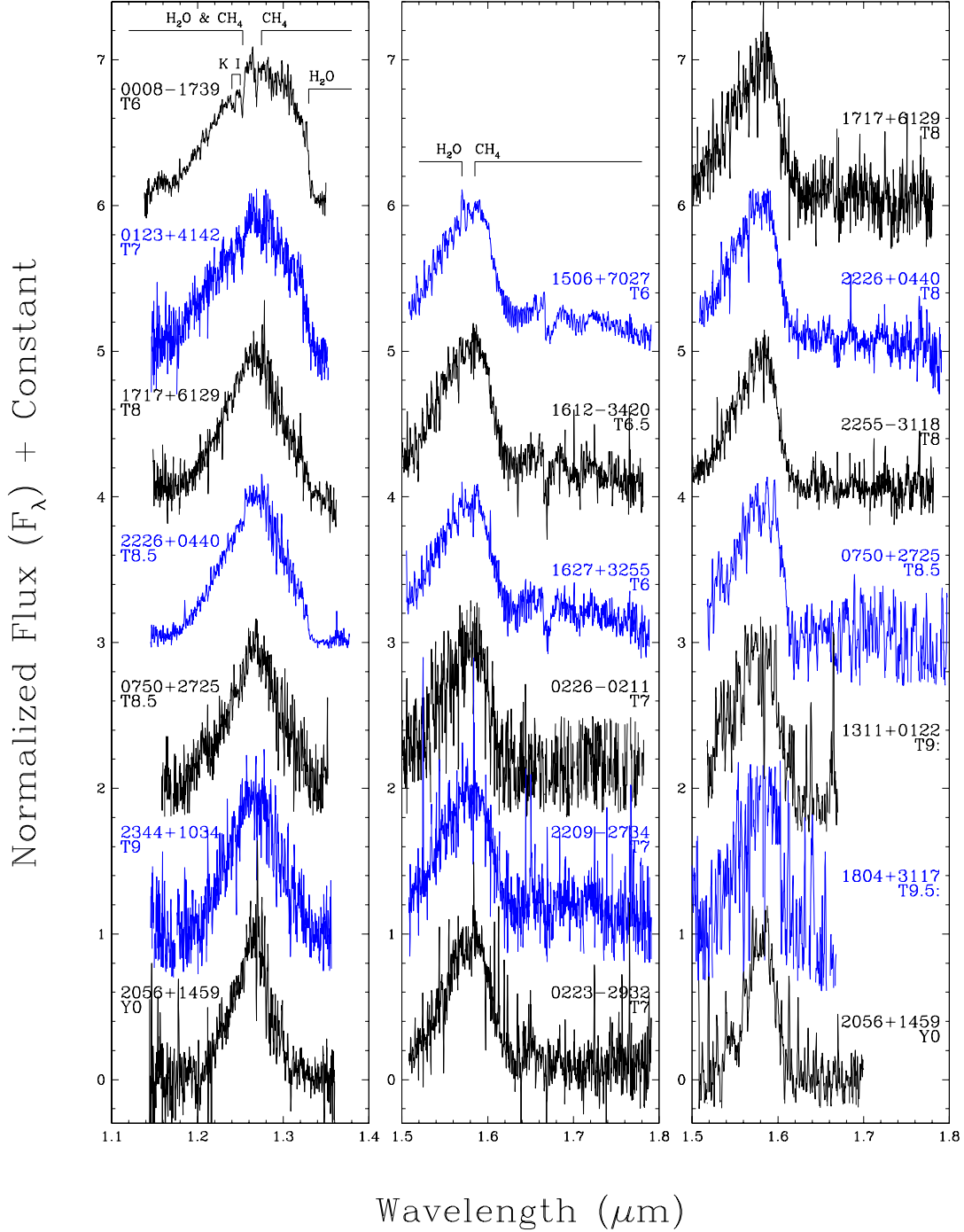


Fig. 26.— Keck/NIRSPEC spectra of confirmed WISE brown dwarfs.  $J$ -band spectra are shown in the left panel and  $H$ -band spectra are shown in the middle and right panels. Spectra have been normalized to one at peak flux and integral offsets have been added to the  $y$ -axis values to separate the spectra vertically. The bottom three spectra in the rightmost plot – those of WISE 1311+0122, WISE 1804+3117, and WISE 2056+1459 – have been smoothed with a five-pixel boxcar. Prominent spectral features are marked.

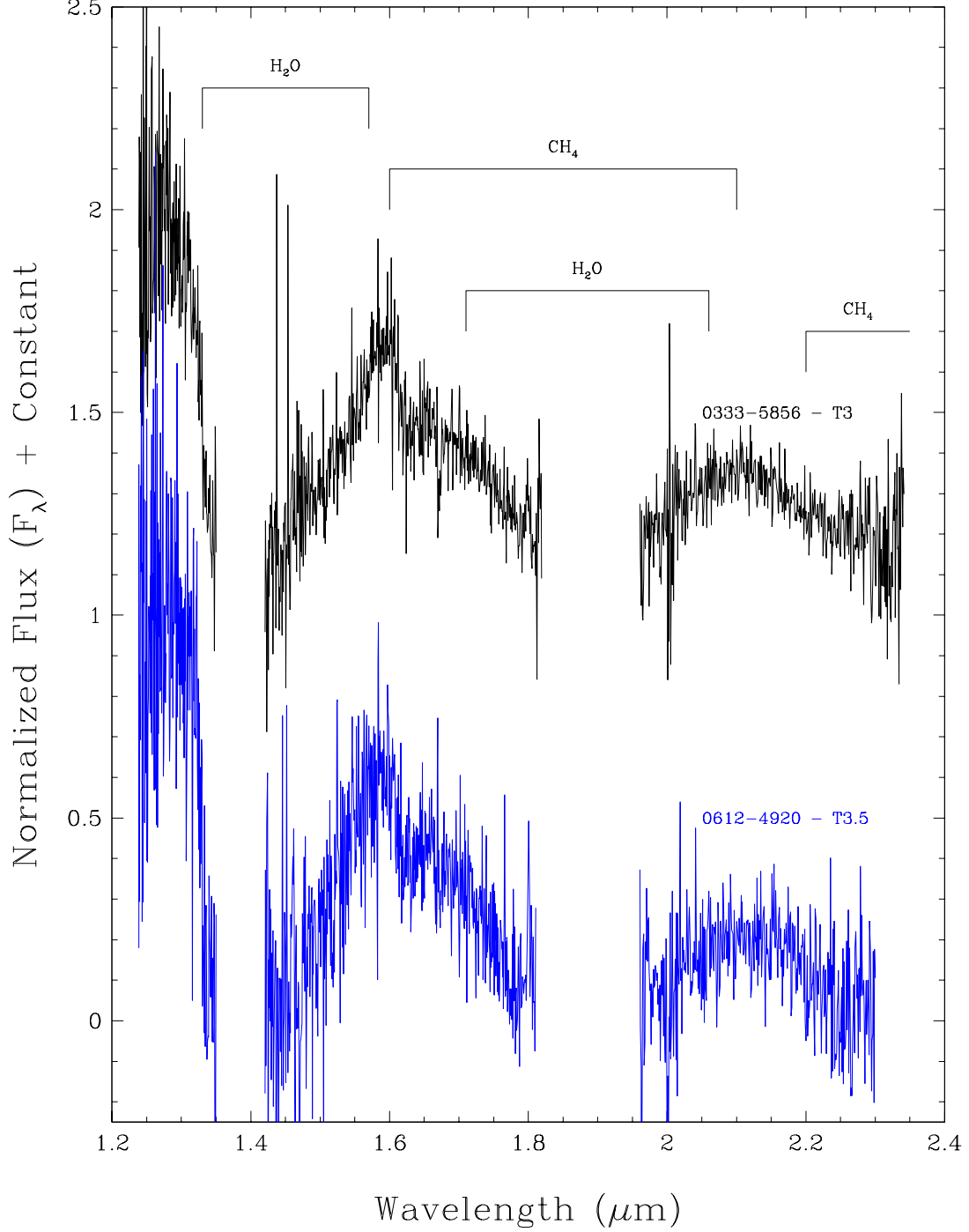


Fig. 27.— SOAR/OSIRIS spectra of two confirmed WISE brown dwarfs. Noisy data in the depths of the telluric water bands near 1.4 and 1.9  $\mu\text{m}$  are not plotted. Spectra have been normalized to one at peak flux and an offset of 1 has been added to the  $y$ -axis value of WISE 0333–5856 to separate it vertically from WISE 0612–4920. Prominent spectral features are marked.

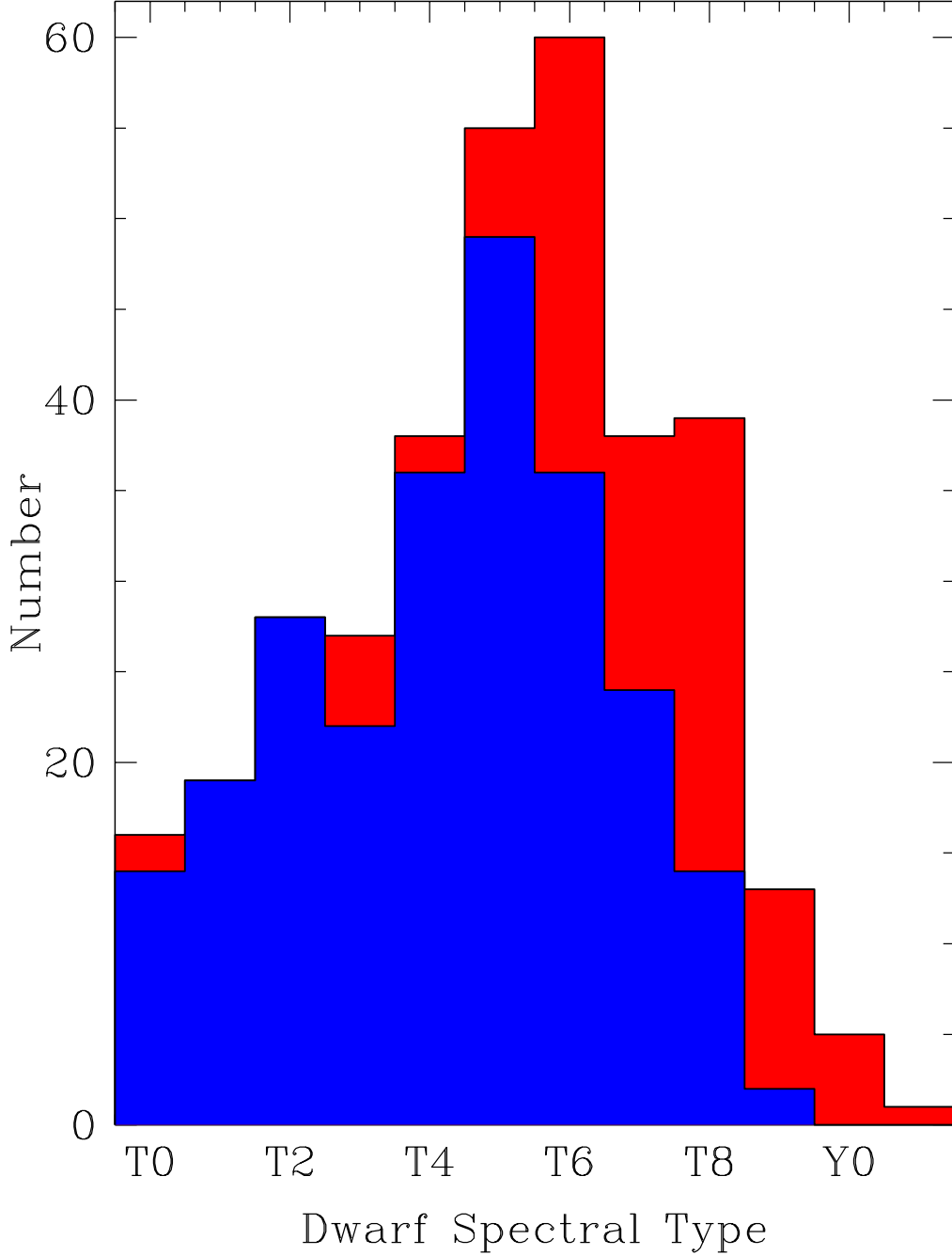


Fig. 28.— A histogram of spectral types for published objects with near-infrared types of T0 or later. The distribution of types of previously published brown dwarfs is shown in blue and the distribution of new types for discoveries in this paper is shown in red. Objects are counted into bins of integral subtypes (e.g., objects of type T7 and T7.5 are shown in the T7 bin). The previously published objects were taken from DwarfArchives.org on 2011 May 15 and are supplemented with new discoveries by Albert et al. (2011) and Burningham et al. (2011).

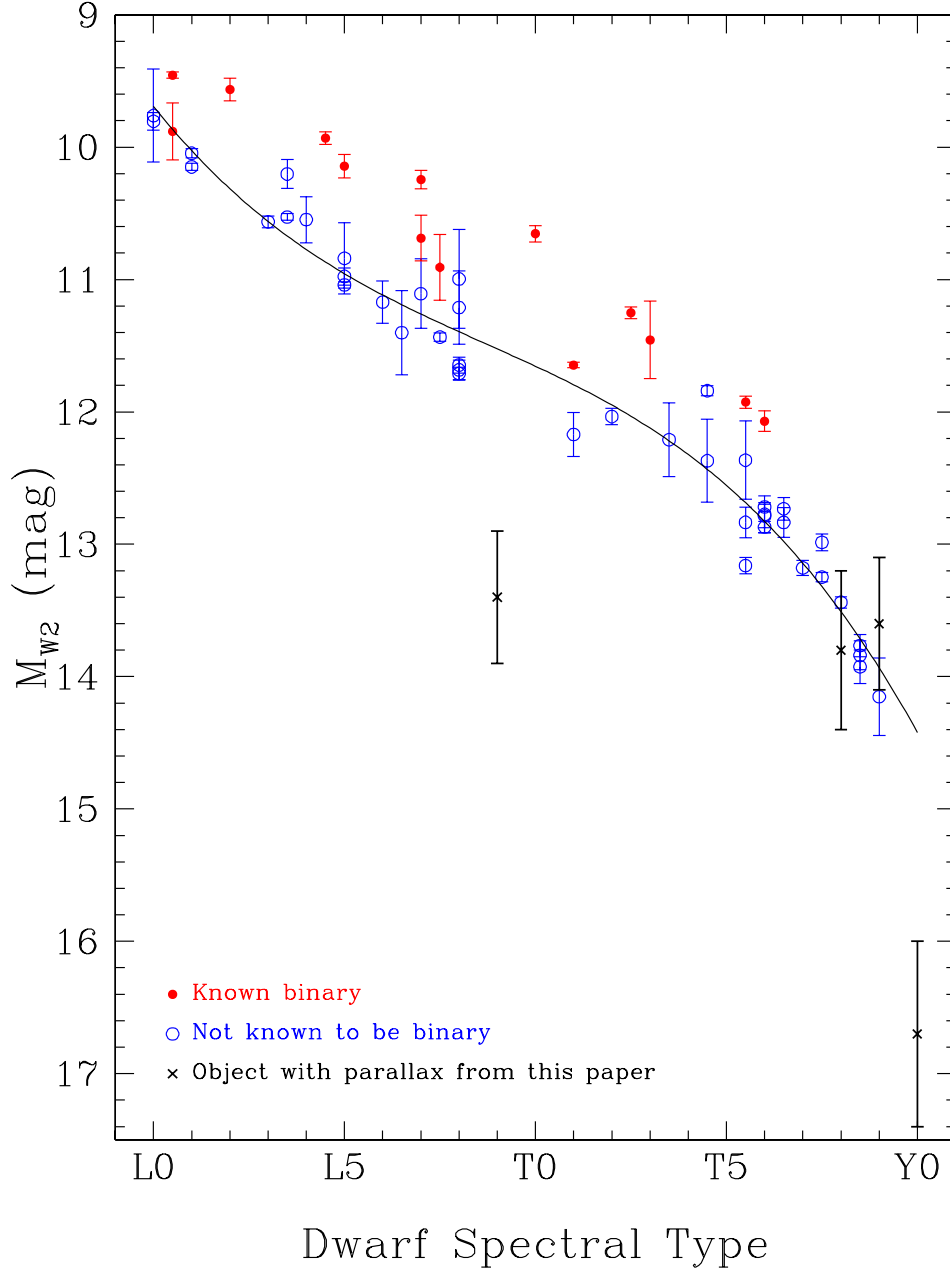


Fig. 29.— Absolute W2 magnitude plotted against spectral type for objects with measured trigonometric parallaxes. Red points are those objects known to be binary through high-resolution imaging. All others are shown as blue points. The solid line shows a third-order relation fit through the blue points, as described in the text. WISE discoveries with trigonometric parallaxes from Table 7 are shown with black x’s. The point for WISE 1541–2250 at lower right, if confirmed via continued astrometric monitoring, suggests that an extrapolation of the fitted relation cooler than T9 may result in Y dwarf spectrophotometric distance estimates that are too large.

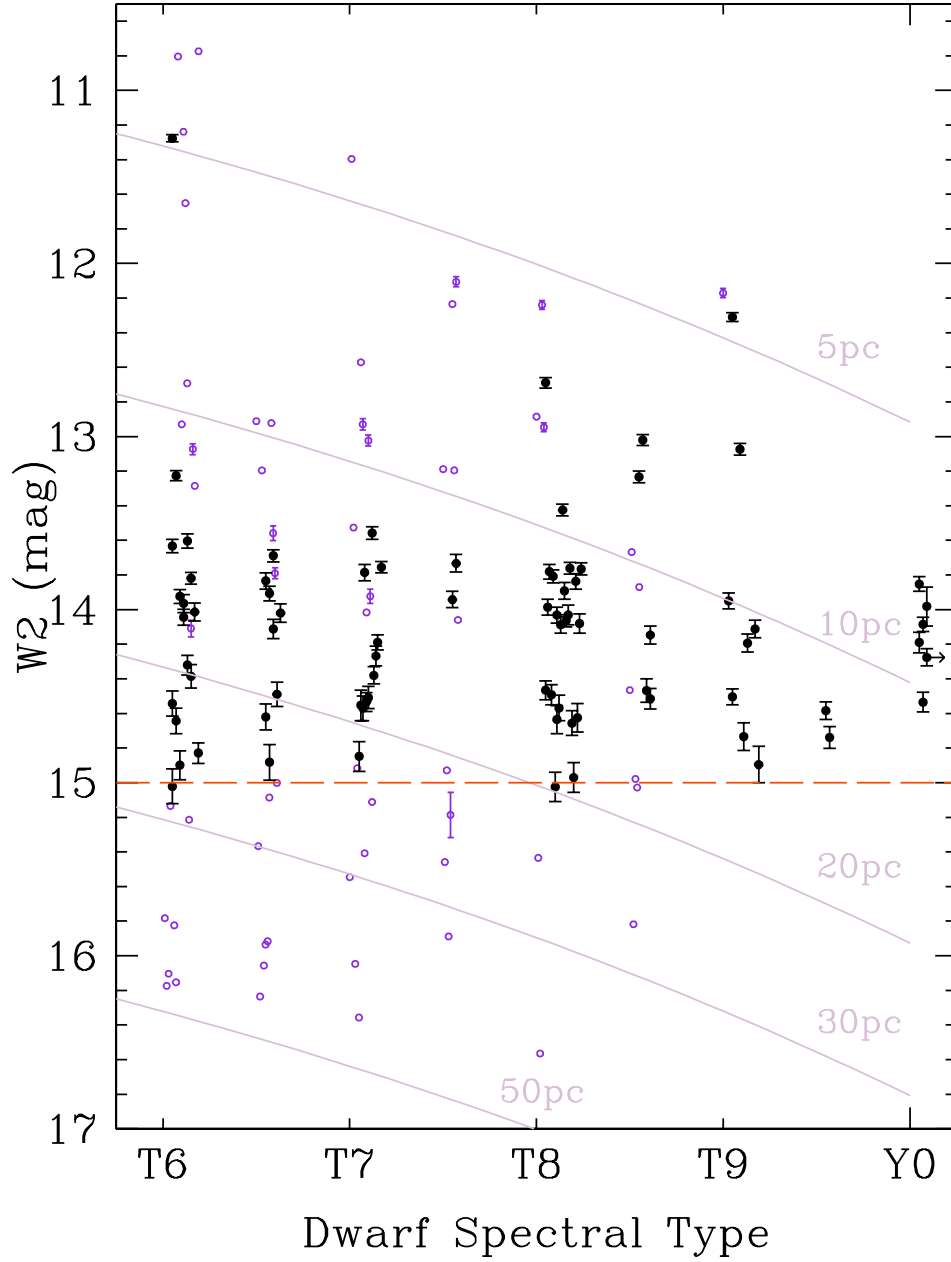


Fig. 30.— W2 vs. spectral type for previously known objects (open, blue violet points) and WISE discoveries (solid, black points). Slight offsets have been added to the spectral subclass of each object so that points suffer from less overlap along the  $x$ -axis. The distance relation from Figure 29 is plotted at various distances from 5 to 50 pc (grey lines) to aid the viewer in estimating distances to plotted objects. The dashed line in orange red shows the approximate W2 magnitude limit of our current WISE search. (Note: Error bars are shown on the open points when W2 photometry is known. Otherwise, open points are plotted at the W2 magnitudes estimated from the objects’ spectral types and near-infrared magnitudes and are plotted without error bars.)

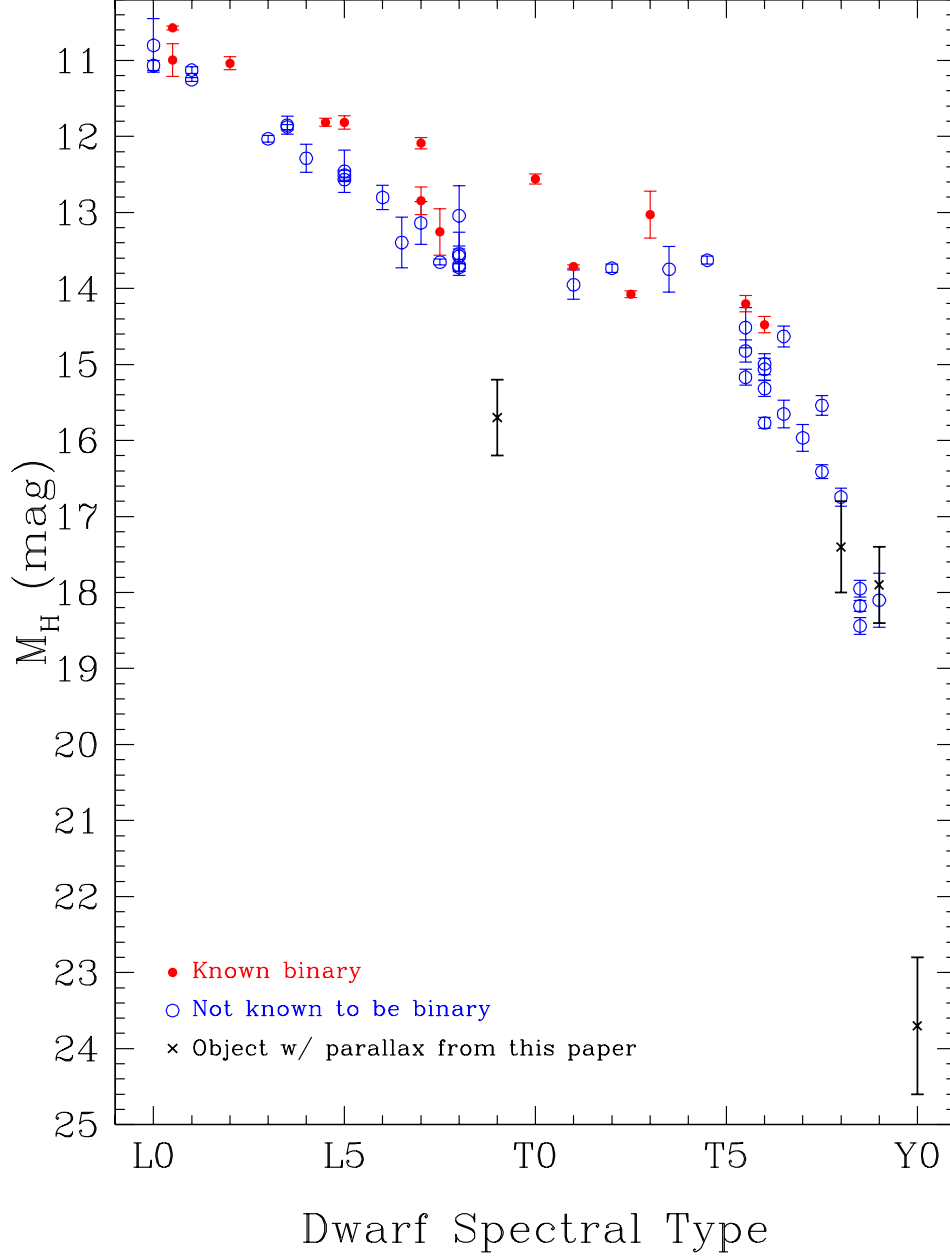


Fig. 31.— Absolute  $H$  magnitude plotted against spectral type for objects with measured trigonometric parallaxes in Figure 29. Note the rapid dimming of the  $H$ -band magnitude at the latest T types. The point for WISE 1541–2250 at lower right, if confirmed via continued astrometric monitoring, suggests that this  $H$ -band dimming accelerates as objects cool to the Y dwarf class.

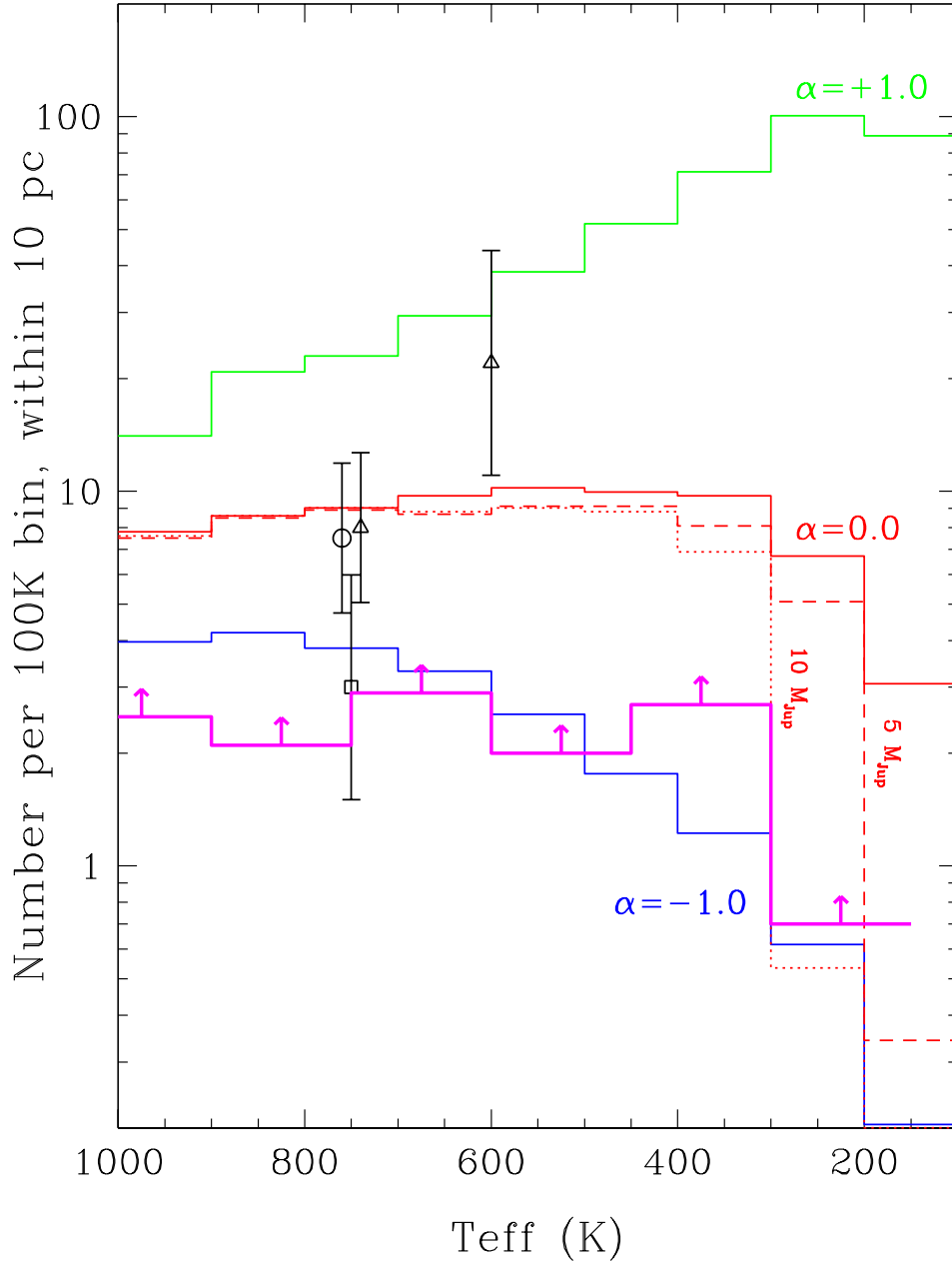


Fig. 32.— The predicted number of brown dwarfs within 10 pc for three different mass functions ( $dN/dM \propto M^{-\alpha}$  with  $\alpha = -1, 0, 1$  shown in green, red, and blue, respectively) having a minimum formation mass of  $1 M_{Jup}$  (Burgasser 2004). Also shown for the  $\alpha = 0$  model (dashed and dotted red lines) is the change in the expected number of brown dwarfs when the minimum formation mass is varied. Recent measurements of the observed space densities of T dwarfs are shown as open symbols – Metchev et al. (2008) (circle), Burningham et al. (2010b) (square), and Reyl   et al. (2010) (triangles). Lower limits to the space densities using a full accounting of objects in the Solar Neighborhood and based largely on early WISE results (Table 8) is shown in magenta.



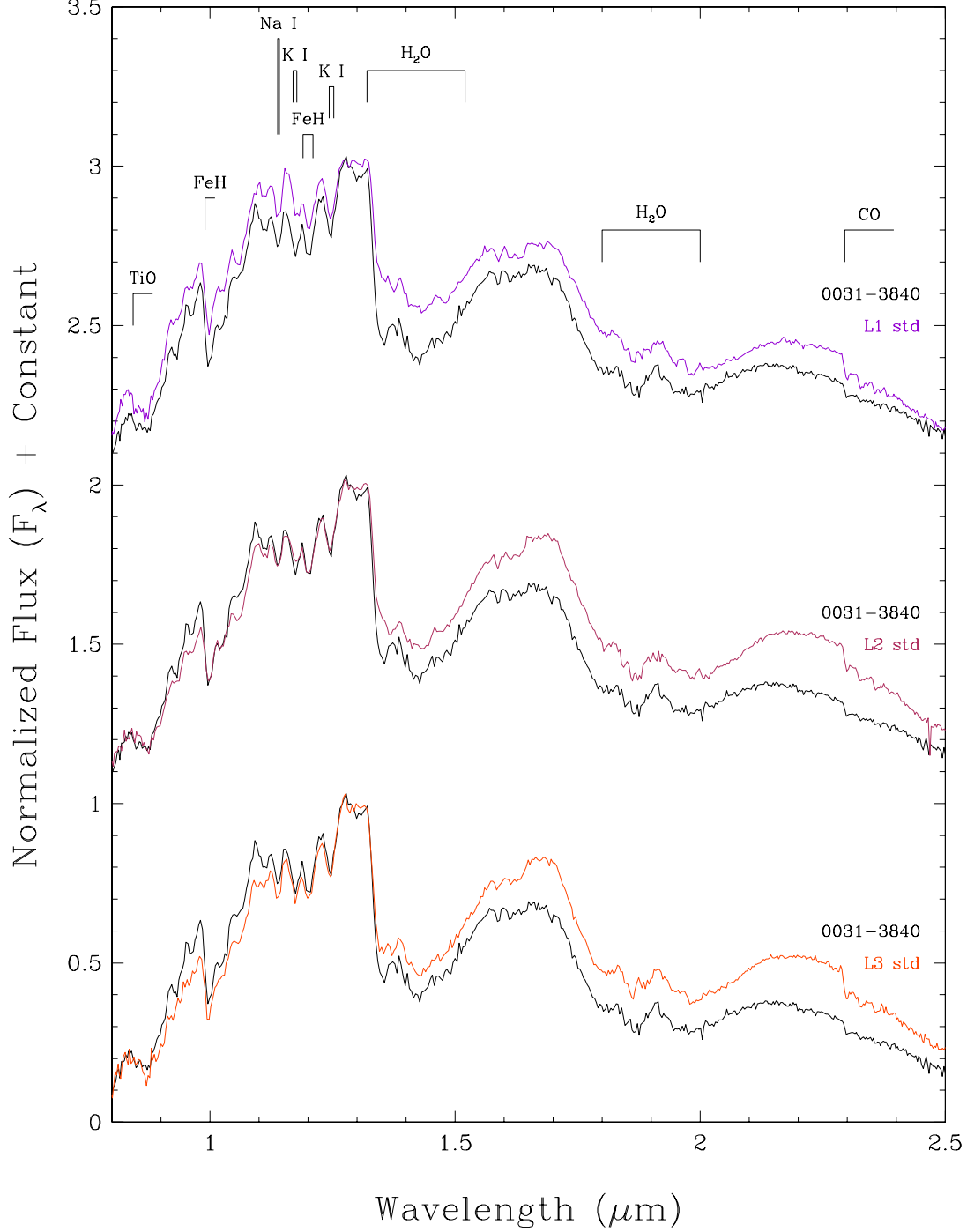


Fig. A1.— The near-infrared spectrum of WISE 0031-3840 (black) compared to the L1 (dark violet), L2 (maroon) and L3 (orange red) spectral standards from Kirkpatrick et al. (2010). Spectra have been normalized to one at 1.28  $\mu\text{m}$  and integral offsets have been added to the  $y$ -axis values to separate the spectra vertically except where overplotting was intended. Prominent spectral features are marked.

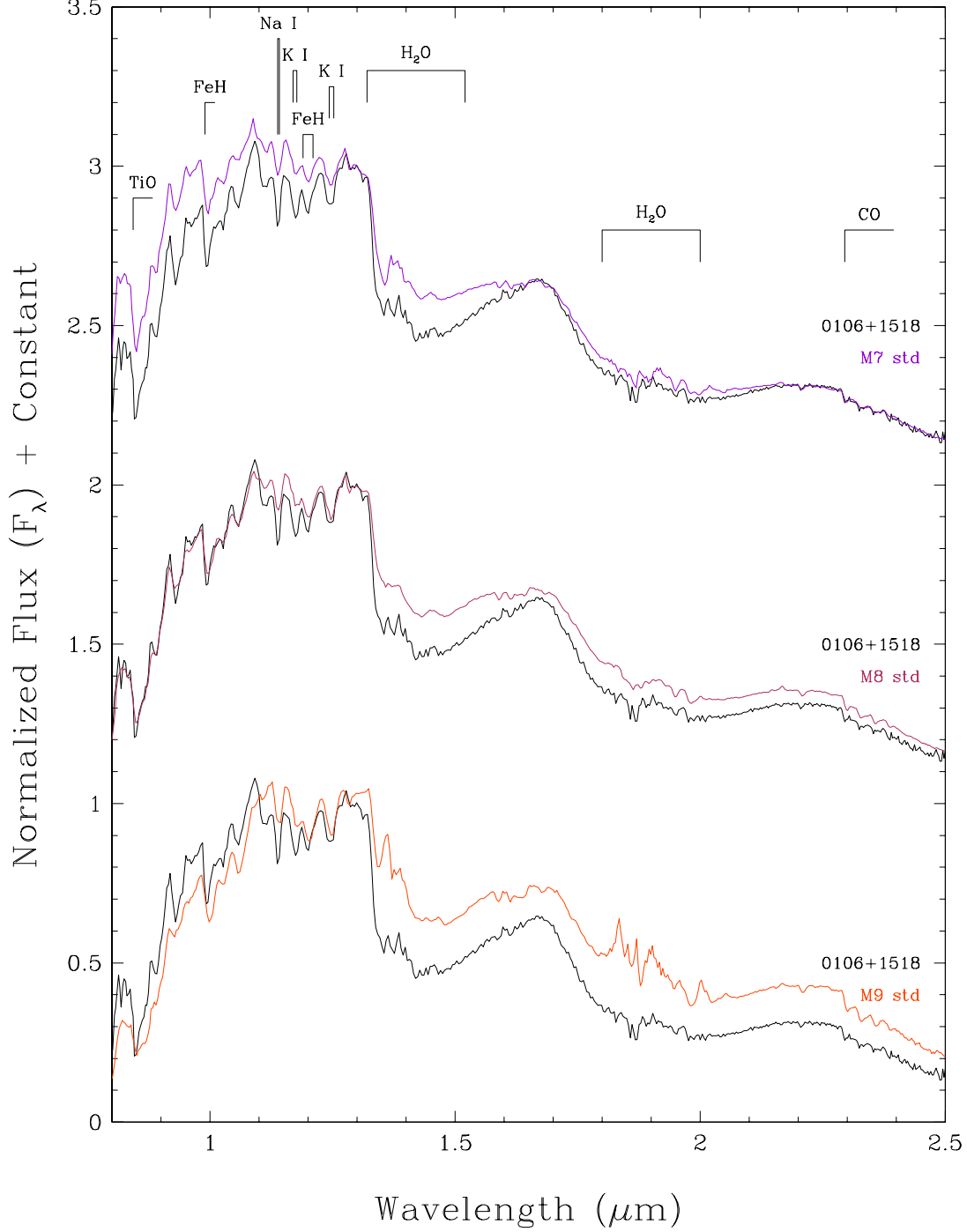


Fig. A2.— The near-infrared spectrum of WISE 0106+1518 (black) compared to the M7 (dark violet), M8 (maroon) and M9 (orange red) spectral standards from Kirkpatrick et al. (2010). Spectra have been normalized to one at 1.28  $\mu\text{m}$  and integral offsets have been added to the  $y$ -axis values to separate the spectra vertically except where overplotting was intended. Prominent spectral features are marked.

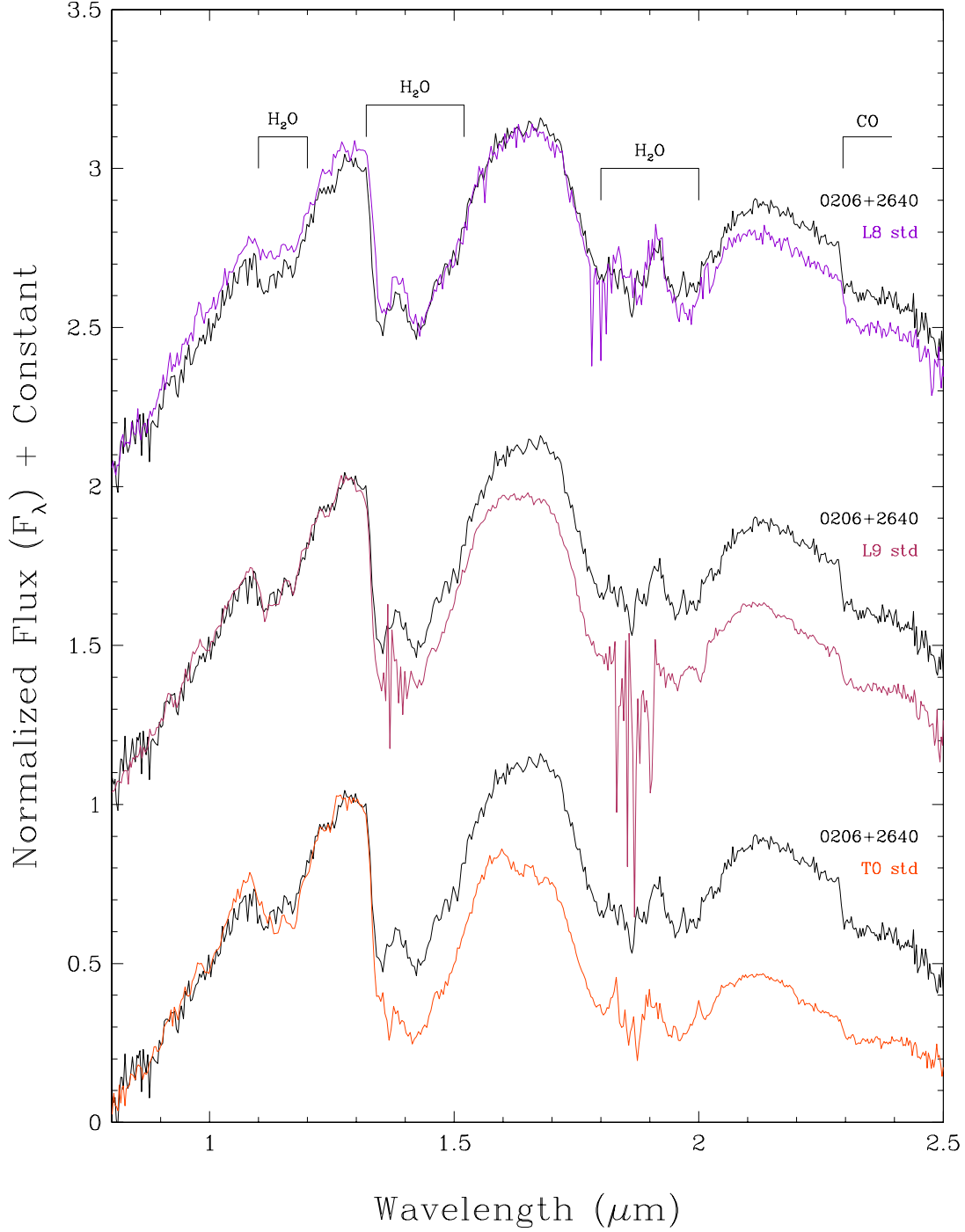


Fig. A3.— The near-infrared spectrum of WISE 0206+2640 (black) compared to the L8 (dark violet), L9 (maroon) and T0 (orange red) spectral standards from Kirkpatrick et al. (2010) and Burgasser et al. (2006). Spectra have been normalized to one at 1.28  $\mu\text{m}$  and integral offsets have been added to the  $y$ -axis values to separate the spectra vertically except where overplotting was intended. Prominent spectral features are marked.

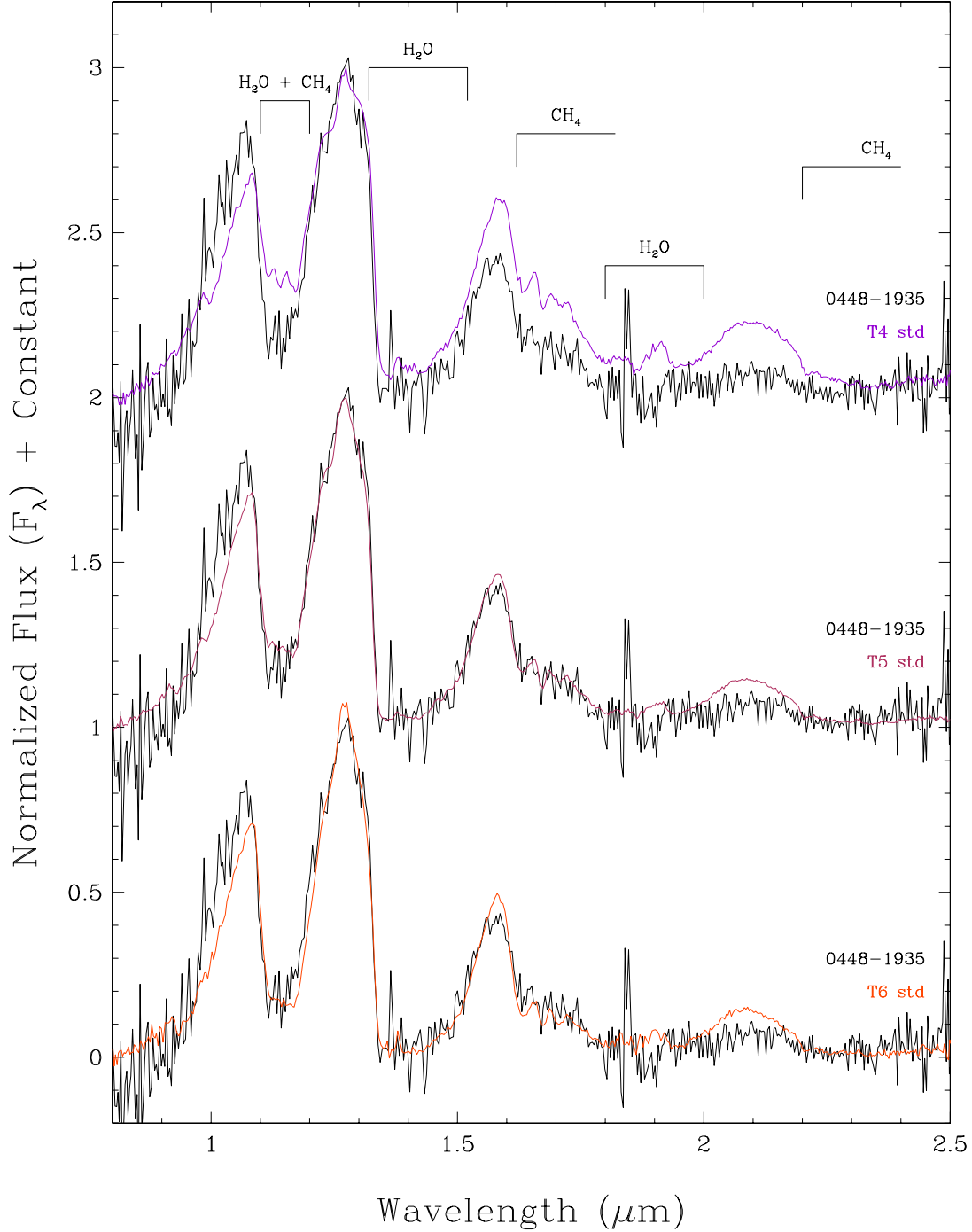


Fig. A4.— The near-infrared spectrum of WISE 0448–1935 (black) compared to the T4 (dark violet), T5 (maroon) and T6 (orange red) spectral standards from Burgasser et al. (2006). Spectra have been normalized to one at  $1.28 \mu\text{m}$  and integral offsets have been added to the  $y$ -axis values to separate the spectra vertically except where overplotting was intended. Prominent spectral features are marked.

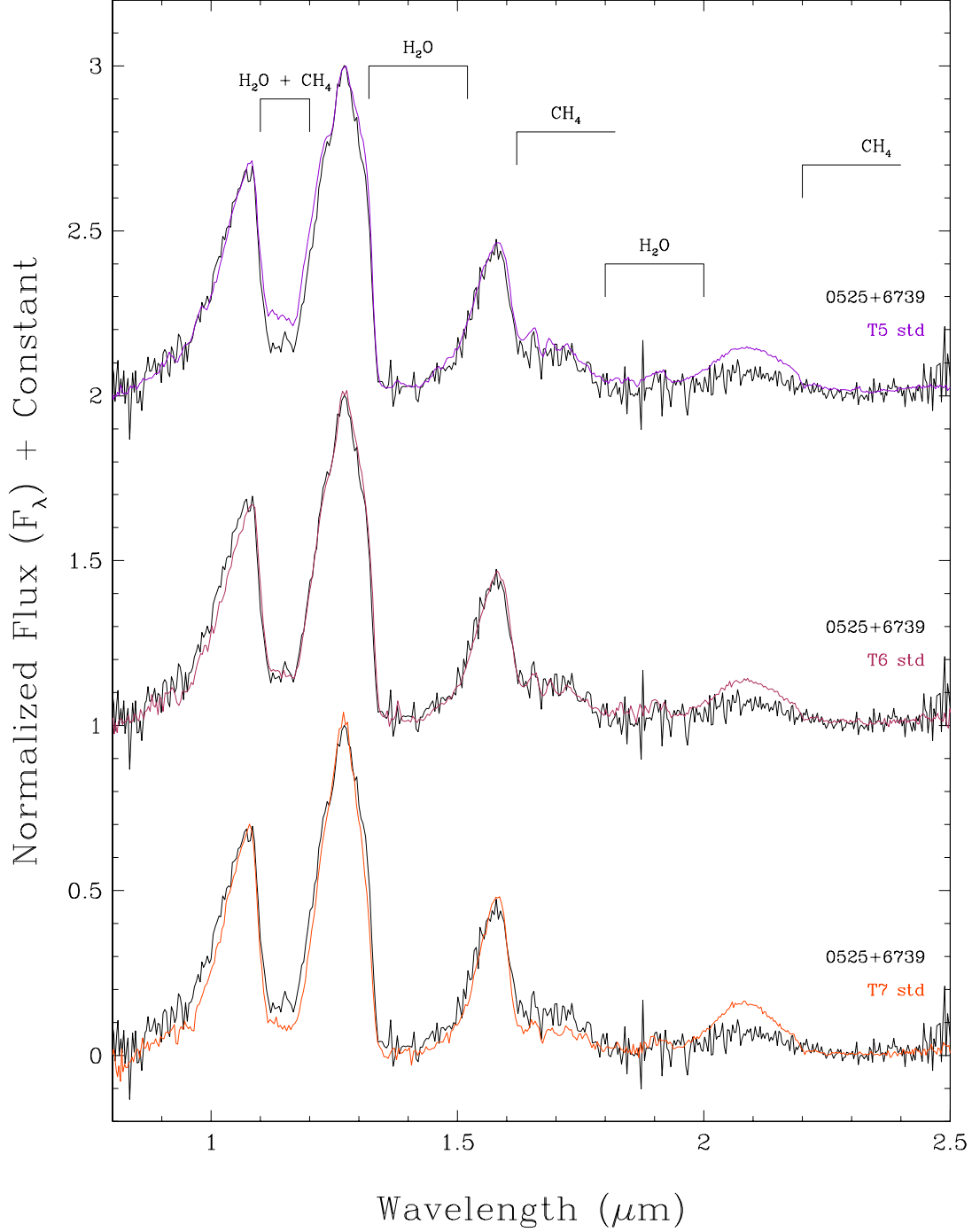


Fig. A5.— The near-infrared spectrum of WISE 0525+6739 (black) compared to the T5 (dark violet), T6 (maroon) and T7 (orange red) spectral standards from Burgasser et al. (2006). Spectra have been normalized to one at  $1.28 \mu\text{m}$  and integral offsets have been added to the  $y$ -axis values to separate the spectra vertically except where overplotting was intended. Prominent spectral features are marked.

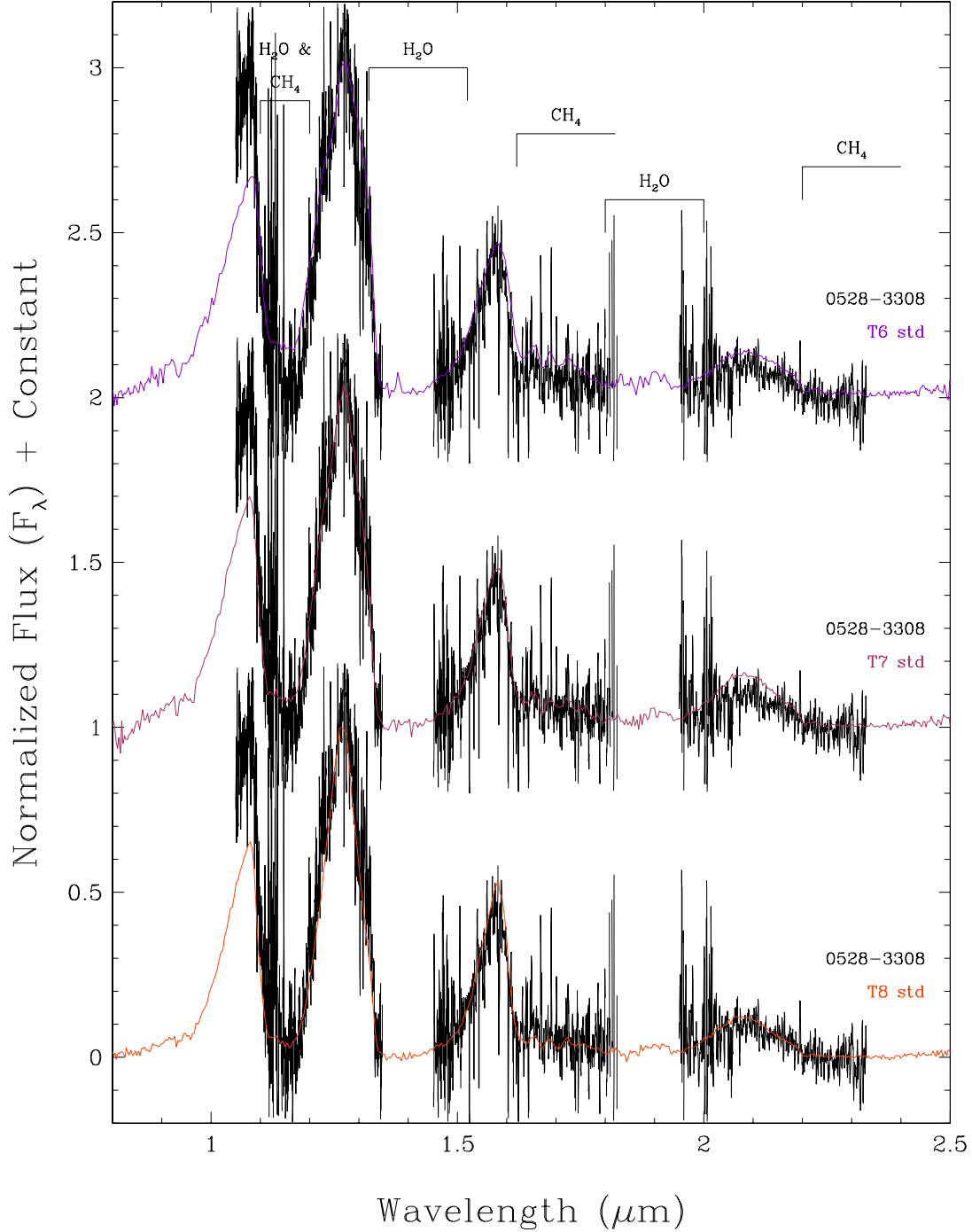


Fig. A6.— The near-infrared spectrum of WISE 0528–3308 (black) compared to the T6 (dark violet), T7 (maroon) and T8 (orange red) spectral standards from Burgasser et al. (2006). Spectra have been normalized to one at  $1.28 \mu\text{m}$  and integral offsets have been added to the  $y$ -axis values to separate the spectra vertically except where overplotting was intended. Prominent spectral features are marked. The spectrum of WISE 0528–3308 has been smoothed with a 5-pixel boxcar.

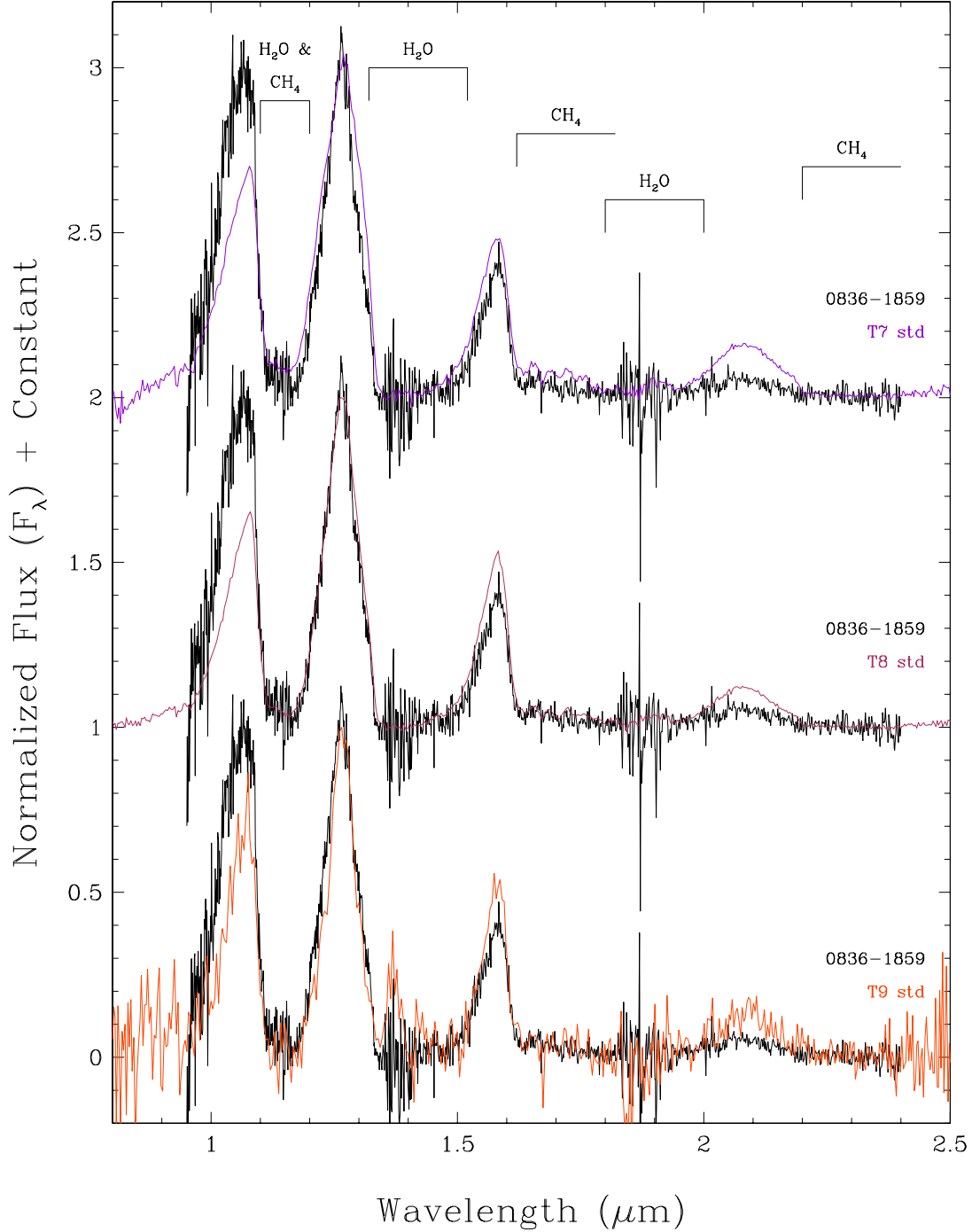


Fig. A7.— The near-infrared spectrum of WISE 0836–1859 (black) compared to the T7 (dark violet), T8 (maroon) and T9 (orange red) spectral standards from Burgasser et al. (2006) and Cushing et al. (accepted). Spectra have been normalized to one at  $1.28 \mu\text{m}$  and integral offsets have been added to the  $y$ -axis values to separate the spectra vertically except where overplotting was intended. Prominent spectral features are marked.

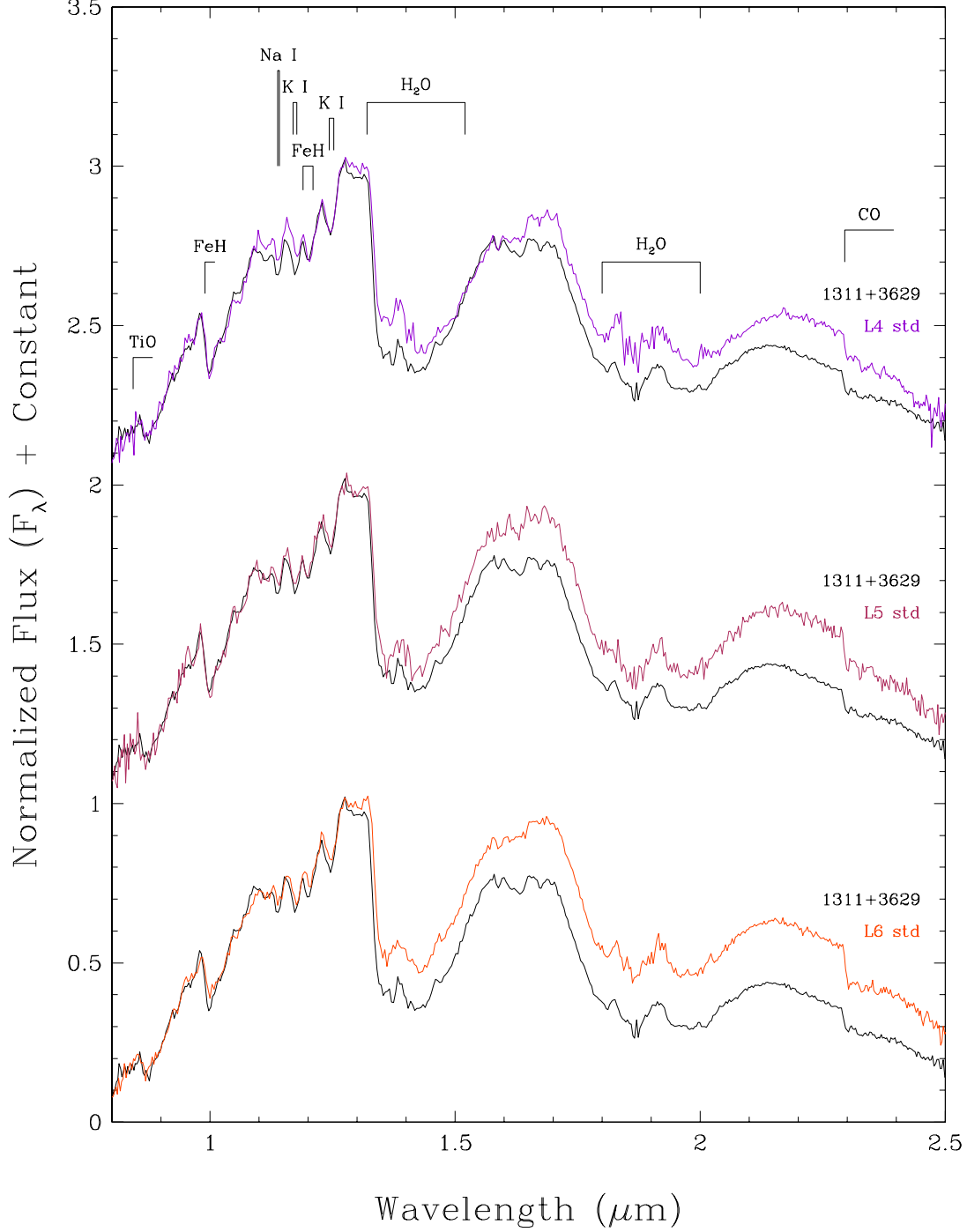


Fig. A8.— The near-infrared spectrum of WISE 1311+3629 (black) compared to the L4 (dark violet), L5 (maroon) and L6 (orange red) spectral standards from Kirkpatrick et al. (2010). Spectra have been normalized to one at  $1.28 \mu\text{m}$  and integral offsets have been added to the  $y$ -axis values to separate the spectra vertically except where overplotting was intended. Prominent spectral features are marked.



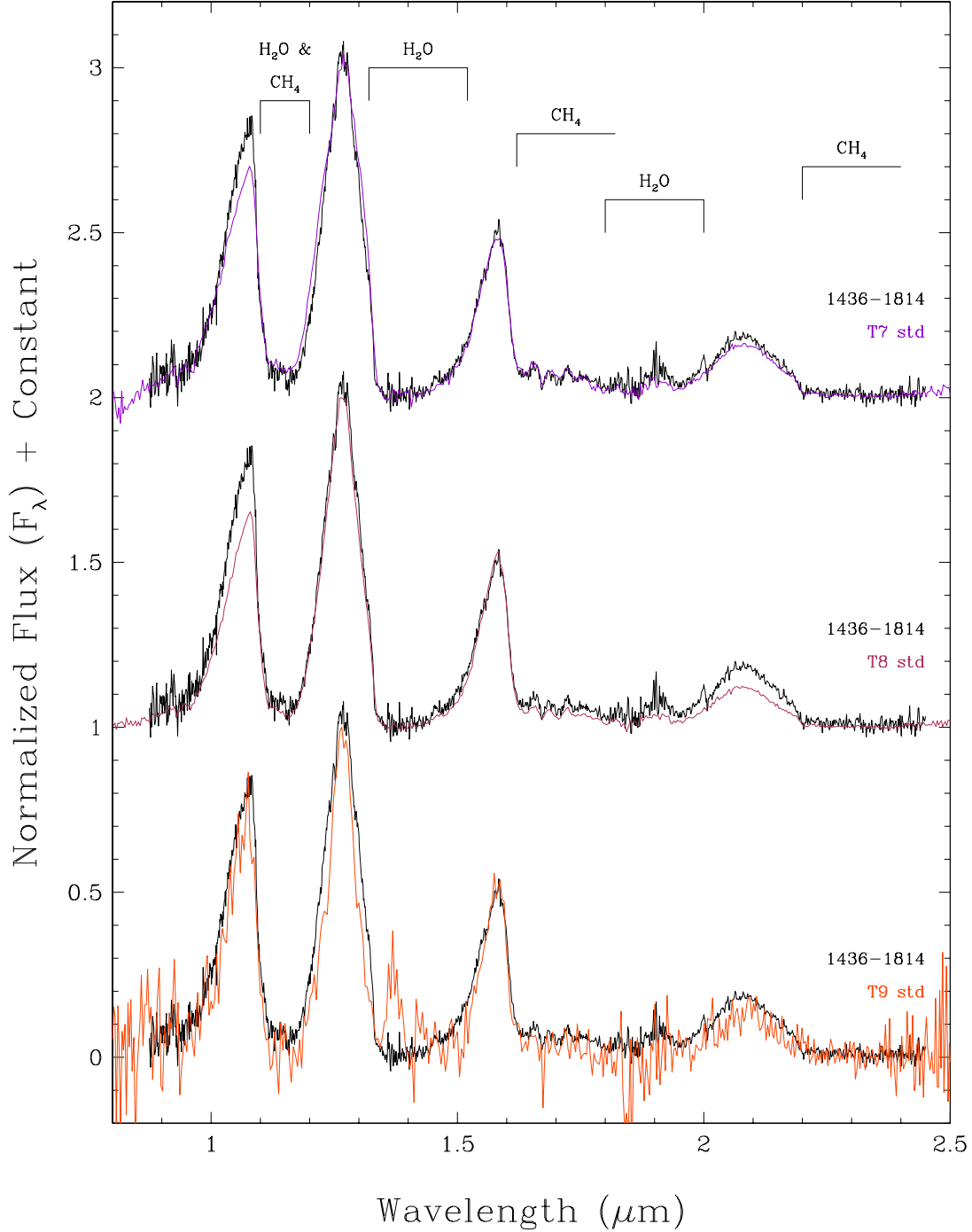


Fig. A9.— The near-infrared spectrum of WISE 1436–1814 (black) compared to the T7 (dark violet), T8 (maroon) and T9 (orange red) spectral standards from Burgasser et al. (2006) and Cushing et al. (accepted). Spectra have been normalized to one at 1.28  $\mu\text{m}$  and integral offsets have been added to the  $y$ -axis values to separate the spectra vertically except where overplotting was intended. Prominent spectral features are marked.

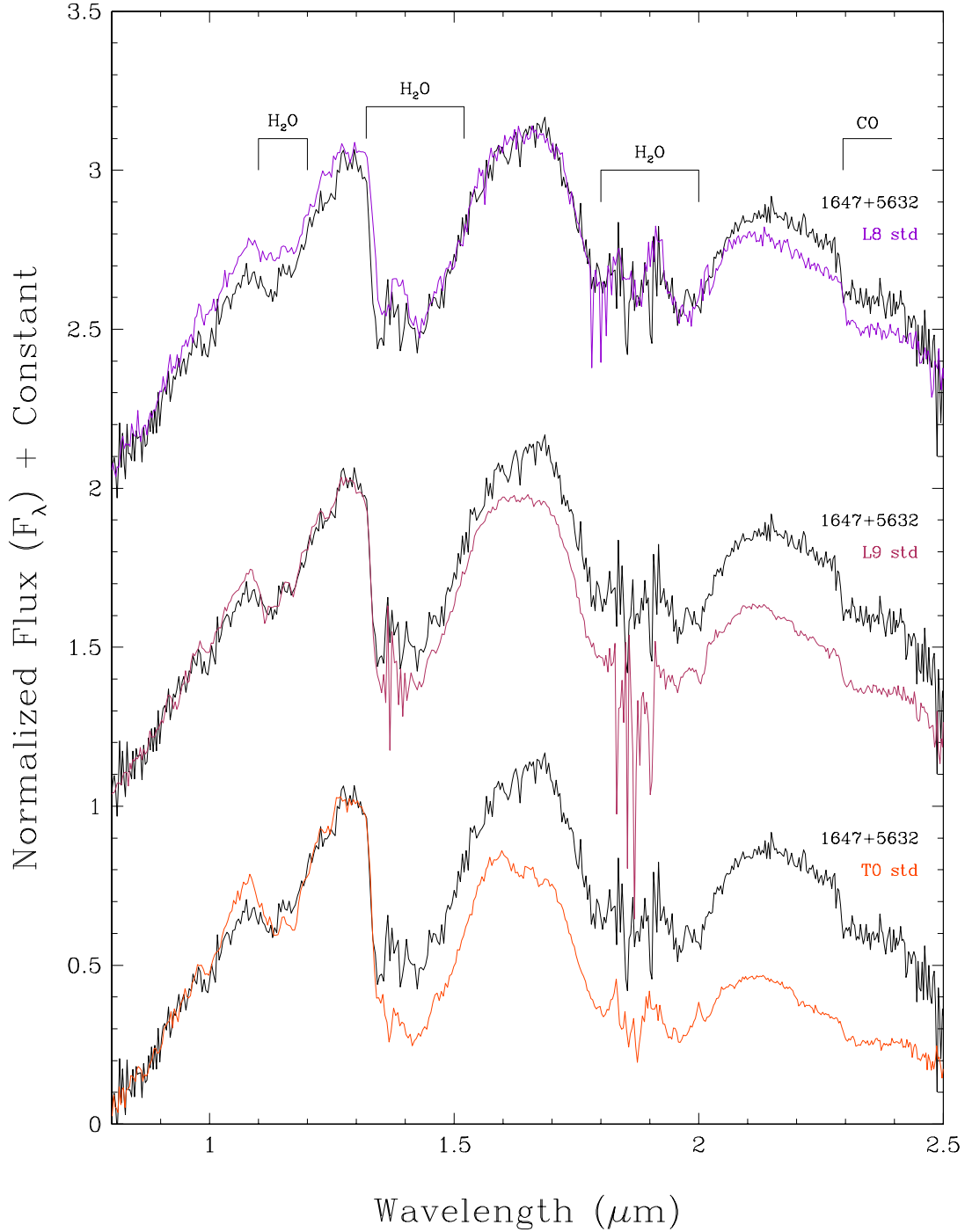


Fig. A10.— The near-infrared spectrum of WISE 1647+5632 (black) compared to the L8 (dark violet), L9 (maroon) and T0 (orange red) spectral standards from Kirkpatrick et al. (2010) and Burgasser et al. (2006). Spectra have been normalized to one at  $1.28 \mu\text{m}$  and integral offsets have been added to the  $y$ -axis values to separate the spectra vertically except where overplotting was intended. Prominent spectral features are marked.

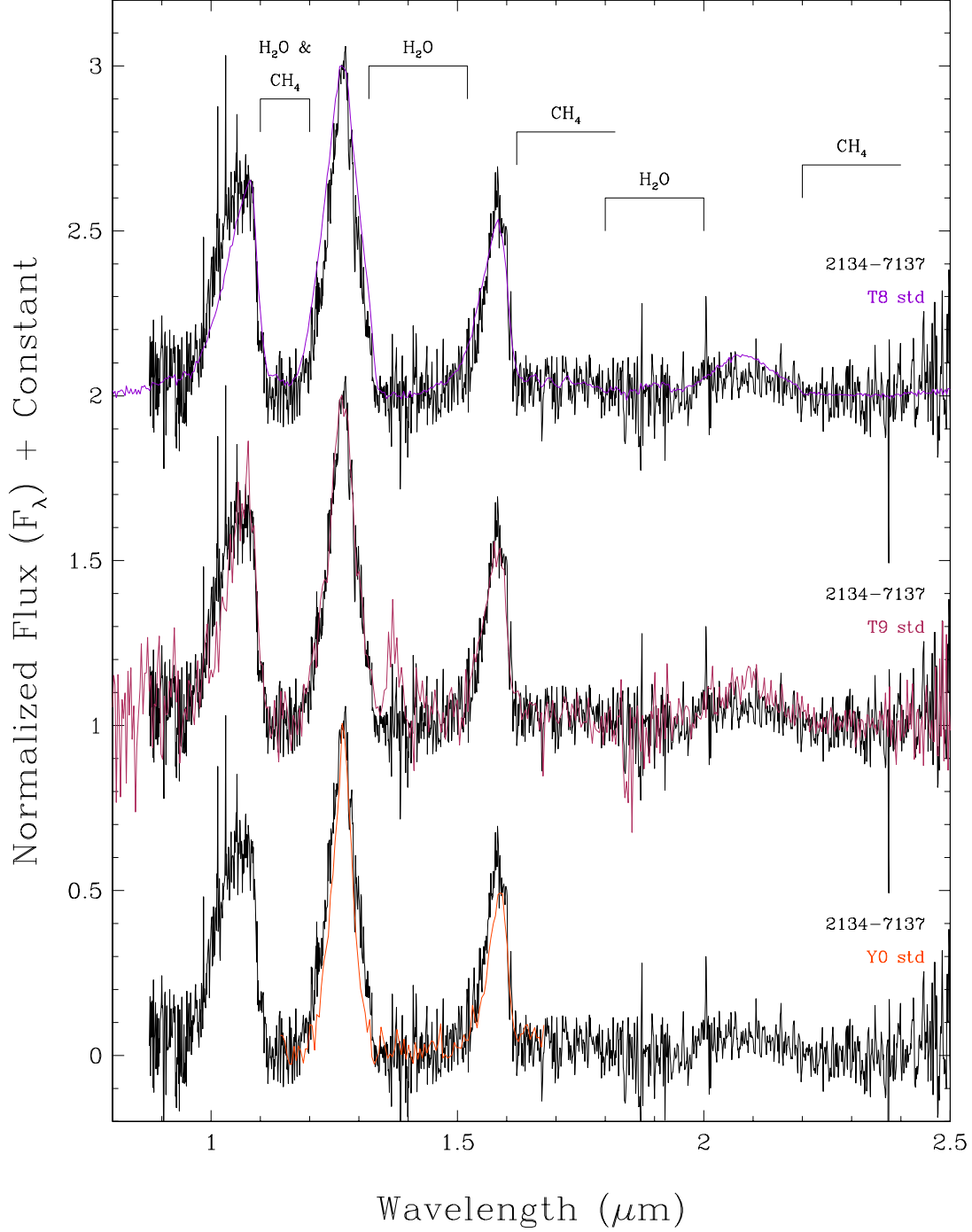


Fig. A11.— The near-infrared spectrum of WISE 2134–7137 (black) compared to the T8 (dark violet), T9 (maroon) and Y0 (orange red) spectral standards from Burgasser et al. (2006) and Cushing et al. (accepted). Spectra have been normalized to one at 1.28  $\mu\text{m}$  and integral offsets have been added to the  $y$ -axis values to separate the spectra vertically except where overplotting was intended. Prominent spectral features are marked.

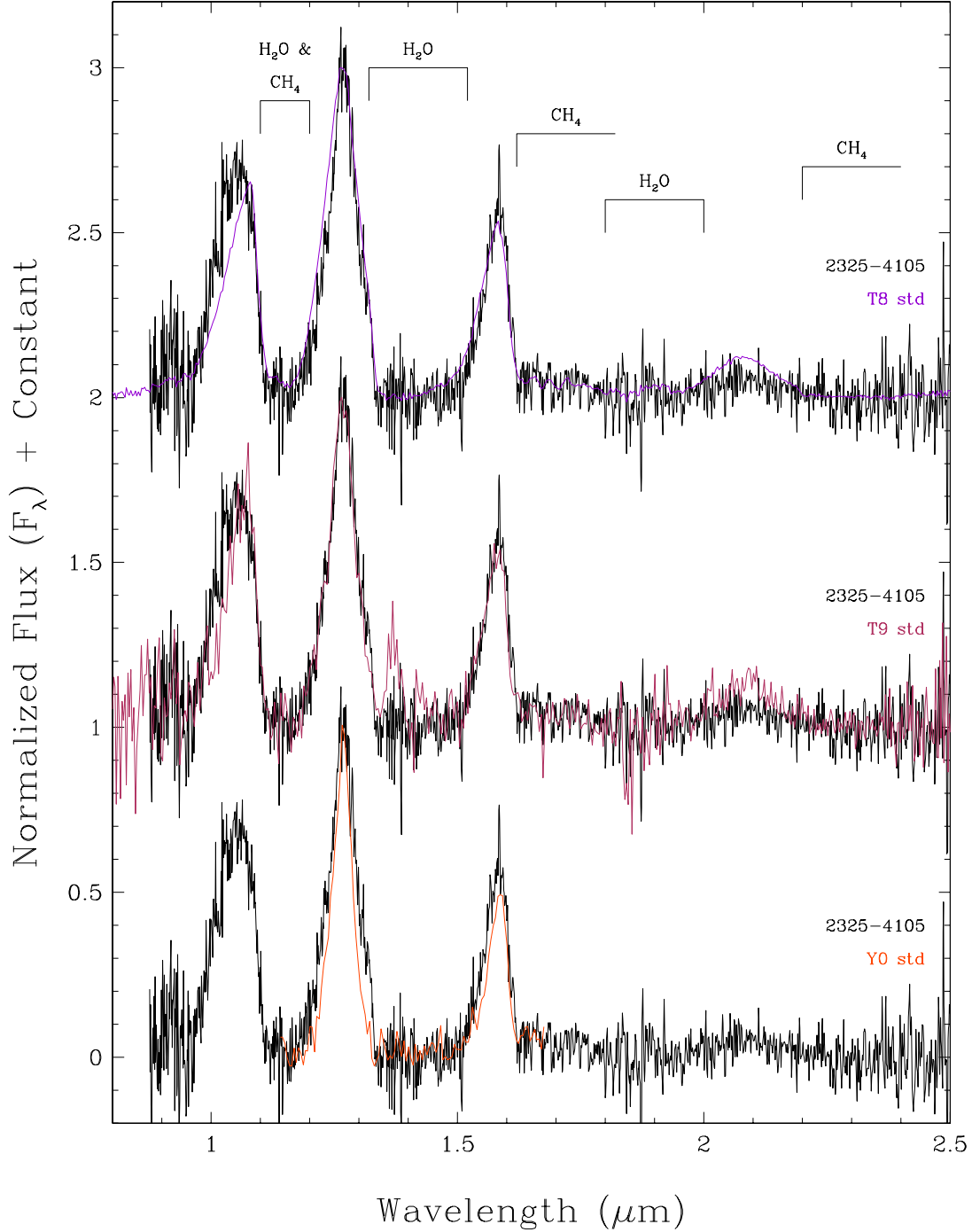


Fig. A12.— The near-infrared spectrum of WISE 2325–4105 (black) compared to the T8 (dark violet), T9 (maroon) and Y0 (orange red) spectral standards from Burgasser et al. (2006) and Cushing et al. (accepted). Spectra have been normalized to one at  $1.28 \mu\text{m}$  and integral offsets have been added to the  $y$ -axis values to separate the spectra vertically except where overplotting was intended. Prominent spectral features are marked.